The Role of the Liver Sinusoidal Endothelial Cells in the Pathophysiology of Insulin Resistance

Mashani Mohamad

A thesis submitted for the degree of Doctor of Philosophy

Ageing and Alzheimer's Institute
ANZAC Research Institute
Faculty of Medicine
The University of Sydney

2016

Declaration of the candidate

I hereby declare that all of the work presented in this thesis is my own original work accomplished under the supervision of Associate Professor Victoria Cogger and Professor David Le Couteur, unless otherwise acknowledged. I acknowledge that the proteomics, microbiota analyses and some of the statistical analyses were performed in the Charles Perkins Centre in the laboratories of Professor Stephen Simpson, Professor Stuart Cordwell and Associate Professor Andrew Holmes.

Mashani Mohamad

Acknowledgments

In the name of Allah, the Most Gracious, the Most Merciful

This PhD journey has been a great and humbling learning experience. First and foremost, I would like to thank my supervisors Assoc. Prof Victoria Cogger and Professor David Le Couteur for giving me the opportunity to perform my work under their guidance. Thank you Victoria for your supervision and assistance in every step throughout this study, and thank you for always looking after me and ensuring that my stay in Sydney was an unforgettable one. Thank you David for your support, guidance, advice and for allowing me to go for attachment and conferences to meet with other passionate scientists. Your continuous and invaluable support will be forever remembered.

I warmly thank and acknowledge all members of the Centre for Education and Research on Ageing (CERA) and Biogerontology laboratory for their advice, assistance and remarkable friendship. Thank you to Dr Alessandra Warren for all the great assistance in microscopy work. Thank you to Dr Aisling McMahon for guiding me in the GF project and animal work. Thank you Shajjia, Jenn, Sam, Rahul, Peter, John and Alice for sharing the student experience together. Thank you Mari Wright for making sure everything goes as smoothly as possible over the years.

I would also like to acknowledge all the amazing scientists and research collaborators that have contributed substantially to the completion of this work. Thank you to Professor Stephen Simpson who allowed me to be a part of the Geometric Framework project. Many thanks to Dr Lindsay Wu, Hassina and Jin from UNSW for the assistance in performing Western Blot that I had difficulties with. Thank you to Dr Fred Sierro of Centenary Institute

and Dr Sue Ying Ying from the Bosch Institute, University of Sydney for assistance in fluorescence microscopy work. Thank you to Dr Stuart Cordwell and Dr Melanie White for the proteomic analysis. Also many thanks go to the staff at the Diagnostic Pathology Unit, Concord Hospital for analysis of blood samples and Molecular Physiology Unit staff for the animal handling assistance. Thanks to the staff and students at the ANZAC Research Institute for providing such a welcoming space to socialise and performing good research.

One chapter of this thesis was completed at the National Institute on Ageing, Baltimore USA. I am grateful to Dr Rafael de Cabo for the privilege to work in his lab. I specially thank Dr Sarah Mitchell for the invaluable help with the project from the beginning to the end, taking care of me and making sure my time in USA was a memorable one.

I gratefully acknowledge funding support from the Ministry of Higher Education Malaysia and ANZAC Research Institute. Thank you to Universiti Teknologi MARA for granting me the study leave to make this study possible. Many thanks to Gurmeet and my other Malaysian friends for sharing the highs and lows of being an international PhD student. Most importantly, I am forever grateful and appreciative to my family who have given me their never ending love and support even from miles away. Thank you Mama, who has always supported and encouraged me to do my best in all matters of life. Last but not least, I wish to thank everyone that I've met along this journey which has been involved in the completion of this thesis in some way either directly or indirectly, for having a significant impact on my life. *Terima kasih semua* ☺

I dedicate this thesis to the loving memory of my father, who had envisioned me becoming a great scientist in the future

Publications and Conference abstracts

Publications derived from the thesis

Mohamad, M., S. J. Mitchell, L. E. Wu, M. Y. White, S. J. Cordwell, J. Mach, S. M. Solon-Biet, D. Boyer, D. Nines, A. Das, S. Y. Catherine Li, A. Warren, S. N. Hilmer, R. Fraser, D. A. Sinclair, S. J. Simpson, R. de Cabo, D. G. Le Couteur and V. C. Cogger (2016). "Ultrastructure of the liver microcirculation influences hepatic and systemic insulin activity and provides a mechanism for age-related insulin resistance." Aging Cell **15**(4): 706-715.

Cogger, V. C., M. Mohamad, S. Solon-Biet, A. M. Senior, A. Warren, J. N. O'Reilly, B. T. Tung, D. Svistounov, A. McMahon, R. Fraser, D. Raubenheimer, A. J. Holmes, S. Simpson and D. G. Le Couteur (2016). "Dietary macronutrients and the aging liver sinusoidal endothelial cell." American Journal of Physiology - Heart and Circulatory Physiology.

Other publications

Wu, L. E., C. C. Meoli, S. P. Mangiafico, D. J. Fazakerley, V. C. Cogger, M. Mohamad, H. Pant, M. J. Kang, E. Powter, J. G. Burchfield, C. E. Xirouchaki, A. S. Mikolaizak, J. Stockli, G. Kolumam, N. van Bruggen, J. R. Gamble, D. G. Le Couteur, G. J. Cooney, S. Andrikopoulos and D. E. James (2014). "Systemic VEGF-A neutralization ameliorates diet-induced metabolic dysfunction." Diabetes **63**(8): 2656-2667.

.

Abstracts from conference presentations

- Mohamad, M., Cogger, V. C. & Le Couteur, D. G. *Effect of liver endothelial defenestration on hepatic insulin and glucose uptake*. Joint ASCEPT-APSA Scientific Conference 2012, Sydney.

- Mohamad, M., Cogger, V. C., Wu, L. E. & Le Couteur, D. G. *Defenestration of liver sinusoidal endothelial cells as a cause of insulin resistance*. 17th International Conference of Cells of Hepatic Sinusoids 2013, Tokyo – Awarded Young Investigator Award.

- Mohamad, M., Cogger, V. C., Wu, L. E. & Le Couteur, D. G. *Effect of liver endothelial cells defenestration on glucose metabolism and insulin resistance.* Australian Society of Medical Research Scientific Conference 2013, Ballarat.

- Mohamad, M., Cogger, V. C., Wu, L. E. & Le Couteur, D. G. *Loss of fenestrations in liver sinusoidal endothelial cells impairs hepatic insulin signaling and glucose homeostasis.* ASCEPT Annual Scientific Meeting 2014, Melbourne.

- Mohamad, M., Cogger, V. C. & Le Couteur, D. G *The role of liver ultrastructure in the pathogenesis of hyperlipidemia and insulin resistance*. Cold Spring Harbor: Lipid Metabolism and Human Metabolic Disorders 2015, China.

- Mohamad, M., Mitchell, S. J., de Cabo, R., Le Couteur, D. G. & Cogger, V. C. *Liver sinusoidal endothelium changes in old age influences hepatic disposition of insulin and metabolism homeostasis*. 18th International Conference of Cells of Hepatic Sinusoids 2015, USA.

Scope of thesis

Ageing is associated with increased prevalence of metabolic syndrome, as well as impaired glucose metabolism, hyperinsulinemia and insulin resistance. The mechanism underlying these associations is poorly understood and is likely to be complex and multifactorial. The liver is the key target for insulin action and while the endothelium has been shown to influence insulin activity in muscle and fat, the role of the liver sinusoidal endothelium on the action of insulin in the liver is unknown.

The liver sinusoidal endothelium is unique: it is perforated with transcellular pores called fenestrations that facilitate unimpeded passage of substrates between blood and hepatocytes. A constellation of age-related morphological changes in the liver sinusoidal endothelium known as pseudocapillarisation have been described in various species including rats, baboons and humans. During ageing, the liver sinusoidal endothelium thickens, there is basement membrane deposition, and the fenestrations are significantly reduced in size and number (defenestration). Age-related pesudocapillarisation has been shown previously to impede the transfer of lipoproteins and medications across the hepatic sinusoidal endothelium.

This thesis tests the hypothesis that changes in the ageing liver contribute to age-related insulin resistance, with alterations of the liver sinusoidal endothelial cell leading to age-related impairment of insulin action and insulin resistance/glucose metabolism.

This work aims to improve the understanding of the effects of ageing processes in the liver on insulin action and glucose metabolism. It investigates the role of age-related

pseudocapillarisation and the acutely induced poloxamer 407 (P407) model of defenestration in hepatic disposition of insulin and glucose metabolism. This thesis also investigates the effect of P407 on the relationship between membrane rafts and fenestrations in SKHep1 cells, a cell line of liver endothelial origin and isolated LSECs. Finally, the effects of dietary macronutrients and calorie intake on fenestrations in old age are examined.

The work contained in this thesis aims to examine the role of age-related pseudocapillarisation in one of the major causes of age-related disease and disability, insulin resistance. In doing so it explores the potential mechanisms involved in these changes and how we may alter the progression of ageing through nutritional intervention.

TABLE OF CONTENTS

LIST OF FIGURES

LIST OF TABLES

LIST OF APPENDICES

List of abbreviations

AUC	Area under the curve
BCA	Bicinchoninic assay
CR	Calorie restricted/restriction
ER	Endoplasmic reticulum
GAMS	Generalised Additive Modelling
GTT	Glucose tolerance test
HOMA	Homeostatic model assessment
HSC	Hepatic stellate cell
IVC	Inferior vena cava
IP	Intraperitoneal
IR	Insulin receptor
KC	Kupffer cell
LSEC	Liver sinusoidal endothelial cell
mTOR	Mechanistic target of rapamycin
MID	Multiple indicator dilution
P407	Poloxamer 407
PAS	Periodic acid Schiff
PBS	Phosphate buffered saline
PV	Portal vein/venule
RT-PCR	Real time-polymerase chain reaction
SEM	Scanning electron microscope/microscopy
SoD	Space of Disse
TEM	Transmission electron microscope/microscopy
Vd	Volume of distribution
VEGF	Vascular endothelial growth factor
vW	Von Willebrand
WAT	White adipose tissue

CHAPTER 1: INTRODUCTION AND LITERATURE REVIEW

1.1 THE LIVER

1.1.1 Anatomy and function of the liver

The liver is the largest internal organ in the body and is responsible for multiple, dynamic functions (Schiff et al., 2007, Cattley and Popp, 2002). As the principle organ for maintaining systemic homeostasis, the liver has a major role in the metabolism, synthesis, storage, detoxification and secretion of numerous substrates. The liver synthesises plasma proteins such as albumin and is involved in the metabolism of lipoproteins and bilirubin, together with bile formation and secretion (Higuchi and Gores, 2003). The liver plays a key role in nutrient storage, processing and the regulation of plasma glucose. The liver also has a major role in maintaining and establishing immune functions such as immune tolerance (Holz et al., 2008) and detoxification of endogenous chemicals, drugs and pathogens (Arias et al., 2011).

The liver is located in the upper right quadrant of the abdominal cavity and contributes to between 2 and 5% of total body weight, with the average adult human liver weighing approximately two kilograms. The liver is functionally divided into four main lobes: left, right, median or quadrate, and caudate, surrounded by a fibrous capsule of connective tissue (Glisson's capsule) and further subdivided into 8 segments by divisions of the right, middle and left hepatic veins, with each segment receiving blood from its own portal pedicle (Fig. 1.1). The histological lobular architecture of the liver is similar in all species (Malarkey et al., 2005).

Uniquely, the liver receives its blood supply from two sources and this bi-channel blood flow is important when considering liver function and structure. Seventy percent of its blood is from the portal vein, which carries deoxygenated blood directly from the splanchnic circulation and contains micro and macro nutrients for processing and storage, and pathogens, drugs, and toxins for metabolism and/or elimination. The remaining 30% of the blood flow comes via the hepatic artery carrying oxygenated blood to the liver. Blood then percolates through the liver sinusoids and collects in the central vein, emptying into hepatic veins before completely draining from the liver via the inferior vena cava (Malarkey et al., 2005, Cattley and Popp, 2002). The bile canaliculus network transfers bile produced in the hepatocytes via the canals of Hering (Saxena and Theise, 2004) to the larger bile ducts and then to the gall bladder or duodenum.

The microscopic structure of the liver consists of repetitive functional units known as ‘classic lobules (Kiernan, 1833). Lobules are roughly hexagonal in shape and contain a central vein surrounded by repeating branches of the portal vein, bile ducts and hepatic artery (known as the portal triad, Fig 1.2). Within each lobule, the anatomical zones are classified as: the periportal/portal zone; midzonal/midlobular; and centrilobular/central zones, depending on the areas proximity to the central veins and portal triads. These zones are depicted in Fig 1.2.

In addition to the classical lobular delineation the liver is divided into acini according to the level of oxygenation and nutrient exposure of the cells (Fig 1.2). Zone 1 (periportal) contains the cells receiving the most oxygenated and nutrient rich blood located closest to the portal triad while zones 2 and 3 respectively contain cells that are exposed to less oxygenated and less nutrient rich blood as they are remote from arteriolar blood and located in the microcirculatory

periphery of the acinus. Each acinus contains approximately one thousand sinusoids that run between the columns of hepatocytes and connect the afferent portal triads to the central vein. This provides an extensive surface area for blood and hepatocytes exchange (McCuskey and Reilly, 1993, McCuskey, 2000, Le Couteur et al., 2008).

The ‘classic lobule’ is the most widely used model describing the liver anatomical unit, and the acinus most commonly used to describe the liver functional unit. Other alternative models of the functional and anatomical units of the liver that have been proposed including the ‘portal lobule’ defined by the central venules with a portal tract at the centre, and the ‘primary lobule’ combining function and anatomy (MacSween et al., 2002, Malarkey et al., 2005, Matsumoto et al., 1979, McCuskey, 2008, Teutsch et al., 1999).

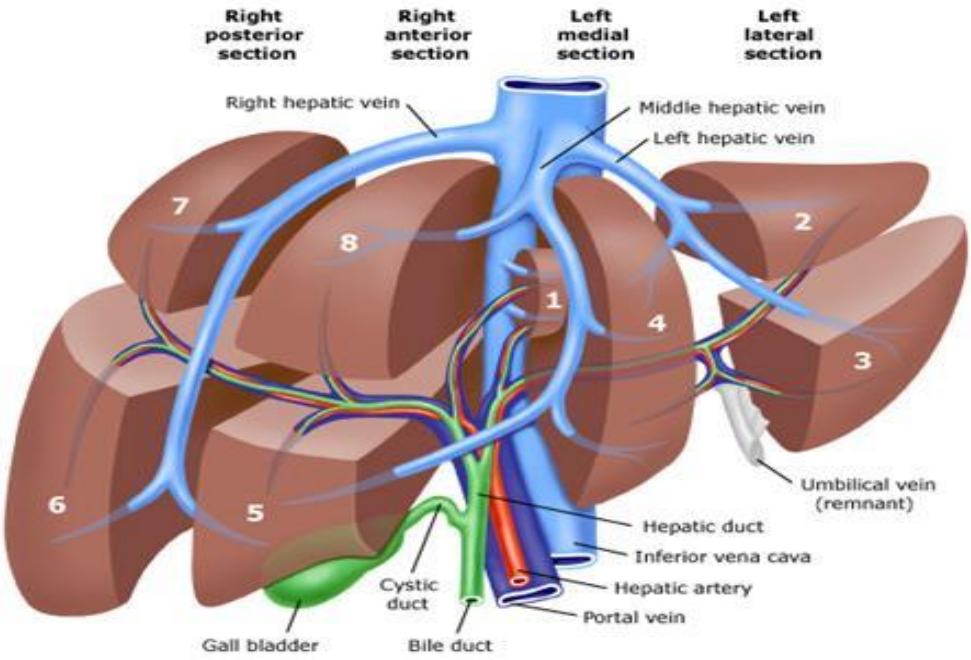

Figure 1.1: Segmental anatomy of the liver showing eight hepatic segments (Schiff et al., 2007)

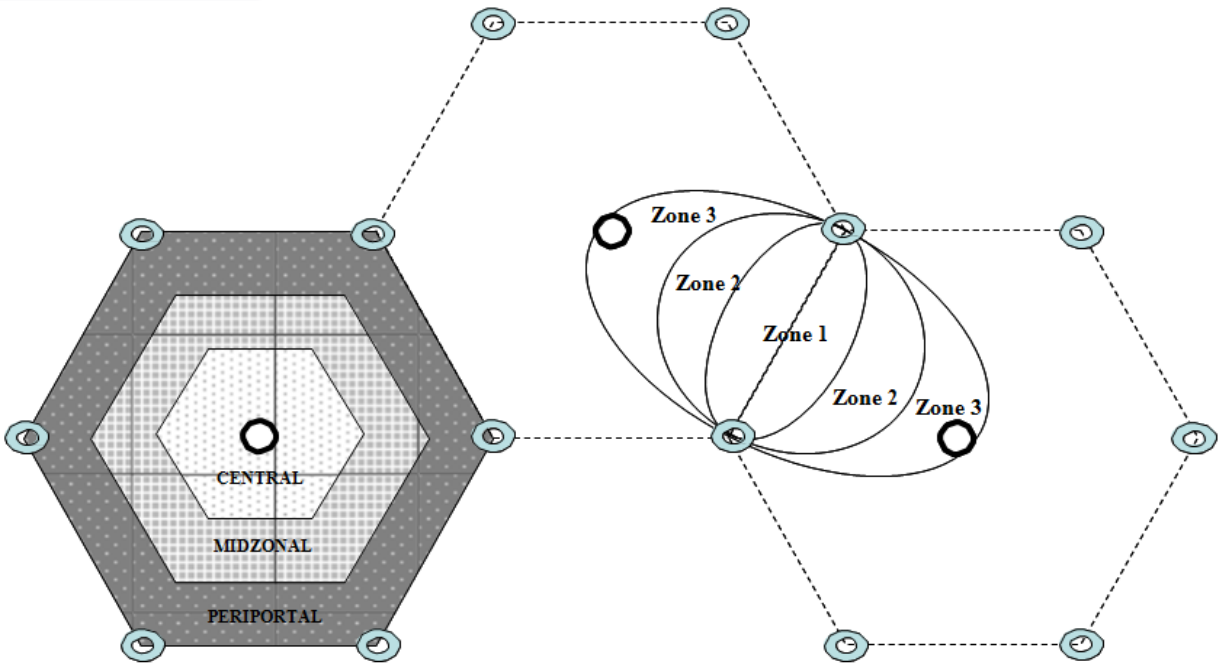

Figure 1.2: A diagrammatic representation of the classic lobule and liver acinus (Cattley and Popp, 2002)

1.2 ULTRASTRUCTURE OF THE LIVER

The liver vasculature is uniquely structured with the main blood vessels separated by a parenchymal mass of cells and connected by the smaller capillaries (sinusoids) at the same time (Arias et al., 2011). The liver is composed of parenchymal cells known as hepatocytes, cholangiocytes and several varieties of resident non-parenchymal cells namely liver sinusoidal endothelial cells (LSEC), hepatic stellate cells, Kupffer cells, natural killer cells and dendritic cells, with each cell having a specific morphology and function. All cells are arranged in a matrix, allowing a coordination of synthesis, metabolism and clearance of a variety of molecules. Each cell type can undergo morphologic or quantitative changes under different disease pathological challenges (Wisse et al., 1996, Fraser et al., 1986).

1.2.1 Hepatocytes

Hepatocytes constitute about 80% of the total volume of the liver and 60% of the liver cells (Kmiec, 2001). They are polyhedral in shape and arranged into plates of single cells, (hepatocyte cords) supported by a fine reticular fibre (collagen III) framework, and are separated by continuous sinusoidal networks, allowing the hepatocytes to have a close contact with the blood (Cattley and Popp, 2002). The hepatocytic membrane has three regions: the sinusoidal domain, the intercellular junction and the bile canalicular surface. The sinusoidal domain/basolateral area of the hepatocyte faces the sinusoid and is characterised by abundant microvilli that increase the area by six-fold for hepatocyte substrate uptake and exchange and extend into the space of Disse (SoD) and even into the sinusoidal lumen through fenestrations (Wisse et al., 1985). The

hepatocyte intercellular regions contain junctional complexes for attachment to and communication with adjacent hepatocytes (Ross et al., 2003). This membrane extends to the sinusoidal lumen and undertakes the extraction of a wide variety of molecules from the blood and simultaneous secretion of molecules synthesised by the hepatocytes (Medlock and Haar, 1983). The canalicular surface of the hepatocytes has villous projections and exporter pumps including the bile salt transporter for biliary excretion (Kullak-Ublick et al., 2000). It is positioned between the lateral surfaces that face adjacent hepatocytes and contain tight junctions that seal the bile canaliculi, and the adhering junctions that link neighbouring hepatocytes and express gap junctions facilitating intercellular communication and exchange (Kuntz and Kuntz, 2009).

The many functions of the hepatocytes include the regulation of carbohydrate, lipid, and amino acid metabolism and storage, blood glucose regulation, and bile, cholesterol, and plasma protein synthesis namely albumin, carrier proteins, coagulation factors, growth factors and hormones (Ghany and Hoofnagle, 2005). They are also the main site of xenobiotic metabolism and transamination reactions in the body (Steinberg et al., 1987) and have the capacity for antigen presentation and T-cell activation (Warren et al., 2006, Crispe, 2011).

Hepatocytes also contain a high density of cytoplasmic organelles that take up 20-30% of the cell volume, and are abundant in mitochondria, smooth and rough endoplasmic reticulum (ER), free ribosomes, Golgi apparatus, lysosomes, and peroxisomes (Kuntz and Kuntz, 2009, Kmiec, 2001, Blouin et al., 1977). They possess significant regenerative capacity, being able to proliferate rapidly in order to replace lost or damaged cells after partial hepatectomy and during disease and toxicity (Fausto and Campbell, 2003).

1.2.2 Cholangiocytes

The cholangiocytes are cells that line the bile ducts and form 1 % of the liver parenchyma. These cells are responsible for the modification of the canalicular bile composition, which occurs through a series of secretory and absorptive processes (Strazzabosco, 2004, Masyuk et al., 2008). Cholangiocytes also interact with other liver cells such as hepatocytes, LSEC, HSC and KC by releasing growth factors, peptides, nucleotides, pro-inflammatory and chemotactic cytokines and other signaling molecules (Strazzabosco, 2004). These cells are involved in regulation of bile formation, liver inflammatory processes, angiogenesis and fibrogenesis because of their interaction with the other liver cells (Masyuk et al., 2008).

1.2.3 Hepatic stellate cells

The hepatic stellate cells (HSC), also known as Ito cells, fat-storing cells, vitamin A-storing cells or lipocytes, are located in the SoD and comprise approximately 1.5% of the total liver cell population (Wake, 1980, Kmiec, 2001). HSC store 80% of the body's retinoids as retinyl palmitate in cytoplasmic fat droplets. The main physiological function of the stellate cells is storage and regulation of retinoids, but also storage of triglycerides, cholesterol and free fatty acids. HSC also synthesise and degrade components of extracellular matrix and other proteins (Senoo, 2004).

During liver injury, HSC respond to inflammatory cytokines such as IL-6 and TGF-β, become activated and acquire a myofibroblast-like phenotype that produces abundant quantities of

collagen types I, III and IV stage. They undergo morphological changes, start proliferating and become contractile, lose their lipid stores and start to secrete fibrogenic and inflammatory cytokines, which can lead to fibrosis (Friedman, 2008). In addition, HSCs are antigen presenting cells, eliciting T-cell responses as efficiently as dendritic cells. Their location in the SoD serve as an early detection point for any pathogens that have crossed the endothelium (Winau et al., 2007).

1.2.4 Kupffer cells

Kupffer cells (KC) are endogenous liver macrophages. They account for 80-90% of the body's resident macrophages (Arii and Imamura, 2000) and are located in the lumen of the hepatic sinusoids, usually in close proximity to the endothelial cells (Wisse, 1972). KC contribute to host defence and tissue homeostasis, and their major function is to clear particulate and foreign materials from the portal circulation. Substrates including microorganisms, endotoxin, old and foreign cells, complement components and immune complexes can be phagocytosed by the KC and broken down by both oxygen dependent and independent mechanisms. KCs also act synergistically with pit cells in the killing of tumour cells (Wisse et al., 1997) and are classified as potential antigen-presenting cells (Bouwens and Wisse, 1992). KC are located within close proximity to the luminal membrane of LSECs, projecting their cytoplasmic processes through fenestrations for further anchorage and contact with HSCs and hepatocytes (McCuskey, 2008).

1.2.5 Natural killer cells

Hepatic natural killer cells or pit cells are located in the hepatic sinusoidal lumen in portal tracts in granuloma-like cellular aggregates. They are often in contact with KCs and are adherent to LSECs by pseudopodia (Wisse et al., 1976). They are considered to be more cytotoxic than other natural killer variants (Melmed et al., 2011). This has significant implications for the liver's early defence against tumours and microbes/virus- infected cells (Nakatani et al., 2004). The liver-associated NK cells exert anti-tumour functions through exocytosis of toxic granules, induction of apoptosis and production of cytokines that augment the activities of other immune cells. The discovery and recognition of the pit cell and their function in the liver helped to establish the liver's early role in the defence against tumour and microbial targets, and the liver as an immunological organ (Nakatani et al., 2004).

1.2.6 Dendritic cells and lymphocytes

Dendritic cells are bone marrow-derived professional antigen presenting cells that travel along the liver sinusoids, capturing and processing antigens before translocating to the portal interstitium and lymphatic vessels (Ohtani et al., 2003). They eventually accumulate in lymph nodes to present the antigens to T- and B-cells for initiation of immune response or tolerance (Matsunol and Ezaki, 2000). Dendritic cells are structurally long, with thin membrane extensions with microvilli for interaction with T-cells (Fisher et al., 2008). Along with LSECs, HSCs, KCs, and hepatocytes, dendritic cells present antigens to lymphocytes from the innate and adaptive immune systems that are located throughout the liver sinusoids and portal tracts (Crispe, 2009).

1.2.7 Liver sinusoidal endothelial cells and fenestrations

The LSECs line the liver sinusoidal capillary wall and are located between the hepatocytes and blood vessels. They are flattened and perforated by transcellular holes/pores termed fenestrations (Bouwens et al., 1991, Wisse et al., 1996). The sinusoidal endothelium lacks a basement membrane, which makes it distinct from all other endothelial cells. They perform a large number of specialised functions and are now considered to play a significant role in liver function. Through their scavenger receptors LSECs are responsible for the clearance by endocytosis of various macromolecules in the sinusoidal blood (Smedsrød et al., 1990). They are also essential components of the liver-centred innate immune system that includes Kupffer cells, natural killer cells and dendritic cells (Arias et al., 2011).

The essential role of the LSEC in liver function is the focus of this thesis and will be discussed in detail in the following sections.

1.2.7.1 Structure and morphology

The LSECs line the vascular lumen of the terminal capillaries of the liver sinusoids. As described above, they lack basement membrane (Bouwens et al., 1991, Wisse et al., 1996) and possess fenestrations with diameters ranging from 50 to 200 nm (Wisse et al., 1996). One of the earliest electron microscopic descriptions of the fenestrated LSEC was by Wisse (Wisse, 1970). This observation described the endothelial cells as containing open fenestrations grouped into sieve plates surrounded by the thin extensions of the cytoplasm. Further studies found that the total area covered by the fenestrations is approximately 5-10% of the LSEC surface area

(Wisse, 1970). Some studies have shown that the diameter of fenestrations decreases and their frequency increases from the periportal (zone 1) to centrilobular zones (zone 3), consistent with an increase in porosity from 6 to 8% (Wisse et al., 1985). Vidal-Vanaclocha and co-workers observed approximately double the number of sieve plates and number of fenestrations per sieve plate in the pericentral sinusoids than the periportal sinusoids (Vidal-Vanaclocha and Barbera, 1985). They classified fenestrations into two types, clustered pores, which are more prevalent in the pericentral sinusoids, and free pores, which are more prevalent in the periportal sinusoids (Vidal-Vanaclocha and Barbera, 1985). Electron microscopy of the sinusoidal endothelium is shown in Fig 1.3.

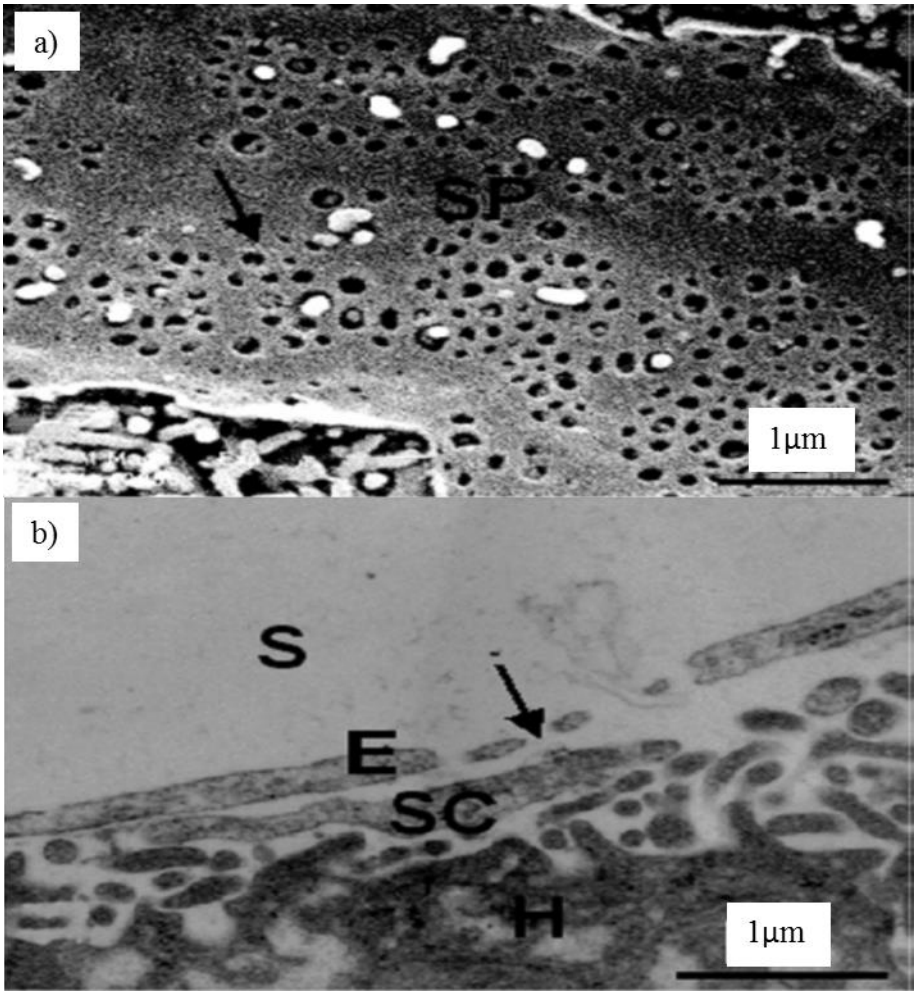

Figure 1.3: Scanning electron micrograph of the liver sinusoidal endothelial cells (Le Couteur et al., 2001). (a) Scanning electron micrograph showing the luminal surface of the liver sinusoidal endothelium. The circular fenestrations that are perforated in the endothelium can be clearly seen (→).The sieve plates (SP) which contains the clusters of fenestrations are clearly visible. Continuous sheets of these cells form a porous endothelium that filters the blood. (b) Transmission electron micrograph showing a cross section through the sinusoids. The thin endothelial cytoplasm (E) is clearly seen with fenestrations (→) through the SoD, which is a low density matrix. The combination of fenestrations and the lack of basement membrane allow direct communication between the sinusoidal lumen and the hepatocytes (H). Hepatic stellate cells (SC) can also be seen in the micrograph.

Fenestrations and sieve plates are structurally supported and demarcated by cytoskeleton elements within the LSEC (Braet et al., 1995). The subendothelial space that lies between the sinusoids and hepatocytes is called the SoD, which contains a low-density matrix of basement membrane constituents and stellate cells. The LSECs containing fenestrations in sieve plates, and the subendothelial SoD, containing extracellular matrix (ECM), together constitute the liver sieve. Molecules from the sinusoidal lumen can translocate directly through the fenestrations, to the low-density matrix of the SoD, to be in contact with hepatocyte microvilli, and vice versa (Wisse et al., 1996, Fraser et al., 1995). Blood constituents that are too large to pass through fenestrations, such as erythrocytes and chylomicrons are excluded from the SoD, while smaller molecules, such as chylomicron remnants are able to pass directly through the fenestrations (Wisse, 1970).

The flow of plasma and macromolecules in and out of the SoD via fenestrations is influenced by the passage of blood cells through the sinusoidal lumen and the composition of ECM. Blood cells are larger than the diameter of the sinusoid and thus squeeze through the luminal space, sometimes modulating their shape to do so. This action has been proposed to promote 'forced sieving' of substances through fenestrations, and compression of the SoD by the movement of larger more rigid white blood cells along the lumens promotes the downstream movement of fluid in the SoD (McCuskey et al., 1978, Wisse et al., 1985). This creates an 'endothelial massage', where erythrocytes and leukocytes may flush plasma through the fenestrations in the endothelium (Wisse et al., 1985). Permeation selectivity of different molecules is regulated by the fenestration and molecule sizes, and the transport kinetics of the molecules relative to steric and frictional properties of the fenestrations (Wisse et al., 1996).

Fenestrations in the LSECs have been described in a very wide range of species with a variation in diameter and frequency has been observed between species as shown in Table 1.1. Fenestrations are conserved and quite similar in size and distribution in animals and humans. All LSECs are fenestrated and these fenestrations are arranged in sieve plates except for rainbow trout (Braet and Wisse, 2002). Porosity is the percentage of the surface area of the sinusoid covered with fenestrations. The frequency of fenestration refers to the number of fenestrations per unit area.

Table 1.1: Inter-species variations in fenestration parameters (Cogger and Le Couteur, 2009)

Species	Porosity (Area %)	Diameter (nm)	Frequency (per μm^2)
Rat (zone 1)	6.0±0.2	111±1	9.1±0.3
Rat (zone 3)	7.9±0.3	105±0.2	13.3±0.5
Rat	4.1±2.3	73±1	2.7±1.1
Mice	4.1±2.2	74±4	
Rabbit	5.2±0.9	60±5	17.3±3.8
Chicken	3.6±1.6	99±15	3.9±0.9
Rainbow trout	-	123	-
Gold Fish	-	50-200	-
Dog	6.7	118±2	7.2
Sheep	-	60±2	-
Baboon	2.6±0.2	50±1	12.1±0.8
Human (zone 1)	3.4±0.2	170±12	9.8±1.8
Human (zone 3)	4.0±0.4	160±10	11.2±2.6

1.2.7.2 Formation and regulation

There is evidence that LSEC fenestrations are formed by a calcium-calmodulin-actomyosin cytoskeleton (Oda et al., 1986, Van Der Smissen et al., 1986). Fenestrations are arranged into sieve plates, creating a network with the cytoskeleton (Braet and Wisse, 2002). The calcium-calmodulin-actomyosin cytoskeleton regulates fenestrations diameter and controls dynamic contraction and dilatation of the fenestrations. Maintenance and induction of this unique endothelial cell phenotype is regulated via paracrine secretion of vascular endothelial growth factor (VEGF) by neighbouring hepatocytes and HSCs, and autocrine production of nitric oxide by endogenous nitric oxide synthase (DeLeve et al., 2004).

An alternative hypothesis has been that fenestrations are formed through the static fusion of caveolae (Oda et al., 2001). Caveolae are plasmalemmal invaginations, which are implicated in endocytosis and transport of substances across the capillary endothelium, signal transduction pathways and calcium regulation (Parton, 2003). Calveolin-1 (Oda et al., 2001) and Ca^{2+}-ATPase pump (Fujimoto, 1993) have been observed both in fenestrations and in caveolae. However, this hypothesis has been largely discounted because the LSEC of caveolin-1 knockout mice are fenestrated and despite the absence of caveolin 1 the fenestrations are arranged in sieve plates (Warren et al., 2010).

Recently it has been shown that the properties of the plasma membrane are highly influential in the formation of fenestrations (Cogger et al., 2013a). Membrane rafts are highly dynamic sterol and sphingolipid enriched lipid-ordered domains of the cell membrane that compartmentalise

cellular signaling molecules. Rafts range from 10-200 nm in diameter and may aggregate into micrometer sized structures that serve as platforms for signal transduction (Viola and Gupta, 2007). They are tethered to the actin cytoskeleton, which is essential for the maintenance of their structure and integrity. Actin disruptors decrease the presence of membrane rafts and increase the number of sieve plates, thus rafts and sieve plates may have an inverse relationship in the LSEC cytoplasm (Svistounov et al., 2012). Fenestrations have been observed to form in non-raft lipid-disordered regions once the stabilising effects of actin and rafts are depleted, and it is possible that fenestrations are created as a result of vesicles that spontaneously form in the cell membrane after it is destabilised (Svistounov et al., 2012). Agents or conditions that increase fenestration number contract or disrupt F-actin, therefore it is also possible that fenestrations spontaneously form in response to stretching and thinning of the cytoplasm between the contracted ring of F-actin (Cogger et al., 2010) that is similar to the manufacture of expanded film ultrafiltration membrane (Baker, 2004). Areas of cytoplasm containing fenestrations are about 50 nm from apical to basolateral surface, approximately half as thick as the cytoplasm surrounding the sieve plates (Cogger et al., 2013a).

Fenestration diameter and number can be altered through induction of cytoskeletal changes (Braet et al., 1995) using acute and chronic exposure to a number of substances and conditions, as shown in Table 1.2. Endothelial fenestration formation has been induced through ‘fenestration forming centres’ within minutes of administration of actin disrupting agents such as cytochalasin B (Steffan et al., 1987). Other actin-disruptor agents including marine-sponge-derived macrolides such as latrunculin A, jasplakinolides, swinholide A and misakinolide A, each with its distinct specific actin-disrupting property, have also been used to study LSEC cytoskeletal

changes and fenestration dynamics (Braet et al., 1996, Braet et al., 2003, Braet et al., 1998, Braet et al., 2002, Spector et al., 1999). Vascular endothelial growth factor receptor expression in endothelial cells is reported to enhance caveolae expression, their fission and fusion, and formation of fenestrations (Chen et al., 2002).

Table 1.2: Modulations of fenestration diameter and number by numerous substances in vivo and in vitro (Arias, 1990, O'Reilly et al., 2010, Braet and Wisse, 2002, Cogger et al., 2013a)

Treatment	Diameter of fenestrations	Number of fenestrations/cell
Actin disruptors		
Cytochalasin B	↑↓	↑
Dihydrohalichondra	↓	↑
Latrunculin A	↓	↑
Misakinolide	↓	↑
Swinholide A	↓	↑
Other Acetylcholine	↑	?
Adrenaline	↓	?
Bethanechol	↑	?
Calmodulin agonist	↑	?
Carbon tetrachloride	↑	↓
Cocaine and ethanol	?	↓
Collagen IV	n.c.	↑
Diethyl nitrosamine	?	↓
Dimethyl nitrosamine	n.c.	↓
DOI (2,5-dimethoxy-4-iodoamphetamine)	↑	↓
Endothelin 1	↓	↓
ET_A-R antagonist (BQ123)	↑	?
Ethanol acute dose	↑	↓
Ethanol chronic dose	↑↓	↓
Fatty liver	?	↓
Hypoxia	↑	?
Hepatectomy	↑	↓
Hepatitis C	↓	↓
Ionophore A23187	↓	?
Irradiation	↑	?
Isoproterenol	↑	?
Jasplakinolide	↓	↑
Laminin	n.c.	↓
Neuropeptide Y	↓	?
Noradrenaline	↓	?
Nicotine	↓	?
Pantethine	↑	↑
Phalloidin	↑	?
Phorbol myristate acetate	n.c.	↑
Pressure	↑	?
Prostaglandin E_1	↑	?
Serotonin	↓	?
Temperature 4 ºC	?	↓
Thioacetamide	↓	↓
Tumour cells	↓	↓
TNF-α	?	↓
Vasoactive intestinal peptide	↑	?
Vascular Endothelial Growth Factor	↑	↑

1.2.7.3 Functional aspects of sinusoidal endothelial cells

In addition to, but as part of the sieving function that has been discussed previously, LSECs are also important for the process of drug clearance. Fenestrations allow the passage of bound and unbound drugs to the SoD for uptake and clearance by the hepatocytes (Braet and Wisse, 2002). The presence of fenestrations also optimises the oxygen delivery from the sinusoids to the hepatocytes (Arias et al., 2011).

The LSECs are the primary scavenger system of the liver and indeed for the entire body. They contain numerous coated pits on their surface which creates a cationic surface charge that allows for endocytosis of negatively charged molecules. Different types of scavenger receptors such as hyaluronan receptors, mannose macrophage receptors and Fc gamma receptors are expressed by LSECs, which allow the removal of various macromolecules from the blood such as proteins, polysaccharides, lipids and nucleic acids (Elvevold et al., 2008). The LSECs internalise macromolecular waste such as extracellular matrix breakdown products (McGary et al., 1989), lysosomal enzymes (Magnusson and Berg, 1989), immune complexes (Mousavi et al., 2007), advanced glycation end products (AGE) (Tamura et al., 2003), acetylated and oxidised low density lipoproteins (Li et al., 2011) and modified proteins (Smedsrød, 2004). There are recent studies that suggest that LSECs might be involved in viral clearance (Ganesan et al., 2011, Liu et al., 2013).

LSECs also express Stabilin-1, a component of stabilin receptor that mediates endocytosis of acetylated LDL (Prevo et al., 2004), secreted protein acidic and rich in cysteine (SPARC)

(Kzhyshkowska et al., 2006), placental lactogen (Kzhyshkowska et al., 2008) and phosphatidylserine (Park et al., 2009). Stabilin-1 also functions as a bacteria-binding protein and modulates angiogenesis (Adachi and Tsujimoto, 2002). It helps in the lymphocyte migration and entry of leukocytes to the site of inflammation (Karikoski et al., 2009).

1.3 PATHOLOGY OF THE LIVER SINUSOIDAL ENDOTHELIAL CELL

Under physiological conditions LSECs are a highly efficient ultrafiltration system; therefore the influence of fenestrations on liver function is mostly seen in diseases and old age where their diameter and frequency are diminished (Cogger and Le Couteur, 2009, Le Couteur et al., 2005, Fraser et al., 2012). Pathology of LSECs in many chronic liver diseases such as cirrhosis is marked by hepatic sinusoidal capillarisation, where the LSEC becomes defenestrated and thickened, resembling the phenotype of a vascular capillary endothelial cell. LSEC capillarisation is generally accompanied by an increased deposition of excessive extracellular matrix and build up in the subendothelial SoD (DeLeve, 2009) and formation of a continuous basement membrane due to deposition of collagen and laminin (Le Bail et al., 1990). Defenestration and capillarisation significantly affects liver function, mainly due to impaired plasma exchange between the sinusoidal lumen and the SoD (Henriksen et al., 1984). Furthermore, it also contributes to hepatocyte hypoxia (DeLeve, 2009, Le Couteur et al., 2005), reduced drug clearance (DeLeve, 2007, Le Couteur et al., 2005), hindered hepatocyte-blood substance exchange (Fraser et al., 1978, Fraser et al., 1995), vasoconstriction and portal hypertension (Iwakiri and Groszmann, 2007), and altered immune function (Iwakiri, 2012, Warren et al., 2007).

1.3.1 Pathology in liver diseases

Capillarisation of the sinusoids in liver disease was first documented by Popper et al. in 1952 and is now well established in many studies (Popper et al., 1952). Capillarisation is associated with hypertrophy and defenestration of the endothelial cells, development of basement membrane, profuse extracellular matrix deposition in the SoD and alterations in HSC morphology.

In cirrhosis, following sinusoidal capillarisation, bridging fibrosis develops along the portal triad-central vein axis, altering blood flow through the liver (Onori et al., 2000). In cases of chronic liver injury, a continuous wound-healing (fibrotic) process is activated that progresses to hepatic cirrhosis in a large number of diseases and drug induced toxicity (Le Bail et al., 1990, Govindarajan and Bonacini, 2003). During cirrhosis, liver function is severely affected as capillarisation of sinusoids, vasoconstriction, and anatomical remodelling, leading to increased vascular resistance that contributes to portal hypertension and venous thrombosis (Iwakiri, 2012). Progressive accumulation of extracellular matrix results in areas of permanent fibrous scar tissue replacing those areas once filled with hepatocytes and sinusoids, a feature that defines cirrhosis (Bosch, 2007, Sánchez-Valle et al., 2012).

Defenestration precedes fibrosis and has been observed in various disease conditions such as primary biliary cirrhosis (Mori et al., 1993), hepatitis (Steffan et al., 1995), specific viral infection of the LSEC (Xu et al., 2003) and with venous administration of endotoxin (Braet and Wisse, 2002, Dobbs et al., 1994). The capillarised LSEC becomes "hypoactive" (Iwakiri and Groszmann, 2007) and loses the ability to revert activated HSCs to a quiescent phenotype (Xie

et al., 2012, DeLeve et al., 2008). HSCs subsequently produce large quantities of ECM, particularly fibrillar collagens type I and III (Bataller and Brenner, 2009, Benyon and Arthur, 1998, Burt, 1993, Reeves and Friedman, 2002). At the same time, there is a decrease in production of NO and other vasodilators in hypoactive capillarised LSECs, enhancing sinusoidal vasoconstriction (Iwakiri, 2012). Fibrosis is also associated with chronic hepatic diseases (Le Bail et al., 1990, Sánchez-Valle et al., 2012) and drug toxicity (Cederbaum, 2006, Iwakiri and Groszmann, 2007, de Araújo et al., 1993).

Concurrent with morphological changes, progressive deterioration of liver function is seen in liver diseases. Impaired exchange and metabolism of substances including lipoproteins and medications are observed in experimental models and clinical cases of liver disease such as cirrhosis (Clark et al., 1988, Martinez-Hernandez and Martinez, 1991, Rogers et al., 1992, McLean and Morgan, 1991). One explanation for progressive loss of liver function is that capillarisation of the sinusoid impedes the passage of substances to the liver parenchyma (McLean and Morgan, 1991, Wanless et al., 1996, Le Couteur et al., 2005).

The study of lipoproteins and the liver sieve has provided more evidence for the formation of a barrier to substrate transfer in sinusoidal capillarisation. Loss of fenestrations in a rat model of cirrhosis inhibits the hepatic uptake of chylomicron remnants, consequently disturbing cholesterol and retinol metabolism (Rogers et al., 1992). Increased blood lipids are found in alcoholics (Clark et al., 1988), and in adults and children with liver disease (SelimoĞlu et al., 2002). Chronic effects of alcohol on the liver sieve may explain the hyperlipidemia associated with cirrhosis, where a chronic high dose of alcohol decreases the number of fenestrations in the

sinusoidal endothelium (Horn et al., 1987). Defenestration may contribute to the hyperlipidemia seen in cirrhosis through capillarisation of the sinusoidal endothelium with the presence of endothelial basement membrane (Schaffner and Poper, 1963). Capillarisation prevents chylomicron remnants from reaching hepatocytes and removes the inhibition of hepatic cholesterol synthesis (Clark et al., 1988).

1.3.2 Pathology in ageing

The ageing liver can be observed macroscopically as undergoing 'brown atrophy' due to brown pigmentation caused by the accumulation of lipofuscin, an end product of lipid peroxidation, in hepatocytes (Popper, 1985, Jansen, 2002, Le Couteur and McLean, 1998). It is estimated that the liver mass is reduced by 44% with age (McLean and Le Couteur, 2004) and blood flow to the ageing liver decreases by up to 53% (Wynne et al., 1989, McLean and Le Couteur, 2004).

On a microscopic level, hepatocytes are seen to increase in size, with increased nuclear polyploidy and binucleation (Watanabe et al., 1984). There are also reported changes in organelle size with age, for example decreased size of smooth endoplasmic reticulum (Schmucker, 1998). The amount of vitamin A that is stored by the liver increases with age (Vollmar et al., 2002) and changes in the extracellular matrix in livers of old rats have been reported (Andrew, 1969). Fibrosis seen in the ageing liver is reportedly due to a reduction in the proteolytic activity of hepatic matrix metalloproteinase (Gagliano et al., 2002). A number of age-related changes in hepatocyte function have already been identified including reduced drug

clearance, changes in enzyme expression and activity and altered transport of drugs across the hepatocyte cell membrane (Schmucker, 2005).

Age-related changes in the ultrastructure of the hepatic sinusoids have been thoroughly described. It was first reported that the sinusoidal endothelium only undergoes a few changes with age (Margreet De Leeuw et al., 1990). Further examinations of the livers of ageing rats with electron microscopy and immunohistochemistry have reported a constellation of age-related changes that have been named pesudocapillarisation (Le Couteur et al., 2001). These changes include reduction in the diameter and density of the fenestrations in the sinusoidal endothelium, thickening of the endothelium, and deposition of collagen and basement membrane with increasing age. Chronic changes in fenestrations are now well established in ageing and become a part of increasingly recognised age-related changes in the liver (Le Couteur and Lakatta, 2010). Vascular endothelial markers, such as von Willebrand factor (vWF) an endothelial glycoprotein that mediates attachment of platelets after endothelial injury, which is not expressed by the sinusoidal endothelium of young rats, is seen in the sinusoids of old rats. The upregulation of vWF in the LSEC is indicative of the pathophysiological state of these cells and has been reported in hepatitis and cirrhosis due to numerous causes (Fukutomi et al., 2005, Albornoz et al., 1999). Increased vWF expression with age likely represents altered platelet adherence with age (Le Couteur et al., 2008).

Pseudocapillarisation is evident across a range of animal models inclusive of rats (Le Couteur et al., 2001), humans (McLean et al., 2003), mice (Warren et al., 2005), and baboons (Cogger et al., 2003) (Table 1.3), an indication that this is a fundamental age-related change. Examples of

electron micrographs of young and old rat livers are shown in Fig. 1.4 and 1.5. Similar changes have been reported in sinusoidal endothelial cells cultured from livers of older humans and in hepatic sinusoidal cells in ageing mice (Ito et al., 2007).

Table 1.3: The effects of old age on porosity (%), fenestration diameter (nm) and thickness (nm) of the hepatic sinusoidal endothelium across four species (Warren et al., 2005). Porosity and fenestration diameter were elucidated using SEM and endothelial thickness using TEM. Y: young, O: old.

Species	Rat		Baboon		Human		Mouse	
	Y	O	Y	O	Y	O	Y	O
Porosity (%)	4.1±2.3	2.5±1.2	4.2±0.5	2.4±0.4	Not done		4.1±2.2	2.2±3.5
Fenestrations diameter (nm)	73±1	60±1	58±1	70±2	Not done		74±4	58±12
Endothelial thickness (nm)	230±50	320±80	130±8	186±9	165±17	289±9	154±4	245±8

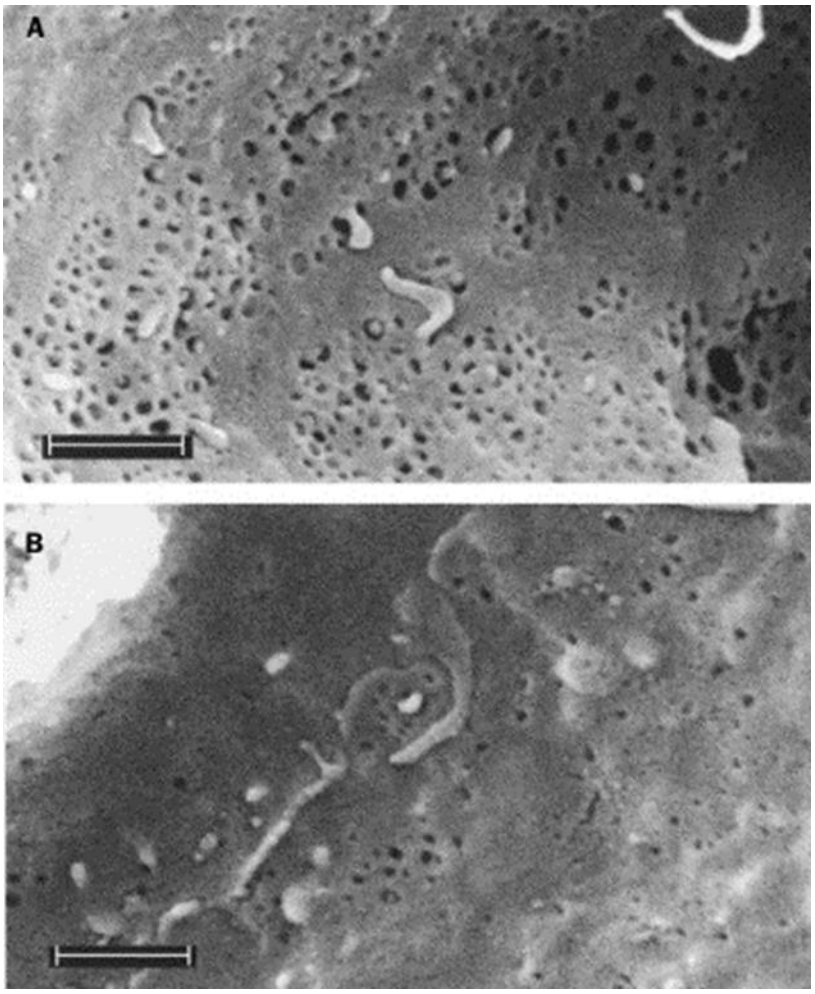

Figure 1.4: Scanning electron micrographs of the sinusoidal surface of the endothelium of (a) young (6 months) and (b) old (26 months) rat showing defenestration of the endothelium of the old rat liver (Le Couteur et al., 2001). Scale bars =1 um.

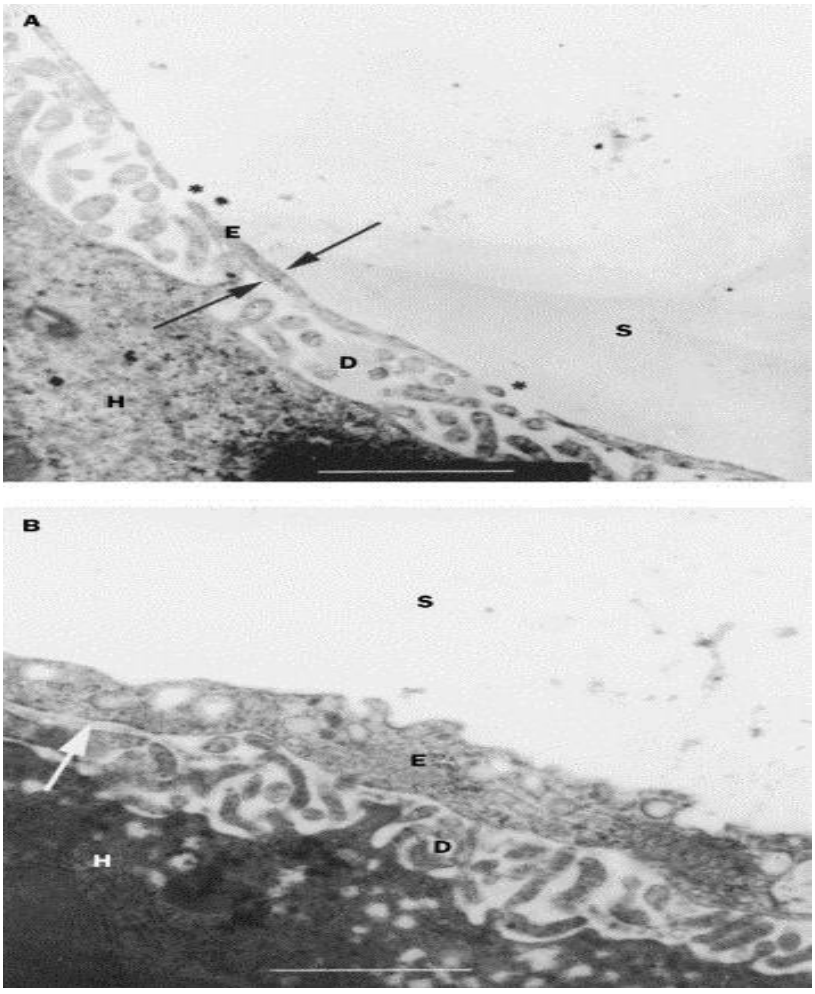

Figure 1.5: Transmission electron micrographs of liver biopsies from a young rat aged 6 months (a) and an old rat aged 26 months (b) showing cross sections of sinusoids (S) with age-related thickening of the sinusoidal endothelium, (E), decreased fenestrations, (*) and laying down of basement membrane in the SoD, (D). H=hepatocytes. (Le Couteur et al., 2001).

1.3.3 Functional implications of morphologic changes in the ageing liver

The study of the ageing process of the liver is important as the liver is the main site for metabolism of many substrates associated with age-related problems such as diabetes, vascular disease, neurotoxicity, xenobiotic detoxification and adverse drug reactions (Le Couteur et al., 2002, Le Couteur and McLean, 1998) and old age is a major risk factor for many liver diseases.

As discussed above the liver undergoes significant changes with age that contribute to the increase risk of the development of disease with age: impaired detoxification and metabolism leading to increased systemic exposure and adverse drug reactions (Le Couteur et al., 2004, Herrlinger and Klotz, 2001), impaired lipid clearance leading to hyperlipidemia (Cassader et al., 1996), a significant risk factor for vascular disease (Weintraub et al., 1996, Krasinski et al., 1990).

The implications of ageing in the liver are also demonstrated by several genetic models of premature ageing, for example the Werner progeria syndrome (Lebel, 2001). Mice with this syndrome have a premature ageing condition that is associated with LSEC pseudocapillarisation, hyperlipidemia (Murata and Nakashima, 1985), and significantly raised levels of serum hyaluronan indicative of decreased LSEC endocytotic capability (Tanabe and Goto, 2001). Pseudocapillarisation was ameliorated with antioxidant (vitamin C) treatment in this animal model of Werner's syndrome (Massip et al., 2010). There are also animal models with ameliorated pseudocapillarisation secondary to caloric restriction, a dietary intervention that delays ageing (Jamieson et al., 2007b).

1.4 INSULIN RESISTANCE

The hypothesis that fenestrations are involved in hepatic insulin action was recently studied by Raines et al (Raines et al., 2011). They studied transgenic mice with partial inactivation of platelet derived growth factor-β (PDGF-β). These mice had leaky, disrupted LSECs as measured by TEM and in vivo fluorescein isothiocyanate (FITC)-dextran uptake. This enhanced transendothelial transport was associated with a dramatic increase in insulin action in the liver, with increased hepatic insulin signaling, improved glucose tolerance tests, increased insulin clearance and an 80% reduction in circulating insulin levels despite euglycemia. These results suggest that insulin and glucose metabolism is also dependent on the LSEC fenestrations, and that pseudocapillarisation might contribute to increased susceptibility with age to hyperinsulinemia, insulin resistance and diabetes. A key focus of this thesis is to study the role of fenestrations on insulin action in the liver, and to determine whether age-related pseudocapillarisation provides a novel mechanism for impaired insulin sensitivity in old age.

1.4.1 Insulin

Insulin was discovered by Best and Banting in 1922 while investigating the role of the pancreas in diabetes mellitus (Banting et al., 1991). It is a hormone that is essential for regulating energy storage and glucose metabolism in the body (Pessin and Saltiel, 2000). Following an increase in the plasma concentration of glucose, insulin is released from the pancreas and stimulates the liver, muscle, adipose tissues and other insulin target cells to commence glucose uptake. The glucose can

be utilised for fuel or stored as glycogen in the liver and muscle. Insulin also reduces glycogenolysis and gluconeogenesis in the liver, decreasing hepatic glucose production (Sesti, 2006).

Insulin resistance is an impaired biological response to insulin where cells become resistant to the effects of insulin, causing normal physiological insulin levels to be insufficient to regulate glucose homeostasis by peripheral target tissues (Petersen and Shulman, 2002). Consequently, a higher amount of insulin is needed to achieve an adequate insulin response. Insulin resistance is one of the earliest changes in individuals with normal glucose tolerance who are progressing towards impaired glucose tolerance and potentially type 2 diabetes. Insulin resistance also has been associated with conditions such as cardiovascular disease, hypertension, obesity, and non-alcoholic fatty liver disease (Cohn et al., 2005).

To understand the insulin mechanism of action, the following section will discuss the insulin network, from insulin secretion, hepatic insulin clearance and insulin signaling.

1.4.1.1 Insulin secretion

Insulin is produced and secreted by β-cells located in the pancreatic islets of Langerhans as a polypeptide hormone with a molecular weight of 58 kDa. It is first synthesised as a single polypeptide, preproinsulin, and undergoes processing in the endoplasmic reticulum to proinsulin, consisting of an α and β chain linked together by disulfide bonds and a C-peptide bridge. After being trafficked to the trans-Golgi network, endopeptidases cleave the C-peptide bridge creating mature insulin which is packed into granules and stored on the plasma membrane. Upon glucose

entry into the pancreatic β-cells through the glucose transporter (GLUT) 2 channels, glucokinase is phosphorylated which stimulates insulin release into the circulation via exocytosis (Melmed et al., 2011).

Impaired insulin secretion can be observed by a reduction in frequency and amplitude of insulin release in response to glucose. This is reported in both individuals with normal fasting plasma glucose and individuals with impaired glucose tolerance, suggesting it can precede insulin resistance and hyperglycaemia (Melmed et al., 2011). Failure of the β-cell to compensate for the insulin resistance is considered an early step for development of impaired glucose tolerance and type 2 diabetes (Abdul-Ghani et al., 2006, Reaven et al., 1989, Weyer et al., 1999a).

1.4.1.2 Hepatic insulin clearance

The liver plays a major role in extracting insulin from the circulation (Meier et al., 2005). Once released from the pancreas, insulin travels to the liver via the hepatic portal vein, followed by binding to the insulin receptor and is either degraded or released into the systemic circulation. The liver is exposed to the highest insulin concentrations of any tissue, with a range between 1,000-5,000 pmol/l (Song et al., 2000), while the systemic circulation receives only ~1% insulin compared to the liver (Song et al., 2000). In addition, the liver reacts directly to changes in insulin concentration by decreasing hepatic insulin clearance when the demand for insulin is increased and vice versa. Therefore, insulin clearance by the liver has major consequences for the maintenance of normal systemic glucose concentrations (Meier et al., 2005).

In general, 80% of total insulin in the body is bound to the insulin receptors in the liver, which extracts ~50% of the secreted insulin during first pass transit (Duckworth et al., 1998, Hovorka et al., 1993). Two molecules have been identified in insulin internalization and degradation: carcinoembryonic antigen-related cell adhesion molecule 1 (CEACAM-1) and insulin degrading enzyme (IDE). CEACAM-1 is involved in mediating the internalization of the insulin-insulin receptor complex (DeAngelis et al., 2008, Najjar, 2002, Poy et al., 2002) and IDE is involved in the inactivation and removal of insulin from the circulation. However, the insulin that is removed from the circulation is not necessarily degraded. A significant amount of receptor bound insulin is released back into the circulation (Hovorka et al., 1993).

Hepatic insulin clearance has been found to be diminished in obesity and type 2 diabetes (Bonora et al., 1983, Bonora et al., 1986, Jones et al., 1997, SANDO et al., 1980). Increased insulin secretion by the pancreas, leading to hyperinsulinemia is a potential compensatory mechanism for maintaining normal blood glucose when hepatic insulin action and clearance is impaired (Rudovich et al., 2004).

1.4.1.3 Insulin Signaling

Insulin regulates a wide range of biological processes that are dependent on tissue type. Apart from regulating glucose/lipid homeostasis, insulin is also responsible for regulating cell growth and differentiation (Dumont et al., 2002). The insulin signaling pathway consists of a complex network of proteins that are also involved in regulating signaling pathways initiated by

other biological stimuli. Although insulin can elicit many biological outcomes, the most important processes are presented as follows and illustrated in Figure 1.6.

a. Insulin receptor

The insulin receptor is the first main component in the insulin signaling pathway. The insulin receptor is a member of the receptor tyrosine kinase superfamily (Ullrich and Schlessinger, 1990), and is present in the form of large heterodimers that consist of two α and β subunits. The α-subunit is located in the extracellular matrix and linked to the intracellular β-subunit via disulfide bonds. Insulin binding to the α-subunit on the surface of target cells leads to conformational changes that induce autophosphorylation of several tyrosine residues on the β-subunit (Kahn and White, 1988, Kasuga et al., 1982, Roth and Cassell, 1983). Autophosphorylation of the β-subunit activates the receptor's protein tyrosine kinase, which activates intracellular substrates responsible for the metabolic consequences of insulin signaling.

b. Insulin receptor substrate (IRS) proteins

The autophosphorylation of tyrosine kinase on insulin receptor activates phosphorylation of the insulin receptor substrate (IRS) proteins. There are several intracellular substrates of IRS that have been identified (Taniguchi et al., 2006), six of them are structurally similar and have been termed insulin receptor substrate proteins 1-6 (IRS1-6) (Cai et al., 2003, Fantin et al., 1999, Lavan et al., 1997, Sun et al., 1991, Sun et al., 1995, White, 1998), with IRS-1 and IRS-2 being the main IRS involved in insulin-mediated metabolic functions in the liver (Thirone et al., 2006).

IRS proteins contain a pleckstrin homology (PH) domain, a protein tyrosine binding domain (PTB) and tyrosine residues that can be phosphorylated by the IR tyrosine kinase (White, 1998). Phosphorylation of IRS tyrosine residues creates docking sites for intracellular molecules with a src-homology-2 (SH2) domain-containing protein. Thus, IRS proteins serve as scaffolds on which the insulin-signaling complex can be arranged in response to the activation of IR (Shaw, 2011, Sun et al., 1993) to facilitate propagation of the insulin signal throughout the cell. Following phosphorylation, IRS proteins are responsible for mediating activation of the two main pathways in insulin signaling which are the phosphatidylinositol 3-kinase (PI3K)-AKT pathway and the Ras-mitogen activated protein kinase (MAPK) pathway (Taniguchi et al., 2006). They also interact with other intracellular targets including Shc (Gustafson et al., 1995), Cbl (Baumann et al., 2000), p62dok (Wick et al., 2001), and GRB2-associated binding proteins (GAB) (Lehr et al., 2000).

Insulin-induced down regulation of IR is a well-established feedback mechanism (Caro and Amatruda, 1980, Knutson et al., 1982, Ramos et al., 2006, Youngren, 2007) that regulates the strength of insulin signaling and is common in hyperinsulinaemic states (Friedman et al., 1997). IRS-1 knockout mice are reported to have glucose intolerance and peripheral insulin resistance (Araki et al., 1994, Tamemoto et al., 1994), whereas IRS-2 knockout mice develop diabetes because of hepatic insulin resistance and lack of pancreatic β-cell compensatory response (Kubota et al., 2000, Withers et al., 1998).

c. PI3-K/AKT pathway

PI3-K is an important kinase involved in mediating metabolic outcomes of insulin signaling (Shepherd et al., 1998). It consists of a regulatory p85 (Escobedo et al., 1991) and a catalytic p110 subunit (Hiles et al., 1992), both of which present in several isoforms (Taniguchi et al., 2006). The p85 subunit has two SH2 domains that interact with the phosphotyrosine residues on IRS-1 (Myers et al., 1992). The PI3-K catalytic subunit is then able to phosphorylate the plasma membrane glycolipid phosphatidylinositol-4,5-bisphosphate (PIP_2) to phosphatidylinositol-3,4,5- triphosphate (PIP_3) (Carpenter and Cantley, 1996). The generation of PIP_3 within the vicinity of the IR/IRS complex allows for the recruitment of protein kinase B, also known as AKT, one of the principal mediators of the metabolic effects of insulin signaling, via its pleckstrin homology (PH) domain (Franke et al., 1997). Once localised to the plasma membrane by binding to PIP_3, AKT can be activated by 3-phosphoinositide-dependent kinase-1 (PDK1) via phosphorylation of threonine 308 (T308) and serine 473 (S473) within AKT's activation loop (Alessi et al., 1997). Following activation, AKT is thought to mediate the majority of the hepatic metabolic outcomes stimulated by insulin (Taniguchi et al., 2006). PDK-1 also activates atypical protein kinase C (aPKC) isoforms ζ and λ for further signaling action.

i. PI3-K/AKT-mediated regulation of glycogen synthesis

AKT and PKCs are essential for insulin-stimulated translocation of glucose transporters, such as GLUT4 that is expressed mainly in muscle and fat, from intracellular pools to the cell surface

(Saltiel and Kahn, 2001). AKT also increases glycogen synthesis by activating glycogen synthase (GS) via inhibition of glycogen synthase kinase 3 (GSK-3) and decreasing glycogenolysis simultaneously (Cross et al., 1995). Insulin has also been shown to target protein phosphatase 1 (PP1) which further increases the dephosphorylation and activation of GSK-3. In addition, AKT promotes protein synthesis by reversing GSK-3-induced inactivation of protein synthesis, eukaryotic initiation factor (eIF)-2B (Pap and Cooper, 2002). AKT also activates mammalian target of rapamycin (mTOR), promoting protein synthesis through p70 ribosomal S6 kinase (S6K1) and inhibition of eIF-4E binding protein (Liu et al., 2002).

ii. PI3-K/AKT-mediated regulation of hepatic glucose output

Insulin regulates hepatic glucose output through direct effects on gene expression (Pilkis and Granner, 1992) and indirect regulation of substrate availability (Saltiel and Kahn, 2001). Insulin inhibits transcription of gluconeogenic genes that code for phosphoenolpyruvate carboxy kinase (PEPCK) (Hall et al., 2007, Hanson and Reshef, 1997), glucose-6-phosphatase (Nakae et al., 2001, Nakae et al., 1999) and fructose-1,6-bisphosphatase, while increasing transcription of genes that code for glycolytic enzymes such as glucokinase (Barzilai and Rossetti, 1993) and pyruvate kinase (Yamada and Noguchi, 1999). Forkhead transcription factor 1 (FOXO-1) (Cheng and White, 2011, Nakae et al., 1999) and the transcriptional co-activator PGC-) (Yoon et al., 2001) are involved in regulating gluconeogenesis in the liver. Specifically, AKT phosphorylates FOXO-1 and prevents it from entering the nucleus and activating transcription of genes that code for glucose-6-phosphatase and PEPCK, an enzyme that catalyses the rate limiting step in gluconeogenesis (Nakae et al., 2001, Puigserver et al., 2003).

iii. PI3-K/AKT-mediated regulation of lipid homeostasis

In addition to the regulatory action of glucose homeostasis, insulin also has a critical role in lipid homeostasis. Insulin deactivates hormone sensitive lipase (HSL) through the PI3-K/AKT pathway thus inhibiting lipolysis in adipose tissue and depriving the liver of fuel from free fatty acids for glucose production (Holm et al., 2000). In the liver, insulin promotes lipogenesis by increasing transcription of lipogenic genes such as acetyl-CoA carboxylase (Munday and Hemingway, 1999). Sterol regulatory element binding protein 1c (SREBP-1c) mediates many of insulin's effects on lipogenesis (Horton et al., 2002). Induction of SREBP-1c transcription appears to be dependent both on AKT (Azzout-Marnich et al., 2000, Fleischmann and Iyendjian, 2000, Matsumoto et al., 2002) and liver X receptor activation (Chen et al., 2004)

iv. Ras/MAPK pathway

The Ras/MAPK pathway is involved in mediating cell growth, differentiation and survival. Insulin causes tyrosine phosphorylation of IRS-1, Gab1 and Shc, thus facilitating binding of growth factor receptor binding protein-2 (Grb-2) (Ogawa et al., 1998). Grb2 recruits the guanyl nucleotide exchange protein, Sos, to the plasma membrane resulting in the activation of G protein Ras (Ogawa et al., 1998). Activated Ras induces a phosphorylation cascade that begins with Ras and ends with activation of the Mitogen activated protein kinase (MAPK)/ Extracellular signal regulated kinases (ERK) pathway. The activated ERKs phosphorylate various intracellular substrates and translocate to the nucleus to phosphorylate transcription factors to promote gene expression. Studies with Ras or SOS dominant negative mutants and with IRS-1

siRNA/antibodies have shown that the Ras/MAPK pathway is important for insulin's effect on cell growth and DNA synthesis (Maassen et al., 1992, RoSE et al., 1994, Sakaue et al., 1995, Waters et al., 1993).

This section has described the upstream components of the insulin-signaling pathway, where AKT is the pivotal step of the pathway because it ties together insulin's major roles in glucose and lipid metabolism (Leavens and Birnbaum, 2011). A detailed description of insulin target tissues following signal transmission will be discussed below.

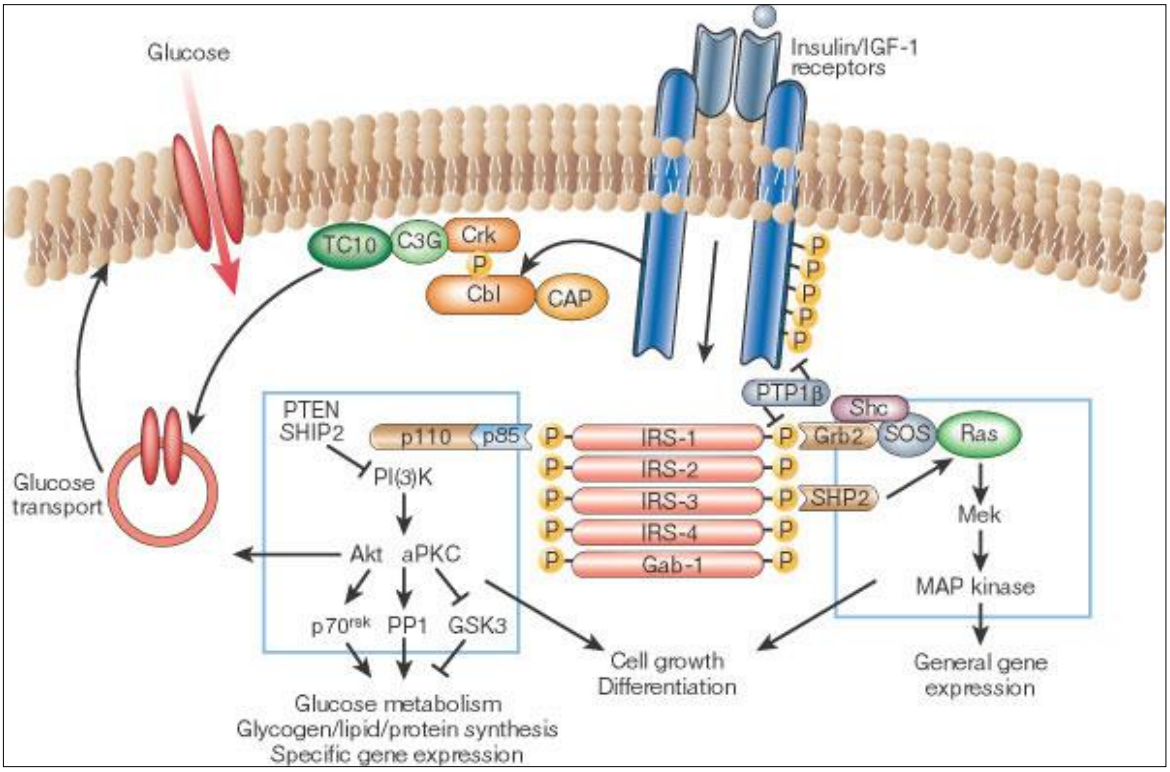

Figure 1.6: Signal transduction in insulin action. The insulin receptor is a tyrosine kinase that undergoes autophosphorylation and catalyses the phosphorylation of cellular proteins, such as members of the IRS family, Shc and Cbl. Upon tyrosine phosphorylation, these proteins interact with signaling molecules through their SH2 domains, resulting in a diverse series of signaling pathways. This includes activation of PI (3) K protein kinases, Ras and the MAP kinase cascade, and the Cbl/CAP and the activation of TC10. These pathways act in a concerted fashion to coordinate the regulation of vesicle trafficking, protein synthesis, enzyme activation and inactivation, and gene expression. This results in the regulation of glucose, lipid and protein metabolism (Saltiel and Kahn, 2001).

1.4.2 Insulin target tissues

Insulin regulates major biological processes including glucose and glycogen metabolism, lipid metabolism and protein synthesis. The effect of insulin in maintaining normoglycaemia in the setting of variable glucose availability is achieved by regulating glucose uptake and endogenous glucose production. The effect of glucose action on target tissues is summarised in Table 1.4.

The three main target tissues of insulin action are liver, muscle and adipose tissue (DeFronzo, 1988). In the postprandial state, insulin levels rise and inhibit the breakdown of glycogen via inhibition of glycogenolysis in muscle and liver tissue as well as inhibiting gluconeogenesis in the liver (Kumar and O'Rahilly, 2005). Insulin also stimulates glucose uptake by muscle and adipose tissue for storage in a form of glycogen and lipids (DeFronzo, 1988). The liver stores both glycogen and lipids, whereas in the normal state the muscle stores only glycogen and the adipose tissue only lipids. In fasting conditions the liver releases glucose via glycogenolysis and gluconeogenesis.

Insulin also has indirect effects on glucose metabolism by decreasing the release of gluconeogenic precursors through regulation of lipid metabolism and protein turnover. Insulin inhibition of lipolysis in adipose tissue reduces the release of free fatty acids and glycerol used for hepatic glucose production. Likewise, insulin inhibition of proteolysis in muscle tissue decreases the release of amino acids necessary for gluconeogenesis (Lewis et al., 1996, Rebrin et al., 1995).

Table 1.4: Classical and non-classical target organs for insulin-regulated glucose metabolism.

A direct effect of insulin on glucose metabolism is defined as an insulin-stimulated change in the flux of glucose through a specific metabolic pathway that is initiated by the insulin receptor in the same tissue. An indirect effect is the regulation of glucose metabolism in one organ resulting from the effect of insulin on other micronutrients (such as lipids) or in other organs (Kumar and O'Rahilly, 2005).

Organ/tissue	**Main effect of insulin on glucose metabolism**	
	Direct	Indirect
Classical targets		
Skeletal and cardiac muscle	↑ Glucose uptake ↑ Glucose oxidation ↑ Glycogen synthesis	↓ NEFA availability and oxidation
Liver	↓Glucose output - ↓Glycogenolysis - ↓ Gluconeogenesis ↑ Glycogen synthesis ↑ Glycolysis ↑ Lipogenesis	↓ NEFA availability and oxidation
Adipose tissue	↑ Glucose uptake ↑ Lipogenesis	Regulation of adipokines synthesis and/or secretion ↓ Lipolysis
Non-classical targets		
Pancreatic beta cells	?	Permissive effect on glucose-stimulated insulin secretion (phase 1 release)
Brain	?	↓ Food intake
Vascular cells	?	↑ Blood flow ↑ Capillary recruitment ↑ NO secretion

Apart from nutrient metabolism, insulin also has effects on non-target tissues such as the central nervous system and vascular cells (DeFronzo, 2009). Insulin signaling in the brain is reported to be involved in appetite suppression (Plum et al., 2006, Schwartz et al., 2000), and has been shown to be reduced in obese, insulin-resistant, normal glucose tolerant individuals (Matsuda et al., 1999). The brain also plays an important role in the physiological control of hepatic glucose production as well as hepatic glucose uptake in response to insulin that usually gives a direct effect on hepatocytes (Rojas and Schwartz, 2014). In vascular cells, insulin is thought to stimulate vasodilatation and capillary recruitment thus enhancing glucose delivery and increasing muscle glucose uptake (Clark et al., 2003).

1.4.3 Development of insulin resistance

Insulin resistance is defined as a reduced biological effect for any given concentration of insulin (Wallace and Matthews, 2002). The characteristics of insulin resistance has been established as the main component in a cluster of abnormalities termed as Syndrome X or metabolic syndrome, that includes type 2 diabetes, obesity, hypertension, dyslipidaemia and cardiovascular disease (Reaven, 1995).

1.4.3.1 Hepatic insulin resistance

Among the three major insulin target tissues, the liver is the primary organ that directly regulates metabolic homeostasis, maintains normoglycaemia during fasting conditions and controls systemic insulin levels via hepatic insulin clearance (Cherrington and Lecture, 1999). Insulin

resistance in the liver is characterised by the inability of insulin to suppress glucose production. Uncontrolled hepatic gluconeogenesis has been shown to contribute to the fasting and overnight hyperglycaemia seen in individuals with type 2 diabetes (Consoli et al., 1989, DeFronzo et al., 1989, Magnusson et al., 1992, Perriello et al., 1997, Weyer et al., 1999b).

Insulin's role in regulating lipid homeostasis is also impaired in hepatic insulin resistance. The overstimulation of lipogenesis by the liver due to hyperinsulinaemic conditions is thought to be a critical component of the overproduction of VLDL particles seen in type 2 diabetes (Adeli et al., 2001). The dyslipidaemia that is often present in individuals with type 2 diabetes is characterised by hypertriglyceridaemia, raised LDL-cholesterol and a low HDL cholesterol profile (Krauss, 2004). Consequently, the abnormal fat storage and ectopic fat deposition in other insulin target tissues has been suggested to have a role in the progressive nature of insulin resistance (Lewis et al., 2002).

1.4.3.2 Peripheral insulin resistance

Insulin resistance in peripheral tissues is characterised by the inability of tissues to take up glucose in response to insulin, affecting glucose disposal and lipolysis. Muscle insulin resistance is present when insulin-mediated glucose disposal through the GLUT4 channel is reduced to the lowest quartile of control subjects (Beck-Nielsen et al., 2005). The progressive hyperinsulinaemia required to overcome the insulin resistance at the muscle is also thought to play a role in the development of metabolic syndrome (Vaag et al., 1995). Furthermore, insulin

resistance in adipose tissue leads to unregulated lipolysis and an increase in circulating free fatty acids, which contributes to increased hepatic glucose output (Groop et al., 1989).

1.4.4 Measurement of insulin resistance

Identification of insulin resistance is an important step in the diagnosis and management of symptoms of metabolic syndrome, especially diabetes. Quantitative measurement of biological action of insulin is used to determine insulin resistance. This is thought to be equal to insulin sensitivity that is reciprocal to insulin resistance (Bergman et al., 1985). Measurement is divided into two groups: non dynamic and dynamic methods (Wallace and Matthews, 2002)

Non-dynamic methods are assessed during steady state using only glucose and insulin measurements. An example for this method is Homeostasis model assessment (HOMA), a mathematical model that calculates insulin sensitivity from fasting plasma glucose and insulin concentrations (Matthews et al., 1985, McAuley et al., 2001). The principle of HOMA is based on the basic understanding of a feedback loop between the liver and the pancreas in the fasting state, where normoglycaemia is regulated by hepatic glucose output. HOMA-IR values of less than or equal to 2.4 have been shown to be reflect normal glucose tolerance and insulin sensitivity (Braatvedt et al., 2006, Geloneze et al., 2009).

Dynamic methods are assessed by makeshift disturbance of the steady state and evaluation upon returning to the steady state. An example of this method is the euglycaemic clamp technique (Wallace and Matthews, 2002). Glucose levels are constantly maintained using an

intravenous infusion and insulin levels are elevated using a constant intravenous of insulin infusion. Once the glucose levels are fixed or 'clamped' at the desired concentration, insulin resistance is inversely related to the glucose infusion rate necessary to maintain the required glucose concentration (Davis et al., 1992). This method is considered a gold standard in measuring insulin sensitivity *in vivo (*Wallace and Matthews, 2002).

Among these two methods, HOMA is more commonly used to determine insulin resistance due to the tests robustness, while euglycaemic clamp is considered to be more invasive, time consuming and a labor intensive procedure (Bergman et al., 1985, Matthews et al., 1985).

1.4.5 Animal models of insulin resistance

Techniques of transgenesis and mutagenesis in rodents have enabled researchers to understand the complex pathogenesis of insulin resistance. Various animal models have been developed to test the hypotheses for insulin resistance, involving transgenic and knockout mice with mutations in genes involved in insulin action and secretion (NANDI et al., 2004). Focus has been targeted at specific insulin target tissue that is created by removal of the insulin receptor using Cre-loxP system (Gu et al., 1994) as shown in Table 1.5.

Table 1.5: Insulin specific target tissue models of insulin resistance

Insulin Receptor	Insulin secretion	Insulin action	Glucose tolerance	Glucose homeostasis	Lipid homeostasis
Muscle (MIRKO)	Normal	Normal	Normal	Normal	↑ FFA ↑ Triglycerides
Fat (FIRKO)	Normal	Improved insulin sensitivity	Improved	Normal	↓Triglycerides
Liver (LIRKO)	Increased	Markedly insulin resistant	Severely Impaired	Hyperglycemia	↓ FFA ↓Triglycerides

The Muscle insulin receptor knockout mouse (MIRKO) was the first insulin specific target tissue model to study insulin resistance because it was thought that the muscle is the most important tissue for glucose uptake (Brüning et al., 1998). However, while MIRKO mice have elevated plasma triglycerides and free fatty acids there is no impairment of glucose homeostasis. It is reported that although muscle was not able not perform glucose uptake, this is compensated by adipose tissue, resulting in increased adiposity and weight gain.

In parallel, fat insulin receptor knockout mice (FIRKO) (Bluher et al., 2002) showed normal glucose homeostasis with improved insulin sensitivity. The mice were surprisingly protected against obesity-induced glucose intolerance and had increased longevity.

The Liver insulin receptor knockout mouse (LIRKO) (Michael et al., 2000) is the only insulin specific target tissue model that exhibited glucose intolerance and insulin resistance. The animal

had both fasting and postprandial hyperglycemia as a result of the liver's inability to inhibit hepatic glucose production. They also had increased insulin secretion and impaired hepatic insulin clearance resulting in marked hyperinsulinaemia with progression to secondary whole body insulin resistance. This indicates that liver is the most relevant tissue in the pathogenesis of insulin resistance compared to muscle and adipose tissue.

Apart from transgenic models, insulin resistance is also studied using high fat diet-induced insulin resistance animals. This model induces primarily hepatic insulin resistance at week 6 and by week 12 there is insulin resistance in the adipose tissue, without effects on the skeletal muscle at any point (Kleemann et al., 2010). This is consistent with LIRKO mice where hepatic insulin resistance precedes systemic insulin resistance.

Studies using the tissue specific insulin receptor animal models and diet-induced models are valuable in studying the pathogenesis of insulin resistance, however complete insulin resistance conditions can only be seen in rare genetic diseases like leprechaunism and type A insulin resistance syndrome (Kahn et al., 1976).

1.4.6 Insulin resistance and the metabolic syndrome

The metabolic syndrome is characterised as a cluster of abnormalities that includes obesity, dyslipidaemia, hypertension and hyperglycemia (Alberti et al., 2005). The pathogenesis of metabolic syndrome is heterogeneous, with central obesity and insulin resistance considered to be the most important causative factors (Anderson et al., 2001). The terms metabolic syndrome

and insulin resistance syndrome have often been used interchangeably, but each term indicates different underlying concepts and observations. The clinical syndromes associated with insulin resistance include, but are not limited to, type 2 diabetes and cardiovascular diseases, hypertension, polycystic ovary syndrome, non-alcoholic fatty liver disease, sleep apnoea and certain cancers (Alberti et al., 2006). The World Health Organization (WHO) has stressed the importance of insulin resistance in the diagnosis of the metabolic syndrome and individuals who are at risk of getting diabetes and cardiovascular diseases (Alberti and Zimmet, 1998).

1.4.7 Insulin resistance and diabetes

There are two types of diabetes mellitus that are generally described: type 1 (T1DM) and type 2 (T2DM). T1DM is characterised by a lack of insulin due to destruction of the insulin-secreting β-cells of the pancreas. Treatment requires regular subcutaneous insulin administration to replace the insulin that would normally be secreted by the pancreas several times a day in order to prevent life threatening hyperglycemia (Sibal et al., 2006). T1DM is usually diagnosed in childhood and the major cause is reported to be from various auto-immune factors and genetic predisposition (Dahlquist, 1993).

T2DM is characterised by hyperglycemia, insulin resistance, and decreased β-cell number and secretory function (Harris et al., 1998, Haslam and James, 2005, Wild et al., 2004). It progresses from an early 'pre-diabetes' stage, which is often asymptomatic, with insulin resistance, to a relatively mild postprandial hyperglycemia, before developing into classic symptomatic diabetes, requiring treatment with insulin and/or oral hypoglycaemic medications. T2DM has mostly been

associated with older age but its prevalence in young people and children is rapidly increasing. There are multiple risk factors for the development of T2DM including age, obesity, family history, lack of exercise and a high calorie diet. T2DM increases susceptibility to multiple microvascular problems such as diabetic retinopathy, diabetic nephropathy and peripheral vascular disease (Hartz et al., 2006).

1.4.8 Liver, insulin resistance and diabetes mellitus

Our understanding of the liver's contribution to the development of insulin resistance has largely focussed on the role of the hepatocyte. For example, it is known that LIRKO mice, which lack the insulin receptor in hepatocytes, exhibit dramatic insulin resistance, severe glucose intolerance and failure of insulin to regulate hepatic gene expression and to suppress hepatic glucose output (Michael et al., 2000). I*n vitro* studies have shown that insulin resistance is induced by interleukin-6 in primary hepatocytes and in human hepatocarcinoma cell line, HepG2 causing a decrease in tyrosine phosphorylation of IRS-1 in response to physiologic insulin levels and inhibition of insulin-dependent activation of AKT, that facilitates downstream insulin metabolic actions (Klover et al., 2002).

However, prior to interaction with the insulin receptor on the hepatocyte, insulin must first cross the LSEC and SoD. The endothelium has been shown to be the rate limiting step for the uptake of insulin in most other tissues such as muscle and fat, however the role of the sinusoidal endothelium in hepatic insulin action has not been specifically investigated (Takamura et al., 2012). Limited evidence has shown that in the normal liver, insulin from the portal vein will be

bound to the hepatocyte insulin receptor within three minutes (Bergeron et al., 1979). The LSEC has limited affinity for insulin and it has been shown that LSECs will only pinocytose insulin in situation of hepatocellular receptor saturation (Bergeron et al., 1979). Abnormalities in liver microcirculatory function, particularly changes in the transfer of insulin from blood to the hepatocytes, may be a critical factor in the development of insulin resistance. However, this possibility largely remains under investigated.

Endothelial dysfunction in metabolic syndrome has been discussed as the cause (Baumgartner-Parzer and Waldhausl, 2001) or the consequence (Avogaro et al., 1997) of insulin resistance. Evidence that endothelial damage occurs before insulin resistance has been shown in offspring and relatives of insulin resistant people with impaired endothelial responses (Jörneskog et al., 2005). Hypertension is commonly associated with both vascular impairment and insulin resistance, hence supporting the important role of the vasculature in insulin sensitivity. A rat model of metabolic syndrome and insulin resistance, with features of NAFLD is shown to have higher in vivo hepatic vascular resistance than control, with increased portal perfusion pressure and decreased endothelium-dependent vasodilation. This occurs before the development of fibrosis or inflammation (Pasarín et al., 2012).

Many liver conditions associated with defenestration and other structural changes in the LSEC are also associated with insulin resistance. This has been ascribed to shunts, hepatocellular failure and reduced hepatic insulin clearance (Takamura et al., 2012). A study in a mouse transgenic model with partial loss of PDGF-beta function, which is responsible for the formation of pericytes showed increased permeability of the LSEC and increased fenestrations. This model

was also associated with a dramatic increase in insulin action in the liver, including increased insulin signaling, improved glucose tolerance test, increased insulin clearance and reduction in circulating insulin levels. Tsuchiya and Accili (2013) examined the effect of knockout of FoxO in mouse endothelium and found that standard chow–fed mice were glucose intolerant and had reduced insulin sensitivity. The defect in insulin action was identified as being in the liver.

With regard to the effect of diabetes on the LSEC and hepatocytes, there are well described changes in the liver in both forms of diabetes mellitus. Diabetes mellitus results in a lipid accumulation in hepatocytes termed fatty liver or hepatosteatosis. Inflammatory cells can infiltrate into the liver causing non-alcoholic steatohepatitis (NASH) and this is associated with mild elevation in liver function tests including the transaminases and alkaline phosphatase (Kalyan et al., 2006). Diabetes is also characterised by a reduction in hepatic insulin sensitivity and decreased insulin mediated suppression of lipolysis in the liver (Marchesini et al., 2001). Excess free fatty acids that occur in diabetes have a toxic effect on hepatocytes, mitochondria and cell membrane (Kaplowitz, 2001). There is also an increase in pro-inflammatory cytokines in the insulin resistant state, such as tumour necrosis factor alpha (TNF-α) which probably contributes to hepatocellular injury (Zhang et al., 2009)

The microvascular complications of diabetes mellitus has been well established in several organs (Singleton et al., 2003), but relatively few studies have reported on the effect of diabetes on liver microvasculature. Bernuau et al. (1982) studied liver biopsies of 12 insulin dependent diabetic patients and found that there is a moderate increase in collagen and basal lamina deposition in the SoD. Some subjects have fatty liver and increased perisinusoidal Masson trichrome staining.

Two other studies (Harrison et al., 2006, Latry et al., 1987) also reported an increase in deposition of collagen and basal lamina in human diabetic liver biopsy samples.

Inaba et al. (1984) examined livers from diabetic patients and found that there was a thickening of endothelium, reduced SoD width and the proliferation of collagen fibres in the SoD. They also reported "obscure pores in the endothelium", which are presumably fenestrations. However this is not quantified and the detection of fenestrations may be below the resolution of the techniques used. A retrospective study of T1DM and T2DM diabetic patients who had undergone liver biopsy has been carried out, reporting an extensive perisinusoidal fibrosis and deposition of basal lamina, termed as 'diabetic hepatosclerosis' (Harrison et al., 2006).

In rats, streptozotocin-induced T1DM rats had increased fenestrations frequency and diameter after five weeks, followed by decreased frequency after 8 weeks, when defenestration is thought to be starting to develop (Jamieson et al., 1999, Jamieson et al., 2001). In diabetic baboons, marked changes in the fenestrations were observed including a decrease in the diameter and the frequency of the fenestrations, leading to a reduction in porosity (Jamieson et al., 2007a). There was also a thicker endothelium compared to control with increased extracellular matrix in the SoD. Fibrosis was observed with increased staining of Masson trichrome and collagen IV immunohistochemistry. This indicates that diabetes accelerated the age-related loss of fenestrations (Jamieson et al., 2007a).

1.5 Scope and aims of this thesis

This chapter has focused on describing hepatic microvasculature and its major, but largely unrecognised, role in liver function. There is now clinical and experimental evidence of diminishing liver function with ageing, while ultrastructural changes have been described in ageing livers that provide a mechanism for these functional changes. Pseudocapillarisation of the hepatic sinusoidal endothelium creates a barrier to the transfer of lipoproteins and drugs from the sinusoidal lumen to the hepatocyte, a barrier that is not present in healthy and young livers. Recent findings have indicated an important role of fenestrations in insulin and glucose metabolism (Raines et al., 2011) which raises the possibility that age-related pseudocapillarisation might contribute to hepatic insulin resistance that is common in old age.

The most consistent age-related change in glucose metabolism is insulin resistance, which is a significant risk factor for diabetes and vascular disease in older people. Although much research on hepatic glucose metabolism has focused on hepatocytes, the role of LSEC, particularly fenestrations has been largely overlooked. This thesis investigates the effect of ultrastructural changes in the ageing liver on insulin resistance.

Chapter 3 examines the effect of age-related pseudocapillarisation on the development of insulin resistance. It is well established that ageing accelerates the development of insulin resistance. It was hypothesised that pseudocapillarisation leads to impaired hepatic disposition of insulin and glucose, leading to impaired systemic glucose homeostasis. To probe this hypothesis the experiments in this chapter examine insulin and glucose action in the liver of young and old mice

and rats in addition to glucose uptake in target tissues and gene and protein expression related to insulin signaling.

Given the significant impact of ageing on insulin and glucose metabolism found in the experiments outlined in Chapter 3, the experiments carried out and presented in Chapter 4 were designed to investigate the impact on glucose and insulin transfer and action in the liver in the absence of other age-related changes. Chapter 4 investigates the effect of P407 induced defenestration on the development of insulin resistance. P407 is a surfactant that is known to selectively target the liver, causing acute and reversible defenestration with severe hyperlipidemia. Here we hypothesised that defenestration, in the absence of any concomitant ageing changes interferes with hepatic disposition of glucose and insulin in the liver, leading to impaired systemic glucose and insulin metabolism. Similar experimental techniques including MID, radiolabeled glucose tolerance test, scanning electron microscopy, real time PCR, immunoblotting and proteomic analysis were used in both Chapters 3 and 4.

Chapter 4 focusses on the implications of loss of fenestrations induced by P407 on insulin action in the liver. Chapter 5 then investigates the mechanisms underlying the loss of fenestrations induced by P407. *In vitro* studies on fenestration modulation are pivotal in elucidating the exact mechanism of fenestration control. The sieve-raft theory states that membrane lipid rafts are associated with the regulation of fenestrations (Cogger et al., 2013a). To further confirm this, Chapter 5 investigates the relationship between membrane rafts and fenestrations using the potent defenestrating agent used in Chapter 4, P407, in both SKHep1 cells, a cell line of endothelial origin and isolated LSECs. It was hypothesised that P407 induces defenestration by

depleting non-raft region of the cell membrane. Scanning electron and light deconvolution microscopy were used to observe the interaction following P407 treatment.

Finally, because fenestrations are known to adapt and change depending on their exposure to nutrients and other substances Chapter 6 examines the role of lifelong macronutrient and caloric intake on fenestrations and insulin and glucose metabolism. In this study, nutritional geometry was used to observe the effects of energy and macronutrients diets on fenestration morphology into older age. Liver biopsies and serum analysis were used to assess the impact of macronutrients and caloric intake on LSEC health at 15 months of age.

The specific hypotheses are:

1. Fenestrations in the LSEC influence the action of insulin in the liver,
2. Age-related pseudocapillarisation of the LSEC contributes to insulin resistance in old age,
3. Loss of fenestrations induced by P407 impairs insulin action in the liver,
4. P407 influences fenestrations by its effects on lipid rafts,
5. Dietary macronutrients influence fenestrations and the development of pseudocapillarisation in old age, with implications for age-related insulin resistance.

CHAPTER 2: METHODOLOGY

2.1 MULTIPLE INDICATOR DILUTION METHOD

This method is also known as tracer dilution method and can be used to measure multiple parameters such as microvascular exchange, transport and metabolism in the liver (Goresky, 1963, Goresky et al., 1973). This is the definitive method to assess the transfer of substrates such as insulin/glucose across the liver endothelium and hepatocellular membrane as described in mice and rats previously (Cogger et al., 2006, Hilmer et al., 2005, Mitchell et al., 2012).

2.1.1 Liver perfusion

Rats were weighed and then anaesthetised by an intraperitoneal (i.p.) injection of 2 ml/kg ketamine (60 mg/ml) and xylazine (6 mg/ml). A midline laparotomy incision was performed and the intestines pushed aside to reveal the portal vein. The portal vein was cannulated with an 18 gauge intravenous cannula (Optiva K, Livingstone, Rosebery, Australia) and the thoracic inferior vena cava was cannulated with a 10 cm length of polyethylene tubing. A single pass perfusion was performed using Krebs-Henseleit bicarbonate buffer (10 mM glucose, saturated with 95 % O_2/5 % CO_2, 2 % bovine serum albumin at 37 ºC) and the perfusate flow rate was maintained at approximately 1 ml/minutes/g of liver using a peristaltic pump (Masterflex L/S, Cole-Palmer, Boronia Australia). Portal venous pressure was measured in centimetres of H_2O according to a manometer connected to the inflow cannula of the portal vein.

2.1.2 Multiple indicator dilution

This step involves 2 separate tracers: (1) ^{3}H-sucrose and ^{14}C-insulin; (2) ^{3}H-sucrose and ^{14}C-glucose (American Radiolabeled Chemicals Inc, St. Louise USA) separately. In some experiments Evans Blue (Sigma Aldrich, Castle Hill Australia) was also added to the injectate. After administration of each injectate (100 µl in volume) through the portal vein, 60 outflow samples were collected using a universal fraction collector (Extech Equipment, Boronia, Australia) at two second intervals, followed by collection at 3 minutes and 5 minutes. Analysis for ^{14}C and ^{3}H specific activity in each outflow sample was performed using a liquid scintillation counter (Packard 1600TR, Australia) by adding 100 µl of outflow to 8 ml of scintillation fluid (UltimaGold, Perkin Elmer, Australia). Radioactivity was measured via disintegration per minute (DPM). A spectrophotometer (BMG Labtech FLUOstar optima microplate reader, Life Technologies, Wembley Australia) was used to quantify the concentration of Evans Blue in the outflow samples.

2.1.3 Data analysis

All outflow data collected was used to generate dose-normalised outflow curves. The hepatic outflow concentrations were expressed as a fraction of the injected dose per ml of outflow. The area under the curve (AUC) and area under the moment of the curve (AUMC) are calculated using the following equations:

$$AUC_{0-120} = \sum_{t=0}^{t=120} C_{n+1}\,(t_{n+1} - t_n)$$

$$AUMC_{0-120} = \sum_{t=0}^{t=120} C_{n+1}\,\frac{(t_{n+1} - t_n)\,(t_{n+1} + t_n)}{2}$$

*t is the sample collection time in seconds.

The mean transit time (MTT) was estimated from the ratio of the AUMC and AUC using the following equation:

$$MTT = \frac{AUMC}{AUC}$$

The value was corrected for the catheter and non-exchanging vessel transit time (t_0), which was estimated from the first appearance of radioactivity above the background levels (Goresky and Silverman, 1964).

The volume of distribution (V) for each substrate was determined from the MTT and the flow rate (Q) using the following equation:

$$V = MTT \times Q$$

Hepatic extraction (E) and substrate recovery (R) from the experiment were determined from the AUC and flow rate (Q) by the following calculation:

$$E = 1 - R = 1 - AUC \times Q$$

2.2 LSEC ISOLATION

2.2.1 Liver perfusion and digestion

LSEC were isolated by perfusing the liver with Collagenase I (Roche, Basel, Switzerland), followed by removal of non-parenchymal cells and Kupffer cells as described previously (Svistounov et al., 2012). Rats were anaesthetised by an intraperitoneal (i.p.) injection of 2 ml/kg ketamine (60 mg/ml) and xylazine (6 mg/ml). After laparotomy, the portal vein was cannulated with an 18 gauge cannula (Optiva K, Livingstone, Rosebery, Australia). Krebs-Henseleit bicarbonate buffer (10 mM glucose, saturated with 95 % O_2/5 % CO_2, 2 % bovine serum albumin at 37 ºC) was perfused through the liver at a steady flow rate to remove the blood from the sinusoids. Livers were perfused with 100 ml collagenase (0.05 % collagenase in PBS) at approximately 5 ml per minutes or until the liver became soft. The liver was then carefully removed and placed in a sterile petri dish with perfusion buffer. Glisson's capsule and major vessels were removed using sterile forceps, with subsequent gentle mincing of the liver into a paste. The cell suspension was filtered through a cell strainer (BD Biosciences, North Ryde, Australia) to remove any undigested tissue then centrifuged in a falcon tube at 100 *g* for 5 minutes at 20 ºC sedimenting most of the hepatocytes into a pellet at the bottom of the tube.

2.2.2 Cell isolation and culture

The supernatant (containing a mixture of sinusoidal liver cells) was removed and centrifuged at 350 *g* for 10 minutes, sedimenting LSECs into a pellet. The pellet was then resuspended in 50 ml PBS and centrifuged for 10 minutes at 350 *g*. The resulting pellet was resuspended in 20 ml PBS. Two 2-step Percoll gradients were made with 15 ml 50 % stock Percoll (in PBS) on the bottom layer, and 20 ml 25 % stock Percoll (in PBS) (Sigma Aldrich, Castle Hill Australia) on the layer above. 10 ml of the cell suspension was carefully added on top of each of the Percoll gradients and centrifuged for 30 minutes at 900 *g*. The resulting intermediate zone enriched in LSECs was carefully removed and diluted with an equal volume of PBS, then centrifuged again at 900 *g* for 10 minutes. The pellet was resuspended in 10 ml complete RPMI-1640 medium (Gibco Grand Island, NY). The cell suspension was then pipetted into uncoated sterile dishes and incubated for 10 minutes (37 ºC, 5 % CO_2) to allow the selective attachment of Kupffer cells to plastic wells, enhancing LSEC purity. LSECs were then collected by firmly washing the dishes with complete RPMI-1640 to maximise the yield. After automated cell counting (Biorad, Gladesville, Australia), LSECs were cultivated at 1.0×10^6 cells per ml in 24-multiwell plates and on collagen-coated Thermanox coverslips for scanning electron microscopy. LSECs were cultured for 3 hours (37 ºC/5 % CO_2) in 1 ml complete RPMI-1640 per well/coverslip. Cells were rinsed in warm PBS prior to treatment.

2.3 ELECTRON MICROSCOPY

The scanning electron microscope (SEM) has a resolving power of 2.5 nm and provides a three dimensional surface image of a specimen such as a cell or block of hepatic tissue. A focused electron beam is scanned across the surface of a prepared specimen under a vacuum. Morphological detail is collected as the electrons hit the specimen surface causing secondary electrons to be released from the specimen (inelastic collisions) and then collected by a detector. An image of the specimen is created according to the secondary electrons' energy, number, and angle of their path. The image is then sent to a computer screen for viewing (Slayter, 1992).

2.3.1 Tissue fixation

To view the integrity of the liver endothelium in the animal models used, livers were prepared for scanning electron microscopy. At the completion of the multiple indicator dilution experiments, the livers were perfused-fixed via the portal vein with 2.5 % glutaraldehyde (EM grade)/2 % formaldehyde in sodium cacodylate buffer (0.1 M sodium cacodylate, 10 mM $CaCl_2$, 1 % sucrose, pH 7.4, 440 mOsmol) as described previously (Cogger et al., 2006). Fixative was perfused through the liver continuously for approximately 5 minutes or until the liver was hardened, indicated by both pale colouration and tissue stiffness. Following fixation, the liver was excised and cut into 1 mm^3 blocks. These blocks were placed in a specimen jar with fresh fixative and left overnight at 4 ^oC prior to subsequent processing.

2.3.2 Tissue preparation and processing

Ten randomly selected blocks per liver were washed 3 times in 0.1 M sodium cacodylate buffer to remove any traces of fixative before incubation in 1 % tannic acid in 0.15 M sodium cacodylate buffer with 1 % sucrose for 1 hour. Blocks were then washed 3 times in sodium cacodylate buffer and post-fixed in 1 % osmium tetroxide in 0.1 M sodium cacodylate buffer (pH 7.4 with 1 % sucrose for 2 hours). The benefit of this step is twofold - osmium tetroxide provides superior lipid fixation to aldehyde fixatives and it saturates the tissue with heavy metal for better interaction with the electron beam. Following incubation, specimens were washed 3 × 10 minutes each in sodium cacodylate buffer and then dehydrated in a series of increasing ethanol gradients: 3 × 50 % (5 minutes each), 3 × 70 % (5 minutes each), 3 × 95 % (5 minutes each), 2 × 100 % (10 minutes each) ethanol and finally 2 × 100 % ethanol (molecular sieve, 10 minutes each). Specimens were treated with hexamethyldisilazane (Sigma Aldrich, Castle Hill Australia) for 10 minutes for complete drying of the tissue. Specimens were left in the fume hood for 10 minutes to remove remaining hexamethyldisilazane and placed in a desiccator overnight. Specimen blocks were then mounted onto SEM stubs using double sided carbon tape, and platinum coated with an autofine coater (JFC 1600, JEOL, Akishima-Shi, Japan), under argon (45 secs at 40 mV).

2.3.3 Tissue visualisation

Images of the sinusoidal endothelium were observed at 15000 × magnification for visualization of fenestrations. Fig. 2.1 shows an example LSEC image with fenestrations. Ten random images

were taken for analysis using ImageJ software (http://rsb.info.nih.gov/ij/) to determine endothelial porosity, average fenestration diameter and frequency. Endothelial porosity (area of the endothelial surface covered with fenestrations) is calculated by dividing the total area of the individual fenestrations in the selected field divided by the total area of the field examined. Fenestration frequency is the total number of fenestrations in the total area of the field examined (Cogger et al., 2014).

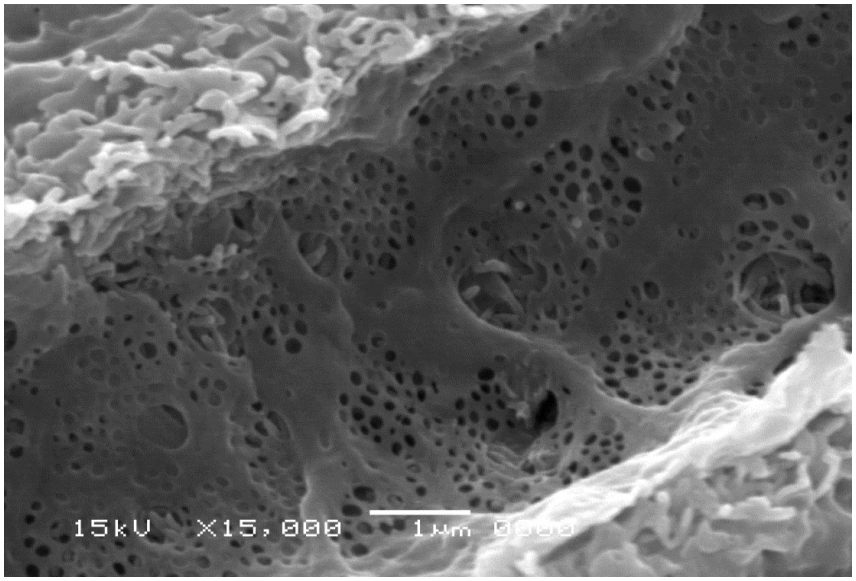

Figure 2.1: An example of image of the fenestrated LSEC taken using JEOL JSM-6380 scanning electron microscope for porosity analysis

2.4 LIGHT MICROSCOPY

Light microscopy was performed to ensure overall tissue integrity and the absence of liver pathologies in all animals used for the experiments contained in this thesis.

2.4.1 Tissue fixation and preparation

At the completion of each experiment, pieces of liver were fixed in 4 % paraformaldehyde buffered saline overnight, dehydrated with ethanol, cleared in xylene and finally embedded in paraffin for light microscopy. Paraffin embedded liver specimens were cut at 4 µm, mounted on glass slides, then subjected to the staining technique of interest as discussed below.

2.4.2 Tissue staining

For staining slide mounted sections were cleared of paraffin and rehydrated to allow affinity for specific dyes. Following staining, they were again dehydrated with ethanol and cleared with xylene before mounted with mounting media (Pertex, Histolab AB, Canning Vale Australia). 2 stains were used in the experiments as follows:

Hematoxylin and eosin

Hematoxylin and eosin (H & E) is a stain routinely used to view the general pathology of the specimen. Hematoxylin stains cell nuclei (chromatin) blue, and eosin stains the cytoplasm and connective tissues different shades of pink, orange, and red, and red blood cells intensely red.

Periodic acid-Schiff

The periodic acid-Schiff (PAS) reaction is used to visualise glycogen, basement membranes, and neutral mucosubstances. Oxidation with periodic acid exposes the aldehyde groups in sugars that subsequently react with the chromophores in Schiff's reagent, producing a bright pink colour. A basic stain such as Harris' Hematoxylin is used as a counterstain to stain the cells blue.

2.4.3 Tissue observation

Once mounting media had completely dried, slides were viewed using EVOS FL Imaging system (Life Technologies, Wembley Australia) using bright field illumination. Pictures were taken at 40 × magnification.

2.5 FLUORESCENCE MICROSCOPY

Fluorescent labelling was used to visualise cell membranes and lipid rafts (Cogger et al., 2010, Svistounov et al., 2012). It is not able to be used to assess fenestrations because there are no fluorescent markers of fenestrations, and the pores are too small to be resolved by standard light microscopy.

2.5.1 Cell fixation

Following culture and treatment, cells were washed with PBS and fixed in 4 % paraformaldehyde buffered saline for 2 hours and then kept in PBS prior to staining.

2.5.2 Cell staining and observation

Cells on coverslips were stained with Cell-Mask Orange (Life Technologies, Wembley Australia), a non-specific cell membrane stain (554/567 nm), and Bodipy FL C5 ganglioside GM1 (505/511 nm) (Life Technologies, Wembley Australia) which stains ordered lipid microdomains of membranes, also known as lipid rafts. Cells were washed and fixed with 4 % fresh paraformaldehyde in PBS. The coverslip were mounted using Prolonged-Gold (Life Technologies, Wembley Australia) to preserve fluorescent signal. The cells were then imaged with red and green channels predetermined for each staining and convolved using Zeiss Wide-field fluorescence deconvolution microscope/Sen Software package. Experiments were performed in triplicate.

2.6 PROTEIN ANALYSIS

Levels of proteins and phosphorylated proteins associated with insulin signaling pathways was assessed using mass spectrometry performed at the Charles Perkins Centre by the laboratory of Professor David James and western blotting.

2.6.1 Proteomic analysis via mass spectrophotometry

Rat liver tissue was collected following the MID procedure was solubilised in SDS/Tris buffer in the presence of phosphatase and kinase inhibitors prior to protein precipitation. Following tryptic digestion, 250 µg of peptide was labelled with one of four isobaric tags (iTRAQ, Sciex) prior to phosphoproteomic enrichment (Jensen et al., 2009, Engholm-Keller et al., 2012). This enrichment generated three peptide populations, singly and multiply phosphorylated peptides (11 fractions); and non-modified peptides (16 fractions). Identification and quantitation of phosphorylated and non-phosphorylated peptides was performed on an Orbitrap Velos Pro mass spectrometer in data dependent acquisition (DDA) mode. All experiments were performed in duplicate. Data was analysed using Proteome Discoverer (Version 1.4; Thermo) and searched using an in-house MASCOT server against the UniProt *mus musculus* database with the following parameters; 2 missed cleavages; 20 ppm mass error (MS) and 0.2 Da mass error (MS/MS); iTRAQ searched as a static modification; carbamidomethyl (Cys), oxidation (Met), acetylation (Protein N-term) and cyclization (Glu and Asp) as dynamic modifications. A false discovery rate of 0.05 was applied to phosphopeptides, with a stricter 0.01 FDR applied to the non-modified cohort. For analysis of MS data, normalization of iTRAQ reporter ions was

calculated using the sum all intensities approach combining both phosphorylated and non-phosphorylated peptide spectral matches (PSM), prior to ratio calculations using young as the denominator for old. Log2 ratios and z-scores were calculated for each PSM, with z-scores determined using a sliding scale based on MS signal intensity (a measure of MS/MS data quality). Median z-scores were calculated with weighted average used to compare medians across experiments for each phosphosite (phosphoproteome enriched), peptide and protein (non-phosphorylated only). To be deemed significantly altered, median z-scores were required to be greater than 1.00 or less than -1.00 for phosphosites. Median z-scores for each non-phosphorylated peptide were calculated preceding determination of protein z-scores. For a protein to be deemed significantly altered, median z-scores >1.96 or <-1.96, equivalent to p values of <0.05 were required. Bioinformatic analysis was performed to reveal pathways associated with ageing using STRING (Jensen et al., 2009, Franceschini et al., 2013, Szklarczyk et al., 2011) and KEGG (Kanehisa and Goto, 2000, Kanehisa et al., 2014) pathway analysis.

2.6.2 Western blotting

Protein immunoblotting is a method used to measure relative amounts of proteins of interest between samples. Frozen liver tissue samples collected after the MID procedure were homogenised (Qiagen TissueLyser, Chadstone Australia) in RIPA buffer containing Tris-HCl, NaCl, Triton x-100, Na-deoxycholate, SDS (Sigma Aldrich, Castle Hill Australia) and protease inhibitor tablets (cOmplete, EDTA-free Protease Inhibitor Cocktail, Roche, Castle Hill Australia). Protein concentrations were determined using the BCA method (Pierce BCA Protein Assay Kit, Thermo Scientific, Scoresby Australia). 20 µg of protein was separated on 4-15 %

gradient mini-protean TGX gels (Bio-Rad, Gladesville Australia) and transferred to a nitrocellulose membrane (Trans-Blot Turbo, BioRad, Gladesville Australia). The membranes were blocked for 1 hour (5 % skim milk in TBS), washed in TBS 0.1 % Tween-20 and incubated overnight in primary antibody solution (5 % BSA, TBS 0.1 % Tween 20). Washed membranes were incubated for one hour in secondary antibody solution (5 % skim milk in TBS 0.1 % Tween, 0.01 % SDS). Probed membranes were analysed on a Licor odyssey system (Millenium Science, Mulgrave Australia) and densitometry analysis was measured using Licor software (Version 3.1).

Antibodies against the following proteins were used: phospho-IRS-1 (Ser612, Cat#2386), IRS-1 (Cat#2382), phospho-AKT (Ser473, Cat#9271), AKT (Cat#4691), and α-tubulin as housekeeping protein (Cat#2144) (Cell Signaling Technology, Arundel, Australia).

2.7 METABOLIC VARIABLES

2.7.1 Blood analysis

Prior to liver perfusion, approximately 1 ml blood was taken from the inferior vena cava (IVC) and transferred into an EDTA tube. Blood was spun at 1500 rpm for 10 minutes at 4 ^{o}C. The plasma was transferred into a clean tube and stored at -20 ˚C. Analysis of lipid and liver function tests was performed by the Biochemistry Department, Diagnostic Pathology Unit, Concord RG Hospital, using the automated Roche Diagnostics Modular Analytics Serum Work Area (F. Hoffman-La Roche Ltd, Hawthorn Australia).

2.7.2 Glucose tolerance and tracer uptake

This method was performed as described previously with modifications (Cooney et al., 2004). Animals were fasted for 6 hours, followed by administration of glucose (2 g/kg i.v.) spiked with 10 µCi ^{14}C-glucose for assessment of insulin storage action in liver, fat and muscle and 10 µCi ^{3}H-2-deoxyglucose for assessment of glucose uptake in fat and muscle. This procedure was done under anaesthesia for rats and using restrainer for mice. It should be noted that ^{3}H 2-deoxyglucose is not a substrate for liver uptake and metabolism. After 15, 30, 45, 60 and 90 minutes, glucose levels were measured with a handheld glucose meter (Accu-Check Performa, Roche, Hawthorn Australia). At 90 minutes, animals were sacrificed and liver, adipose tissue and quadriceps muscle were excised, weighed and either snap frozen in liquid nitrogen or placed in 4 % phosphate buffered paraformaldehyde, dehydrated and embedded in paraffin for histology. Blood was collected at 0 (fasted) and 90 minutes (fed) to determine insulin levels (Rat Ultrasensitive Insulin ELISA, Alpco Diagnostics, Kurnell Australia), c-peptide levels (Rat C-peptide ELISA, Alpco Diagnostics, Kurnell Australia) and glucagon levels (Sigma Aldrich, Castle Hill , Australia). This procedure was done under anaesthesia for rats and using restrainer for mice.

2.7.3 Insulin uptake

Whole body insulin extraction was performed in another batch of rats, where ^{14}C-insulin (1 µCi/g) was injected via the inferior vena cava of anesthetised animals. Five minutes later the

animals were exsanguinated by cardiac puncture and in addition to the blood, the liver, white adipose tissue (WAT) and muscle tissue were collected for measurement of ^{14}C-insulin.

2.7.4 Tissue processing for tracer uptake

To determine the incorporation of ^{14}C-labelled glucose to glycogen, liver, muscle and adipose tissue were digested in potassium hydroxide (KOH) (Sigma Aldrich, Castle Hill , Australia) at 70 ºC, followed by addition of saturated $NaSO_4$ (Sigma Aldrich, Castle Hill , Australia) and precipitated with 95 % ethanol for liquid scintillation counting. The amount of ^{14}C glucose incorporated into glycogen was calculated by correcting for the area under the curve for ^{14}C-glucose during GTT and for the weight of the tissue sample used. Tissue ^{3}H-2-deoxyglucose uptake was determined by homogenizing in 0.5 % perchloric acid (PCA) (Sigma Aldrich, Castle Hill, Australia) and homogenates were centrifuged and neutralised with KOH. One aliquot was counted directly to determine total radioactivity (^{3}H-2-deoxyglucose and ^{3}H-2-deoxyglucose-6-phosphate). A second aliquot was treated with barium hydroxide (BaOH) and zinc sulfate ($ZnSO_4$) (Sigma Aldrich, Castle Hill , Australia) to remove ^{3}H-2-deoxyglucose-6-phosphate and any tracer incorporated into glycogen, and then was counted to determine ^{3}H-2-deoxyglucose radioactivity. Total ^{3}H-2-deoxyglucose-6-phosphate is the difference between the two aliquots and normalised to tissue weight. Blood samples were deproteinised using BaOH and $ZnSO_4$ to quantify plasma radioactivity by liquid scintillation counting. Tissue specific glucose uptake index, Rg was calculated using the following equation:

$$Rg = \frac{(3H-2-deoxyglucose-6-phosphate)\,tissue}{AUC\,(3H-2-deoxyglucose)\,plasma}\,.\,\text{glucose plasma}$$

2.7.5 Insulin tolerance

Insulin tolerance tests were performed after a 3 hours fast. Insulin (1.5 IU kg^{-1} body weight) (Sigma Aldrich, Castle Hill , Australia) was administered via i.p. injection and blood glucose levels were read using a handheld glucose meter (Accu-Check Performa, Roche, Hawthorn Australia) through tail bleeds at 0, 15, 30, 60 and 90 minutes.

2.7.6 Pyruvate tolerance

Animals were fasted for 6 hours prior to an i.p injection of pyruvate (2 g/kg; Sigma Aldrich, Castle Hill, Australia) and glucose levels were read using a handheld glucose meter (Accu-Check Performa, Roche, Hawthorn Australia) through tail bleeds at 0, 15, 30, 60 and 90 minutes. Total AUC was calculated using the trapezoidal formula.

2.8 REVERSE TRANSCRIPTION AND QUALITATIVE REAL TIME PCR ARRAY ANALYSIS

Total RNA was isolated from frozen liver tissue samples using RNeasy Plus Mini Kit (Qiagen Pty Ltd, Chadstone, Australia) according to the manufacturer's instruction, with DNase treatment included. RNA quantification was performed using a Nanodrop (Thermofischer, Wilmington, DE, USA) and samples with OD>2.0 were selected for subsequent step. Reverse transcription of 1 µg of total RNA was carried out using RT^2 First strand kit (Qiagen Pty Ltd, Chadstone, Australia). The cDNA was then added to the RT^2 SYBR green qPCR mastermix, loaded onto 96-

well RT^2 Profiler PCR array plate (PARN-030-ZD, Qiagen Pty Ltd, Chadstone, Australia) and amplified on Biorad CFX Connect Real Time PCR Detection system (Roche Diagnostics, Hawthorn Australia) for 40 cycles. PCR array data was analysed according to the manufacturer's instructions. Relative gene expression was determined using the $\Delta\Delta C_t$ method normalised against five housekeeping genes (Actb, B2m, Hprt1, Ldha and Rplp1) and changes in gene expression were shown as a fold increase or decrease compared to control group.

2.9 STATISTICAL ANALYSIS

All statistical analysis was performed using SigmaStat Statistics Software (Sigmaplot v12.5, Systat Software, Germany) unless specifically stated. Data are presented as the mean ± standard error of the mean (SEM). Statistical significance for the differences between two groups (e.g. young and old) was calculated using two-tailed Students T test. Correlations between two measures were calculated using the Pearsons Product Moment correlation coefficient. Statistical significance was assumed at $p<0.05$.

CHAPTER 3: AGE-RELATED DEFENESTRATION AND HEPATIC INSULIN AND GLUCOSE DISPOSITION

Chapters 3 and 4 have been combined for the following publication:

Mohamad, M., S. J. Mitchell, L. E. Wu, M. Y. White, S. J. Cordwell, J. Mach, S. M. Solon-Biet, D. Boyer, D. Nines, A. Das, S. Y. Catherine Li, A. Warren, S. N. Hilmer, R. Fraser, D. A. Sinclair, S. J. Simpson, R. de Cabo, D. G. Le Couteur and V. C. Cogger (2016). "Ultrastructure of the liver microcirculation influences hepatic and systemic insulin activity and provides a mechanism for age-related insulin resistance." Aging Cell **15**(4): 706-715.

3.1 INTRODUCTION

Insulin resistance, characterised by elevated basal and stimulated levels of insulin, is inextricably associated with older age (Fink et al., 1983, Oya et al., 2014). The liver is the key target organ for insulin activity and under normal physiological conditions the entire output of endogenous insulin from the pancreas travels through the liver vasculature before entering the systemic circulation (Izzo and Bartlett, 1969). Once it has entered the liver parenchyma, most likely through the liver sinusoidal endothelial cells (LSEC) fenestrations, insulin regulates a myriad of metabolic processes such as glycogen storage, gluconeogenesis and fatty acid synthesis. The primary role of the liver in the development of insulin resistance is demonstrated by the fact that insulin resistance occurs in liver-specific insulin receptor knockout mice (Fisher and Kahn, 2003), but not in muscle-(Brüning et al., 1998) or fat-(Bluher et al., 2002) specific insulin receptor knockout mice. Further evidence comes from the observation that glucose intolerance that occurs during the early stages of high fat feeding is due to the development of insulin resistance in the liver before other tissues develop metabolic changes (Turner et al., 2013). Hyperinsulinemia and insulin resistance are common conditions associated with altered liver function, particularly those associated with structural changes in the liver endothelium such as old age and liver disease (Chai et al., 2014, Kotronen et al., 2007, Takamura et al., 2012, Kawaguchi et al., 2011, Fink et al., 1983, Bose and Ray, 2014, Taguchi et al., 2014, Muller et al., 1992).

The transfer of insulin across the endothelium is the rate limiting step for the uptake and action of insulin in muscle and fat (Majumdar et al., 2012, Sandqvist et al., 2011). Despite its important

impact on the disposition of many other substrates, the effect of the endothelium on insulin activity in the liver has largely been overlooked (Fraser et al., 1995, Cogger et al., 2006, Cogger and Le Couteur, 2009). As discussed in Chapter 1, the main endothelial cells in the liver are the LSECs, which are specialised endothelial cells that line the wall of the hepatic sinusoid. The thin cytoplasmic extensions of LSECs are perforated with fenestrations that are non-diaphragmed, transcellular pores 50-150 nm in diameter. Between 2-20% of the surface of the LSECs are covered by fenestrations clustered into groups called liver sieve plates (Cogger and Le Couteur, 2009, Fraser et al., 1995, Wisse et al., 1985). These ultrastructural features facilitate transfer of plasma and small particulate substrates between the blood and the hepatocytes. Under normal conditions, LSECs are a highly efficient ultrafiltration system; therefore the influence of fenestrations on liver function is mostly seen in diseases and old age where their diameter and frequency are diminished (Cogger and Le Couteur, 2009, Cogger et al., 2006, Fraser et al., 2012).We propose that fenestrations also provide a portal for the hepatic uptake, and subsequent clearance and activity of insulin, and that the loss of fenestrations, such as that which occurs with old age, provides a novel mechanism for hepatic insulin resistance. Such a discovery would have considerable clinical significance as it provides a novel mechanism for the insulin resistance seen in ageing and with liver diseases where there is a reduction in fenestrations (Le Couteur et al., 2001, Cogger et al., 2006, Furrer et al., 2011).

In this study the role of age-related pseudocapillarisation in hepatic insulin resistance has been examined; in particular the effects of loss of fenestrations on the disposition and activity of insulin in the liver and systemically. Defenestration seen in old age has been shown to impair the transendothelial transfer and hepatic clearance of several substrates including lipoproteins,

acetaminophen and diazepam (Cogger et al., 2006, Mitchell et al., 2010, Mitchell et al., 2012, Mitchell et al., 2011). Therefore, the aim of this study was to investigate the role of LSEC fenestrations in the hepatic disposition and action of insulin.

3.2 METHODS

3.2.1 Animals

Male Fischer 344 rats (for MID methodologies) and male C57/Bl6 mice (for metabolic parameter assessments) aged 3 months (young) and 24-27 months (old) were obtained from the National Institutes of Ageing (Baltimore, MD). Due to limited availability of older rats and the technical limitations of the liver perfusion studies are, rats were prioritised for the MID studies and mice were used for the remaining in vivo studies. The animals were allowed free access to water and standard chow. All animals were treated in accordance with Animal Care guidelines. This study was approved by the Animal Care and Users Committee of the National Institute on Ageing, National Institutes of Health (protocol number: 429-TGB-2017).

3.2.2 Liver perfusion and multiple indicator dilution method

This procedure was performed as described in Sections 2.3.2 and 2.3.3. Briefly the young and old F344 rats were weighed and anaesthetised and liver was perfused with Krebs buffer followed by a tracer injectates of either: (1) ^{3}H-sucrose and ^{14}C-insulin or (2) ^{3}H-sucrose and ^{14}C-glucose. Analysis for ^{14}C and ^{3}H specific activity from outflow samples was performed in a Packard 1600TR liquid scintillation counter and data were used to generate dose-normalised outflow curves. The area under the curve (AUC), area under the moment of the curve (AUMC), mean transit time (MTT) and recovery of each indicator were determined.

3.2.3 Scanning electron microscopy

At the completion of MID experiments, liver specimens were perfusion-fixed with 3 % glutaraldehyde/2 % paraformaldehyde in 0.1 M sodium cacodylate buffer and processed for scanning electron microscopy as described in Section 2.4.5. Fenestrations of the liver endothelium were examined using a Jeol 6380 Scanning electron microscope at 15000X magnification. Ten random images of sinusoids per sample were taken for each liver at 15000X for analysis of fenestration diameter and porosity using ImageJ software (1.41 NIH, USA) as described in Section 2.4.5.4.

3.2.4 Metabolic parameters

3.2.4.1 Glucose tolerance and tracer uptake

Young and old C57/Bl6 mice were fasted for 6 hrs, followed by administration of glucose (2 g/kg i.v.) spiked with 10 µCi ^{14}C-glucose for assessment of insulin action in liver, fat and muscle and 10 µCi ^{3}H-2-deoxyglucose for assessment of glucose uptake in fat and muscle as described in Section 2.6.2.

3.2.4.2 Insulin uptake

Whole body insulin extraction was performed in another group of young and old mice, where ^{14}C-insulin (1 µCi/g) was injected via the inferior vena cava of anesthetised animals as described in Section 2.6.3.

3.2.4.3 Tissue processing for tracer uptake

Incorporation of radiolabelled glucose to glycogen, ^{3}H-2-deoxyglucose uptake and ^{14}C-insulin uptake were determined using the mice liver from Sections 3.2.4.1 and 3.2.4.2 according to methods as described in Section 2.6.4.

3.2.4.4 Insulin tolerance

Young and old C57/Bl6 mice were fasted for 3 hrs followed by insulin injection (1.5 IU/kg i.p.) and glucose levels were read using a handheld glucose meter as described in Section 2.6.5.

3.2.4.5 Pyruvate tolerance

A fourth cohort of young and old C57/Bl6 mice were fasted for 6 hours prior to an i.p injection of pyruvate (2 g/kg; Sigma Aldrich) and glucose levels were read using a handheld glucose meter as described in Section 2.6.6.

3.2.5 Histology

Liver tissue from mice described in Section 3.2.4.1 was fixed in 4% paraformaldehyde, paraffin embedded, sectioned and subjected to H&E and PAS staining, followed by observation as described in Section 2.3.2.

3.2.6 Reverse transcription and quantitative real time-PCR array analysis

Total RNA was isolated from frozen rat liver tissue samples using a RNeasy Plus Mini Kit (Qiagen Pty Ltd, Chadstone, Australia), followed by subsequent reverse transcription and real time-PCR as described in Section 2.8.

3.2.7 Proteomic studies

3.2.7.1 Mass Spectrometry

This procedure was performed as described in Sections 2.6.1. Briefly rat liver tissue from the MID procedure was solubilised in SDS/Tris buffer in the presence of phosphatase and kinase inhibitors prior to protein precipitation. Following tryptic digestion, 250 µg of peptide was labeled with one of four isobaric tags (iTRAQ, Sciex) prior to phosphoproteomic enrichment (Jensen et al., 2009, Engholm-Keller et al., 2012). Identification and quantitation of phosphorylated and non-phosphorylated peptides was performed on an Orbitrap Velos Pro mass spectrometer in data dependent acquisition (DDA) mode. All experiments were performed in

duplicate. Data was analysed using Proteome Discoverer (Version 1.4; Thermo) and searched using an in-house MASCOT server against the UniProt *mus musculus* database, which is the closest one to rat available. For analysis of MS data, normalization of iTRAQ reporter ions was calculated using the sum all intensities approach combining both phosphorylated and non-phosphorylated peptide spectral matches (PSM), prior to ratio calculations using young as the denominator for old. Bioinformatic analysis was performed to reveal pathways associated with ageing using STRING (Jensen et al., 2009, Franceschini et al., 2013, Szklarczyk et al., 2011) and KEGG (Kanehisa and Goto, 2000, Kanehisa et al., 2014) pathway analysis.

3.2.7.2 Western Blots

This procedure was performed as described in Sections 2.6.1. Briefly frozen liver tissue samples collected after the MID procedure were homogenised in RIPA buffer containing Tris-HCl, NaCl, Triton X-100, Na-deoxycholate, SDS (Sigma Aldrich) and protease inhibitor tablets. Protein concentrations were determined using the BCA method (Pierce BCA Protein Assay Kit, Thermo Scientific). The protein extract were subjected to immunoblotting according to protocol as described previously (Hoehn et al., 2008). Antibodies against the following proteins were used: phospho-AKT (Ser473, Cat#9271), AKT (Cat#4691) and α-tubulin (Cat#2144) (Cell Signaling Technology, Arundel, Australia).

3.2.8 Data analysis

Data analysis was performed using Microsoft Excel. All values are expressed as the mean ± SEM. Statistical significance was calculated using two-tailed Students T-test and Pearson's Product Moment correlation coefficient (Sigmaplot v11, Systat Software, Germany).

3.3 RESULTS

3.3.1 Histology and Electron Microscopy

Post mortem examination of the whole animal and haematoxylin and eosin staining of liver sections from the old and young animals confirmed all animals included in the study were free of gross and liver pathology (Fig. 3.1).

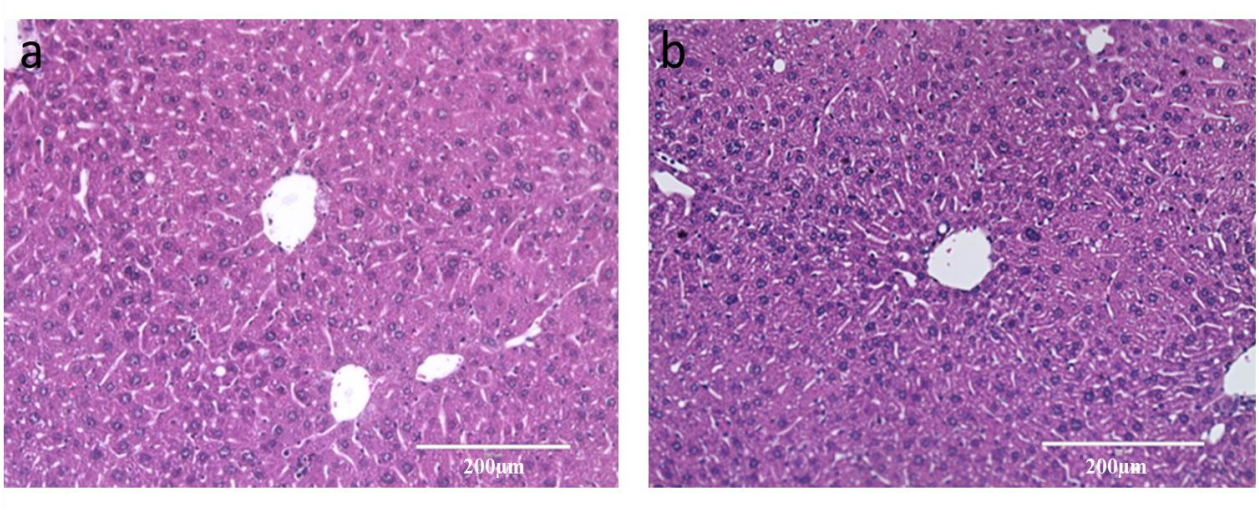

Figure 3.1: Haematoxylin and Eosin staining of young (a) and old (b) Fischer F344 rats. No signs of pathology were found in both liver groups.

Scanning electron microscopy (Fig. 3.2) was performed to confirm age-related defenestration of the LSEC that has been described previously in many species including rats, mice and humans. LSEC morphology was analysed as described in Table 3.1 and an age-related reduction in porosity was found. These findings are consistent with previous studies (Le Couteur et al., 2001, Le Couteur et al., 2008a).

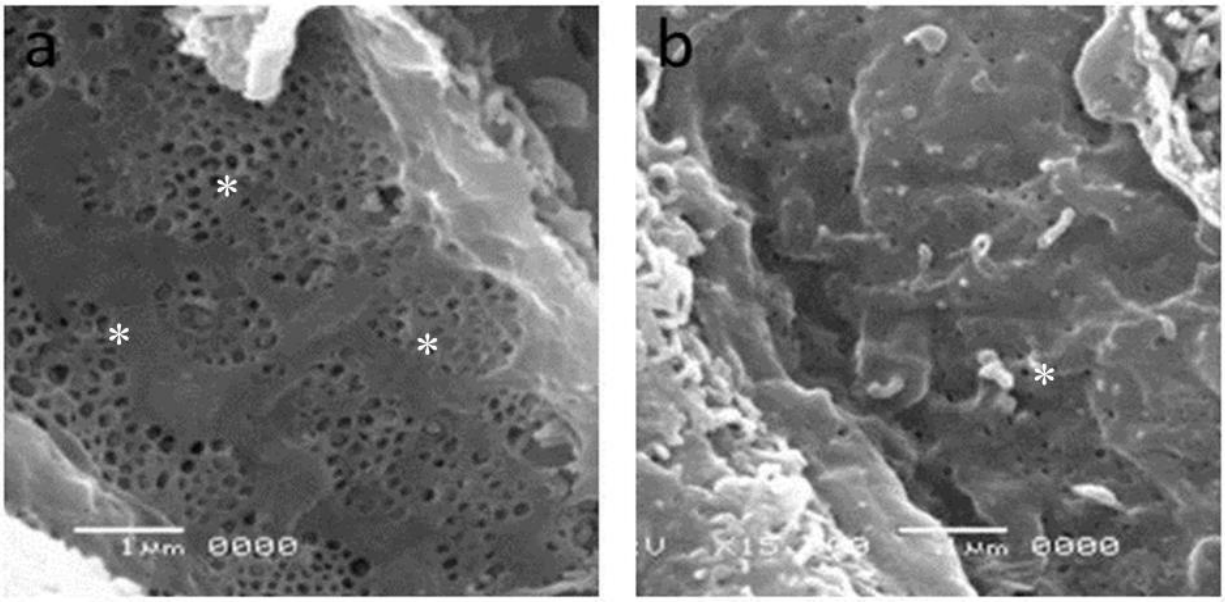

Figure 3.2: Representative Scanning electron micrographs of the perfused LSEC in young (a) and old (b) Fischer F344 rats. Fenestrations are indicated by an *. Significant defenestration is observed with age. Original micrographs taken at 15000 × magnification**.**

Table 3.1: Quantification of the fenestrations in LSECs. There is a significant decrease in liver porosity (P=0.006), but no change in the fenestration diameter in the old group. Data is presented as mean ± SEM.

Animal group	**n**	**Porosity (%)**	**Diameter (nm)**	**Frequency (per um^2)**
Young	5	4.88±0.5	96.4±0.6	4.72±0.4
Old	5	2.64±0.2*	73.2±0.4	4.03±0.2

3.3.2 Age-related pseudocapillarisation impairs the access of insulin, but not glucose to the extracellular space of the liver

To establish a causal relationship between age, age-related defenestration of the liver endothelium and insulin resistance, MIDs were performed in young and old rats. Outflow insulin curves from the MID experiments are shown in Fig. 3.3.

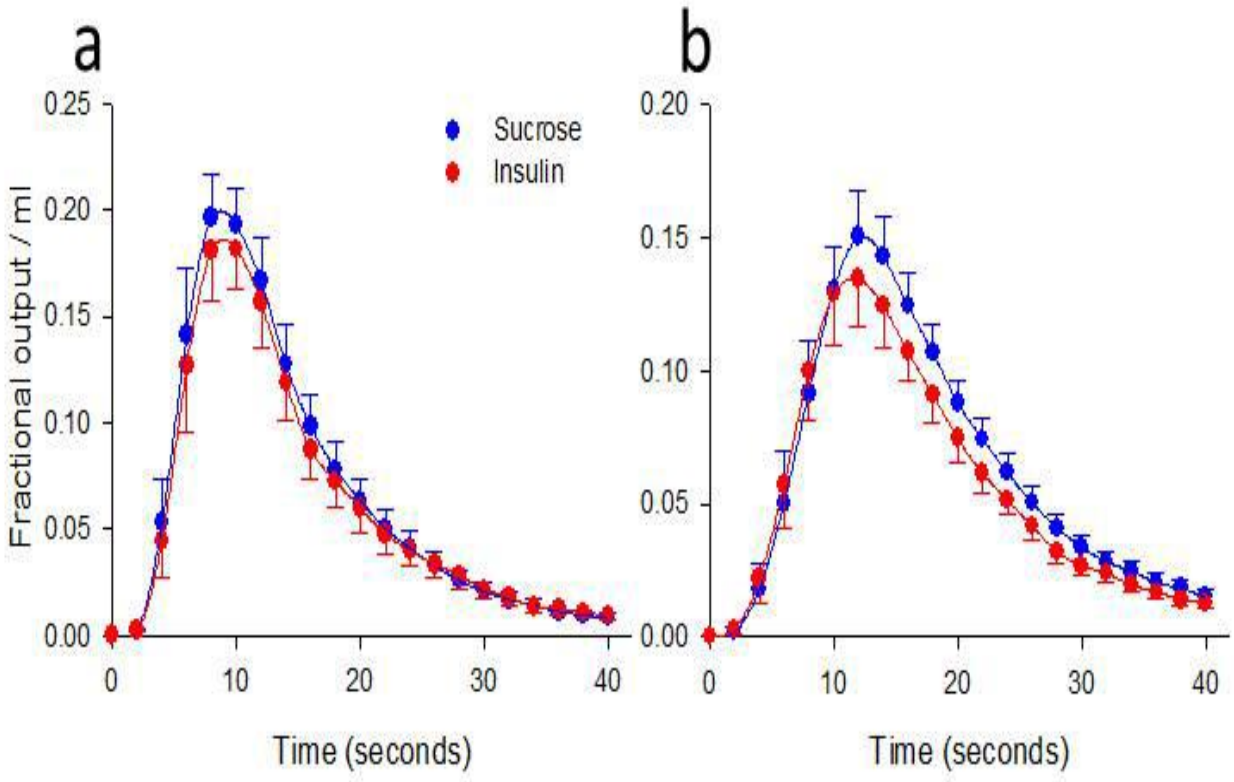

Figure 3.3: MID outflow curves for insulin and the extracellular marker sucrose (n=9 young and n=9 old). Insulin exits the liver after sucrose in young rats (a) whereas the order is reversed in the old animals (b) indicating restricted access to the entire extracellular space with age-related defenestration.

In young animals, the insulin curve overlaps the sucrose curve (Fig 3.3a), indicating that insulin has unimpeded access to the entire extracellular ('sucrose') space. However in old animals, the insulin curve appears earlier than the sucrose curve (Fig 3.3b), indicating that insulin has a smaller volume of distribution than sucrose. The recovery and apparent volume of distribution of insulin and tracers are shown in Table 3.2. There was no difference in the recovery of Evans Blue or sucrose between the age groups.

Table 3.2: The effect of age on recovery and volume of distribution (Vd) of Evans blue, insulin and sucrose.

	Young (n=9)	**Old (n=9)**
Fractional recovery		
Evans blue	0.97±0.03	0.88±0.06
Insulin	0.68±0.05	0.68±0.06
Sucrose	0.73±0.05	0.76±0.05
Vd (ml/g)		
Evans blue	0.26±0.04	0.28±0.02
Insulin	0.28±0.04	0.28±0.01
Sucrose	0.26±0.04	0.30±0.02
Ratio		
Insulin/Evans blue	1.09±0.08	1.03±0.04
Insulin/Sucrose	1.10±0.07	0.95±0.02

Analysis of the curves showed that old age was associated with a statistically significant reduction in the volume of distribution of insulin normalised to the extracellular marker sucrose volume of about 20 % (P=0.01, Fig. 3.4).

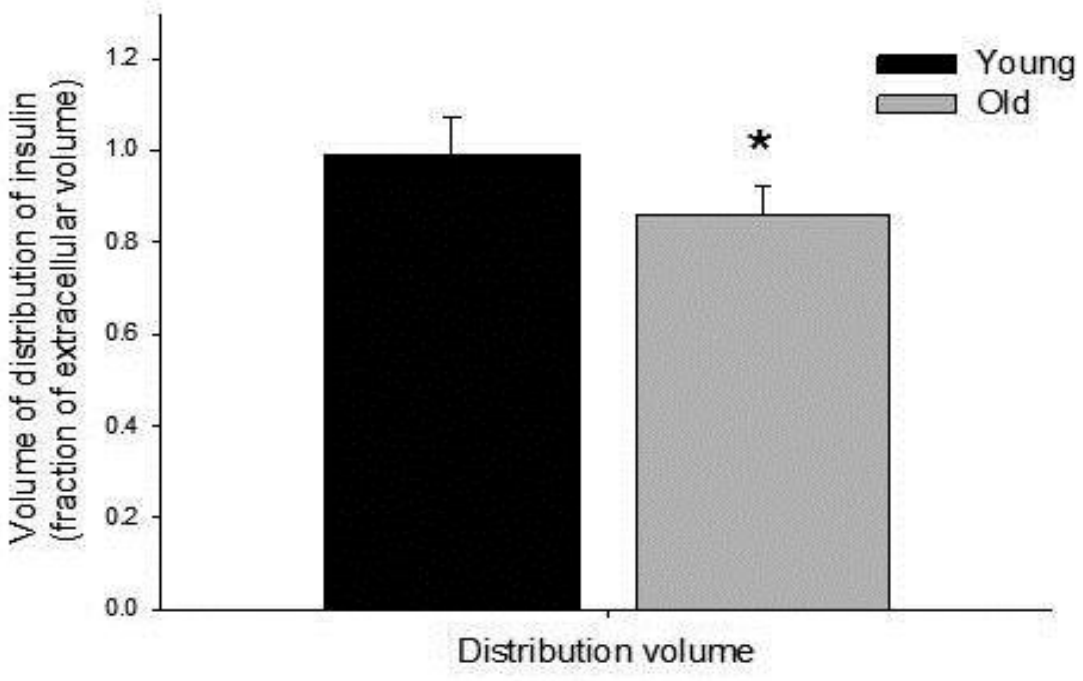

Figure 3.4: Volume of distribution of insulin as a percentage of extracellular volume. There is a 20 % reduction in the fractional volume of distribution of insulin with age (n = 9 young and 9 old F344 rats, P=0.01).

Contrary to insulin, there was no difference in the appearance of the glucose and sucrose curves for young and old, indicating a similar distribution (Fig 3.5a-b). Analysis of the curves for recovery and volume of distribution are shown in Table 3.3. There was no difference in the recovery of Evans Blue, glucose or sucrose between both groups. The ratio of volume of

distribution of glucose compared to Evans Blue and sucrose was not influenced by age (p=0.07, Fig 3.6).

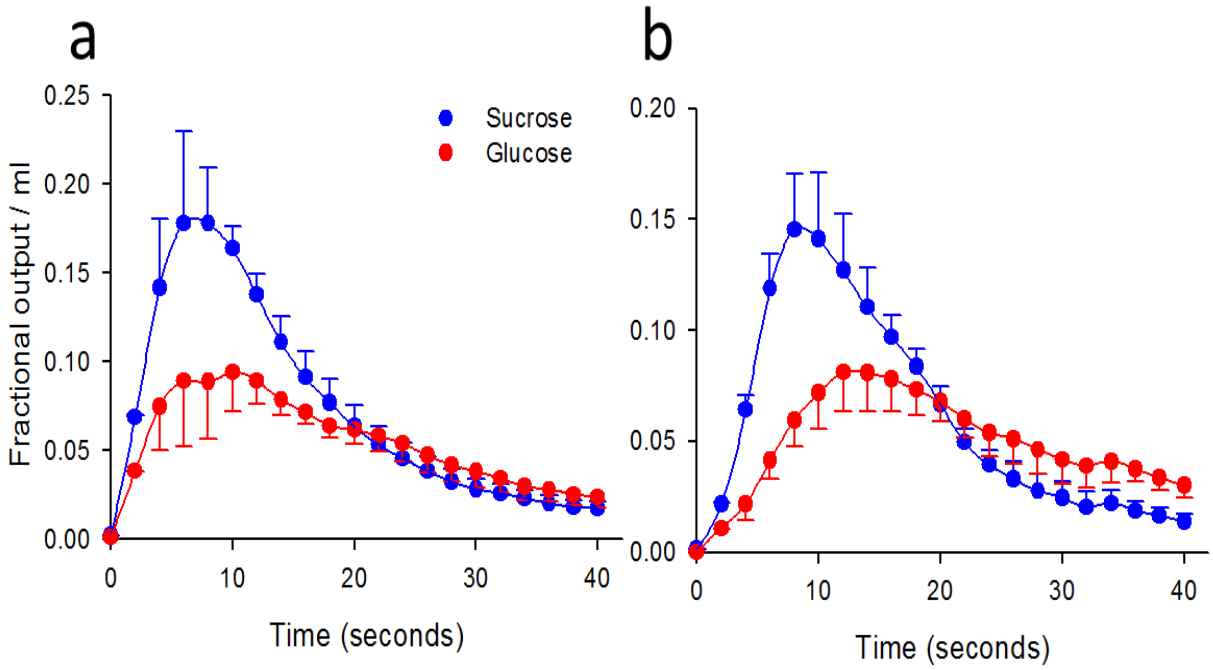

Figure 3.5: Average MID outflow curves for glucose and the extracellular marker sucrose. Both the young (a) and old (b) glucose curves are delayed compared to sucrose, consistent with its access to extracellular and intrahepatocytic spaces; however there was no difference in the glucose appearance between young and old groups.

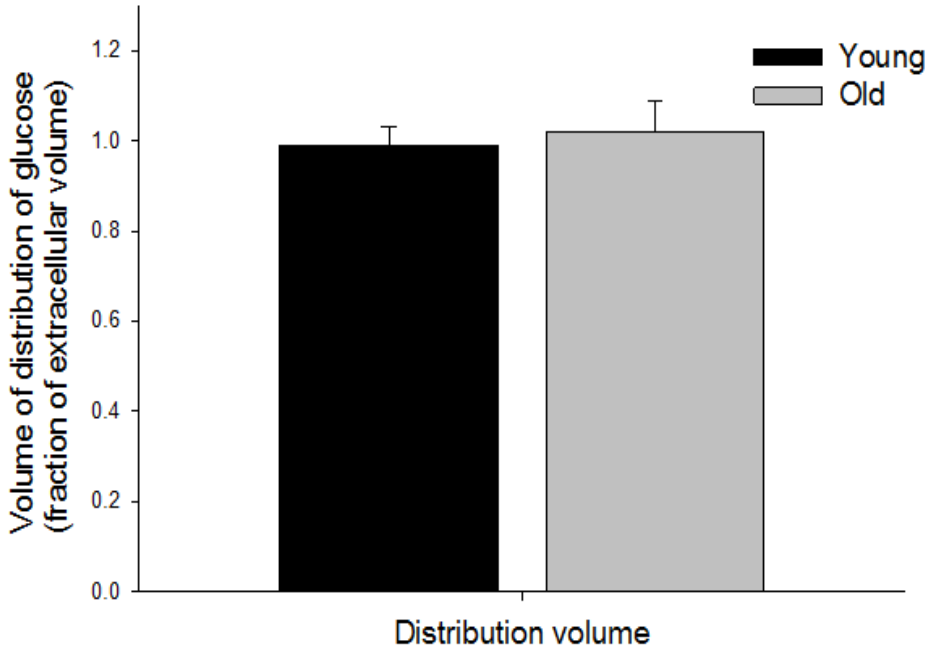

Figure 3.6: Volume of distribution of glucose as a percentage of extracellular volume. There were no differences in the fractional volume of distribution of glucose with age, (n = 9 young and n = 10 old F344 rats).

Table 3.3: The effect of age on recovery and volume of distribution (Vd) of Evans blue, glucose and sucrose

	Young (n=9)	Old (n=9)
Fractional recovery		
Evans blue	1.00±0.03	0.88±0.10
Glucose	0.70±0.03	0.76±0.07
Sucrose	0.85±0.04	0.79±0.08
Vd (ml/g)		
Evans blue	0.36±0.04	0.32±0.05
Glucose	0.58±0.08	0.55±0.07
Sucrose	0.40±0.05	0.34±0.04
Ratio		
Glucose/Evans blue	1.57±0.16	1.86±0.26
Glucose/Sucrose	1.41±0.05	1.65±0.22

3.3.3 Metabolic parameters

3.3.3.1 Insulin levels and systemic metabolism

As a consequence of reduced hepatic uptake of insulin, the basal insulin concentrations were significantly increased in the old mice, both in the fasted and fed states when compared to their younger counterparts (Fig 3.7a). C-peptide levels were unchanged in the old group during the fasted state (Fig. 3.7b), indicating that hyperinsulinemia is established through reduced clearance of insulin by the liver rather than increased pancreatic insulin secretion. In the fed state, C-peptide levels increased significantly with age, suggesting that increased insulin secretion is required to maintain glucose tolerance with age. Glucagon levels were significantly lower in the old, compared to the young mice, when fasting (Fig. 3.7c).

To determine if age is associated with only impaired liver insulin uptake hepatic, systemic insulin uptake was also measured using an intravenous dose of ^{14}C-insulin. Although intraperitoneal insulin tolerance performance was similar between groups (Appendix 1), insulin uptake by the liver was reduced by about 30 % in 24 month old C57/Bl6 mice, but unchanged in fat and muscle (Fig. 3.7d).

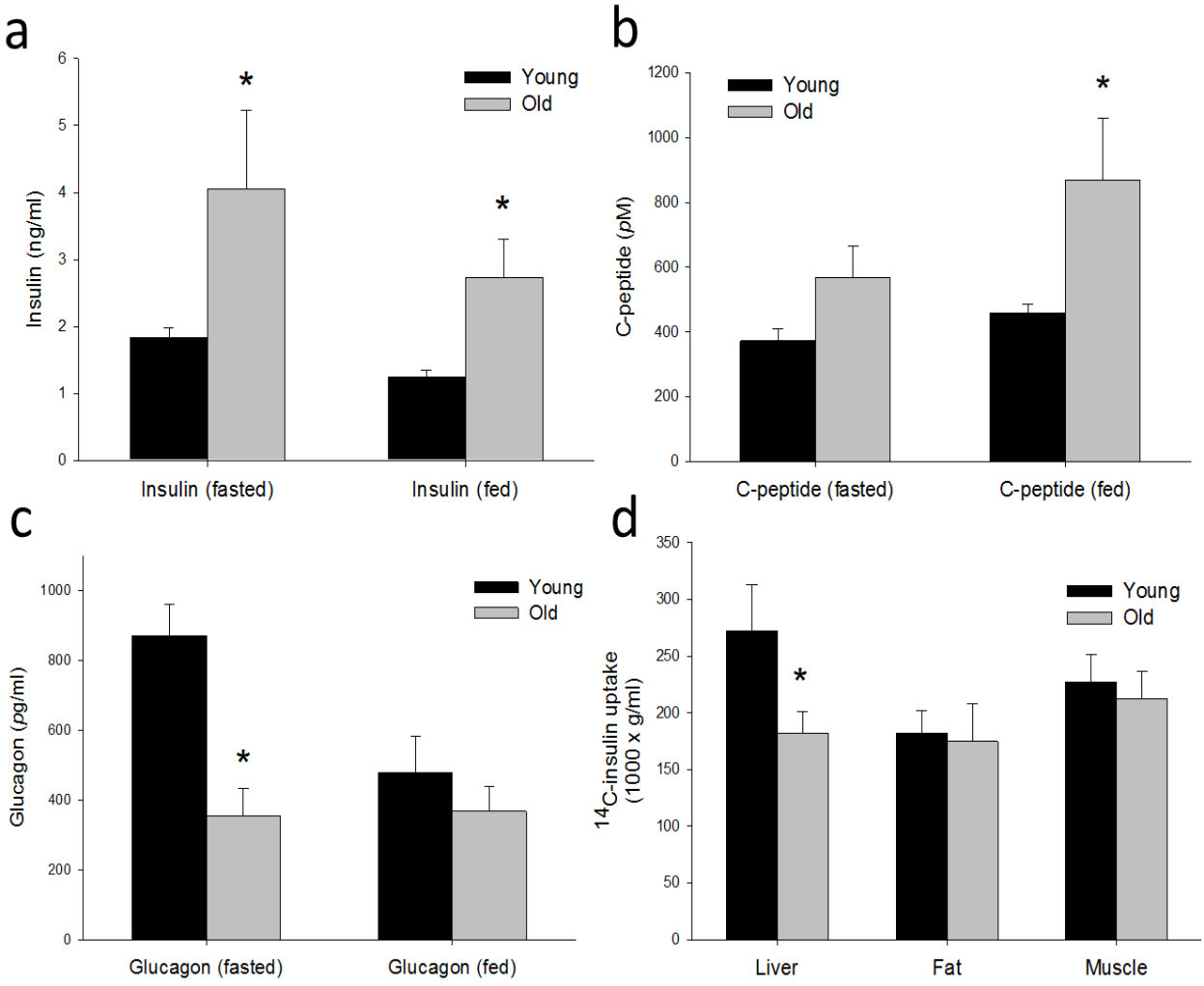

Figure 3.7: (a) Fasting and fed insulin levels were significantly elevated with age in C57/Bl6 mice (n = 6 young and 5 old C57/Bl6 mice, $P < 0.05$). (b) C-peptide levels were significantly elevated with age in the fed state (n = 4 young and 5 old C57/Bl6 mice, $P = 0.02$) and (c) Glucagon levels were supressed in the fasting state in old mice (n = 6 young and 5old C57/Bl6 mice, $P = 0.02$). (d) ^{14}C labelled insulin uptake by the liver was significantly reduced with age, but remained constant in muscle and fat (n = 10 young and 10 old C57/Bl6 mice, $P < 0.05$).

3.3.3.2 Glucose tolerance and tracer uptake

Despite impaired hepatic insulin uptake associated with defenestration, glucose tolerance tests conducted on the 3 month and 24 month old mice showed no impairment with age and in fact tended to be lower (Fig. 3.8a).

However, because of the very high insulin levels, the homeostatic model assessment index for insulin resistance (HOMA-IR), which is calculated from the fasting glucose-insulin product, was increased by more than two-fold in the old mice, indicating insulin resistance (Fig. 3.8b).

To further determine which tissues were contributing to the insulin resistance, ^{14}C-glucose and ^{3}H-2-deoxyglucose and were administered during glucose tolerance tests and the uptake measured in muscle, white adipose tissue (WAT) and liver. The clearance of ^{14}C-glucose into glycogen was significantly reduced in liver but this was associated with a trend for an increase in muscle clearance (Fig 3.9a). In addition, there was significant increase in ^{3}H 2-deoxyglucose uptake, which is not a substrate for liver uptake and metabolism, in both muscle and fat with age (Fig 3.9b). The data indicate that the reduction in hepatic glucose uptake and hyperinsulinemia is associated with a compensatory age-related increase in glucose uptake in muscle and fat (as well as depleted glycogen stores, see below), thereby normalising the glucose tolerance test.

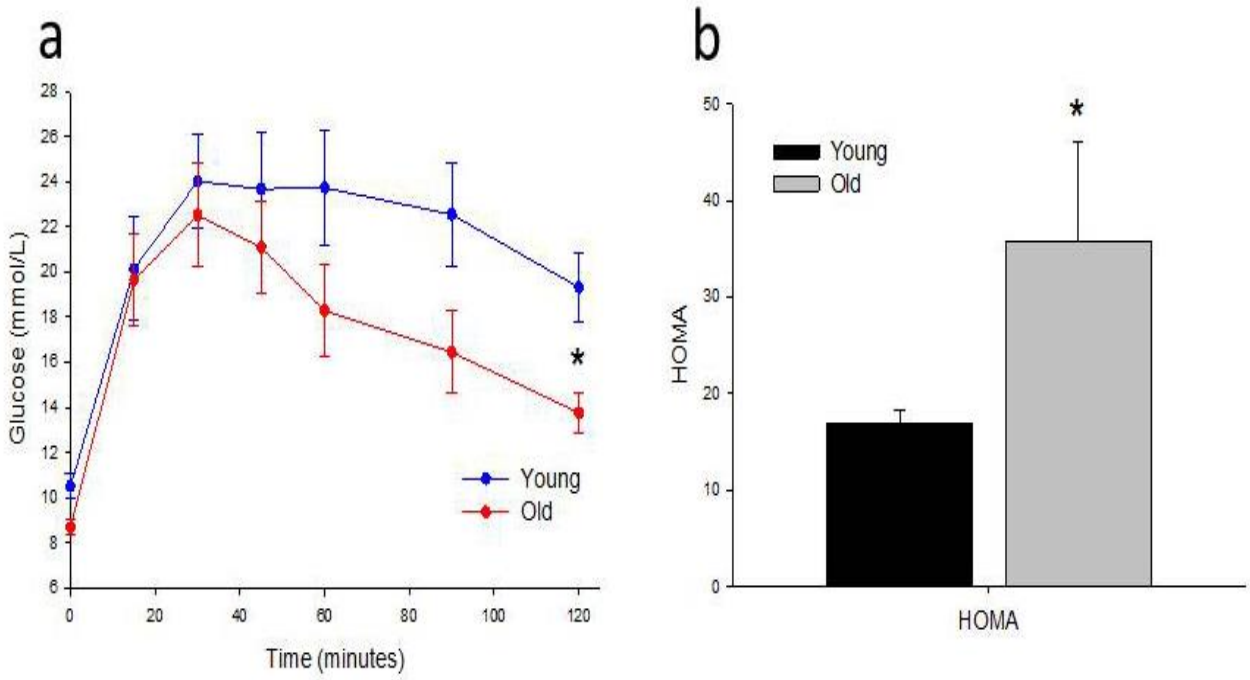

Figure 3.8: (a) Glucose tolerance was maintained in the hyperinsulinemic state seen with age in the C57/Bl6 mice (n = 8 young and 5 old C57/Bl6 mice). (b) The HOMA index was significantly increased with age reflecting the high insulin levels required with age to maintain glucose homeostasis (n = 6 young and 5 old C57/Bl6 mice, P = 0.03).

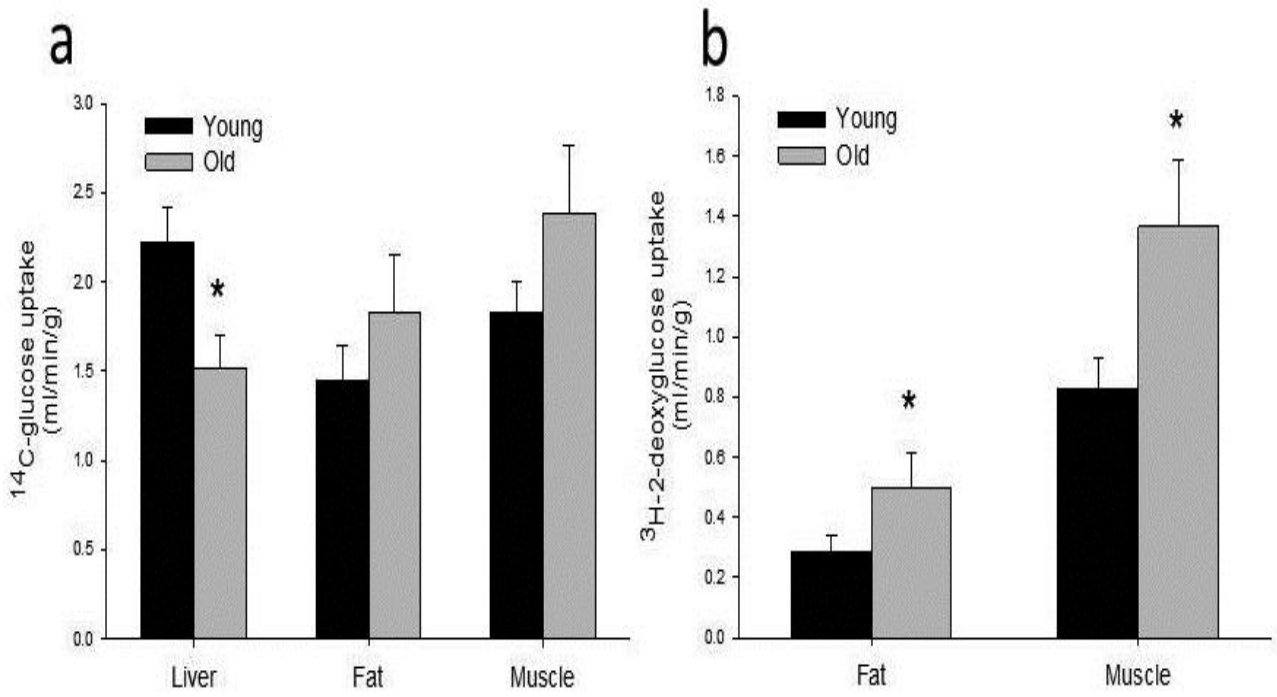

Figure 3.9: (a) There is a significant reduction in incorporation of ^{14}C labelled glucose into glycogen ($P < 0.05$) and a trend towards increased incorporation into glycogen by muscle and fat with age (n = 8 young and n = 5 old C57/Bl6 mice). (b) ^{3}H-2-deoxyglucose uptake into fat and muscle was significantly increased with age (n = 8 young and n = 5 old C57/Bl6 mice, $P < 0.05$).

Consistent with the selective impact of age-related defenestration on hepatic insulin sensitivity, hepatic glycogen storage measured by PAS staining showed a marked reduction in glycogen in the old animals (Fig. 3.10).

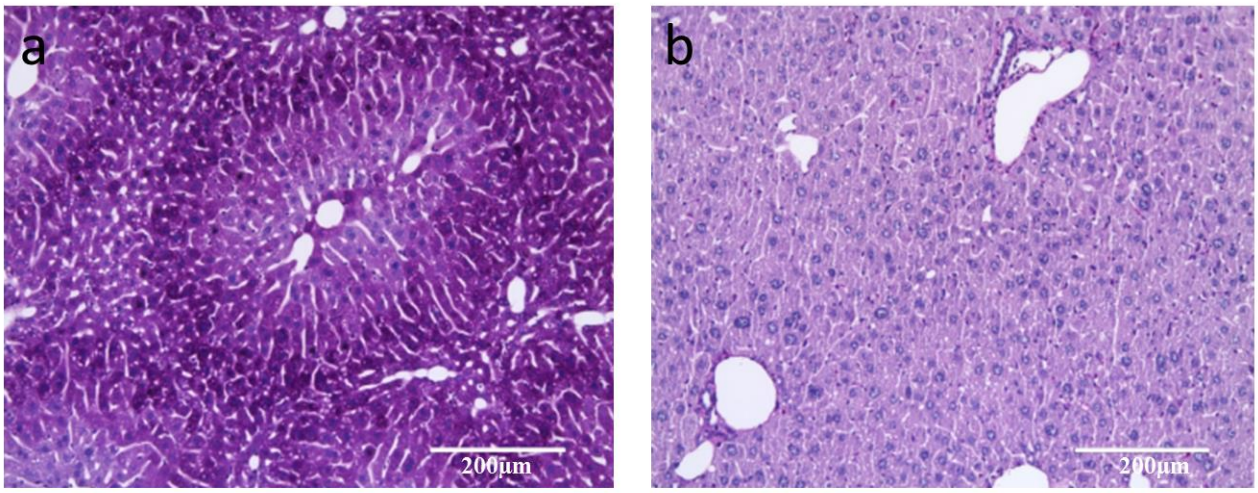

Figure 3.10: PAS staining of the liver in young (a) and old (b) mice showing significantly reduced glycogen storage with age (n = 8 young and n = 5 old mice).

3.3.3.3 Pyruvate tolerance

We also performed a pyruvate tolerance test (Fig. 3.11) to examine the impact of age on insulin-mediated inhibition of gluconeogenesis. Old age was associated showed a lower conversion of pyruvate to glucose. Although initially surprising, this is consistent with the observation that in rodents, some of the effects of insulin on hepatic gluconeogenesis are mediated via the brain, rather than a direct effect on hepatocytes (Rojas and Schwartz, 2014). Therefore age-related hyperinsulinemia will drive brain-mediated inhibition of gluconeogenesis even though its direct hepatic activity is reduced.

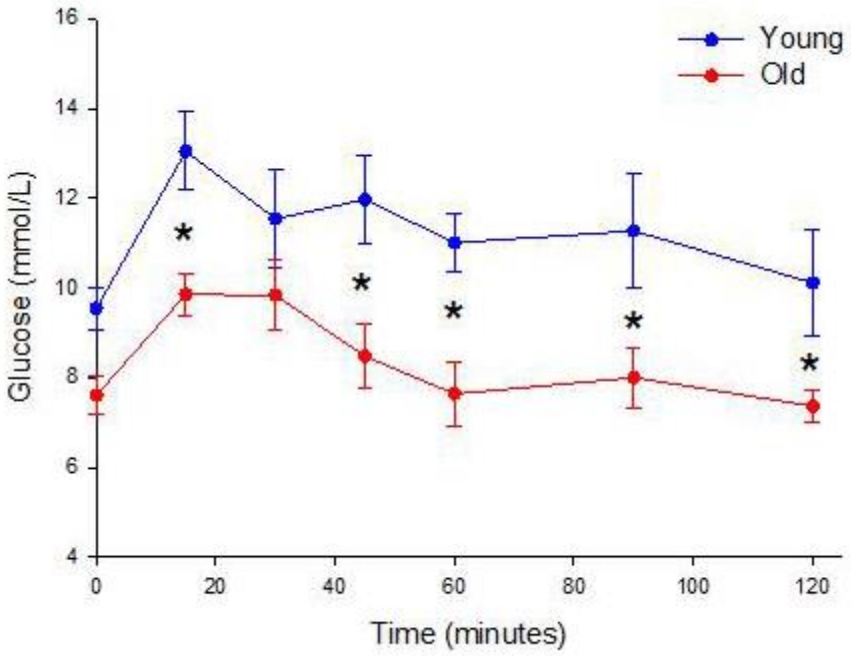

Figure 3.11: Pyruvate tolerance tests revealed impaired gluconeogenesis in the hyperinsulinemic setting seen with age (n = 8 young and n = 8 old C57/Bl6 mice, P = 0.003).

3.3.4 Reverse transcription and quantitative real time-PCR array analysis

To identify gene expression that might be altered by ageing, a quantitative RT-PCR (qRT-PCR) screening array for 84 key genes in the insulin signaling pathway was conducted (Appendix 2). Gene expression profiles showed no changes in insulin signaling pathway genes with age. Fatty acid synthase, a protein responsible for fatty acid synthesis was the only gene in this panel shown to be downregulated with age in the liver (p=0.02).

3.3.5 Proteomic studies

Western blot analysis revealed that phosphorylation of the hepatocellular insulin receptor substrate AKT was reduced in the old mice (Fig. 3a-b). To further probe phosphoprotein changes we utilised a large-scale, unbiased phosphoproteomic approach and liquid chromatography coupled to tandem mass spectrometry (LC-MS/MS) to identify changes in protein and phosphopeptide abundances, which enabled signal pathway mapping in liver tissues from young and old mice. LC-MS/MS of phosphopeptide-enriched samples identified 7,208 sites of phosphorylation (*n*=5,156 phosphopeptides from *n*=2,400 proteins), of which 1,580 were statistically significantly altered in abundance (*z*-score <-1.00 or >+1.00; Appendix 3). Non-phosphorylated peptides from the same samples were also identified and revealed only 281 proteins (*z*-score <-1.96 or >+1.96; Appendix 3) that were significantly altered in abundance, confirming that the major changes at the biochemical level between young and old mouse livers were those associated with signaling. We next specifically examined the set of altered phosphopeptides and used functional cluster analysis to identify Kyoto Encyclopaedia of Genes and Genomes (KEGG) pathways associated with ageing in the liver. Functional clusters contained within this dataset were compared against the mouse genome to determine their over-representation compared to background. The most over-represented KEGG pathways were ErbB (*p*-value 9.77 e^{-9}), neurotrophin (4.10 e^{-7}), GnRH (4.27 e^{-7}), MAPK (7.96 e^{-7}) and insulin (1.05 e^{-6}) signaling. The diversity of these pathways reflects the likely multifactorial nature of ageing, however changes associated with insulin signaling are consistent with reduced access of insulin to hepatocytes in old age. We next performed site-specific analysis of the phosphopeptides that were statistically significantly altered in aged livers by performing kinase recognition motif

analysis using MotifX. These data showed that the Akt recognition motifs R-X-R-X-X-pS and R-S-X-pS were enriched 11.5-fold and 10-fold respectively, compared with background in the dataset of peptides displaying reduced phosphorylation with ageing (Fig. 3.12c), which is consistent with the AKT Western blot data (Fig. 3.12a-b), and confirms a significant reduction in AKT signaling in aged livers. Motifs containing acidic residues, consistent with casein kinase 2 (CK2) activation were also enriched, however these were found in both the up- and down-regulated phosphopeptide datasets.

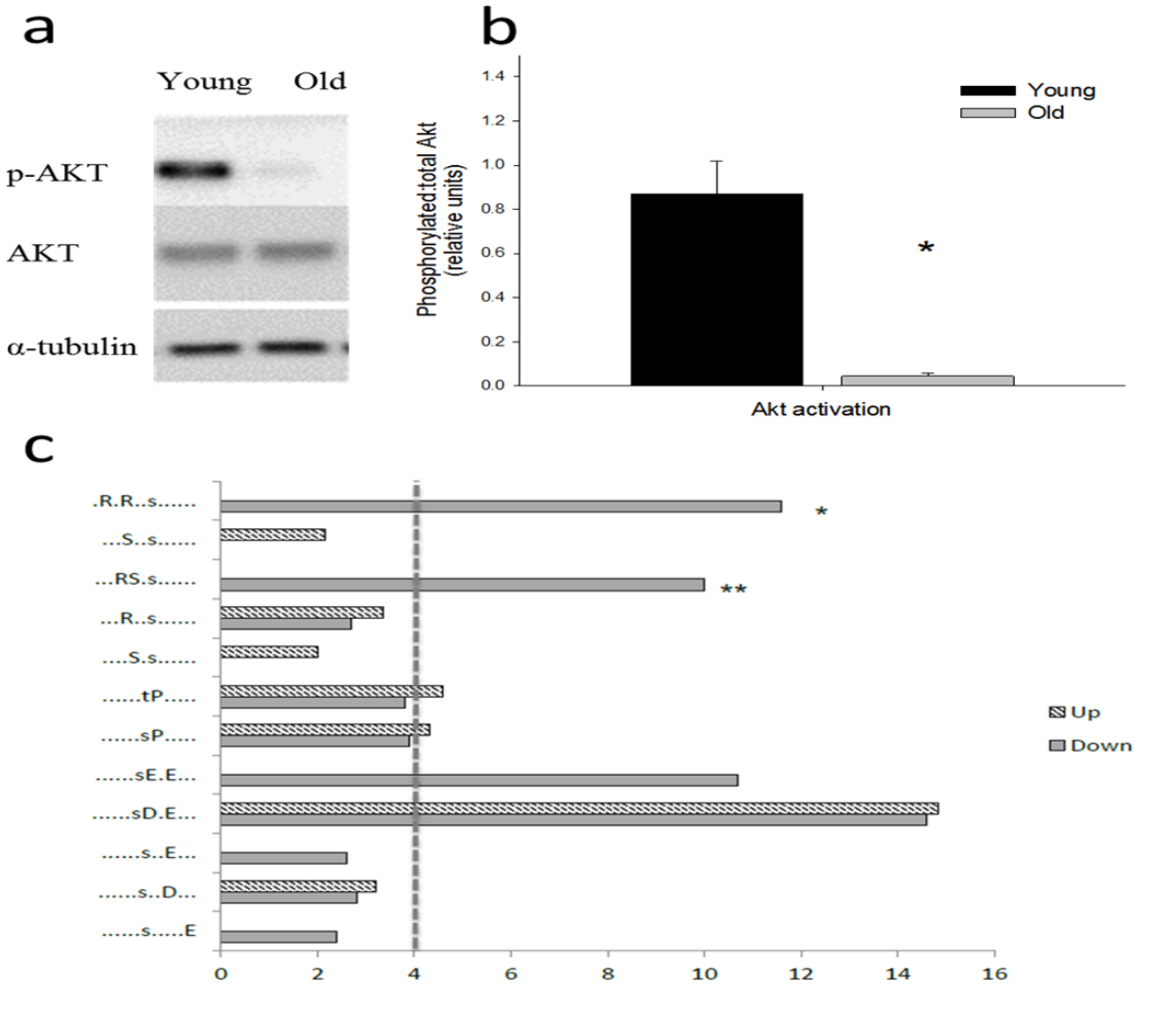

Figure 3.12: (a) Representative western blots of p-AKT and AKT showing significantly decreased phosphorylation of AKT in insulin stimulated old rat livers compared to young**.** (b) Densitometry analysis of phosphorylated: total AKT from western blots (n = 6 young and n = 6 old F344 rats, P = 0.002). (c) Fold over-representation of kinase recognition sequences from phosphoproteome analysis of young versus aged livers. Reduced Akt signaling is indicated by the prevalence of Akt recognition sequences * = 'R-x-R-x-x-pS' (11.5-fold) and ** = 'R-S-x-pS' (10-fold) in the set of phosphopeptides with reduced abundance in aged livers. Dotted line indicates cut-off for significant fold-change (>4-fold).

3.4 DISCUSSION

This study demonstrates that age-related defenestration of the LSEC restricts insulin access to the insulin receptor on the hepatocyte membrane through impaired transendothelial transfer. This resulted in hyperinsulinemia, impaired hepatic insulin signaling, depleted glycogen stores, compensatory increases in muscle and fat uptake of insulin and glucose and dysregulated gluconeogenesis. In fat and muscle, the blood vessels are the rate limiting step for the uptake of insulin (Majumdar et al., 2012, Sandqvist et al., 2011) The data show that under physiological conditions, the liver endothelium does not provide a barrier for the uptake of insulin which attests to its remarkable role in facilitating the transfer of substrates between blood and liver cells (Le Couteur et al., 2005) However, in conditions associated with structural changes in the LSECs, the liver blood vessels become a barrier for the transfer of insulin. This is a significant development in our understanding of insulin resistance seen with age and liver disease.

As we have previously reported, ageing is associated with significant defenestration of the LSECs (Cogger et al., 2006, Warren et al., 2011, Mitchell et al., 2010). Using the multiple indicator dilution methodology we have determined the disposition of insulin in perfused livers, and shown that ageing restricts access of insulin to the extravascular space. My laboratory has previously shown that defenestration associated with old age is mechanistically linked to reduced transendothelial transfer of other substrates including lipoproteins (Hilmer et al., 2005, Cogger et al., 2006) and both albumin-bound and dissolved medications (Mitchell et al., 2010, Le Couteur et al., 2005). Fenestration loss is also known to occur in streptozotocin-induced diabetic baboon and in rat models (McMahon et al., 2013, Jamieson et al., 2007a). Fenestrations appear to be an

important portal for the efficient transfer of many xeno- and endo-biotics (Cogger and Le Couteur, 2009). There was no change seen in glucose transfer across the LSEC with age, suggesting fenestrations are not a rate limiting step in glucose transfer across the endothelium to the hepatocellular membrane.

Accompanying the impaired transendothelial access of insulin to the hepatocytes, there were significant systemic changes including reduced hepatic insulin uptake and clearance, and increased insulin levels and insulin resistance. This was associated with insulin resistance as assessed by the HOMA-IR calculation, but surprisingly the glucose tolerance test was normal, or actually slightly improved in the aged mice. We propose that this might be secondary to the long term age-related compensatory effects on glucose uptake in muscle and fat, and the reduction in hepatic glycogen storage.

Despite elevated circulating insulin levels, ageing was associated with impairment of hepatic insulin signaling as measured by a full hepatic proteome screen using LCMS/MS and glycogen stores. The full proteome screen showed that the most age-related changes observed in the liver are at the biochemical level rather than due to protein expression changes. Western blot confirmed this with no change detected in protein levels but significant reductions seen in hepatic AKT phosphorylation in insulin-stimulated livers.

No age-related changes were found in the expression of genes associated with the insulin signaling pathway as measured by qRT-PCR. This further supports the suggestion that all

changes we are seeing in hepatic insulin signaling with age are occurring post translationally, which we propose is secondary to defenestration.

It has recently been postulated that the LSEC plays a significant role in insulin action in the liver. Tsuchiya et al. (2013) proposed a causal relationship for insulin resistance through LSEC mediated nitric oxide pathways (Tsuchiya and Accili, 2013). Raines et al. 2011 reported the effects of LSEC structure on insulin activity in a murine transgenic model with partial loss of platelet-derived growth factor-beta (PDGF-β) function. These mice developed highly permeable, disrupted LSECs as measured by transmission electron microscopy and *in vivo* FITC-dextran uptake (Raines et al., 2011). Such changes in the LSEC were associated with a dramatic increase in insulin action in the liver, evidenced by increased insulin signaling in liver, improved glucose tolerance tests, increased insulin clearance and an 80% reduction in circulating insulin levels despite euglycemia (Raines et al., 2011).

While this work clearly indicates that patent fenestrations are essential for efficient hepatic insulin uptake, clearance and signaling, there are some limitations in the study which require further investigation. Ageing is a multifactorial process during which the entire body undergoes significant adaptations and changes which all could play a role in overall metabolic homeostasis, but are not within the scope of this project. Further investigation of the role of LSEC defenestration in the absence of all other systemic age-related adaptations will further substantiate the key role of fenestrations in hepatic insulin transfer, which will be addressed in Chapter 4. A further limitation is the use of mixed rodent models. Australia does not presently hold an ageing rat or mouse facility, all animals used were acquired through the National

Institutes of Ageing, USA. The combination of rats for the MIDs and proteomics and mice for all of the metabolic parameters was a decision made to allow the most rigorous probing of the role of fenestrations in hepatic insulin uptake. Ageing rats are considerably more expensive and more difficult to obtain than ageing mice but are essential for technically sound MID experiments, animal usage was prioritised on the grounds of these considerations. The combination of rats and mice was well considered and this is not thought to reduce the novelty or validity of the findings. Furthermore, defenestration as a result of ageing is well established in both the mouse and rat models used within this study, thus we believe that our results are valid despite this limitation.

In conclusion, defenestration of the LSECs provides a novel mechanism that contributes to insulin resistance associated with advanced age and potentially other conditions associated with loss of fenestrations such as chronic liver disease. Maintaining the structural integrity of the LSECs is a potential therapeutic target for insulin resistance in old age.

CHAPTER 4: P407 INDUCED DEFENESTRATION AND HEPATIC INSULIN AND GLUCOSE DISPOSITION

4.1 INTRODUCTION

It is recognised clinically and experimentally that many conditions associated with impaired hepatic microcirculation such as ageing, cirrhosis, non-alcoholic fatty liver disease are also associated with impaired insulin handling by the liver (Chai et al., 2014, Fink et al., 1983, Kawaguchi et al., 2011, Muller et al., 1992). One of the hallmark changes of the liver microcirculatory system in ageing and cirrhosis is the loss of liver sinusoidal endothelial cell (LSEC) integrity with defenestration, endothelial thickening and deposition of basal lamina (Le Couteur et al., 2001, McLean et al., 2003). The importance of the impacts of these changes on substrate exchange between the blood and hepatocyte is gaining recognition (Furrer et al., 2011, Lesurtel and Clavien, 2014).

In Chapter 3 it was shown that age-related defenestration is causally associated with impaired hepatic insulin transfer and subsequent signaling and control. The results in Chapter 3 strongly supported the key role of fenestrations in insulin transfer from the sinusoidal blood vessels to the hepatocellular membrane and the insulin receptor. However, it is recognised that ageing is a multifactorial process where many fundamental cellular processes are affected and considerable adaptations develop overtime to support metabolic homeostasis.

Given the complexity of ageing, testing the role of LSEC fenestrations in insulin transfer in a singular model of defenestration is important. One model for testing the acute effects of loss of fenestrations (‘defenestration’) on liver function is poloxamer 407 (P407). This is a non-ionic surfactant that causes marked defenestration of the LSEC without the development of fibrosis

(Warren et al., 2011, Cogger et al., 2006). Defenestration induced by P407 has been shown to impair the transendothelial transfer and hepatic clearance of several substrates including lipoproteins, acetaminophen and diazepam (Cogger et al., 2006, Mitchell et al., 2010, Mitchell et al., 2012). Here P407 was used to determine whether acute defenestration interferes with the hepatic disposition and action of insulin and whether this has any systemic implications. This would also provide further evidence that defenestration is a mechanism for the development of hepatic insulin resistance and hyperinsulinemia.

4.2 METHODS

4.2.1 Animals and P407 treatment

Male Fischer 344 rats aged 8-10 weeks and weighing 200 g were obtained from Animal Research Centre (Perth, Australia). The animals were allowed free access to water and standard chow. The treatment group received an intraperitoneal injection (i.p.) of P407 (1 g/kg, BASF Ltd, Southbank, Australia) 24 hrs prior to liver perfusion, prepared by mixing with normal saline and kept in liquid form at 4 ºC. Control animals included those that received a volume-matched i.p. injection of normal saline or were untreated. There were no differences between control animals given saline or no treatment, therefore their data were pooled. All animals were treated in accordance with Animal Care guidelines. This study was approved by the Sydney Local Health District Animal Welfare Committee (AWC Protocol #2012/005A).

4.2.2 Liver perfusion and multiple indicator dilution method

This procedure is described in detail in sections 2.3.2, 2.3.3 and 3.2.2.

4.2.3 Blood analysis

Prior to liver perfusion, approximately 1 ml blood was taken from the inferior vena cava (IVC) during surgery and transferred into an EDTA tube, followed by processing and analysis as described in section 2.7.1.

4.2.4 Scanning electron microscopy

Liver tissue was perfused for scanning electron microscopy for measurement of intact endothelial fenestrations as described in 2.2.2.

4.2.5 Metabolic parameters

4.2.5.1 Glucose tolerance and tracer uptake

Animals were fasted for 6 hrs, followed by administration of glucose (2 g/kg i.v.) spiked with 10 µCi ^{14}C-glucose for assessment of insulin action in liver, fat and muscle and 10 µCi ^{3}H-2-deoxyglucose for assessment of glucose uptake in fat and muscle as described in 2.6.2.

4.2.5.2 Insulin uptake

Whole body insulin extraction was performed in another batch of rats, where ^{14}C-insulin (1 µCi/g) was injected via the inferior vena cava of anesthetised animals as described in 2.6.3.

4.2.5.3 Pyruvate tolerance

A third cohort of P407 and control animals were fasted for 6 hours prior to an i.p injection of pyruvate (2 g/kg; Sigma Aldrich, Castle Hill Australia) and glucose levels were read using a handheld glucose meter as described in section 2.6.6.

4.2.6 Histology

Liver tissue was fixed in 4 % paraformaldehyde, paraffin embedded, sectioned and subjected to H&E and PAS staining, followed by observation as described in section 2.3.2.

4.2.7 Reverse transcription and quantitative real time-PCR array analysis

Total RNA was isolated from liver tissue samples using a RNeasy Plus Mini Kit (Qiagen Pty Ltd, Chadstone, Australia), followed by subsequent reverse transcription and real time-PCR as described in section 2.8.

4.2.8 Proteomic studies

4.2.8.1 Mass Spectrometry

Mass Spectrometry was performed as described in Section 2.6.1. Bioinformatic analysis was performed to reveal pathways associated with P407 treatment using STRING (Jensen et al., 2009, Franceschini et al., 2013, Szklarczyk et al., 2011) and KEGG (Kanehisa and Goto, 2000, Kanehisa et al., 2014) pathway analysis.

4.2.8.2 Western Blots

Frozen liver tissue samples were processed as described in section 2.6.2. The protein extract were subjected to immunoblotting according to protocol as described previously (Hoehn et al., 2008). Antibodies against the following proteins were used: phospho-IRS-1 (Ser612, Cat#2386), IRS-1 (Cat#2382), phospho-mTOR (Ser2448, Cat#2971), mTOR (Cat#2972), IRS-2 (Cat#4502) and α-tubulin (Cat#2144) (Cell Signaling Technology, Arundel, Australia).

4.2.9 Data analysis

Data analysis was performed using Microsoft Excel. All values are expressed as the mean ± SEM. Statistical significance was calculated using two-tailed Student's T test and Pearson's Product Moment correlation coefficient (Sigmaplot v11, Systat Software, Germany).

4.3 RESULTS

4.3.1 Histology, blood analysis and Electron Microscopy

At 24 hr following P407 treatment, blood samples were observed to be lipemic. Blood analysis showed a significantly higher serum cholesterol and triglycerides in the treated group compared to control (Fig. 4.1a) with no difference in aspartate transaminase (AST) and alanine transaminase (ALT) levels between groups (Fig. 4.1b). Post mortem examination of the whole animal and haematoxylin and eosin staining of liver sections from the control and P407 animals confirmed all animals included in the study were free of gross and liver pathology (Fig. 4.2).

Scanning electron microscopy (Fig. 4.3) was performed to confirm P407 induced defenestration of the LSEC that has previously been described (Mitchell et al., 2012, Warren et al., 2011, Cogger et al., 2006). LSEC morphology was analysed as described in Table 4.1. P407 administration led to reduced fenestration diameter and porosity. These findings are consistent with previous studies (Warren et al., 2011, Cogger et al., 2006).

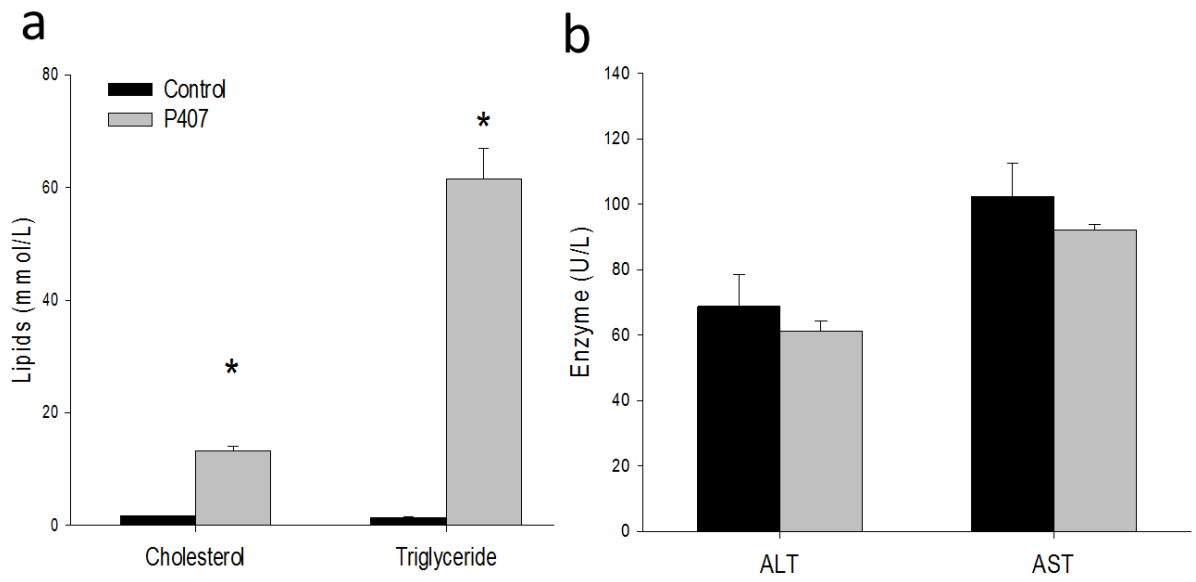

Figure 4.1: Blood analysis of serum (a) lipid and (b) liver function parameters for control and P407 treated rats. Blood cholesterol and triglycerides were markedly increased 24 hours after P407 administration (* P<0.001) while serum ALT and AST is similar between groups. Data is presented as mean ± SEM, n = 5 control and n=5 P407 treated F344 rats.

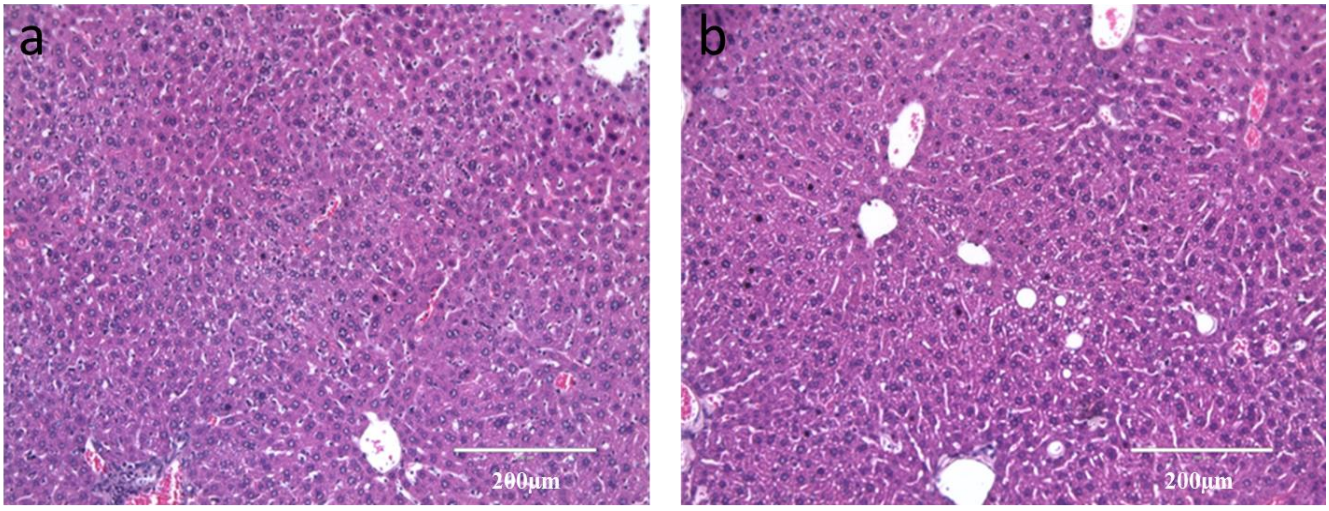

Figure 4.2: Representative Haematoxylin and Eosin staining of (a) control and (b) P407 F344 rats. No signs of pathology were found.

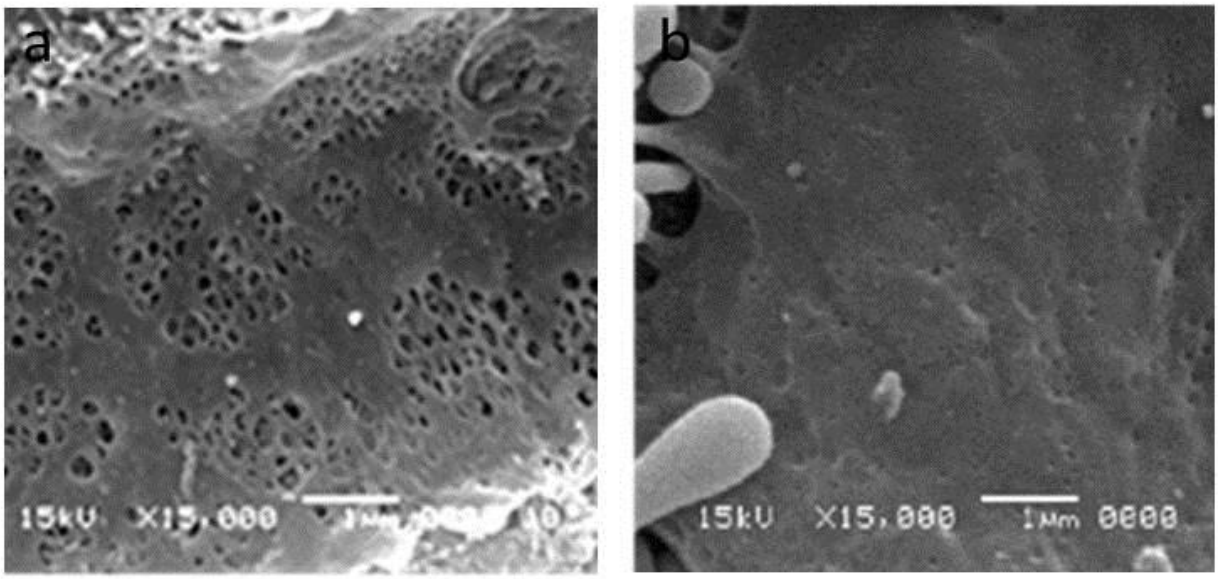

Figure 4.3: Representative Scanning electron micrographs of the perfused the LSEC in (a) control and (b) P407 F344 rats. Significant defenestration is observed with P407 administration. Original micrographs taken at 15000 × magnification**.**

Table 4.1: Quantification of the LSEC fenestrations. There is decreased liver porosity in P407 treated group (P=0.02). Data is presented as mean ± SEM.

Animal group	**n**	**Porosity (%)**	**Diameter (nm)**	**Frequency (per um^2)**
Control n = 10	5	5.44±0.5	104.5±3.5	3.68±0.2
P407-treated n = 11	5	3.64±0.5*	85±4.3	4.04±0.3

4.3.2 P407 induced defenestration impairs the access of insulin and glucose to the extracellular space of the liver

To further probe the relationship between defenestration of the liver endothelium and insulin resistance, MIDs were performed on livers from rats treated with P407 and their matched controls. Outflow insulin curves from the MID experiments are shown in Fig. 4.4.

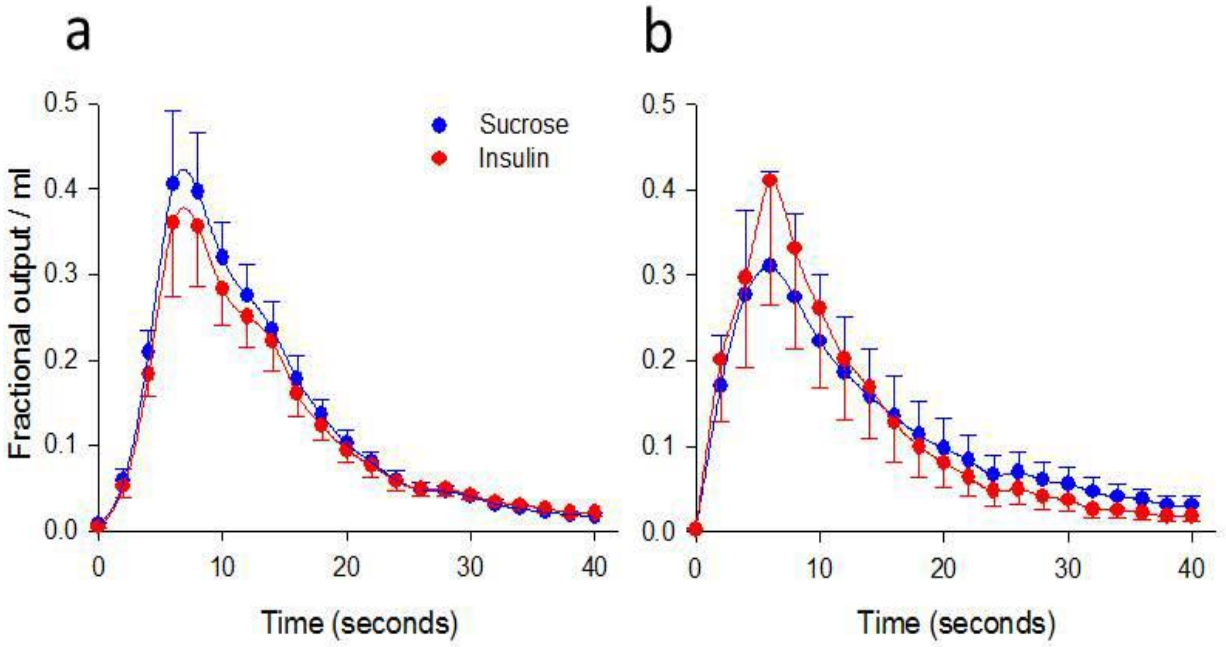

Figure 4.4: Average MID outflow curves for insulin and the extracellular marker sucrose (n=12 control and n=8 P407). Insulin exits the liver after sucrose in (a) control rats whereas the order is reversed in the (b) P407 animals indicating restricted access to the extracellular space with acute defenestration.

In control animals, the insulin curve overlaps the sucrose curve (Fig. 4.4a), indicating that insulin has unimpeded access to the entire extracellular ('sucrose') space. Following P407 treatment, the

insulin curve appears earlier than the sucrose curve (Fig. 4.4b), indicating that insulin has a smaller volume of distribution than sucrose. The recovery and apparent volume of distribution of insulin and tracers are shown in Table 4.2. There was no difference in the recovery of Evans Blue or sucrose between groups. Analysis of the curves showed that P407 was associated with a significant reduction in the volume of distribution of insulin, normalised to sucrose volume, of about 20 % (Fig. 4.5, $P<0.05$). P407 induced defenestration was associated with a trend towards higher recovery of insulin (75 ± 10% controls *vs* 86 ± 4% P407-treated).

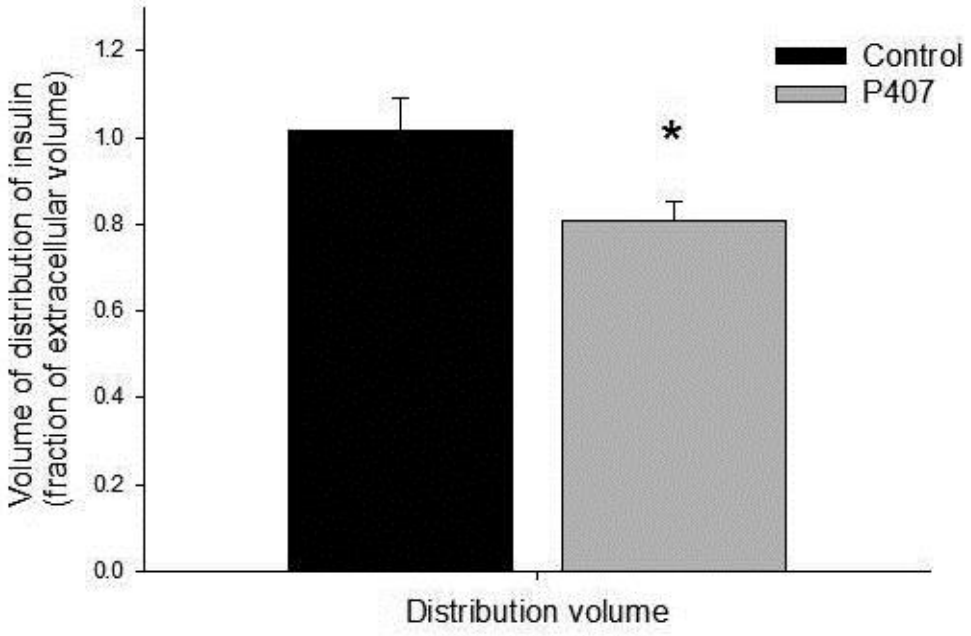

Figure 4.5: There was a 20 % reduction in the fractional volume of distribution of insulin with acute defenestration (n = 12 control and n= 8 P407 F344 rats, P = 0.01).

Table 4.2: The effect of P407 on recovery and volume of distribution (Vd) of Evans blue, insulin and sucrose. * P<0.05.

	Control (n=12)	**P407 (n=8)**
Fractional recovery	value	value
Evans blue	0.83±0.08	0.77±0.07
Insulin	0.78±0.07	0.83±0.05
Sucrose	0.93±0.06	0.83±0.05
Vd (ml/g)		
Evans blue	0.25±0.02	0.23±0.03
Insulin	0.27±0.03	0.23±0.03
Sucrose	0.26±0.03	0.29±0.04
Ratio		
Insulin/Evans blue	1.07±0.09	0.97±0.05
Insulin/Sucrose	1.02±0.07	0.81±0.04*

There was a similar trend seen with the glucose outflow curves (Fig 4.6). In control animals the glucose curves were delayed compared with the sucrose curves (Fig. 4.6a), indicating that in normal livers, glucose has access to the entire extracellular space and enters the hepatocytes as well. Following P407 treatment, the glucose curves appear earlier than seen in the control experiments (Fig. 4.6b), indicating a reduction in its volume of distribution. Analysis of the curves for recovery and volume of distribution are shown in Table 4.3. There was no difference in the recovery of Evans Blue, glucose or sucrose between both groups. The ratio of volume of

distribution of glucose compared to Evans Blue was not influenced by P407. However, there was a reduction in the volume of distribution of glucose compared to sucrose. Analysis of the curves showed that P407 was associated with a significant reduction in the volume of distribution of glucose, normalised to sucrose volume, of about 24 % (Fig. 4.7, $P<0.05$).

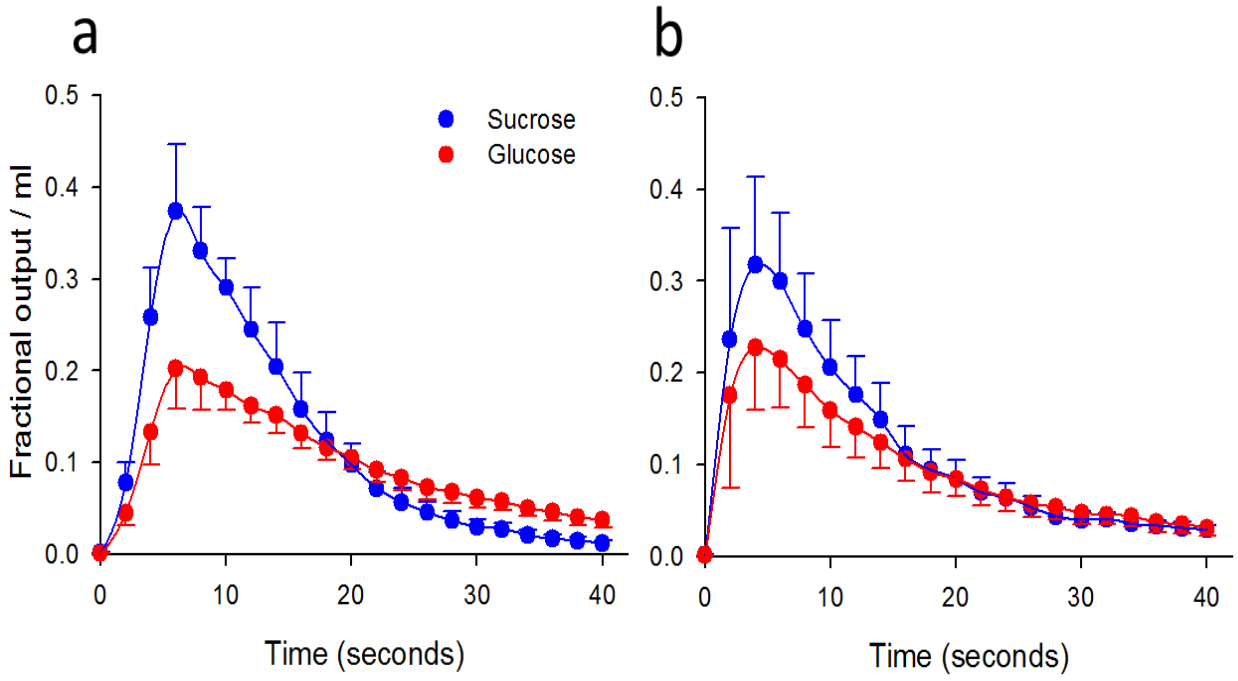

Figure 4.6: Average MID outflow curves for glucose and the extracellular marker sucrose. Glucose exits the liver after sucrose for both **a.** control and **b**. P407 rats, with P407 rats shows an earlier appearance of glucose compared to control.

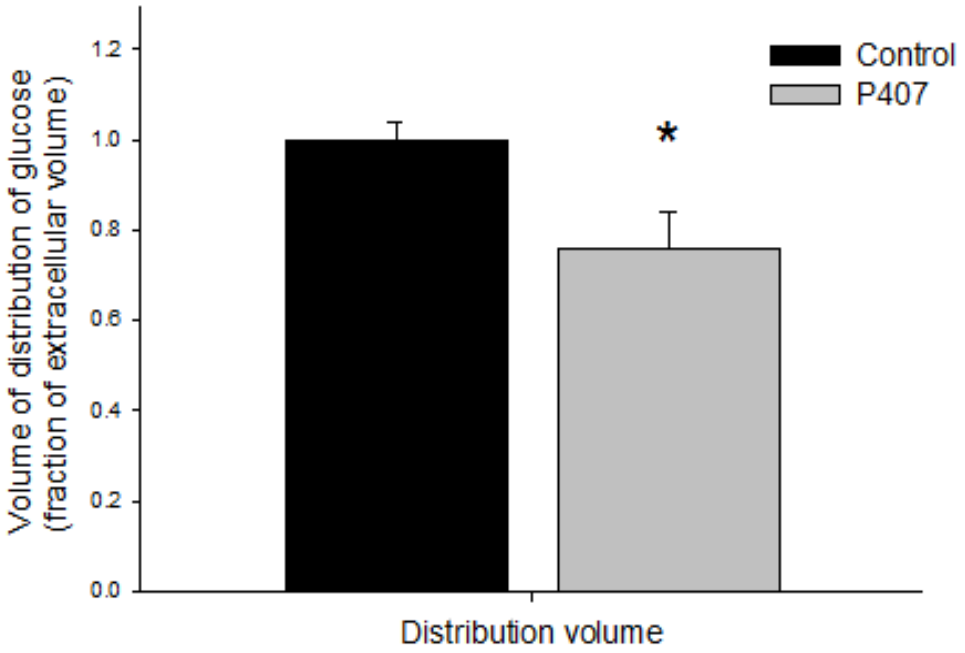

Figure 4.7: There was a 24 % reduction in the fractional volume of distribution of glucose with acute defenestration (n = 12 control and n= 8 P407 F344 rats, P = 0.01).

Table 4.3: The effect of P407 on recovery and volume of distribution (Vd) of Evans blue, glucose and sucrose

	Control (n=12)	P407 (n=8)
Fractional recovery		
Evans blue	0.87±0.07	0.73±0.09
Glucose	0.82±0.05	0.71±0.09
Sucrose	0.89±0.04	0.82±0.1
Vd (ml/g)		
Evans blue	0.24±0.02	0.22±0.03
Glucose	0.37±0.04	0.31±0.05
Sucrose	0.25±0.02	0.29±0.06
Ratio		
Glucose/Evans blue	1.56±0.06	1.34±0.10
Glucose/Sucrose	1.50±0.06	1.10±0.10*

4.3.3 Metabolic parameters

4.3.3.1 Insulin levels and systemic metabolism

Impaired hepatic uptake of insulin due to P407 induced defenestration led to significantly elevated basal and fed insulin levels in the P407 rats when compared to their control counterparts (Fig. 4.8a).

The elevated circulating insulin was not due to increased insulin secretion by the pancreas as shown in Fig. 4.8b. C-peptide levels were unchanged in the P407 group during the fasted state, indicating that hyperinsulinemia is established through reduced clearance of insulin by the liver rather than increased pancreatic insulin secretion. In the fed state, C-peptide levels increased in the control animals while remaining steady in the P407 animals, reflecting impaired secretion of insulin in the acutely defenestrated animal. Glucagon levels were significantly lower in the P407 compared to the control mice when fasting (Fig. 4.8c).

Whole body insulin handling assessed by intravenous injection of ^{14}C-insulin revealed that insulin uptake by the liver was reduced by 20% in P407-treated animals (Fig. 4.8d $P=0.04$), but was unchanged in muscle and fat.

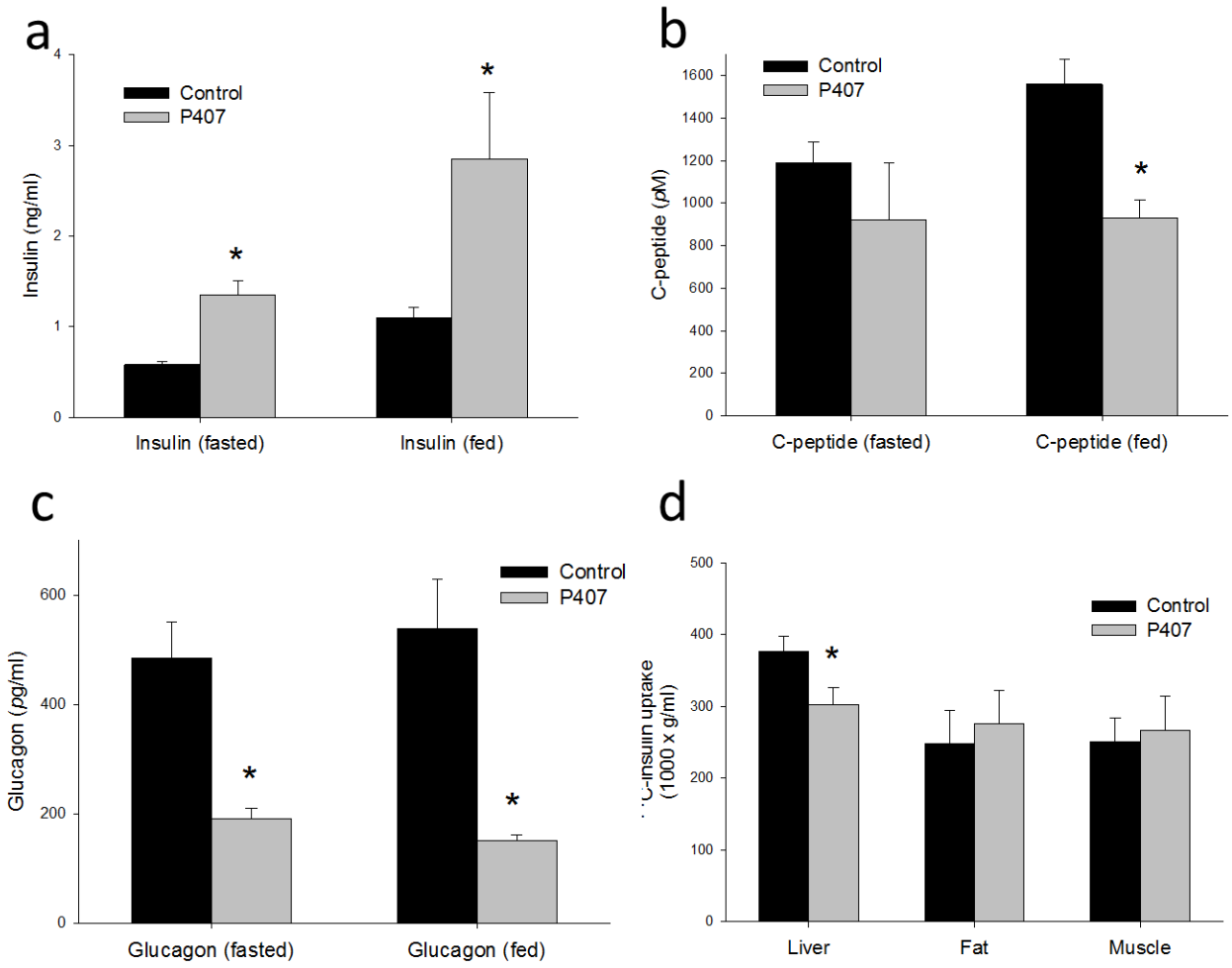

Figure 4.8: (a) Fasting and fed insulin levels were significantly elevated following P407 induced defenestration (n = 6 control and 6 P407 F344 rats, fasting $P < 0.05$, fed $P = 0.005$). (b) C-peptide levels were significantly decreased with P407 induced defenestration in the fed state (n = 5 control and 5 P407 F344 rats, $P = 0.03$) and (c) Glucagon levels were supressed in the fasting and fed states in P407 treated rats (n = 4 control and 4 P407 F344 rats, fasting $P = 0.02$, fed, $P = 0.16$). (d) ^{14}C labelled insulin uptake by the liver was significantly reduced with defenestration, but remained constant in muscle and fat (n = 6 control and 6 P407 F344 rats $P = 0.04$).

4.3.3.2 Glucose tolerance and tracer uptake

To determine whether altered hepatic disposition of insulin had any effect on systemic glucose metabolism, we performed glucose tolerance tests. The incremental area under the curve (iAUC), calculated from the glucose tolerance curve (Fig. 4.9a, n=13 controls n=10, P=0.04). indicated impaired glucose tolerance in the P407 animals Further, because of the very high insulin levels, the homeostatic model assessment index for insulin resistance (HOMA-IR), which is calculated from the fasting glucose-insulin product, was increased by more than two-fold in the P407 mice, indicating insulin resistance (Fig.. 4.9b).

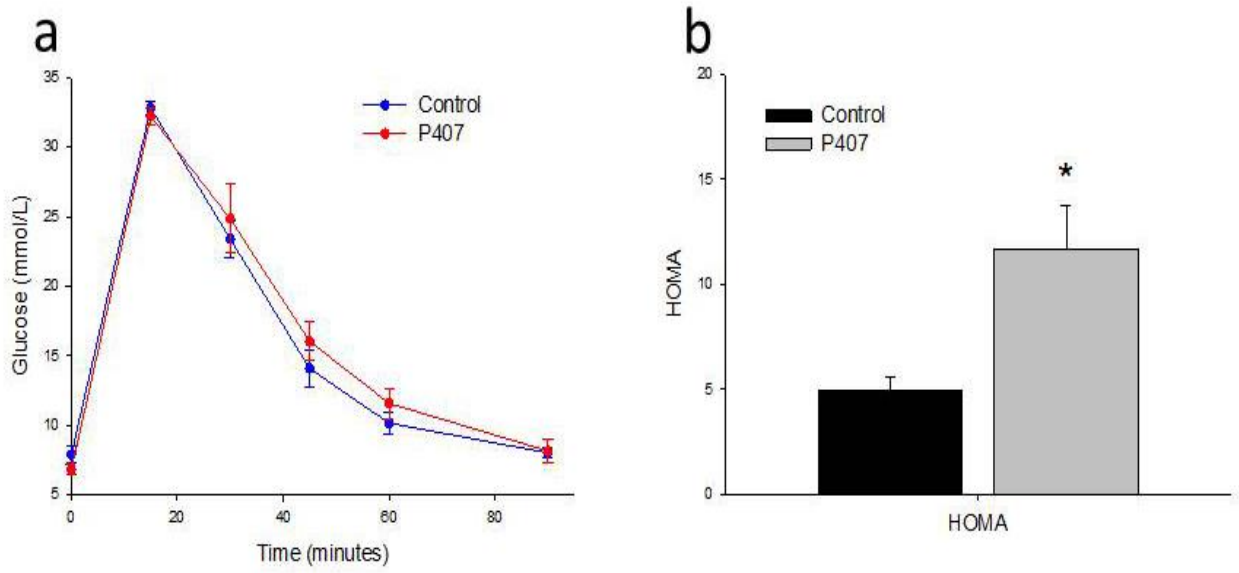

Figure 4.9: (a) Glucose tolerance curve of control and P407 rats. The iAUC calculated the curve was increased by P407-induced defenestration (n = 10 control and 8 P407 F344 rats). (b) The HOMA-IR index was significantly increased by P407 induced defenestration (n = 6 control and 6 P407 F344 rats, P = 0.002)

To further determine which tissues were contributing to the insulin resistance, ^{14}C-glucose and ^{3}H-2-deoxyglucose and were administered during glucose tolerance tests and the uptake measured in muscle, WAT and liver. The incorporation of ^{14}C-glucose into glycogen was significantly reduced in liver of P407 treated rats with no change in WAT or muscle incorporation (Fig. 4.10a). There was no change in ^{3}H 2-deoxyglucose uptake, which is not a substrate for liver uptake and metabolism, in both muscle and fat with P407 treatment (Fig. 4.10b). The data indicate that the reduction in hepatic glucose incorporation into glycogen and hyperinsulinemia lead to abnormal glucose tolerance in acutely defenestrated rats.

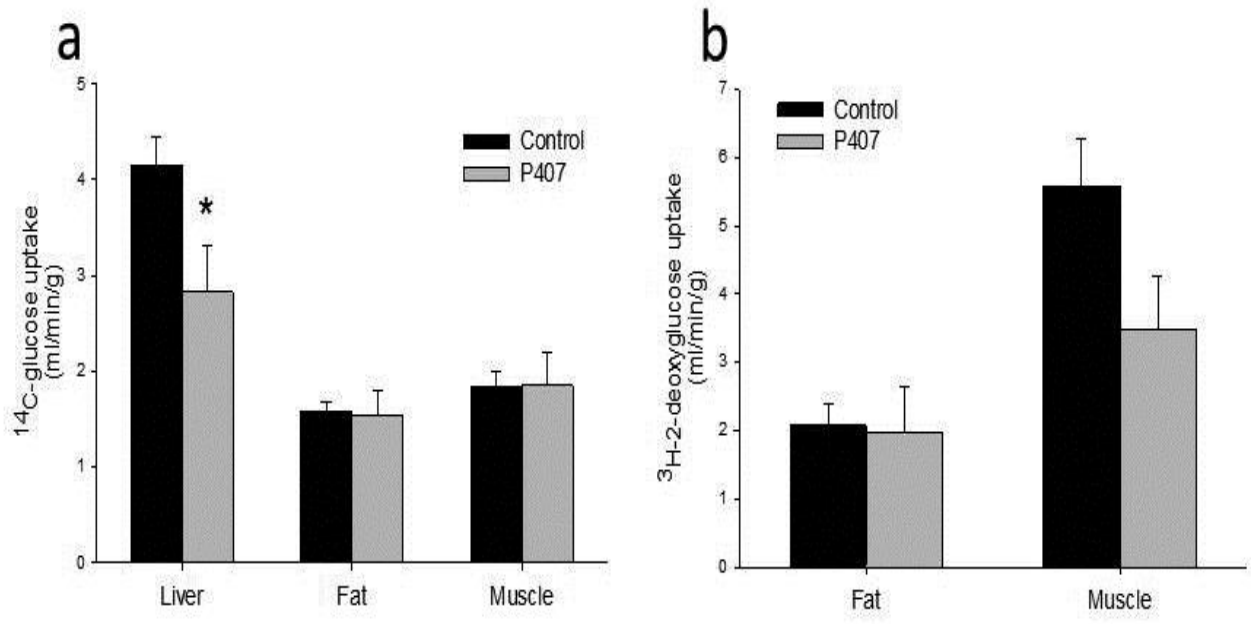

Figure 4.10: (a) There was a significant reduction in hepatic incorporation of ^{14}C labelled glucose into glycogen, with no change in muscle and fat incorporation (n = 10 control and 8 P407 F344 rats, $P < 0.05$). (b) ^{3}H-2-deoxyglucose uptake into fat and muscle was unchanged following P407 treatment, although muscle uptake was more pronounced in P407 but it is not significant (n = 10 control and 8 P407 F344 rats, $P = 0.06$).

Consistent with the significant impact of acute defenestration on hepatic insulin sensitivity and glucose homeostasis hepatic glycogen storage measured by PAS staining showed a marked reduction in glycogen in the P407 animals (Fig. 4.11).

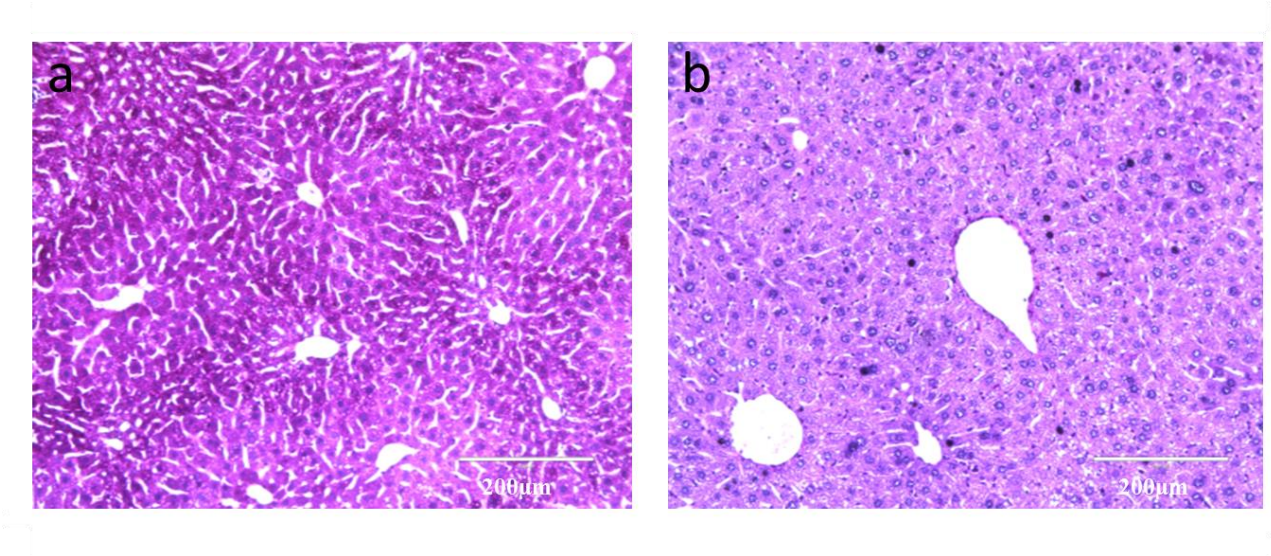

Figure 4.11: PAS staining of the liver in (a) control and (b) P407 treated rats showing significantly reduced glycogen storage with defenestration (n = 10 control and 8 P407 F344 rats).

4.3.3.3 Pyruvate tolerance

The pyruvate tolerance test demonstrated a paradoxical reduction in gluconeogenesis in P407 rats upon injection of pyruvate as a substrate for gluconeogenesis (Fig. 4.12). MID experiments were further conducted and the results showed that pyruvate disposition was not restricted by loss of fenestrations (Appendix 4, Vd: 1.64 ± 0.1 ml/g n=6 controls *vs* 1.58 ± 0.1 ml/g n=6 P407 treated). This indicates that reduced gluconeogenesis associated with P407 is not caused by the effects of defenestration on pyruvate uptake.

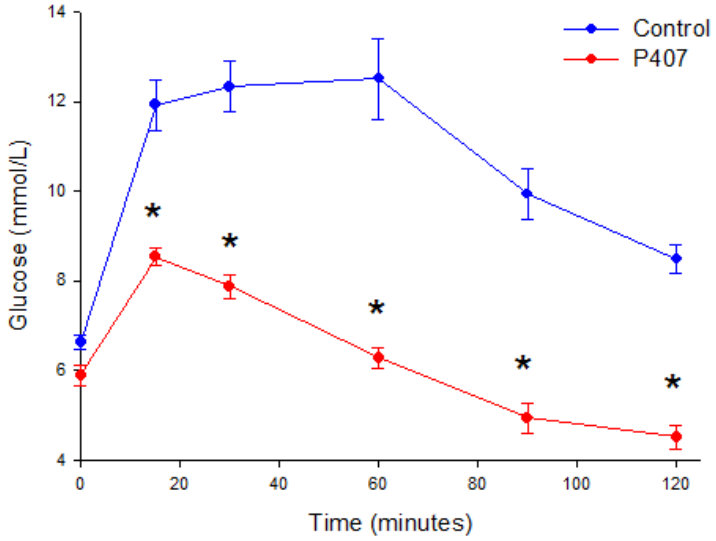

Figure 4.12: Pyruvate tolerance tests revealed impaired gluconeogenesis in the hyperinsulinemic setting (n = 13 control and 9 P407 F344 rats, $P < 0.05$).

4.3.4 Reverse transcription and quantitative real time-PCR array analysis

To identify gene expression that might be altered by reduced transendothelial access of insulin to the hepatocyte insulin receptor, a qRT-PCR screening array for 84 key genes in the rat insulin signaling pathways was conducted (Appendix 5). As outlined in Table 4.4 gene expression profiles showed that IRS-2 was upregulated (1.76-fold; p=0.02) and thyroglobulin, which has a role as secondary effector target genes for insulin signaling was downregulated (1.88-fold; p=0.01, Table 4.4). There was also upregulation of leptin coding gene Cebpa that is a primary target gene for insulin signaling (6.08-fold) and downregulation of G6pc gene involved in glucose and glycogen metabolism (3.53-fold), but this was not significant.

Table 4.4: Significant changes in PCR array profiles with following administration of P407 in rats.

Symbol	Gene name	Up or down regulation	p value
Irs2	Insulin receptor substrate 2	1.76	0.02*
Tg	Thyroglobulin	-1.88	0.018*
Cebpa	CCAAT/enhancer binding protein (C/EBP), alpha	6.08	0.95
G6pc	Glucose-6-phosphatase, catalytic subunit	-3.53	0.84

4.3.5 Proteomic studies

Western blot analysis revealed that phosphorylation of IRS-1, the phosphorylation target of the activated insulin receptor, was significantly reduced by over 50% in P407 rats as compared to controls (0.98 ± 0.3 n=9 controls *vs* 0.4 ± 0.10 n=10 P407-treated, $P<0.05$). Conversely, the expression of total IRS-2 protein was increased in the P407 rats (0.21 ± 0.03 n=4 controls *vs* 0.78 ± 0.06 n=4 P407-treated, $P<0.05$). There is no difference in the phosphorylation of mTOR which is involved in downstream insulin signaling (Fig 4.13a-c).

We again utilised large-scale phosphoproteomics to determine the effects of P407 on hepatic cell signaling pathways, which further highlighted loss of fenestration-specific effects without the multi-factorial processes involved in ageing. LC-MS/MS identified 1,480 sites of phosphorylation that were statistically significantly altered in abundance (*z*-score <-1.00 or > +1.00; Appendix 3). Analysis of non-phosphorylated peptides revealed only 189 proteins that were significantly altered in abundance, and these contained no discernible functional or spatial pattern. Proteins containing significantly altered phosphopeptides were subjected to functional cluster analysis and compared against the mouse genome as background. The most over-represented KEGG functional pathway was the insulin signaling pathway (*p*-value 9.24 e^{-10}). Site-specific analysis using MotifX again showed an 11-fold over-representation of the Akt recognition sequence (R-X-R-X-X-pS) in the set of phosphopeptides significantly reduced by P407 treatment (Fig. 4.14), which is consistent with the data observed for aged liver tissue.

Comparison of significantly altered phosphoproteins between the ageing and P407-related samples revealed that 396 and 481 non-redundant gene products were unique to P407 and ageing respectively, with 530 common to both comparisons. The sets of phosphoproteins unique to P407 and ageing showed no statistically significant over-represented KEGG functional pathways, however proteins contained in the overlapping set with phosphopeptides altered in abundance by both P407 and ageing were functionally most typically associated with insulin signaling (*p*-value 1.83 e^{-8}). We next took the large-scale data and performed phosphosite level interrogation using PhosphoSite Plus (www.phosphosite.org) to specifically examine changes to known insulin-regulated sites from proteins within the KEGG insulin signaling pathway in aged and P407-treated liver. In total, we identified 49 phosphopeptides containing known insulin-regulated sites from 23 insulin signal pathway proteins. In aged liver, 39/49 phosphopeptides were significantly altered and 34 of these were reduced in phosphorylation (from IRS-1, SHC-1, Sos1, Raf1, Erk1/2, PI3K, Foxo1, Gys1, Trip10, Acaca, PP1, Rps6 and Eif4ebp1; Appendix 3), which is consistent with reduced insulin signaling. Fifteen of these phosphopeptides also showed reduced phosphorylation in P407-treated livers (from IRS-1, SHC-1, Erk1/2, PI3K, Foxo1, Gys1, PP1 and Trip10). Four phosphopeptides were elevated in abundance in both aged and P407-treated liver (from Akt1, PP1 and IRS-2). Seven phosphopeptides containing known insulin-regulated sites (from BAD, TSC1/2, mToR and p70S6K) were unaltered by either ageing or P407. While we did not observe the IRS-1 tyrosine sites targeted by the insulin receptor (Fig. 14), we did observe the phosphorylation target of the insulin receptor on SHC-1 (Tyr423), which was significantly reduced in abundance in both aged and P407-treated livers (Appendix 3). These data confirm that defenestration leads to altered hepatic insulin signaling that strongly correlates with the effects of ageing on this pathway.

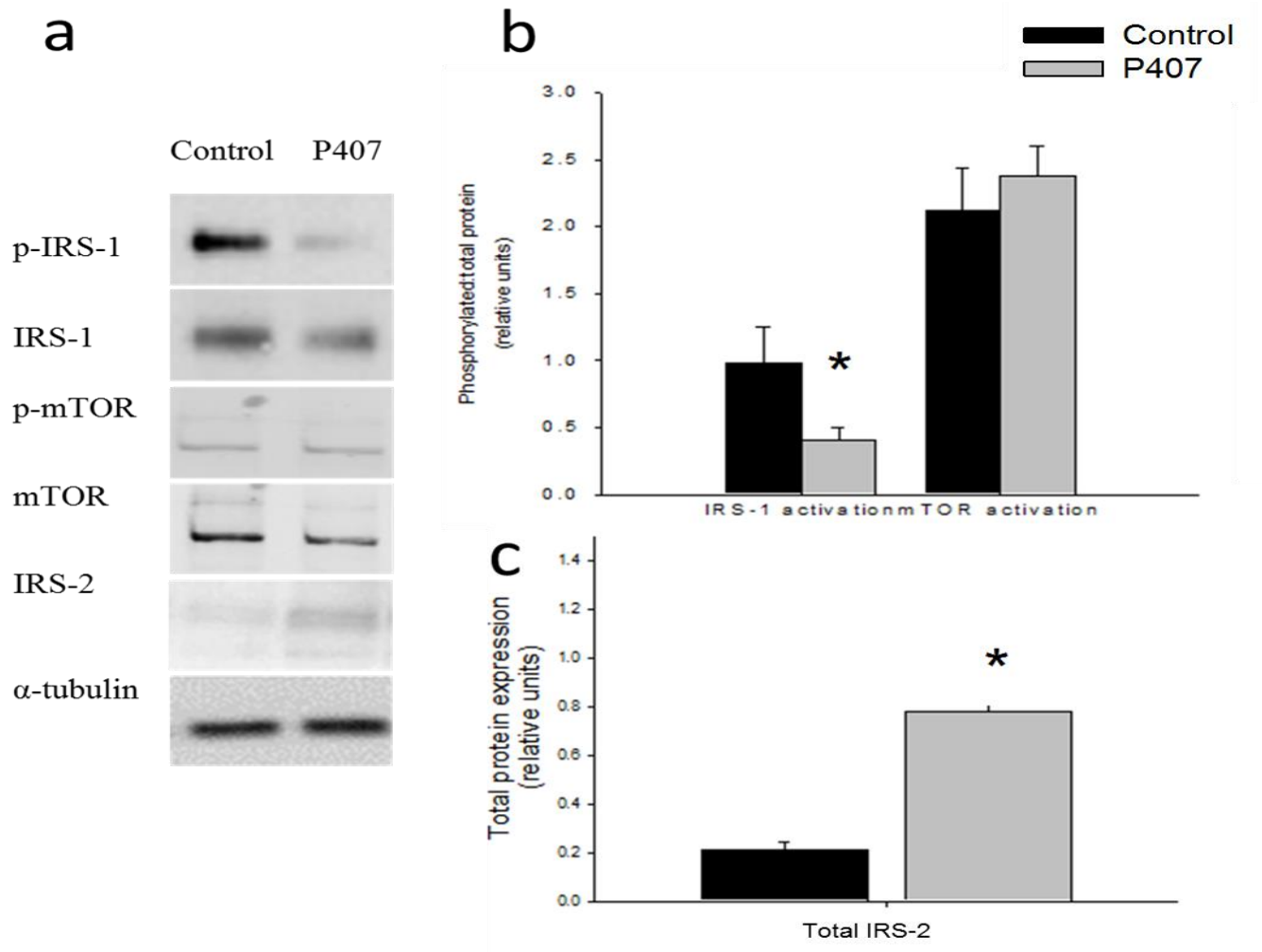

Figure 4.13: (a) Representative Western Blots of p-IRS-1, IRS-1, p-mTOR, mTOR and IRS-2 from control (n=6) and P407 livers (n=6). (b) Densitometry showing significantly decreased phosphorylation of IRS-1 in insulin stimulated P407 livers compared to control (P=0.002) while there are no changes in mTOR phosphorylation as a downstream target protein. (c) Densitometry showing significantly increased total IRS-2 protein in P407 livers compared to control (P<0.001), probably as a compensatory mechanism due to decreased IRS-1 activation.

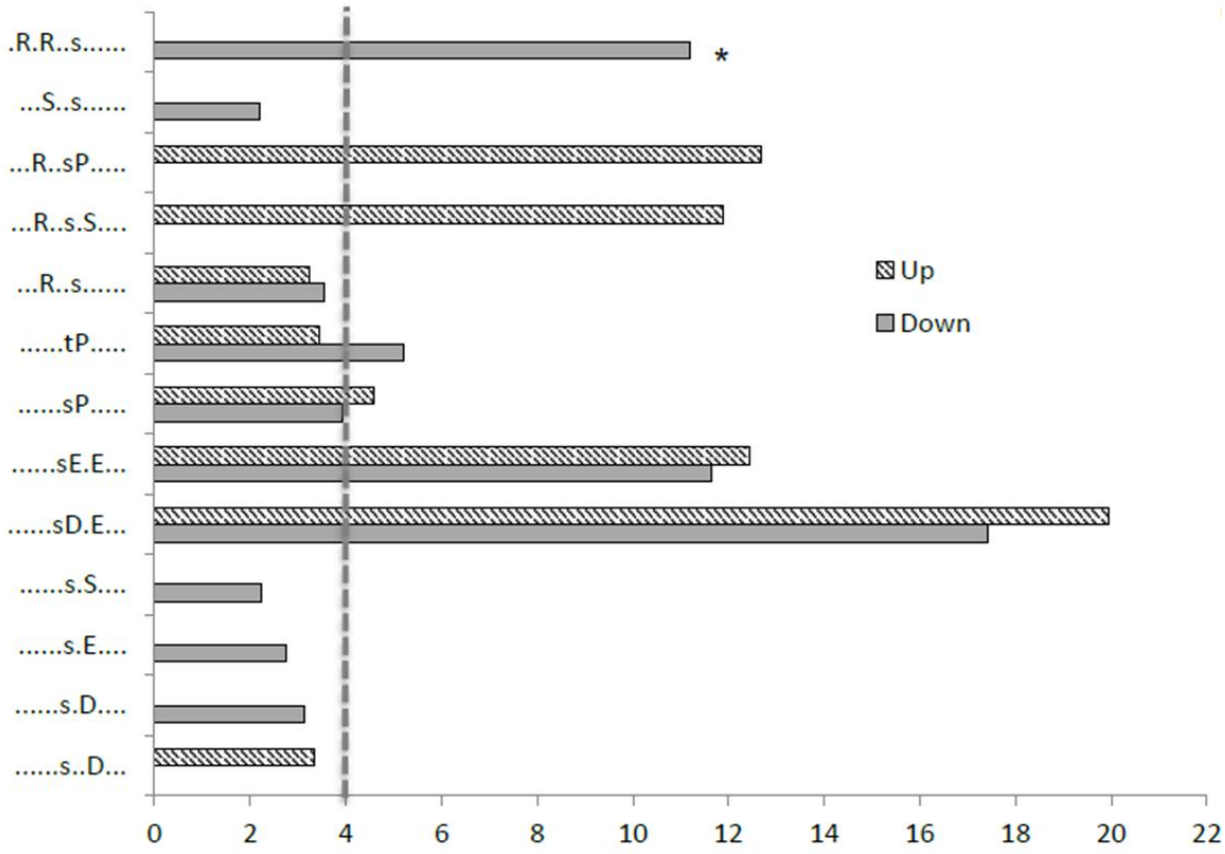

Figure 4.14: Fold over-representation of kinase recognition sequences from phosphoproteome analysis of control versus P407-treated livers. Reduced Akt signaling is indicated by the prevalence of Akt recognition sequence *= 'R-x-R-x-x-pS' (11-fold) in the set of phosphopeptides with reduced abundance in P407-treated livers. Dotted line indicates cut-off for significant fold-change (>4-fold).

4.4 DISCUSSION

This study assesses the effect of acute defenestration of the LSEC, induced by the synthetic surfactant, P407, on hepatic disposition of insulin and glucose. In addition, it examines the implications of these changes in hepatic glucose and insulin disposition for whole body glucose homeostasis.

As previously reported, within 24 hours of a single injection of P407 there was a marked hyperlipidaemia with normal liver function (Johnston, 2004, Palmer et al., 1998, Cogger et al., 2006, Mitchell et al., 2010, Mitchell et al., 2012, Warren et al., 2011, Johnston and Palmer, 1993, Dumortier et al., 2006). P407 is a ubiquitous block co-polymer surfactant that has been widely studied as a model for hyperlipidaemia (Johnston, 2004) and also used as a vehicle for nanoparticle drug delivery (Kabanov et al., 2002, Moghimi, 1999). The hyperlipidaemic response to P407 has been linked to altered activity of enzymes involved in lipoprotein metabolism, in which hypertriglyceridemia is caused by lipoprotein lipase inhibition and hypercholesterolemia by indirect effects on HMG CoA reductase activity (Johnston, 2004). It is reported that this condition is also caused by inhibition of lipid metabolizing enzyme activities (Wasan et al., 2003). However, P407 also induces defenestration of the LSEC which has been shown to impair the chylomicron passage into the hepatocytes, thus providing an additional explanation for hyperlipidaemia (Cogger et al., 2006).

P407 targets the liver after intraperitoneal injection (Li et al., 1996) and the observation of lipemic blood is an indicator that it has successfully enter blood circulation (Wout et al., 1992).

Apart from causing hyperlipidaemia, P407 is regarded as a non-toxic substance and is widely used in pharmaceutical preparations (Dumortier et al., 2006). P407 is used for the study of pharmacokinetics and pharmacodynamics of various medications used to treat hyperlipidaemia (Shayeganpour et al., 2008, Lee et al., 2012).

Scanning electron microscopy of the LSEC revealed ultrastructural changes of defenestration as previously reported (Cogger et al., 2006, Mitchell et al., 2010, Mitchell et al., 2012, Warren et al., 2011). P407 significantly defenestrates LSECs within 12 - 36 hours after injection in mice in association with a 10 fold increase in plasma lipids (Cogger et al., 2006). Transmission electron microscopy analysis of mouse livers one day after P407 injection showed that LSECs developed large vacuoles full of lipids and/or P407 micelles in conjunction with LSEC defenestration and swelling observed on scanning electron microscopy, as a response to remove excess lipid and P407 from the blood (Warren et al., 2011). Mitochondria and ATP production are not affected by P407, therefore it is most likely that it interacts directly with the cell membrane (Cogger et al., 2006).

Using multiple indicator dilution methodology, the disposition of insulin and glucose was studied in perfused livers. These studies showed that P407-induced defenestration was associated with restricted access of insulin and glucose to the extracellular space. In control animals, both substrates had access to the entire sucrose space (extracellular and vascular space) but following P407, this was reduced by approximately about 20% for insulin and glucose as compared to the sucrose space (equivalent to the vascular space). Defenestration associated with P407 has been reported to be associated with restricted access of substrates transiting from the sinusoidal lumen

across into the SoD. These substrates include lipoproteins (Cogger et al., 2006) and medicines such as acetaminophen and diazepam (Mitchell et al., 2010, Mitchell et al., 2012). It is of note that the hepatic clearance of several other medicines has been found to be reduced following P407 (Lee et al., 2012), but in these reports, the effect on endothelium and transfer across the endothelium were not specifically investigated.

Systemically, P407 was associated with relatively normal glucose levels, but impaired glucose tolerance, increased insulin levels and insulin resistance (as assessed by the fasting insulin-glucose product, HOMA-IR). The hyperinsulinemic condition of the P407-treated animals was not secondary to increased insulin secretion by the pancreas because there was suppression of C-peptide levels. Instead, it can be inferred from the data that hyperinsulinemia was caused by reduced hepatic insulin clearance; a conclusion also supported by decreased liver insulin uptake in the whole body insulin uptake experiments. Glucagon levels were also significantly lower in P407-treated animals, which is possibly a response to the serum high insulin levels measured in the study.

Despite elevated circulating insulin levels, glycogen content of the livers as shown by PAS staining was significantly diminished in P407-treated animals. This is again consistent with reduced activation of insulin signaling pathways in the liver. Insulin resistance has been shown to decrease glycogen synthetase activity and glycogen content in skeletal muscle (Cline et al., 1999) and the liver (Kusunoki et al., 2002) as a result of impaired insulin action.

Following P407, there was reduced gluconeogenesis in the pyruvate tolerance test which is consistent, paradoxically, with increased insulin activity. This was not secondary to impaired pyruvate transfer across the endothelium as determined by multiple indicator dilution study. This is most likely caused by hyperinsulinemia acting via brain control of hepatic glucose metabolism (Rojas and Schwartz, 2014) and parallels the changes seen in old age.

After establishing that defenestration reduces the hepatic volume of distribution of insulin and glucose, the impact of this reduced transfer of hepatocyte insulin signaling was examined using large scale proteomics and western blots. Large scale proteomics showed that in the acute defenestration, the most significantly affected pathway is insulin signaling. Western blots showed P407-induced defenestration were associated with reduced hepatic IRS-1 phosphorylation consistent with reduced access of insulin to the hepatocellular membrane. However, consistent with the exponential nature of signaling pathways and with previous work (Hoehn et al., 2008), alteration at the level of IRS-1 signaling was insufficient to cause changes in the expression of downstream signaling intermediates proteins such as mTOR.

Interestingly, there was an increase in total IRS-2 expression with P407 treatment. A similar finding was observed in the liver insulin stimulated-LIRKO mice, where there was a 5-fold increase in IRS-2 expression in the liver due to loss of insulin signaling (Michael et al., 2000). IRS-2 is reported to have a predominant role in β-cell development and compensation of peripheral insulin resistance, working with IGF-1 to maintain glucose homeostasis (Withers et al., 1999) and the increase in IRS-2 expression is likely to be a compensatory response to the reduction in IRS-1 phosphorylation.

In agreement with the protein expression findings PCR array analysis of gene expression profiles showed that IRS-2 gene expression was upregulated, in parallel with increased total IRS-2 protein expression from western blotting. Increased IRS-2 expression is also associated with steatohepatitis and altered lipid and insulin metabolism in humans (Rametta et al., 2013). The pattern of downregulation in G6pc gene expression observed is subsequently reflected by decreased gluconeogenesis in P407 during the pyruvate tolerance test.

It is of note that repeated administration of P407 has recently been reported to induce type 2 diabetes mellitus in rats, with sustained hyperglycemia occurring after several weeks of daily treatment (Bharti et al., 2013). In another study, a single dose of P407 did not influence glucose or insulin, however a smaller dose (0.5 g/kg) was used in mice rather than rats (Johnston and Waxman, 2008). In this study of rats, a single dose of P407 (1 g/kg) induced insulin resistance with elevated insulin levels and impaired glucose tolerance, although the glucose levels were still within the normal range. Our data indicate that this is mediated, at least in part, by defenestration of the LSEC.

In conclusion, defenestration of the LSEC induced by P407 reduced the transfer of insulin and glucose from the sinusoid into the extracellular space and reduced insulin action in hepatocytes with an impact on glucose homeostasis. This was associated with hyperinsulinaemia, glucose intolerance and deranged glucose metabolism in the liver. These results are in agreement with previous reports showing that defenestration of the LSEC leads to impaired transendothelial transfer of various other substances such as lipoproteins and medications into the liver (Hilmer et al., 2005, Mitchell et al., 2012, Mitchell et al., 2011). Therefore the endothelium in the liver, as

in other tissues, can have a significant impact on insulin action. Moreover, the results suggest a novel mechanism linking defenestration associated with liver diseases and ageing with insulin resistance and possibly diabetes mellitus.

CHAPTER 5: THE RELATIONSHIP OF FENESTRATIONS AND LIPID RAFTS IN VITRO

5.1 INTRODUCTION

LSECs have a unique phenotype compared to the endothelial cells of other organs. They are highly differentiated cells with attenuated cytoplasmic extensions approximately 100 nm thick that are perforated by non-diaphragmed transcellular fenestrations and have no associated basement membrane. The fenestrations which cover approximately 5-20 % of the LSEC surface area function as a filter for substrate transfer between blood and hepatocytes. Individual fenestration diameter ranges from 50-150 nm and the majority are arranged into groups known as sieve plates. As discussed previously the size and number of the fenestrations is important for the passage of selective substrates, such as insulin across the LSEC (Wisse et al., 1985).

Due to their small size, fenestrations are below the optical resolution limit and their observation has been significantly performed by electron microscopy (Cogger and Le Couteur, 2009). This technical limitation has hampered the use of living cells or fluorescent probes to investigate the distinctive biological structure of LSECs (Braet et al., 2007). While the details of fenestration ultrastructure have been observed and documented many times, there remains no specific cell surface protein that can reliably differentiate fenestrations from the non-fenestrated membrane sections of the LSEC or that assists in probing the exact spatial and temporal events of fenestration formation and loss.

Advancement in microscopy has recently provided opportunities that overcome the diffraction limit of optical resolution. Fenestrations are now able to be resolved using three-dimensional structured illumination microscopy (3D-SIM), an ultra-high resolution light microscopy that uses

interference patterns to convert structures below the resolution limit of light microscopy into observable construct by generating difference frequency called moiré fringes (Cogger et al., 2010). The three dimensional structure of fenestrations has been successfully resolved using Cell Mask Orange membrane stain, where fenestrations are seen clustered in sieve plates, similar to observation with scanning electron microscopy. Additional structures were observed intercalated with between the sieve plates, postulated as membrane rafts, highly dynamic sterol and sphingolipid enriched lipid-ordered domains of the cell membrane that compartmentalise cellular signaling molecules.

To confirm this hypothesis, studies were undertaken in our laboratory on the relationship between fenestrations, actin and lipid rafts have been conducted using 3D-SIM, TIRFM and SEM (Svistounov et al., 2012). It was found that fenestrations form in non-rafts regions of LSEC once the membrane-stabilizing effects of actin cytoskeleton and membrane rafts are diminished. The inverse relationship between fenestrations and membrane rafts has raised the hypothesis of sieve-raft theory for the regulation of fenestrations (Cogger et al., 2013a) whereby lipid rafts regulate the formation of fenestrations in sieve plates.

The mechanisms for the loss of fenestrations induced by P407 such as seen in Chapter 4 have not been investigated. P407 has previously been shown to cause loss of fenestrations by examination with scanning electron microscopy (Cogger et al., 2006), but the effects of P407 on the lipid rafts of the LSEC membranes are unknown. The objective of this study is to investigate the effect of P407 on the relationship between membrane rafts and fenestrations in SKHep1 cells (a cell line

of liver endothelial origin) and isolated LSECs. It is proposed that P407 induces defenestration by depleting non-raft region of the cell membrane (Cogger et al., 2008).

5.2 METHODS

5.2.1 Animals

Male Fischer 344 rats aged 8-10 weeks and weighing 200 g were obtained from Animal Research Centre (Perth, Australia). The animals were allowed free access to water and standard chow. All animals were treated in accordance with Animal Care guidelines. This study was approved by the Sydney Local Health District Animal Welfare Committee (AWC Protocol #2012/005A).

5.2.2 SKHep1 cell culture and treatment

SKHep1 cells were obtained from the American Type Tissue Culture Collection (ATCC, VA). Cells were cultured in a humidified 5 % CO_2 incubator at 37 ºC and grown in DMEM supplemented with 10 % fetal calf serum and antibiotics. Cells were grown on Thermanox coverslip for SEM and collagen coated glass coverslip for fluorescent microscopy. Once cells were 75 % confluent, cells were treated with normal saline or 0.5 mg/ml P407. After 1 hr of treatment, cells were rinsed 3 times with PBS and fixed as described in section 5.2.4 and 5.2.5.

5.2.3 LSEC isolation and treatment

This procedure is described in detail in sections 2.3.2 and 2.3.3. Briefly the animals were weighed and anaesthetised and liver was perfused with Collagenase solution. Cell suspension

was centrifuged and the supernatant was layered on a two-step Percoll gradient for the removal of non-parenchymal cells other than LSECs. LSEC purity was enhanced by selective adherence of Kupffer cells to plastic. LSECs were quantified and seeded on Thermanox coverslips for SEM and collagen coated glass coverslips for fluorescence microscopy in serum free RPMI-1640 media. After 3 hours, cells were treated with normal saline or 0.5 mg/ml P407. Following 1 hr of treatment, cells were rinsed 3 times with PBS and fixed as described in section 5.2.4 and 5.2.5.

5.2.4 Cell fixation, processing and imaging for SEM

Following treatment, Thermanox-mounted SKHep1 cells and isolated LSECs were fixed for scanning electron microscopy in 2.5 % glutaraldehyde in 0.1 M Cacodylate buffer (0.1 M sodium cacodylate buffer with 1 % sucrose pH 7.4) for 1 hour. Cells were washed, filtered and 1 % Tannic acid in 0.1 M Cacodylate buffer (pH 7.4) was added to cells for 1 hour and rinsed thoroughly. Cells were osmicated (1 % OsO4/0.1 M Cacodylate buffer pH 7.4 for 1 hour) and dehydrated in an ethanol gradient. After treatment with hexamethyldisilazane, coverslips were left to dry in a desiccator. Coverslips were then mounted on stubs using double-sided tape, coated with platinum in a sputter coater and examined using a Jeol 6380 Scanning Electron Microscope. Experiments were performed in triplicate.

5.2.5 Cell fixation, processing and imaging for fluorescence microscopy

Following treatment, cells, SKHep1 cells and isolated LSECs on glass coverslips were fixed with 4 % paraformaldehyde in PBS overnight. Cells were washed and stained with Cell Mask Orange,

a cell membrane marker and Bodipy FL C5 ganglioside GM1 (Life Technologies, Wembley Australia) which is a marker of membrane rafts. The cells were then fixed and mounted with Prolong Gold (Invitrogen, Scoresby Australia). Imaging was performed using Zeiss Wide-field fluorescence deconvolution microscope and images were convolved using Sen Software package (Carl Zeiss AG, Hamburg Germany). Experiments were performed in triplicate.

5.3 RESULTS

5.3.1 Loss of fenestrations is observed in P407 treated SKHep1 cells and isolated LSECs

Scanning electron microscopy of the untreated SKHep1 cells showed numerous pores similar to fenestrations (Fig. 5.1). Some of the pores are grouped evenly representing a sieve plate. Following one hour treatment with P407, there is a reduction of pore size and number as compared to saline treated cells (Fig. 5.1).

LSECs were successfully isolated and grown in RPMI culture. Fenestrations clustered in sieve plates are seen on scanning electron microscopy (Fig. 5.2a-b). Treatment with P407 reduced the size and number of fenestrations in isolated LSECs (Fig. 5.2c-d) as reported previously (Cogger et al., 2006). The sieve plates of the treated cells are smaller compared to saline treated cells. The presence of gaps in the cytoplasm is an artefact caused by isolation and culture of the LSECs.

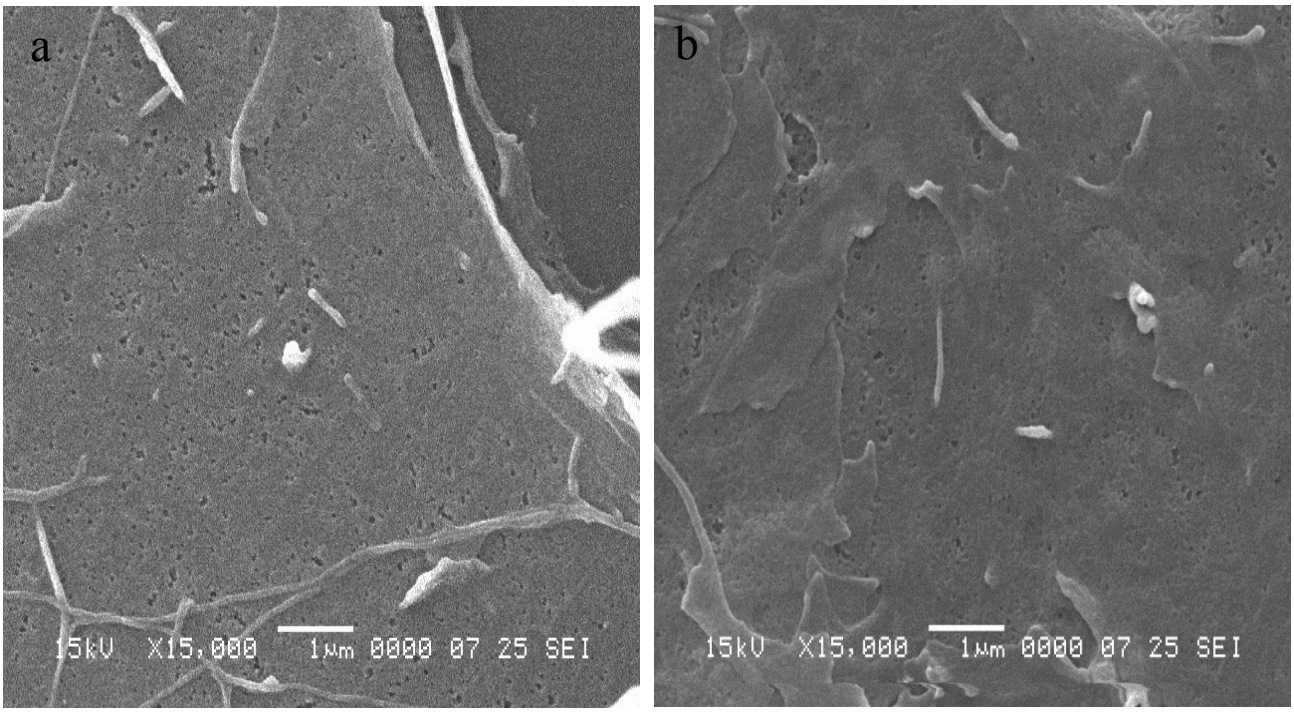

Figure 5.1: Scanning electron microscopy of saline-treated SKHep1 cells showing numerous pores on the cell membrane (a). Following treatment with P407 (b) cells showed a reduced number of fenestrations.

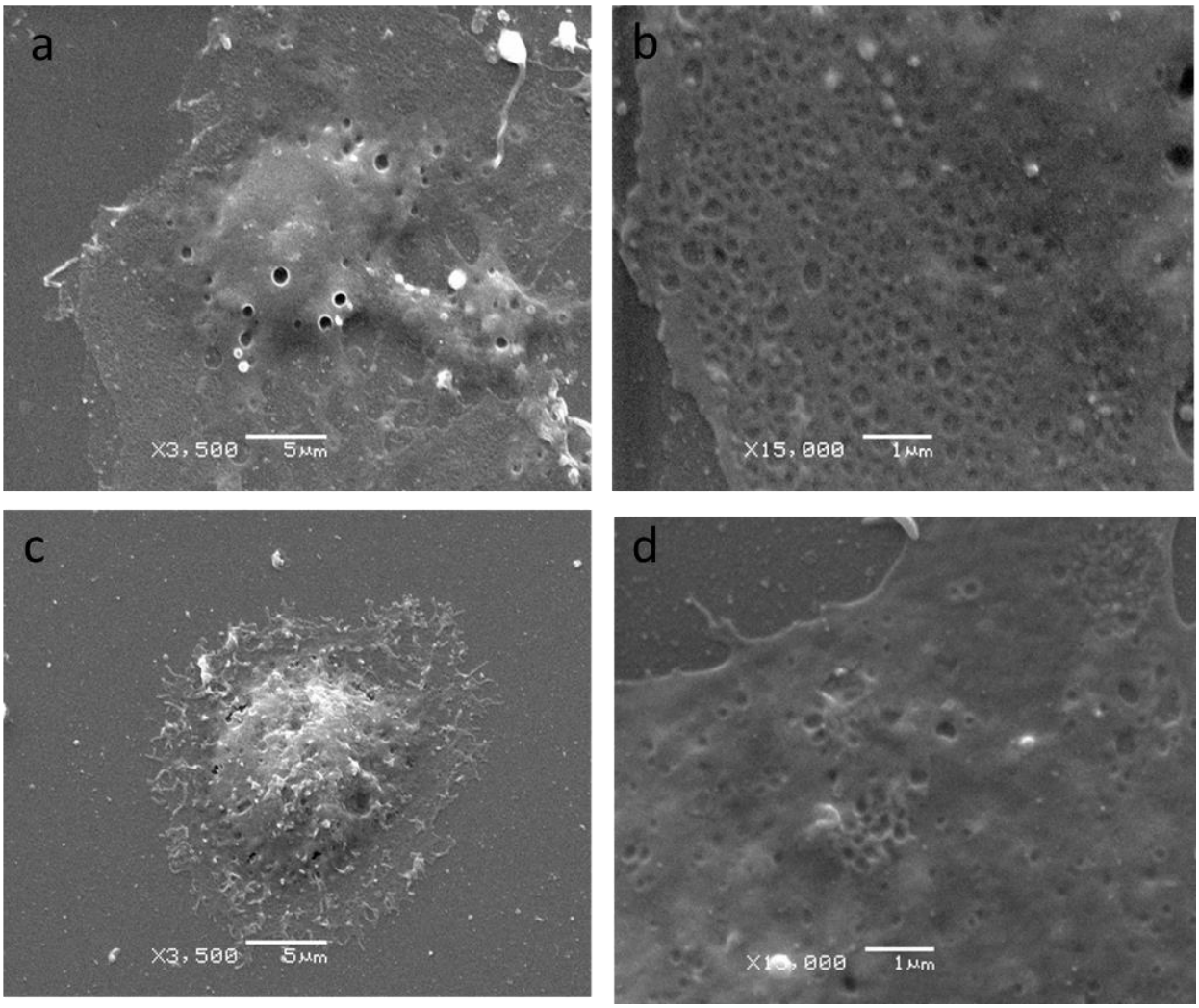

Figure 5.2: Scanning electron microscopy of saline-treated isolated LSECs in lower (a) and higher (b) magnification, showing numerous fenestrations clustered into sieve plates. Following treatment with P407, lower magnifications showed a smaller cell diameter (c) and higher magnification showed loss of fenestrations and smaller sieve plates (d) of LSECs.

5.3.2 Lipid rafts are increased in P407 treated SKHep1 cells and isolated LSECs

In order to determine whether P407 induces defenestration by depleting the non-raft component of the LSEC membranes, both cells were stained with the cell membrane marker Cell Mask Orange and the specific raft marker Bodipy FL C5 ganglioside GM1. SKHep1 cells showed a capillary-like structure under fluorescence microscopy with 95 % confluency (Fig. 5.3a). The cells have a consistent distribution of rafts along the perimeter of the cells. Following P407 treatment SKHep1 cells exhibited a strong staining of lipid rafts seen as clusters at the perinuclear region (Fig. 5.3b). This indicates a marked change in the distribution and intensity of lipid rafts compared to control.

Low magnification fluorescence microscopy of the isolated LSECs revealed the cells were growing in a monolayer with about 50 % confluency (Fig. 5.4). Higher magnification of individual LSECs revealed multiple unresolvable regions representing sieve plates in the peripheral regions of the cell (Fig. 5.5a). As reported previously sieve plates are present in attenuated areas of the cell membrane. These regions can be less than 100nm in thickness which renders them unresolvable under conventional confocal microscopy. Lipid rafts can be seen localised to the perinuclear region of the saline treated LSEC. There was a marked increase in raft staining following treatment with P407 indicating depletion of non-raft cell membrane areas (Fig. 5.5b). A very thin and discontinuous cytoplasm is seen in between sieve plates as a result of disordered cell membrane. As revealed by the merged images (Fig. 5.5) after P407 treatment the LSEC membrane is predominantly characterised by Bodipy positive membranes, indicating a predominance of raft microdomains.

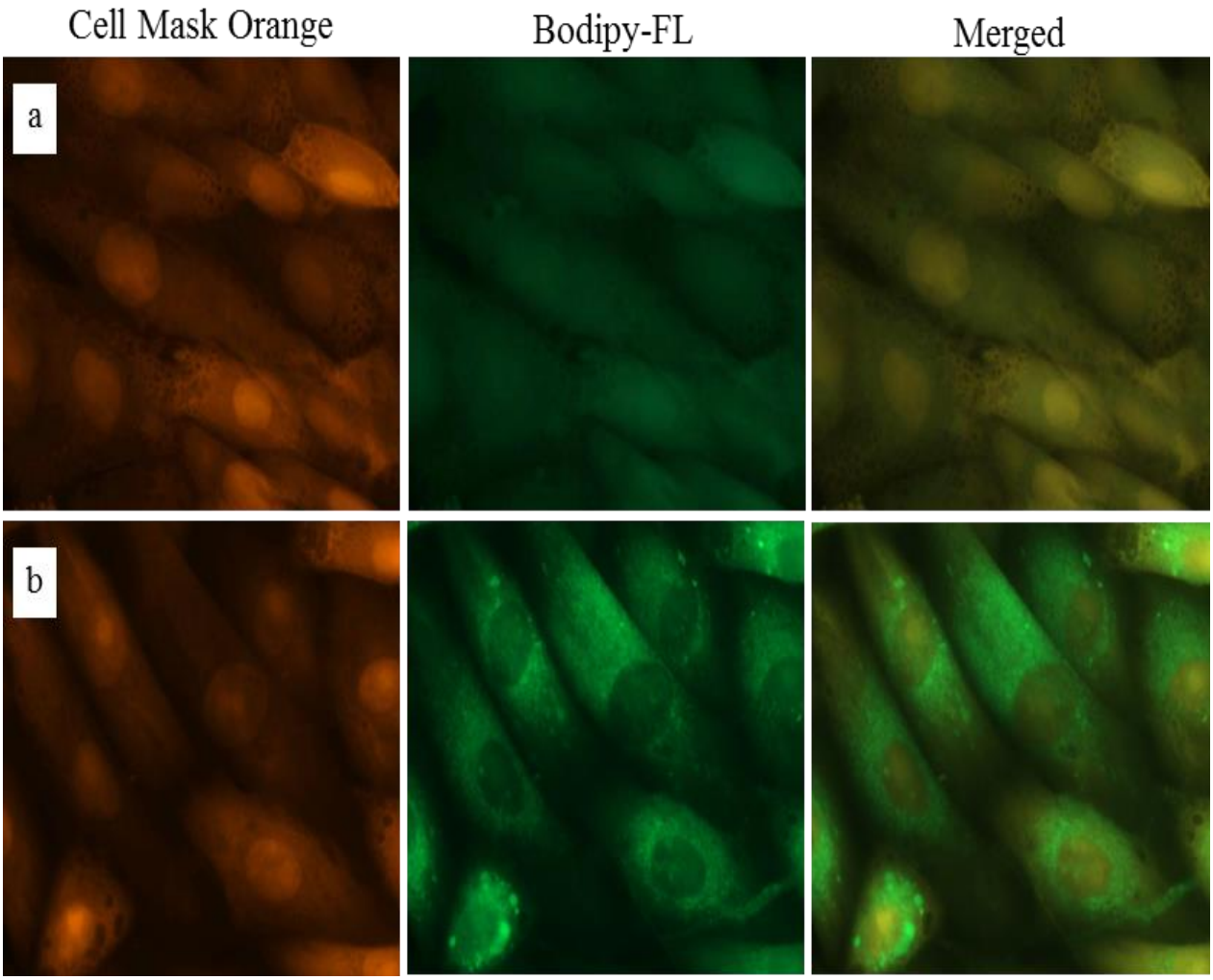

Figure 5.3: Fluorescent image of SKHep1 cells stained with cell membrane and lipid raft marker showing low distribution of lipid raft in saline-treated cells (a) Following treatment with P407, there was an increase green staining, at the perinuclear region of the cells (b) with inverse distribution of cell membrane.

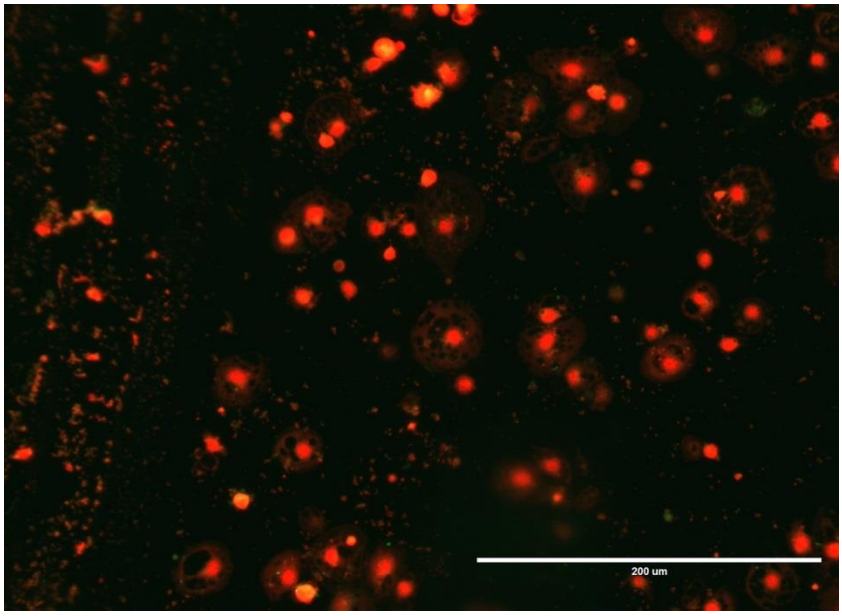

Figure 5.4: Low magnification (20X) of the isolated LSECs showing cells growing in a monolayer with about 50 % confluency.

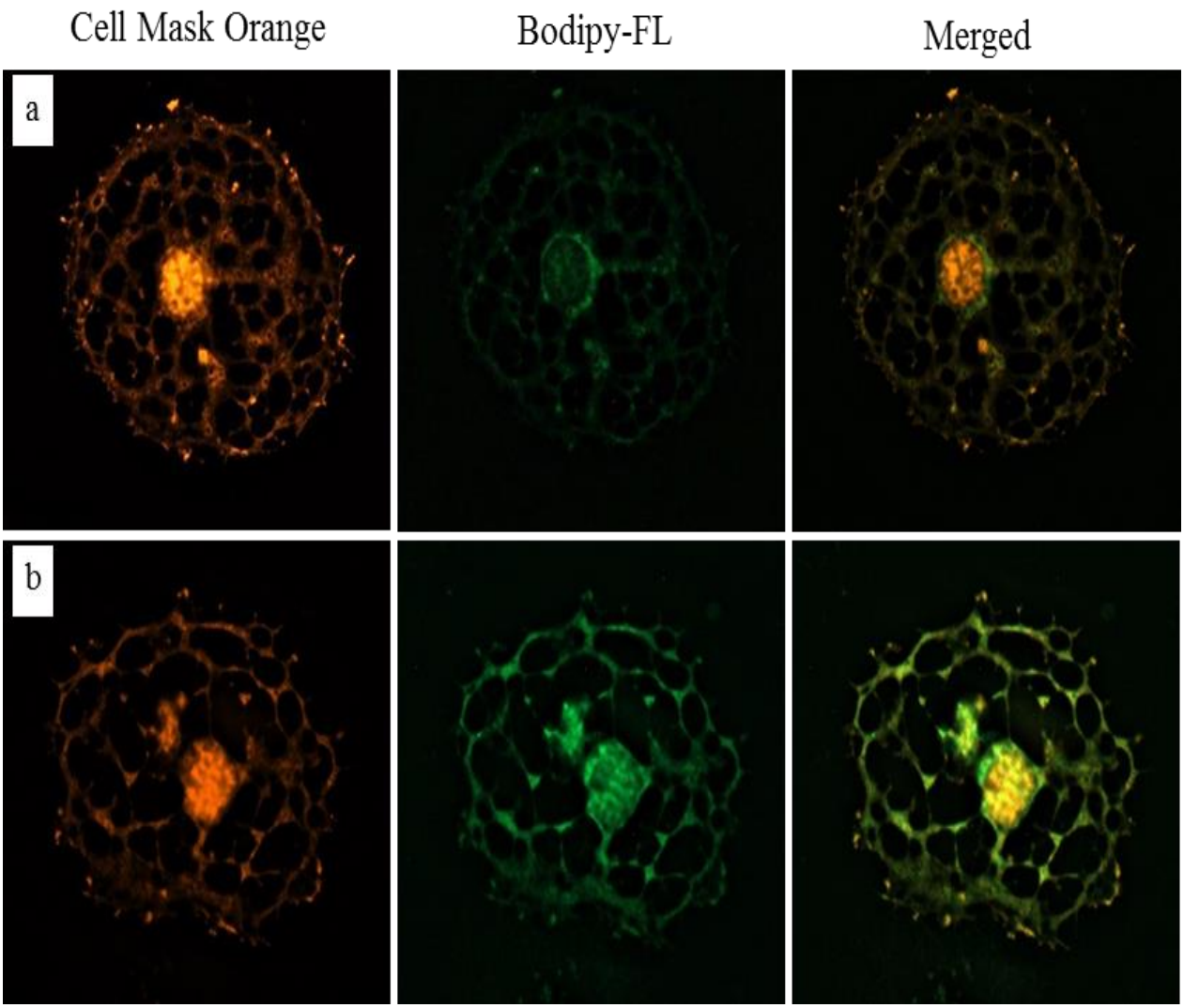

Figure 5.5: Fluorescent image of isolated LSECs stained with cell membrane and lipid raft marker showing a minimal lipid raft distribution at the perinuclear region in saline-treated cells (a). Following treatment with P407, there was an increase green staining at the perinuclear and peripheral region of the cells (b) consistent with depletion of non-lipid raft membrane.

5.4 DISCUSSION

This study assesses the relationship between membrane rafts, fenestrations and defenestration following P407 treatment in SKHep1 and isolated LSECs.

Concordant with its *in vivo* effect, this study has shown that P407 induced significant loss of fenestrations in isolated LSECs. While this has previously been reported, here it was also found that P407 treatment leads to an increase in fluorescent staining for lipid raft membranes (Bodipy FL C5 ganglioside GM1) in SKHep1 cells and isolated LSECs, consistent with the sieve-raft theory. Although deconvolution microscopy is not able to visualise individual fenestrations, the distribution of the fluorescent raft stains confirmed the findings from 3D-SIM, where rafts are preferentially distributed in the perinuclear regions of LSECs and are inversely distributed with respect to sieve plates (Svistounov et al., 2012). Utilizing deconvolution microscopy, isolated LSECs are seen to be growing intact on the coverslip in a monolayer. The lace-like network of the sieve plates are identified by their F-actin stress fibres via 3D-SIM (Cogger et al., 2010) and the membrane of these F-actin fibres can be seen in these studies (Fig. 5.4). The net-like structure of LSEC has also been reported to be formed by clathrin heavy chain coated vesicles via fluorescent microscopy. This is a unique feature of LSEC compared to other cell types that show a well-known punctate staining pattern representing the clathrin-coated vesicles (Falkowska-Hansen et al., 2007).

In previous studies using Triton X, another non-ionic detergent that is known to deplete non-raft regions of the cell membrane, LSEC porosity was reduced by ~90% (Svistounov et al., 2012)

and it is plausible that P407 induced defenestration is triggered by the same mechanism. Millar et al. (2005) has compared Triton WR-1339 and P407 in the determination of triglyceride and lipoprotein metabolism and concluded that P407 is equivalent to Triton WR-1339 in triglyceride production but without the unwanted side effects of Triton (Millar et al., 2005). It is interesting to note that Poloxamer 188, a related polymer has been shown to insert into fluid phase lipid membranes and act as a stabiliser of these domains (Maskarinec et al., 2002) while this process does not extract lipids from non-raft regions of membranes it acts to increase raft regions of membranes through stabilisation.

As supported by the data presented here defenestration by P407 most likely occurs by a direct mechanism on the cell membranes of the target cell without influence from other residents cells of the liver such as Kupffer cells, stellate cells or hepatocytes (Cogger et al., 2006).

Multiple studies on the regulation of fenestrations have reported that the actin cytoskeleton plays a role in the maintenance of fenestrations (Vermijlen et al., 2002, Nagai et al., 2004, Van Der Smissen et al., 1986), and VEGF has the ability to increase fenestration via retraction of the actin cytoskeleton (Cogger et al., 2008, Funyu et al., 2001, Yokomori et al., 2003). It has been shown that membrane fusion and pore formation is restricted by dynamic resistance of the actin network in experimental membrane fusion models (McGuire et al., 1992), and in the generation of membrane vesicles, which are also associated with increased lipid-disordered, non- raft microdomains (Owen et al., 2010). This suggests that the formation of fenestrations requires retraction and/ or rearrangement of the normal sub-membrane actin cytoskeleton, while stabilisation of the membrane requires actin support.

Lipid rafts have been associated with numerous physiological and pathological conditions in individual types of liver cells (Dolganiuc, 2011). Beyond the reciprocal relationship between fenestration and lipid rafts described here, the more proximal details of fenestration formation in LSECs are not known. In other endothelial cells of vascular system, lipid rafts play a major role in functionality where disruptions of lipid rafts causes loss of cell viability and altered cell morphology (Bao et al., 2010, Kline et al., 2010). Membrane lipid rafts have been studied using fluorescent microscopy, showing higher lipid order for the areas of the membrane associated with active signaling and adhesive events (Owen et al., 2006). Various agents have been applied to isolate raft or non-raft membranes including 7-ketocholesterol which disorders membrane rafts (Kahn et al., 2011). Treatment of isolated LSECs with 7-ketocholesterol causes a marked increase in the number and size of sieve plates associated with the increase in disordered non-raft membranes (Svistounov et al., 2012). In hepatocytes lipid rafts have also been associated with the triggering of calcium waves, which regulate fluid and electrolyte secretion and exocytosis (Ito et al., 1997, Kasai and Augustine, 1990). Immunofluorescence studies in isolated hepatocytes showed that the disruption of lipid rafts impairs accumulation of the inositol 1,4,5-triphosphate receptor responsible for calcium wave polarization (Nagata et al., 2007).

Research on LSECs has been limited by multiple factors. *In vivo* experiments are restricted to a single treatment for each animal (Cogger et al., 2008). In vitro work is limited because isolation of LSECs involves lengthy, complicated procedures that yields only sufficient LSEC for 6-12 single experimental samples and the *in vitro* viability of the differentiated cells is limited to less than 12 hours (DeLeve et al., 2006, Elvevold et al., 2008). To overcome low yields of LSEC, Gerlach (2001) developed a method of isolation from pig livers but this not feasible in most

animal facilities due to ethical considerations, complicated equipment needs and procedures (Gerlach et al., 2001). The M1 (MILEC) cell line has been established as an immortal LSEC cell line, but observation with electron microscopy revealed it is not fenestrated unless treated with actin disruptors and co-cultured with other cells (Saito et al., 2004). While this is the first observation of P407 effect on SKHep1 cells, previous studies have utilised this cell to study fenestrations. SKHep1 cells are catalogued as immortalised cell lines derived from the ascetic fluid of a 52 year old male with hepatic adenocarcinoma. It is described as a hepatoma origin but various results have shown that this cell is actually an endothelial origin (Heffelfinger et al., 1992, Kawai et al., 2001, Seow et al., 2001). This is further confirmed by observation of pores and thin cytoplasmic extension via SEM (Cogger et al., 2008). VEGF has shown to increase SKHep1 porosity and diameter, observed by contraction of actin cytoskeleton and attachment of caveolin-1 towards the nucleus via fluorescent microscopy. This makes SKHep1 cells a good model for LSEC research, similar to the use of HepG2 cells to study hepatocytes (Javitt, 1990).

The establishment of fluorescent microscopy for the study for fenestrations has continued to evolve with a recent, promising study using direct stochastic optical reconstruction (dSTORM). This work further resolved LSECs to a spatial resolution of ~20nm by using a dSTORM add on to an Olympus IX71 microscope (Mönkemöller et al., 2014). The characteristics of LSEC were readily identified including the very thin membranes that divide individual fenestrations. This improved technical capacity will potentially expand the LSEC field and allow dynamic and greater probing of fenestration biology without the technical limitations of electron microscopy.

The important physiological role of the LSEC has become increasingly recognised in normal and various pathological conditions of liver, as well as ageing. While these studies are not able to address how defenestration occurs in ageing it will be interesting to observe the cell membrane of LSECs isolated from old animals to see if there are increased raft membranes in these cells with age. This would provide a plausible mechanism for age-related defenestration and would be in line with the observations of other studies that have reported detrimental lipid raft changes in ageing (Marquet-de Rouge et al., 2013, Eckert et al., 2003). Future studies will be aimed at addressing these questions in an ageing LSEC model.

In conclusion, loss of fenestrations by P407 is caused by the depletion of the non-raft areas in LSEC membrane, inhibiting the formation of fenestrations. Fluorescence imaging has been used to observe the increased raft area and defenestration has been confirmed by SEM. This finding has strengthened the sieve-raft hypothesis and further facilitates the study of fenestration biology as the changes can be detected by fluorescence rather than electron microscopy. As there is increased recognition of the role of LSECs in liver pathology, an understanding of the mechanisms that regulate fenestrations is essential for the development of therapies directed to the management of diseases and old age where there is reduction in fenestrations.

CHAPTER 6: DIETARY MACRONUTRIENTS AND THE AGEING LIVER SINUSOIDAL ENDOTHELIAL CELL

A manuscript version of Chapter 6 has been published in the following publication:

Cogger, V. C., M. Mohamad, S. Solon-Biet, A. M. Senior, A. Warren, J. N. O'Reilly, B. T. Tung, D. Svistounov, A. McMahon, R. Fraser, D. Raubenheimer, A. J. Holmes, S. Simpson and D. G. Le Couteur (2016). "Dietary macronutrients and the aging liver sinusoidal endothelial cell." American Journal of Physiology - Heart and Circulatory Physiology

6.1 INTRODUCTION

Liver sinusoidal endothelial cells (LSEC) have key physiological roles in endocytosis, immune function and the transfer of substrates between blood and hepatocytes via patent pores called fenestrations (Sorensen et al., 2008, Sorensen et al., 2012, Fraser et al., 2012). With ageing, there are significant ultrastructural changes in the LSEC that have been termed pseudocapillarisation (Le Couteur et al., 2001, Le Couteur et al., 2008a). These include a marked reduction in fenestration porosity, diameter and frequency, associated with increased endothelial thickness and altered expression of several endothelial and extracellular matrix proteins including von Willebrand factor and collagen. Pseudocapillarisation has been detected in old age in mice, rats, non-human primates and humans (Le Couteur et al., 2001, Le Couteur et al., 2008a) and has been documented in premature ageing syndromes in mice (Cogger et al., 2013b, Gregg et al., 2011). Fenestrations are dynamic, non-diaphragmed, transcellular pores that allow the free passage of substrates between the sinusoidal blood and hepatocytes (Fraser et al., 2012). Therefore loss of fenestrations with pseudocapillarisation contributes to impaired hepatic clearance of substrates such as lipoproteins and medications in old age (Hilmer et al., 2005, Le Couteur et al., 2005).

Caloric restriction (CR) has been known as the most robust, non-genetic intervention that for increasing lifespan and reducing disease (Everitt et al., 2005), including age-related loss of liver function, is associated with increased LSEC porosity, reduced extracellular matrix deposition and significantly attenuated LSEC thickening into very old age (Jamieson et al., 2007b). CR also improves blood lipoprotein profiles and delays the development of vascular disease in animal

models function (Zhu et al., 2004). Given our understanding of the role of fenestrations in lipoprotein uptake by the liver it can be hypothesised that improved LSEC morphology into old age through CR is at least partially responsible for CR mediated improvements in liver function and blood lipid profiles. Fenestration number and size are altered with fasting (O'Reilly et al., 2010), caloric restriction (Jamieson et al., 2007b) and following systemic exposure to any bioactive molecule of gut bacterial origin, which are delivered via the portal vein directly to the liver (Dobbs et al., 1994, Cheluvappa et al., 2008). These properties suggest that fenestrations are regulated by diet perhaps via the effects of diet on the composition of the gut microbiome. Therefore, in this study we determined the effects of dietary macronutrients and calorie intake on fenestrations in old age. Livers were studied from a large cohort of 15 month old mice that had been ad libitum-fed one of 25 diets varying in the amounts of protein, fat, carbohydrate and energy density in order to study the relationship between energy intake, macronutrients, ageing and lifespan (Solon-Biet et al., 2014, Solon-Biet et al., 2015, Le Couteur et al., 2014). In addition to the direct role of individual macronutrients on fenestrations we were able to explore the potential effect of different populations of gut-derived bacteria on the structural integrity of the LSEC.

6.2 METHODS

6.2.1 Animals and Husbandry

C57/Bl6 male and female mice (3 weeks old; n = 858) (Animal Resources Centre, WA, Australia) were housed three per cage in standard approved cages (Technoplast, Varese, Italy) in the Molecular Physiology Unit of the ANZAC Research Institute, a specific pathogen-free facility designed for housing transgenic mice. A custom-designed two-chamber Perspex insert, designed to collect food spillage (Sorensen et al., 2008), was placed beneath the food hopper of each cage to collect food waste for quantification. Mice were maintained at 24 ºC-26 ºC and 44%-46% humidity under a 12 hr light:12 hr dark photoperiod, with lights on at 0600hrs. All protocols were approved by the Sydney Local Health District Animal Welfare Committee (Protocol No. 2009/003).

25 experimental diet treatments were custom-designed and manufactured in dry, pelleted form by Gordon's Specialty Feeds, Sydney, Australia (Solon-Biet et al., 2014). The diet treatments were adequate in terms of addressed both nutritional quantity and quality. To manipulate diet quantity, indigestible cellulose was added to diet treatments, yielding 3 total energy (caloric) density regimes fixed at 8, 13 and 17 kJ g^{-1} (referred to as low, medium and high energy).

Mice were provided ad libitum access throughout their lifetime to 1 of 25 diets varying in content of protein, carbohydrate, and fat and overall energy density. Food intake was closely monitored throughout life to accurately determine food intake. Mice were checked daily, and

body weight measurements were recorded to correspond with food intake measurements. Animals losing more than 20% body weight were excluded from the study.

6.2.2 Tissue and blood collection

At 15 months of age, one-third of the animals were anaesthetised using ketamine and xylazine (1:1) via i.p injection. Animals were culled, blood was collected via cardiac puncture and tissues harvested for a variety of analyses. Liver samples were obtained and perfused-fixed for 1 minute with electron microscope fixative solution (3% glutaraldehyde, 2% paraformaldehyde, 2 mM calcium chloride, 1% sucrose in 0.1 M sodium cacodylate buffer). Following fixation, 1 mm^3 samples were taken, post-fixed, washed and then stored in 0.1M sodium cacodylate buffer at 4 ℃ as previously described (Cogger et al., 2014).

6.2.3 Blood parameters

Blood parameters were all measured in the fasting state. Blood glucose levels were determined using tail bleeds and a handheld glucometer (Accu-Check Performa, Roche, Hawthorn Australia). Blood was analysed for insulin and leptin by ELISA (ALPCO Diagnostics, Kurnell Australia). Circulating amino acid determinations were analysed at the Australian Proteome Analysis Facility, Macquarie University, using the Waters AccQ-Tag Ultra Chemistry Kit (Waters Corporation, Rydalmere, Australia). Free fatty acids were analysed by Metabolomics Australia.

6.2.4 Tissue processing and observation

This procedure is described in section 2.3.2 and 2.3.3 in Chapter 2: Methodology. Briefly, fixed liver blocks were treated with 1% osmium tetroxide in 0.1M sodium cacodylate buffer for two hours, followed by dehydration in an increasing ethanol gradient and final critical point drying with hexamethyldisilazane. Samples were mounted on stub and sputter coated with platinum, followed by observation using JEOL JSM-6380 scanning electron microscope (SEM). Ten random sinusoids pictures were taken at 15000x magnification for analysis using ImageJ for liver porosity, fenestrations diameter and fenestrations frequency per surface area. Samples were analysed in random order and category was blinded during analysis. In addition to electron microscopy haematoxylin and eosin staining was undertaken to ensure the livers were free of pathology.

6.2.5 Gut microbiome

The cecum contents were collected, metagenomic DNA recovered and the microbial community sampled by 454 sequencing of the 3' end of the 16S ribosomal RNA (907-1492) using primers specific for the domain Bacteria. Sequence reads were assigned to OTUs at 97% identity and then classified using both QIIME and Mothur.

6.2.6 Statistical analysis

The effects of macronutrients on fenestrations were analysed according to the Geometric Framework approach, with response variables fitted as response surfaces onto macronutrient intake (protein, carbohydrate and fat) arrays, using thin-plate spline procedures in R, accompanied by Generalised Additive Modelling (GAMs) to test the main and interactive effects of the three macronutrients. These methods are described elsewhere (Solon-Biet et al., 2014, Solon-Biet et al., 2015, Le Couteur et al., 2014).

To explore the relationship between fenestrations, dietary macronutrients and the gut microbiome correlations with fenestrations were performed using the Spearman's test in SigmaPlot (SPSS Version 12.5) were performed in the first instance (data presented are mean ± SD and $P<0.05$ considered significant). To further explore these relationships we then tested whether abundance of circulating metabolites (fatty acids and amino acids) and bacterial families correlated with fenestration morphology using an information theoretic, model averaging approach with linear models (LMs) (Burnham & Anderson, 2002). We assessed whether dietary correlates affected three aspects of fenestrations: 1) percent porosity (converted to a proportion and logit transformed to normalise; (Warton and Hui, 2010)), 2) diameter of the fenestration and 3) fenestration frequency (+0.5 and log transformed to normalise;(Yamamura, 1999)). LMs were fitted using the 'lm' function in the *base* package of *R (*R-Development-Core-Team, 2015), and model averaging was performed using the package *MuMIn (*Bartoń, 2015). These analyses were undertaken by Dr Alistair Senior in the laboratory of Professor Simpson at the Charles Perkins Centre, University of Sydney.

6.3 RESULTS

6.3.1 Geometric framework analysis of the relationship between macronutrients and LSEC fenestrations.

Response surfaces showing the relationship between macronutrients, dietary energy and fenestration morphology are shown in Fig. 6.1 (n=129 mice) and representative scanning electron micrographs are shown in Fig. 6.2. Fenestration porosity was influenced by dietary fat intake (P=0.016, for GAMs tables see Table 6.1), with low to intermediate fat intakes (around 20 kJ/mouse/day) associated with highest porosity, and porosity falling both as fat intake increased or decreased to very low levels indicating a non-linear effect (quadratic). There was no statistically significant impact of the intake of energy, protein or carbohydrate on porosity. The response of fenestration frequency was similar to that of porosity, being associated only with fat intake (P=0.001). On the other hand, fenestration frequency was inversely associated with protein and carbohydrate intakes (P=0.028 and P=0.006, respectively). Low carbohydrate or low protein intake were both associated with increased fenestration diameter. However, there were no interactions between protein and carbohydrate, and their impact on diameter was not sufficient to translate into a change in total porosity.

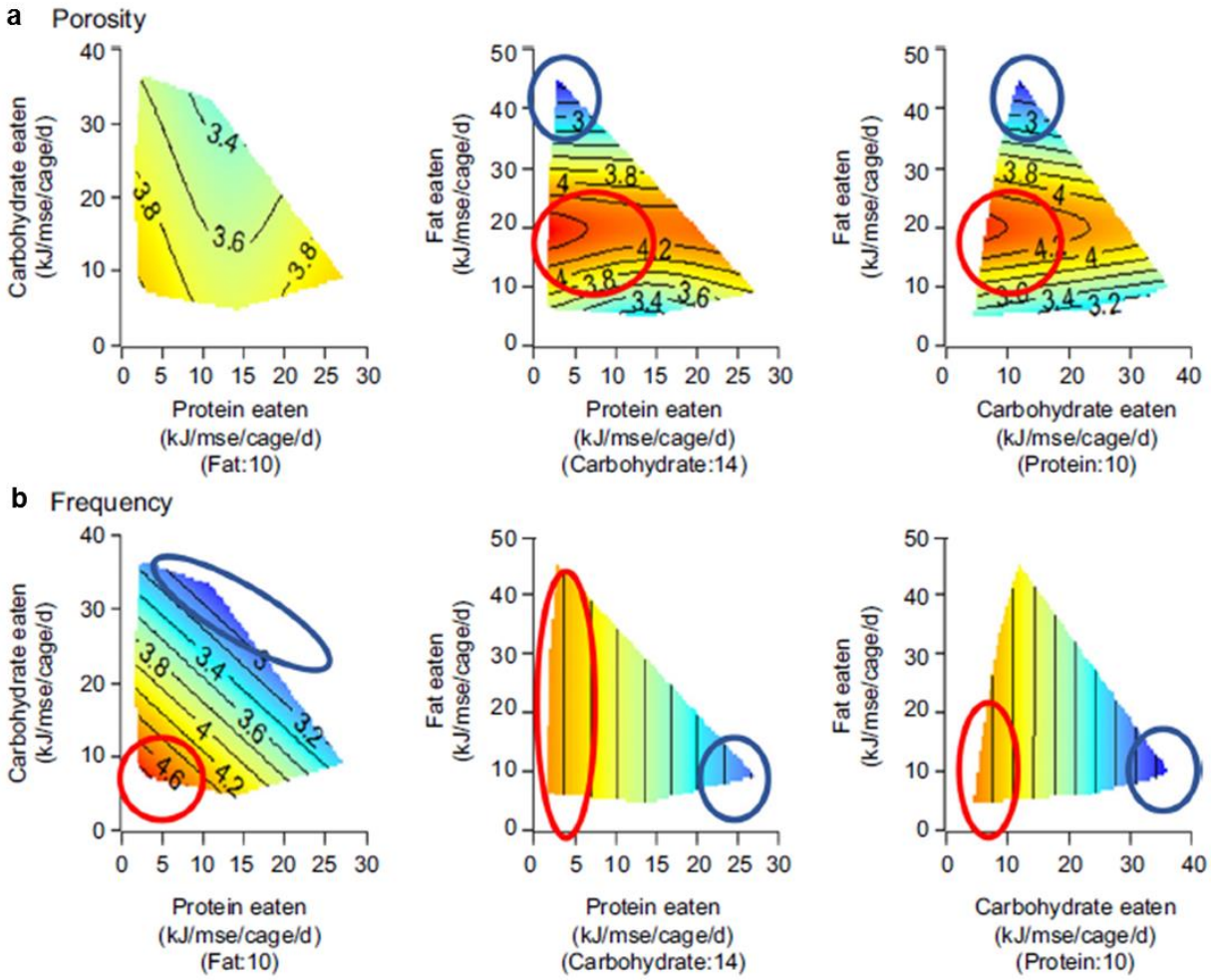

Figure 6.1: Geometric Framework analysis showing relationship between macronutrients and fenestration porosity (a) and diameter (b). In each surface the blue represents the lowest value while the red represents the highest value. Each graph represents a slice through the median value of the third macronutrient (value provided in parenthesis below the x-axis label). Three graphs are provided demonstrating the interactions between protein and carbohydrate, protein and fat, and carbohydrate and fat. The regions with the highest fenestration diameter porosity or diameter are encircled in red, while those with the lowest are encircled with blue. Fat had a significant effect on porosity (P=0.016) while protein and carbohydrate had significant effects on diameter (P=0.028 and P=0.006, respectively).

Table 6.1: Generalised Additive Modelling (GAMs) for Figure 6.1.

	edf	Degrees of freedom	F	p-value
Porosity (Fig. 1a)				
Protein eaten	5.447e-05	8	0.000	0.5569
Carbohydrate eaten	5.508e-01	8	0.153	0.1218
Fat eaten	1.874	8	0.698	0.0157 *
Protein, carbohydrate eaten	1.595e-05	3	0.000	0.7683
Protein, fat eaten	8.597e-01	3	0.538	0.1076
Carbohydrate, fat eaten	5.143e-05	3	0.000	0.5844
Frequency (Fig. 1b)				
Protein eaten	7.904e-01	8	0.000	0.02760*
Carbohydrate eaten	8.628e-01	8	0.000	0.00633**
Fat eaten	6.362e-05	8	0.000	0.38350
Protein, carbohydrate eaten	2.451e-06	3	0.000	0.89405
Protein, fat eaten	4.171e-06	3	0.000	0.73794
Carbohydrate, fat eaten	7.106e-06	3	0.000	0.88118

Fig. 1a: *R* sq. (adj.) = 0.0942. Deviance explained = 11.7%. REML = 234.77. Scale est. = 2.1008; n = 129. Fig 1b: *R* sq.(adj.) = 0.052. Deviance explained = 6.42%. REML = 272.02. Scale est. = 3.8373; n = 129. GAMs, generalized additive modelling; edf, estimated degrees of freedom; REM, restricted maximal likelihood. *$P < 0.05$; **$P < 0.01$.

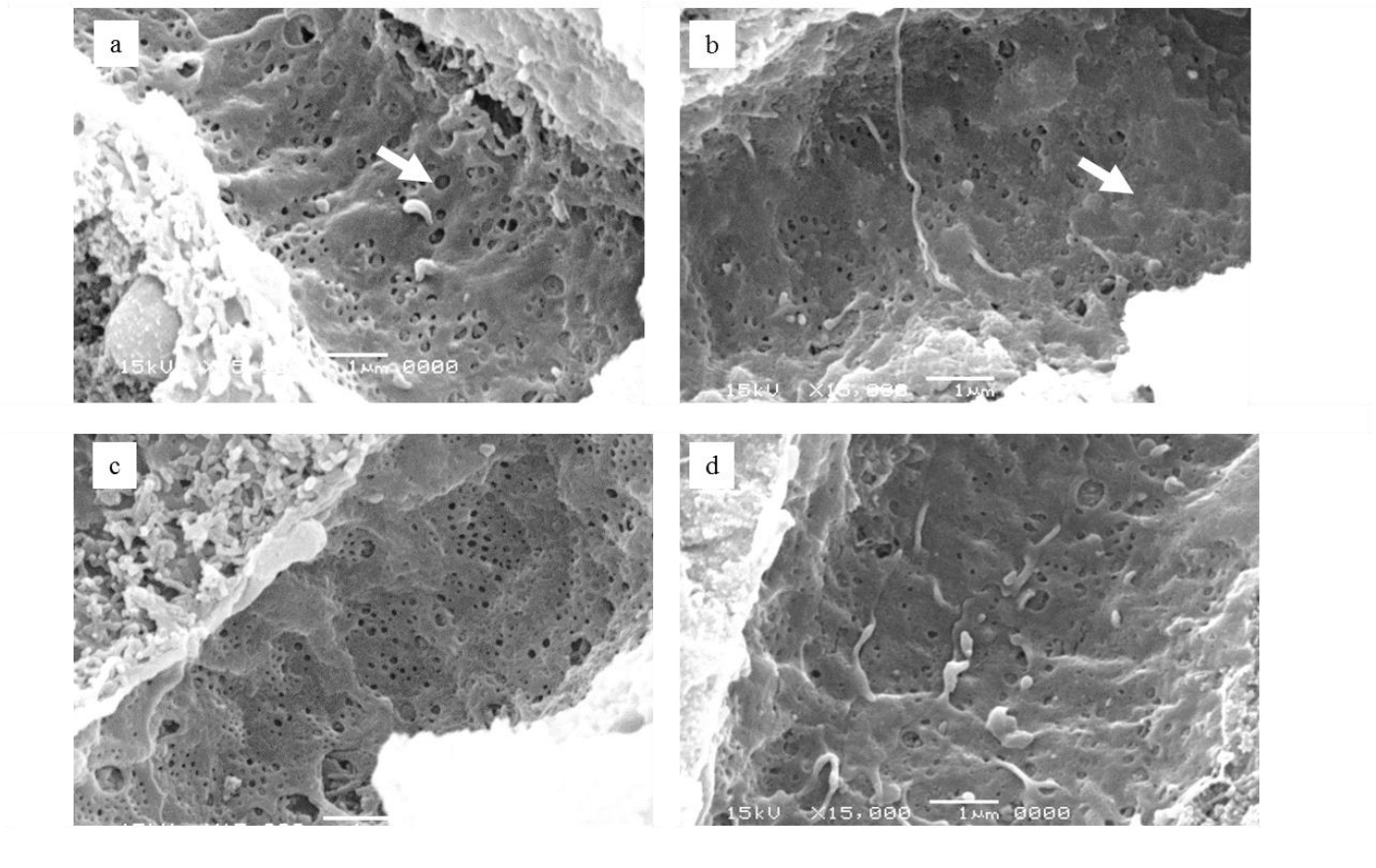

Figure 6.2: Scanning electron micrographs of the luminal surface of the liver sinusoidal endothelial cells. Some fenestrations are indicated with an arrow. (a). Increased fenestration diameter induced by diets low in carbohydrate or protein. (b) fenestration diameter is decreased in diets high in carbohydrates or protein, (c) Increased porosity induced by fat intake of approximately 20 kJ/mouse/day and (d) Diets high in fat lead to reduced endothelial porosity through loss of fenestrations (Original magnification 15000 ×).

6.3.2 Relationship between fenestrations and gut microbiome.

There were 78 mice where a complete dataset was available for both electron microscopy of the LSEC and gut microbiome analysis. In this cohort of samples the most abundant taxa were the *Firmicutes* and *Bacteroidetes* phyla, followed by *Clostridia, Bacillae, Erysipelotrichia, Deferribacteres, Verrucomicrobia, Lachnospiraceae, Clostridiaceae, Ruminococcaceae, Eubacteriaceae, Rikenellaceae,* and *Bacteroidaceae*. There were significant positive relationships between fenestration porosity and diameter with the abundance of the *Firmicutes* phylum (Fig. 6.3, P=0.046 and P=0.0057 respectively). There was a significant negative relationship between fenestration diameter and the abundance of the *Bacteroidetes* phylum (P=0.045) and a non-significant negative trend with fenestration porosity and *Bacteroidetes* (Fig. 6.3, P=0.087).

Model averaging of lower taxonomic orders suggested no bacterial families were particularly good predictors of fenestration diameter or porosity (all families had a relative importance < 0.6), and for both responses the top model sets included the null models (see Supplementary Tables 2, 3, 4 and 5). However, in concordance with the relationships suggested above, model averaging suggested that increasing *Bacteroidaceae* abundance (a member of the *Bacteroidetes* Phylum) was associated with a decreasing frequency of fenestrations (LM Est. [LCI to UCI] = -0.603 [-0.954 to -0.252]; Supplementary Table 6) and increasing abundance of *Lachnospiraceae (*a member of the *Firmicutes* phylum) was associated with an increase in fenestrations (LM Est. [LCI to UCI] = 0.422 [0.063 to 0.781]; Supplementary Table 7).

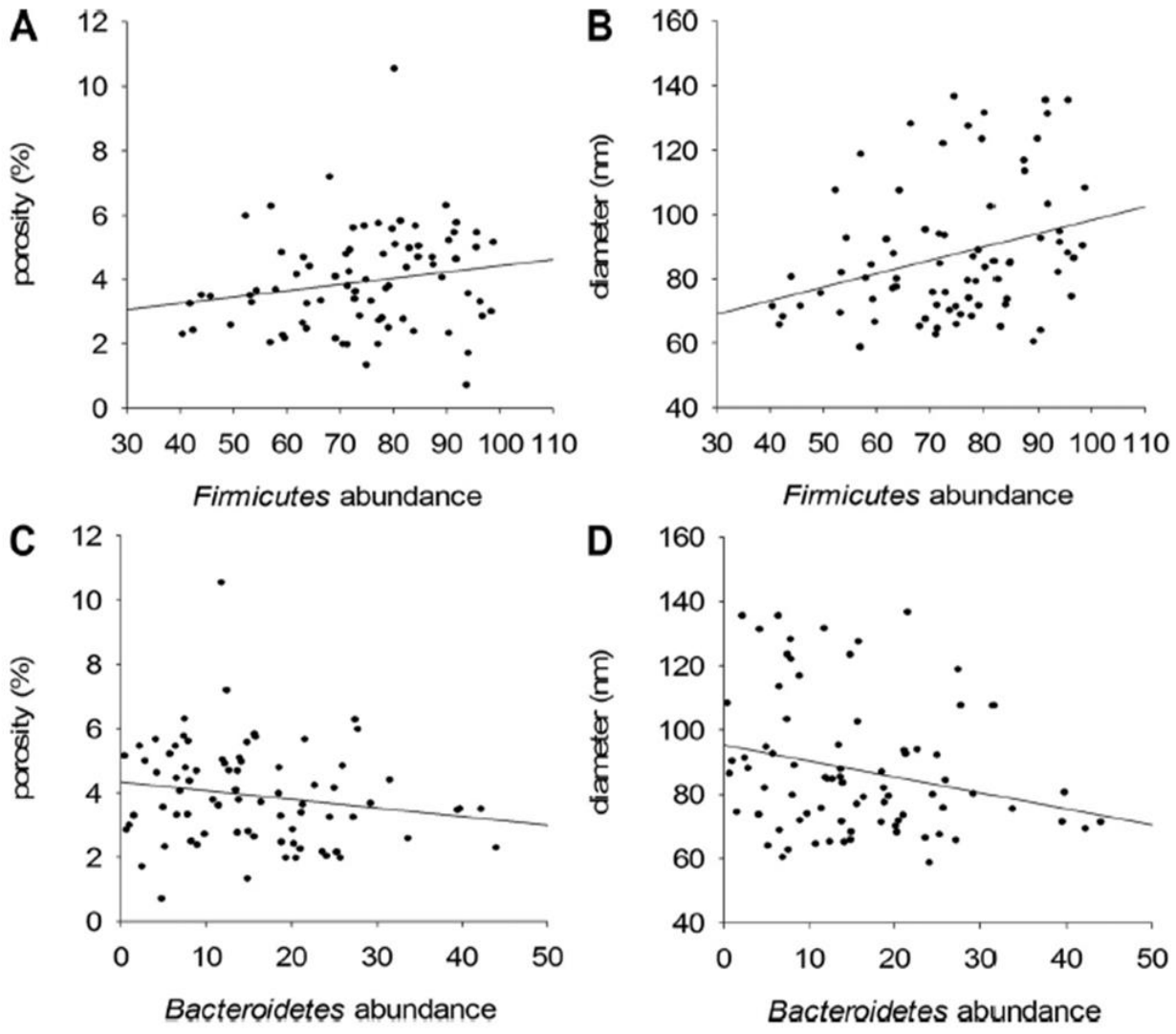

Figure 6.3: The relationship between fenestrations (diameter, porosity) and gut microbiome phyla (*Firmicutes, Bacteroidetes*). There was a significant positive relationship between fenestration porosity and diameter with *Firmicutes* abundance (a, b, Spearmans correlation, P=0.046 and P=0.0057 respectively). There was a significant negative relationship between fenestration diameter and *Bacteroidetes* abundance (d, P=0.045) and a non-significant negative trend with fenestration porosity and *Bacteroidetes* (c, P=0.087)

6.3.3 Relationship between fenestrations and circulating metabolites and other substrates influenced by diet.

Correlative analysis of individual free fatty acids found negative relationships between C16:0 (palmitic acid) and C20:4 (arachidonic acid) with fenestration porosity (P=0.027 and P=0.037, respectively, n=95 mice), while C19:0 (nonadecanoic acid) had negative associations with fenestration diameter (P=0.020, Fig. 6.4), as well as frequency (P=0.048, Appendix 6). However, model averaging of free fatty acid groups showed that despite the strong influence that dietary fat intake has on fenestration morphology, circulating levels of fatty acids are not good predictors of fenestration responses, in all cases the relative importance of predictors was less than 0.45, and for all three responses the top model set contained the null model (see Supplementary Tables 8, 9, 10, 11, 12 and 13 in Appendix 6). In addition there were no associations between fenestrations and other measures that reflect metabolic health including blood glucose, insulin, triglycerides, cholesterol or leptin, although there was a non-significant trend towards a negative relationship between fenestration diameter and fasting insulin.

There were no significant relationships between fenestration porosity, diameter or frequency with circulating levels of total amino acids, total branched chain amino acids or any of the individual amino acids except phenylalanine which had a negative relationship with porosity (P=0.037, n=94 mice, Fig. 6.4) and aspartic acid which had a negative relationship with diameter (P=0.047). Model averaging of more complex models also indicated that the concentration of circulating amino acids were not a good predictor of fenestration diameter or frequency; in both cases the top model sets contained the null models (see Supplementary Tables 14, 15, 16 and 17

in Appendix 6). The best predictor was abundance of hydroxyl and sulfur selenium amino acids, which had a relative importance of 0.832 for the fenestration diameter response, and was estimated to have a positive effect but with very poor precision (LM Est. [LCI to UCI] = 11.779 [-1.075 to 24.633]; Supplementary Table 15). For fenestration porosity, abundance of aliphatic amino acids had a relative importance of 1, appearing in all models in the top model set (Supplementary Tables 18 and 19). Model averaged estimates indicate that increases in aliphatic amino acids were associated with decreases in the porosity of fenestrations (LM Est. [LCI to UCI] = -0.431 [-0.799 to 0.063]; Supplementary Table 19).

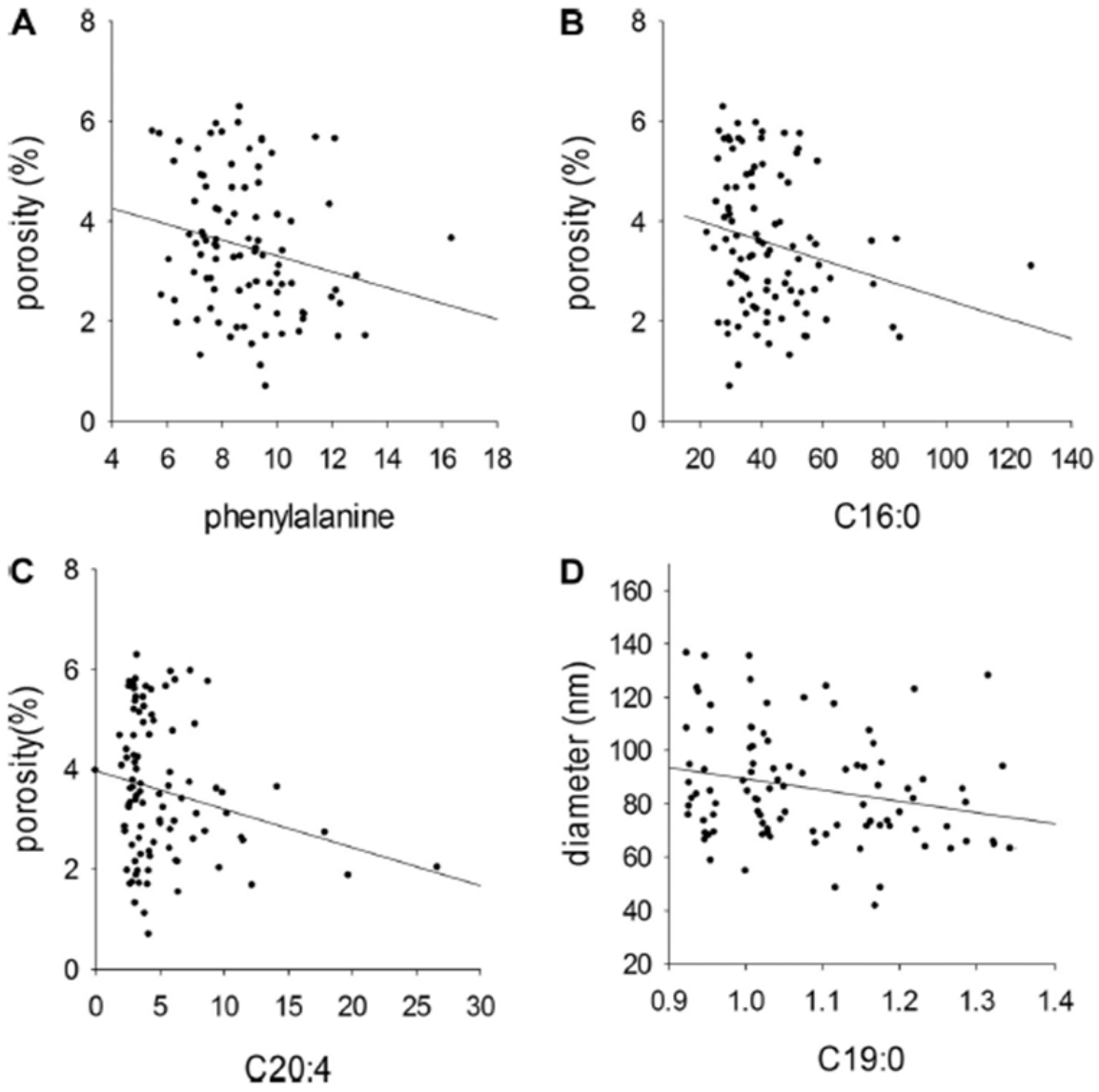

Figure 6.4: The relationship between phenylalanine, and the fatty acids C16:0, C19:0 and C20:4. There were significant correlations between porosity and circulating phenylalanine (P=0.037), C16:0 (P=0.027) and C20:4 (P=0.037) and between fenestration diameter and C19:0 (P=0.020).

6.4 DISCUSSION

In previous studies, fenestrations have been reported to be influenced by reduced intake of food and dietary energy. In one study, my laboratory showed that a 48 hour period of fasting in rats was associated with increased fenestration diameter of about 10%(O'Reilly et al., 2010). In another study from my laboratory it was found that caloric restriction over a lifetime in rats was associated with increased fenestration frequency and porosity of about 60% in old age (Jamieson et al., 2007b). These studies indicate that fenestrations are dynamic structures that are influenced by dietary manipulation. However, such studies where only one nutritional dimension, energy, is manipulated cannot determine whether the outcome is a result of a reduction in total energy or one of the individual macronutrient components of the diet (Simpson et al., 2015). One of the key advantages of using the Geometric Framework is that the different components of the diet – energy, protein, carbohydrates and fat plus their interactions – can be evaluated across a nutritional landscape (Simpson and Raubenheimer, 2012). The results of this study have revealed that the main dietary component that influences fenestration porosity is fat, such that higher fat intakes are associated with reduced fenestration frequency and overall porosity. A low fat intake of approximately 20 kJ/mouse/day was associated with maximum porosity below which porosity decreased again slightly. According to the phenotype response surfaces, porosity varied between about 2.8% and 4.4% depending upon the dietary fat intake. Fat intake had its main impact on fenestration frequency while protein and carbohydrate intakes influenced fenestration diameter, although this was not sufficient to alter total porosity.

A number of nutritional interventions have been found to influence ageing and lifespan. The most widely studied is caloric restriction. We have previously shown that caloric restriction is associated with increased fenestrations in old age (Jamieson et al., 2007b). The results in our current study suggest that this might be secondary to a reduction in each of the macronutrients acting via different mechanisms: the reduction in fat intake leads to increased fenestration diameter, the reduction in protein and carbohydrate intake leads to increased fenestration frequency. On the other hand, our studies in insects (Lee et al., 2008) and mice (Solon-Biet et al., 2014) have indicated that low protein, high carbohydrate diets are linked with longer lifespan and improved latelife health. We did not find any direct beneficial impact of low protein, high carbohydrate diets on fenestrations, perhaps as a consequence of the opposing effects of low protein and high carbohydrate on fenestration diameter.

Having established that macronutrients influence fenestrations we then sought to elucidate possible mechanisms that could link diet with LSEC ultrastructure. We performed analysis of gut microbiome and circulating fatty acids and amino acids. Analysis of the gut microbiome data showed that there was a positive relationship between fenestrations and diet-induced changes in the *Firmicutes* phylum and a negative relationship and/or trend with the *Bacteroidetes* phylum. *Firmicutes* and *Bacteroidetes* make up the most abundant phyla within the gut microbiome. Although the abundances of *Firmicutes* and *Bacteroidetes* have been linked to various health states, these phyla include a broad diversity of different taxa of bacteria, thus analysis limited to *Firmicutes* and *Bacteroidetes* can only be considered to be a blunt interpretation of gut microbiota (Jandhyala et al., 2015, Ha et al., 2014). It is interesting that the abundance of *Firmicutes* declines with age while *Bacteroidetes* increases (Jandhyala et al., 2015, Mariat et al.,

2009). Ageing is associated with a reduction in fenestrations which is a key part of age-related pseudocapillarisation of the hepatic sinusoid (Le Couteur et al., 2008a, Le Couteur et al., 2001) which might therefore be mechanistically linked with age-related changes in the relative abundances of *Firmicutes* and *Bacteroidetes*. There has also been a growing focus on the role of the gut microbiome in the pathogenesis of hepatic diseases including in particular hepatosteatosis and cirrhosis (Wieland et al., 2015). This is in part because the liver receives the majority of its blood supply from the intestinal portal circulation, and is therefore exposed to a diverse array of microbial toxins and metabolites. Hepatosteatosis has been reported to be associated with reduced *Firmicutes* and increased *Bacteroidetes*, while various liver diseases are associated with leaky gut with subsequent increased exposure of the liver to bacterial toxins and bacteria (Wieland et al., 2015, Paolella et al., 2014, Dobbs et al., 1994). With respect to the LSEC, we have shown that defenestration can be caused by direct exposure to two bacterial toxins: lipopolysaccharide endotoxin (Dobbs et al., 1994) and pseudomonal pyocyanin (Cheluvappa et al., 2007).

We then investigated the relationship between circulating substrates that might reflect changes in dietary intake of macronutrients. Our previous studies have demonstrated that fenestrations form in the non-lipid raft segments of the LSEC cell membrane (Svistounov et al., 2012). Moreover, interventions that disrupted lipid rafts and the non-raft membranes had significant effects on fenestrations and porosity. We concluded that one of the factors regulating fenestrations were lipid rafts (Svistounov et al., 2012, Cogger et al., 2013a). Lipid rafts are potentially influenced by diet, in particular dietary fatty acids (Pike, 2009). The lipid rafts contain a high proportion of saturated fatty acids while long chain polyunsaturated fatty acids increase the clustering of

proteins within lipid rafts (Pike, 2009). A number of different fatty acids, including arachidonic acid (C20:4) partition rapidly into cell membranes and perturb lipid rafts (Catalá, 2012). Further it has been demonstrated that metabolites of arachidonic acid have been shown to contribute to LSEC dysfunction in the setting of portal hypertension (Bosch et al., 2010). Therefore it is of note that circulating levels of the saturated fatty acids, C16:0, C19:0 and the polyunsaturated fatty acid, C20:4 were associated with fenestrations. However, more complex models could not find substantial correlations between fatty acid groups and fenestrations.

In the Geometric Framework study of the effects of macronutrients on ageing, it was found that branched chain amino acids appeared to mediate some of the benefits of a low protein high carbohydrate diet on age-related health and lifespan (Solon-Biet et al., 2014). Here we did not find any association between branched chain amino acids and fenestrations. Examination of the other amino acids revealed an inverse association between porosity and phenylalanine concentrations Although this could be a chance finding, it is of note that an elevated level of phenylalanine is a risk factor for hypertriglyceridemia (Mook-Kanamori et al., 2014), while defenestration is a mechanism for hyperlipidemia through impaired hepatic uptake of chylomicron remnants (Hilmer et al., 2005).

In conclusion, macronutrients had complex effects on LSEC fenestrations. Overall, reduced intake of macronutrients was associated with increased measures of fenestration frequency and/or diameter, with fat having the dominant influence on porosity mediated by its effect on the frequency of fenestrations. There was an association between microbiome (*Firmicutes,*

Bacteroidetes) and free fatty acids with fenestrations which might provide mechanistic links between dietary macronutrients and LSEC ultrastructure in old age.

CHAPTER 7: GENERAL DISCUSSION

The liver is the main organ in the body responsible for a wide variety of biological processes regulated by insulin such as glucose homeostasis and hepatic insulin clearance. Glucose metabolism is significantly impaired with ageing (Fink et al., 1983) and impaired insulin action with age contributes to disease and morbidity.

Age-related changes in the liver have been established in a variety of species. In addition to a reduction in both liver size and blood flow, the endothelial changes of pseudocapillarisation- decreased porosity, increased thickness and increased basal lamina - have been reported. These alterations have contributed to reduced hepatic clearance of many substrates with age. My laboratory has previously demonstrated that ageing is associated with an impaired clearance of chylomicron remnant secondary to defenestration in ageing, contributing to the development of atherosclerosis. Similarly it has been shown here that age- and disease related loss of fenestrations may form a barrier for insulin action, contributing to insulin resistance in ageing.

The majority of previous liver studies examining insulin action focus on the hepatocyte, however as postulated here the cells of the hepatic sinusoid are also crucial to liver function. The work of this thesis focuses on the vital role of the LSEC on insulin action and glucose homeostasis in the liver during health, ageing and also toxicity (P407).

In Chapter 3, the impact of age-related pseudocapillarisation of the liver sinusoidal endothelium has shown, for what we believe is the first time, that fenestrations are essential for efficient insulin transfer across the liver sinusoidal endothelium and subsequent insulin and glucose homeostasis. Mechanistically, we have demonstrated defenestration such as occurs in ageing and

liver disease, restricts insulin access to the hepatocellular membrane through impaired trans-endothelial transfer, resulting in hyperinsulinemia, impaired hepatic insulin signaling, reduced glycogen storage, compensatory muscle and fat uptake of insulin and glucose and dysregulated gluconeogenesis. Future studies showing a correlation between insulin transfer and consequent signaling events are needed to obtain a full picture of the LSEC role in metabolism homeostasis.

However, as it is recognised that ageing is a multifactorial process where many fundamental cellular processes are affected and considerable adaptations develop overtime to support metabolic homeostasis, testing the role of LSEC fenestrations in insulin transfer in a singular model of defenestration is important. Chapter 4 used P407 induced defenestration to explore the impact of acute defenestration on insulin and glucose transfer. This work showed that defenestration alone reduced the transfer of insulin and glucose from the sinusoid into the extracellular space and reduced insulin action in hepatocytes with an impact on glucose homeostasis. This was associated with hyperinsulinaemia, glucose intolerance and deranged glucose metabolism in the liver. While not all of the ageing changes in the liver are recapitulated by P407 these results are in agreement with the findings in Chapter 3, and are also in parallel with a previous study showing that defenestration of the LSEC in ageing leads to impaired transendothelial transfer of various other substances such as lipoproteins and medications into the liver (Hilmer et al., 2005, Mitchell et al., 2012, Mitchell et al., 2011).

Following up on the loss of fenestrations *in vivo* by P407 in Chapter 4, an *in vitro* analysis of isolated LSECS treated with P407 was performed in Chapter 5. This work explored the mechanism for defenestration in this model and demonstrates that loss of fenestrations is caused

by the depletion of the non-lipid raft domains in the LSEC membrane, inhibiting the formation of fenestrations. . Further studies will need to be performed to further support this work and should include observations of these changes via live-cell imaging or with additional treatment of insulin to add to the results obtained *in vivo*. This finding has strengthened the sieve-raft hypothesis and further facilitated the study of fenestration biology as the changes can be detected by fluorescence rather than electron microscopy. As there is increased recognition of the role of LSECs in liver pathology, it is important that the mechanisms that regulate fenestrations are elucidated so we can enhance understanding of the risk factors for LSEC changes and potentially target these mechanisms for development of therapies for the management of diseases and old age. Future studies examining the cellular mechanisms behind age- and disease-related defenestration are required, however extrapolating from these and other related studies suggest that examining the lipid properties of the cell membranes would be beneficial.

Chapter 6 investigates the effects of macronutrient intake on the ageing vasculature of the liver and its association with gut microbiome and circulating fatty acids. Reduced intake of macronutrients was associated with increased fenestration frequency and/or diameter, with fat having the dominant influence on porosity mediated by its effect on the frequency of fenestrations. There was an association between microbiome (*Firmicutes, Bacteroidetes*) and free fatty acids with fenestrations which might provide mechanistic links between dietary macronutrients and LSEC ultrastructure in old age. This indicates that the rate of development of changes in LSEC is influenced not only by ageing but also by dietary manipulation, and possibly that pseudocapillarisation may be attenuated or indeed prevented by diet.

The studies in this thesis have shed light on the importance of the endothelium in the liver, as similarly in other tissues, in the maintenance of normal function and regulation of metabolic homeostasis. This establishes not only the importance of the fenestrated endothelium for the transfer of insulin in the liver, but also further validates the poloxamer 407 model for examining substrate transfer across the ageing sinusoidal endothelium. The role of pseudocapillarisation in age-related insulin resistance could be further established using experimental models that defenestrate the normal LSEC and/or regenerate fenestrations in aged-related pseudocapillarisation. Future studies are needed to understand fenestration biology and the mechanism that underlies loss of fenestrations. This understanding may allow the prevention of pseudocapillarisation and initiate the development of therapies to attenuate age-related structural changes. Such interventions are important for the prevention and management of impaired metabolic homeostasis such as insulin resistance and hyperlipidemia in older people.

In conclusion, the integrity of the liver microvasculature is essential for the lifelong maintenance of insulin and glucose homeostasis. The morphology of the liver sinusoidal endothelial cell is dependent on the properties of the cell membranes, which can be altered through diet and exposure to circulating macronutrients and gut microbiome-derived factors. These results suggest interesting avenues to pursue for the treatment and prevention of age-related defenestration and the diseases and morbidities associated with age. Future research should focus on therapeutic agents that maintain the ultrastructure of the LSEC in old age as a potential therapy for the treatment and prevention of insulin resistant and diabetes in older people

REFERENCES

Abdul-Ghani, M. A., Jenkinson, C. P., Richardson, D. K., Tripathy, D. & Defronzo, R. A. 2006. Insulin secretion and action in subjects with impaired fasting glucose and impaired glucose tolerance results from the veterans administration genetic epidemiology study. *Diabetes,* 55**,** 1430-1435.

Adachi, H. & Tsujimoto, M. 2002. FEEL-1, a novel scavenger receptor with in vitro bacteria-binding and angiogenesis-modulating activities. *Journal of Biological Chemistry,* 277**,** 34264-34270.

Adeli, K., Taghibiglou, C., Van Iderstine, S. C. & Lewis, G. F. 2001. Mechanisms of hepatic very low-density lipoprotein overproduction in insulin resistance. *Trends in Cardiovascular Medicine,* 11**,** 170-176.

Alberti, K., Zimmet, P. & Shaw, J. 2006. Metabolic syndrome—a new world-wide definition. A consensus statement from the international diabetes federation. *Diabetic medicine,* 23**,** 469-480.

Alberti, K. G., Zimmet, P., Shaw, J. & Group, I. D. F. E. T. F. C. 2005. The metabolic syndrome--a new worldwide definition. *Lancet,* 366**,** 1059-62.

Alberti, K. G. M. M. & Zimmet, P. F. 1998. Definition, diagnosis and classification of diabetes mellitus and its complications. Part 1: diagnosis and classification of diabetes mellitus. Provisional report of a WHO consultation. *Diabetic medicine,* 15**,** 539-553.

Albornoz, L., Alvarez, D., Otaso, J. C., Gadano, A., Salviú, J., Gerona, S., Sorroche, P., Villamil, A. & Mastai, R. 1999. Von Willebrand factor could be an index of endothelial dysfunction in patients with cirrhosis: relationship to degree of liver failure and nitric oxide levels. *Journal of Hepatology,* 30**,** 451-455.

Alessi, D. R., James, S. R., Downes, C. P., Holmes, A. B., Gaffney, P. R., Reese, C. B. & Cohen, P. 1997. Characterization of a 3-phosphoinositide-dependent protein kinase which phosphorylates and activates protein kinase Bα. *Current Biology,* 7**,** 261-269.

Anderson, P. J., Critchley, J. A., Chan, J. C., Cockram, C. S., Lee, Z. S., Thomas, G. N. & Tomlinson, B. 2001. Factor analysis of the metabolic syndrome: obesity vs insulin resistance as the central abnormality. *International Journal of Obesity and Related Metabolic Disorders,* 25**,** 1782-8.

Andrew, W. 1969. Comparative study of aging of the liver (日本解剖学会第 74 回総会特別講演). *解剖学雑誌,* 44**,** 70-71.

Araki, E., Lipes, M. A., Patti, M.-E., Brüning, J. C., Haag Iii, B., Johnson, R. S. & Kahn, C. R. 1994. Alternative pathway of insulin signalling in mice with targeted disruption of the IRS-1 gene. *Nature,* 372 (6502), 186-190.

Arias, I., Wolkoff, A., Boyer, J., Shafritz, D., Fausto, N., Alter, H. & Cohen, D. 2011. *The Liver: Biology and Pathobiology*, John Wiley & Sons.

Arias, I. M. 1990. The biology of hepatic endothelial cell fenestrae. *Progress in Liver Diseases,* 9**,** 11-26.

Arii, S. & Imamura, M. 2000. Physiological role of sinusoidal endothelial cells and Kupffer cells and their implication in the pathogenesis of liver injury. *Journal of Hepato-Biliary-Pancreatic Surgery,* 7**,** 40-48.

Avogaro, A., Piarulli, F., Valerio, A., Miola, M., Calveri, M., Pavan, P., Vicini, P., Cobelli, C., Tiengo, A., Calo, L. & Del Prato, S. 1997. Forearm nitric oxide balance, vascular relaxation, and glucose metabolism in NIDDM patients. *Diabetes,* 46**,** 1040-6.

Azzout-Marniche, D., Becard, D., Guichard, C., Foretz, M., Ferre, P. & Foufelle, F. 2000. Insulin effects on sterol regulatory-element-binding protein-1c (SREBP-1c) transcriptional activity in rat hepatocytes. *Biochemical Journal,* 350**,** 389-393.

Baker, R. W. 2004. Membrane transport theory. *Membrane Technology and Applications, Second Edition***,** 15-87.

Banting, F., Best, C., Collip, J., Campbell, W. & Fletcher, A. 1991. Pancreatic extracts in the treatment of diabetes mellitus: preliminary report. 1922. *CMAJ: Canadian Medical Association Journal,* 145**,** 1281.

Bao, J.-X., Jin, S., Zhang, F., Wang, Z.-C., Li, N. & Li, P.-L. 2010. Activation of membrane NADPH oxidase associated with lysosome-targeted acid sphingomyelinase in coronary endothelial cells. *Antioxidants & redox signaling,* 12**,** 703-712.

Bartoń, K. 2015. *Mumin: Multi-model inference* [Online]. http://CRAN.R-project.org/package=MuMIn.

Barzilai, N. & Rossetti, L. 1993. Role of glucokinase and glucose-6-phosphatase in the acute and chronic regulation of hepatic glucose fluxes by insulin. *Journal of Biological Chemistry,* 268**,** 25019-25025.

Bataller, R. & Brenner, D. A. 2009. Hepatic Fibrosis. *The Liver: Biology and Pathobiology, Fifth Edition***,** 433-452.

Baumann, C. A., Ribon, V., Kanzaki, M., Thurmond, D. C., Mora, S., Shigematsu, S., Bickel, P. E., Pessin, J. E. & Saltiel, A. R. 2000. CAP defines a second signalling pathway required for insulin-stimulated glucose transport. *Nature,* 407**,** 202-207.

Baumgartner-Parzer, S. M. & Waldhausl, W. K. 2001. The endothelium as a metabolic and endocrine organ: its relation with insulin resistance. *Experimental and Clinical Endocrinology & Diabetes,* 109 Suppl 2**,** S166-79.

Beck-Nielsen, H., Alford, F. & Hother-Nielsen, O. 2005. Insulin resistance in glucose disposal and production in man with specific reference to metabolic syndrome and type 2 diabetes. *Insulin Resistance Insulin action and its disturbances in disease. West Sussex: Wiley***,** 155-79.

Benyon, R. C. & Arthur, M. J. 1998. Mechanisms of hepatic fibrosis. *Journal of Pediatric Gastroenterology and Nutrition,* 27**,** 75-85.

Bergeron, J. J., Sikstrom, R., Hand, A. R. & Posner, B. I. 1979. Binding and uptake of 125I-insulin into rat liver hepatocytes and endothelium. An in vivo radioautographic study. *The Journal of Cell Biology,* 80**,** 427-443.

Bergman, R. N., Finegood, D. T. & Ader, M. 1985. Assessment of Insulin Sensitivity in Vivo*. *Endocrine Reviews,* 6**,** 45-86.

Bernuau, D., Guillot, R., Durand, A.-M., Raoux, N., Gabreau, T., Passa, P. & Feldmann, G. 1982. Ultrastructural aspects of the liver perisinusoidal space in diabetic patients with and without microangiopathy. *Diabetes,* 31**,** 1061-1067.

Bharti, S. K., Krishnan, S., Kumar, A., Rajak, K. K., Murari, K., Bharti, B. K. & Gupta, A. K. 2013. Antidiabetic activity and molecular docking of fructooligosaccharides produced by Aureobasidium pullulans in poloxamer-407-induced T2DM rats. *Food Chemistry,* 136**,** 813-21.

Blouin, A., Bolender, R. P. & Weibel, E. R. 1977. Distribution of organelles and membranes between hepatocytes and nonhepatocytes in the rat liver parenchyma. A stereological study. *The Journal of cell biology,* 72**,** 441-455.

Bluher, M., Michael, M. D., Peroni, O. D., Ueki, K., Carter, N., Kahn, B. B. & Kahn, C. R. 2002. Adipose tissue selective insulin receptor knockout protects against obesity and obesity-related glucose intolerance. *Developmental Cell,* 3**,** 25-38.

Bonora, E., Zavaroni, I., Coscelli, C. & Butturini, U. 1983. Decreased hepatic insulin extraction in subjects with mild glucose intolerance. *Metabolism,* 32**,** 438-446.

Bonora, E., Zavaroni, I., Manicardi, V., Coscelli, C. & Butturini, U. 1986. Further evidence that insulin metabolism is a major determinant of peripheral insulin response to oral glucose in subjects with mild glucose intolerance. *Journal of endocrinological investigation,* 9**,** 371-374.

Bosch, J. 2007. Vascular deterioration in cirrhosis: the big picture. *Journal of clinical gastroenterology,* 41**,** S247-S253.

Bosch, J., Abraldes, J. G., Fernández, M. & García-Pagán, J. C. 2010. Hepatic endothelial dysfunction and abnormal angiogenesis: new targets in the treatment of portal hypertension. *Journal of Hepatology,* 53**,** 558-567.

Bose, S. K. & Ray, R. 2014. Hepatitis C virus infection and insulin resistance. *World Journal of Diabetes,* 5**,** 52-8.

Bouwens, L., De Bleser, P., Vanderkerken, K., Geerts, B. & Wisse, E. 1991. Liver cell heterogeneity: functions of non-parenchymal cells. *Enzyme,* 46**,** 155-168.

Bouwens, L. & Wisse, E. 1992. Pit cells in the liver. *Liver,* 12**,** 3-9.

Braatvedt, G., Gamble, G. & Kyle, C. 2006. Metabolic characteristics of patients with apparently normal fasting plasma glucose. *The New Zealand Medical Journal,* 119.

Braet, F., De Zanger, R., Crabbe, E. & Wisse, E. 1995. New observations on cytoskeleton and fenestrae in isolated rat liver sinusoidal endothelial cells. *Journal of Gastroenterology and Hepatology (Australia),* 10**,** S3-S7.

Braet, F., De Zanger, R., Jans, D., Spector, I. & Wisse, E. 1996. Microfilament-disrupting agent latrunculin A induces an increased number of fenestrae in rat liver sinusoidal endothelial cells: Comparison with cytochalasin B. *Hepatology,* 24**,** 627-635.

Braet, F., Muller, M., Vekemans, K., Wisse, E. & Le Couteur, D. G. 2003. Antimycin A-induced defenestration in rat hepatic sinusoidal endothelial cells. *Hepatology,* 38**,** 394-402.

Braet, F., Spector, I., De Zanger, R. & Wisse, E. 1998. A novel structure involved in the formation of liver endothelial cell fenestrae revealed by using the actin inhibitor misakinolide. *Proceedings of the National Academy of Sciences of the United States of America,* 95**,** 13635-13640.

Braet, F., Spector, I., Shochet, N., Crews, P., Higa, T., Menu, E., De Zanger, R. & Wisse, E. 2002. The new anti-actin agent dihydrohalichondramide reveals fenestrae-forming centers in hepatic endothelial cells. *BMC Cell Biology,* 3.

Braet, F. & Wisse, E. 2002. Structural and functional aspects of liver sinusoidal endothelial cell fenestrae: A review. *Comparative Hepatology,* 1.

Braet, F., Wisse, E., Bomans, P., Frederik, P., Geerts, W., Koster, A., Soon, L. & Ringer, S. 2007. Contribution of high-resolution correlative imaging techniques in the study of the liver sieve in three-dimensions. *Microscopy Research and Technique,* 70**,** 230-242.

Brüning, J. C., Michael, M. D., Winnay, J. N., Hayashi, T., Hörsch, D., Accili, D., Goodyear, L. J. & Kahn, C. R. 1998. A muscle-specific insulin receptor knockout exhibits features of the metabolic syndrome of NIDDM without altering glucose tolerance. *Molecular cell,* 2**,** 559-569.

Burt, A. D. 1993. Cellular and molecular aspects of hepatic fibrosis. *The Journal of pathology,* 170**,** 105-114.

Cai, D., Dhe-Paganon, S., Melendez, P. A., Lee, J. & Shoelson, S. E. 2003. Two new substrates in insulin signaling, IRS5/DOK4 and IRS6/DOK5. *Journal of Biological Chemistry,* 278**,** 25323-25330.

Caro, J. F. & Amatruda, J. M. 1980. Insulin receptors in hepatocytes: postreceptor events mediate down regulation. *Science,* 210**,** 1029-1031.

Carpenter, C. L. & Cantley, L. C. 1996. Phosphoinositide kinases. *Current opinion in Cell Biology,* 8**,** 153-158.

Cassader, M., Gambino, R., Ruiu, G., Marena, S., Bodoni, P. & Pagano, G. 1996. Postprandial triglyceride-rich lipoprotein changes in elderly and young subjects. *Aging (Milano),* 8**,** 421-8.

Catalá, A. 2012. Lipid peroxidation modifies the picture of membranes from the "Fluid Mosaic Model" to the "Lipid Whisker Model". *Biochimie,* 94**,** 101-109.

Cattley, R. C. & Popp, J. A. 2002. 31 - Liver. *In:* WALLIG, W. M. H. G. R. A. (ed.) *Handbook of Toxicologic Pathology (Second Edition).* San Diego: Academic Press.

Cederbaum, A. I. 2006. Cytochrome P450 2E1-dependent oxidant stress and upregulation of anti-oxidant defense in liver cells. *Journal of Gastroenterology and Hepatology,* 21**,** S22-S25.

Chai, S. Y., Pan, X. Y., Song, K. X., Huang, Y. Y., Li, F., Cheng, X. Y. & Qu, S. 2014. Differential patterns of insulin secretion and sensitivity in patients with type 2 diabetes mellitus and nonalcoholic fatty liver disease versus patients with type 2 diabetes mellitus alone. *Lipids in Health and Disease,* 13**,** 7.

Cheluvappa, R., Cogger, V. C., Kwun, S. Y., O'reilly, J. N., Le Couteur, D. G. & Hilmer, S. N. 2008. Liver sinusoidal endothelial cells and acute non-oxidative hepatic injury induced by Pseudomonas aeruginosa pyocyanin. *International Journal of Experimental Pathoogyl,* 89**,** 410-8.

Cheluvappa, R., Jamieson, H. A., Hilmer, S. N., Muller, M. & Le Couteur, D. G. 2007. The effect of Pseudomonas aeruginosa virulence factor, pyocyanin, on the liver sinusoidal endothelial cell. *Journal of Gastroenterology and Hepatology,,* 22**,** 1350-1.

Chen, G., Liang, G., Ou, J., Goldstein, J. L. & Brown, M. S. 2004. Central role for liver X receptor in insulin-mediated activation of Srebp-1c transcription and stimulation of fatty acid synthesis in liver. *Proceedings of the National Academy of Sciences of the United States of America,* 101**,** 11245-11250.

Chen, J., Braet, F., Brodsky, S., Weinstein, T., Romanov, V., Noiri, E. & Goligorsky, M. S. 2002. VEGF-induced mobilization of caveolae and increase in permeability of endothelial cells. *American Journal of Physiology - Cell Physiology,* 282**,** C1053-C1063.

Cheng, Z. & White, M. F. 2011. Targeting Forkhead box O1 from the concept to metabolic diseases: lessons from mouse models. *Antioxidants & redox signaling,* 14**,** 649-661.

Cherrington, A. D. & Lecture, B. 1999. Control of glucose uptake and release by the liver in vivo. *Diabetes-New York-,* 48**,** 1198-1214.

Clark, M. G., Wallis, M. G., Barrett, E. J., Vincent, M. A., Richards, S. M., Clerk, L. H. & Rattigan, S. 2003. Blood flow and muscle metabolism: a focus on insulin action. *American Journal of Physiology-Endocrinology And Metabolism,* 284**,** E241-E258.

Clark, S., Cook, H. B., Oxner, R. G., Angus, H., George, P. & Fraser, R. 1988. Defenestration of hepatic sinusoids as a cause of hyperlipoproteinaemia in alcoholics. *The Lancet,* 332**,** 1225-1227.

Cline, G. W., Petersen, K. F., Krssak, M., Shen, J., Hundal, R. S., Trajanoski, Z., Inzucchi, S., Dresner, A., Rothman, D. L. & Shulman, G. I. 1999. Impaired glucose transport as a cause of decreased insulin-stimulated muscle glycogen synthesis in type 2 diabetes. *New England Journal of Medicine,* 341**,** 240-6.

Cogger, V., O'reilly, J., Warren, A. & Le Couteur, D. 2014. A standardized method for the analysis of liver sinusoidal endothelial cells and their fenestrations by scanning electron microscopy. *Journal of Visualized Experiments: JoVE*.

Cogger, V. C., Arias, I. M., Warren, A., Mcmahon, A. C., Kiss, D. L., Avery, V. M. & Le Couteur, D. G. 2008. The response of fenestrations, actin, and caveolin-1 to vascular endothelial growth factor in SK Hep1 cells. *American Journal of Physiology Gastrointestinal and Liver Physiology,* 295**,** G137-G145.

Cogger, V. C., Hilmer, S. N., Sullivan, D., Muller, M., Fraser, R. & Le Couteur, D. G. 2006. Hyperlipidemia and surfactants: the liver sieve is a link. *Atherosclerosis,* 189**,** 273-81.

Cogger, V. C. & Le Couteur, D. G. 2009. Fenestrations in the liver sinusoidal endothelial cell. *In:* Arias, I. M., Wolkoff, A., Boyer, J. L., Shafritz, D. A., Fausto, N., Alter, H. & Cohen, A. (eds.) *The Liver: Biology and Pathobiology.* 5th Edition ed. Hoboken, NJ: John Wiley & Sons, Ltd.

Cogger, V. C., Mcnerney, G. P., Nyunt, T., Deleve, L. D., Mccourt, P., Smedsrød, B., Le Couteur, D. G. & Huser, T. R. 2010. Three-dimensional structured illumination microscopy of liver sinusoidal endothelial cell fenestrations. *Journal Of Structural Biology,* 171**,** 382-388.

Cogger, V. C., Roessner, U., Warren, A., Fraser, R. & Le Couteur, D. G. 2013a. A Sieve-Raft Hypothesis for the regulation of endothelial fenestrations. *Computational and Structural Biotechnology Journal,* 8**,** e201308003.

Cogger, V. C., Svistounov, D., Warren, A., Zykova, S., Melvin, R. G., Solon-Biet, S. M., O'reilly, J. N., Mcmahon, A. C., Ballard, J. W., De Cabo, R., Le Couteur, D. G. & Lebel, M. 2013b. Liver Aging and Pseudocapillarization in a Werner Syndrome Mouse Model. *Journals of Gerontology A Biological Sciences and Medical Sciences*.

Cogger, V. C., Warren, A., Fraser, R., Ngu, M., Mclean, A. J. & Le Couteur, D. G. 2003. Hepatic sinusoidal pseudocapillarization with aging in the non-human primate. *Experimental Gerontology,* 38**,** 1101-7.

Cohn, G. S., Kittleson, M. M. & Blumenthal, R. S. 2005. Toward an improved diagnosis of the metabolic syndrome other clues to the presence of insulin resistance. *American Journal Of Hypertension,* 18**,** 1099-1103.

Consoli, A., Nurjhan, N., Capani, F. & Gerich, J. 1989. Predominant role of gluconeogenesis in increased hepatic glucose production in NIDDM. *Diabetes,* 38**,** 550-557.

Cooney, G. J., Lyons, R. J., Crew, A. J., Jensen, T. E., Molero, J. C., Mitchell, C. J., Biden, T. J., Ormandy, C. J., James, D. E. & Daly, R. J. 2004. Improved glucose homeostasis and enhanced insulin signalling in Grb14-deficient mice. *EMBO Journal,* 23**,** 582-93.

Crispe, I. N. 2009. The liver as a lymphoid organ. *Annual Review of Immunology,* 27**,** 147-163.

Crispe, I. N. 2011. Liver antigen-presenting cells. *Journal of Hepatology,* 54**,** 357-365.

Cross, D. A., Alessi, D. R., Cohen, P., Andjelkovich, M. & Hemmings, B. A. 1995. Inhibition of glycogen synthase kinase-3 by insulin mediated by protein kinase B. *Nature,* 378**,** 785-789.

Dahlquist, G. 1993. Etiological aspects of insulin-dependent diabetes mellitus: an epidemiological perspective. *Autoimmunity,* 15**,** 61-65.

Davis, S., Monti, L., Piatti, P., Moller, N., Ng, L., Coppack, S., May, M., Brown, M., Orskov, H. & Alberti, K. 1992. Estimates of insulin action in normal, obese and NIDDM man: comparison of insulin and glucose infusion test, CIGMA, minimal model and glucose clamp techniques. *Diabetes Research (Edinburgh, Scotland),* 23**,** 1-18.

De Araújo, M. S. T., Gérard, F., Chossegros, P., Guerret, S., Barlet, P., Adeleine, P. & Grimaud, J.-A. 1993. Cellular and matrix changes in drug abuser liver sinusoids: a semiquantitative and morphometric ultrastructural study. *Virchows Archiv A,* 422**,** 145-152.

Deangelis, A. M., Heinrich, G., Dai, T., Bowman, T. A., Patel, P. R., Lee, S. J., Hong, E.-G., Jung, D. Y., Assmann, A. & Kulkarni, R. N. 2008. Carcinoembryonic antigen-related cell adhesion molecule 1 a link between insulin and lipid metabolism. *Diabetes,* 57**,** 2296-2303.

Defronzo, R. A. 1988. The triumvirate: β-cell, muscle, liver. A collusion responsible for NIDDM. *Diabetes,* 37**,** 667-687.

Defronzo, R. A. 2009. From the triumvirate to the ominous octet: a new paradigm for the treatment of type 2 diabetes mellitus. *Diabetes,* 58**,** 773-795.

Defronzo, R. A., Ferrannini, E. & Simonson, D. C. 1989. Fasting hyperglycemia in non-insulin-dependent diabetes mellitus: contributions of excessive hepatic glucose production and impaired tissue glucose uptake. *Metabolism,* 38**,** 387-395.

De Leve, L. D. Hepatic microvasculature in liver injury. Seminars in liver disease, 2007. 390-400.

De Leve, L. D. 2009. The hepatic sinusoidal endothelial cell: morphology, function, and pathobiology. *The Liver: Biology and Pathobiology, Fifth Edition***,** 371-388.

De Leve, L. D., Wang, X. & Guo, Y. 2008. Sinusoidal endothelial cells prevent rat stellate cell activation and promote reversion to quiescence. *Hepatology,* 48**,** 920-930.

De Leve, L. D., Wang, X., Hu, L., McCuskey, M. K. & McCuskey, R. S. 2004. Rat liver sinusoidal endothelial cell phenotype is maintained by paracrine and autocrine regulation. *American Journal of Physiology-Gastrointestinal and Liver Physiology,* 287**,** G757-G763.

De Leve, L. D., Wang, X., McCuskey, M. K. & McCuskey, R. S. 2006. Rat liver endothelial cells isolated by anti-CD31 immunomagnetic separation lack fenestrae and sieve plates. *American Journal of Physiology-Gastrointestinal and Liver Physiology,* 291**,** G1187-G1189.

Dobbs, B., Rogers, G., Xing, H. & Fraser, R. 1994. Endotoxin-induced defenestration of the hepatic sinusoidal endothelium: a factor in the pathogenesis of cirrhosis? *Liver,* 14**,** 230-233.

Dolganiuc, A. 2011. Role of lipid rafts in liver health and disease. *World Journal Of Gastroenterology,* 17**,** 2520.

Duckworth, W. C., Bennett, R. G. & Hamel, F. G. 1998. Insulin degradation: progress and potential 1. *Endocrine reviews,* 19**,** 608-624.

Dumont, J. E., Dremier, S., Pirson, I. & Maenhaut, C. 2002. Cross signaling, cell specificity, and physiology. *American Journal of Physiology-Cell Physiology,* 283**,** C2-C28.

Dumortier, G., Grossiord, J. L., Agnely, F. & Chaumeil, J. C. 2006. A review of poloxamer 407 pharmaceutical and pharmacological characteristics. *Pharmaceutical Research,* 23**,** 2709-28.

Eckert, G. P., Kirsch, C. & Muller, W. E. 2003. Brain-membrane cholesterol in Alzheimer's disease. *Journal of Nutrition Health and Aging,* 7**,** 18-23.

Elvevold, K., Smedsrød, B. & Martinez, I. 2008. The liver sinusoidal endothelial cell: a cell type of controversial and confusing identity. *American Journal of Physiology-Gastrointestinal and Liver Physiology,* 294**,** G391-G400.

Engholm-Keller, K., Birck, P., Storling, J., Pociot, F., Mandrup-Poulsen, T. & Larsen, M. R. 2012. TiSH--a robust and sensitive global phosphoproteomics strategy employing a combination of TiO2, SIMAC, and HILIC. *Journal of Proteomics,* 75**,** 5749-61.

Escobedo, J. A., Navankasattusas, S., Kavanaugh, W. M., Milfay, D., Fried, V. A. & Williams, L. T. 1991. cDNA cloning of a novel 85 kd protein that has SH2 domains and regulates binding of PI3-kinase to the PDGF β-receptor. *Cell,* 65**,** 75-82.

Everitt, A. V., Roth, G. S., Le Couteur, D. G. & Hilmer, S. N. 2005. Caloric restriction versus drug therapy to delay the onset of aging diseases and extend life. *Age (Dordr),* 27**,** 39-48.

Falkowska-Hansen, B., Falkowski, M., Metharom, P., Krunic, D. & Goerdt, S. 2007. Clathrin-coated vesicles form a unique net-like structure in liver sinusoidal endothelial cells by assembling along undisrupted microtubules. *Experimental Cell Research,* 313**,** 1745-1757.

Fantin, V. R., Lavan, B. E., Wang, Q., Jenkins, N. A., Gilbert, D. J., Copeland, N. G., Keller, S. R. & Lienhard, G. E. 1999. Cloning, Tissue Expression, and Chromosomal Location of the Mouse Insulin Receptor Substrate 4 Gene 1. *Endocrinology,* 140**,** 1329-1337.

Fausto, N. & Campbell, J. S. 2003. The role of hepatocytes and oval cells in liver regeneration and repopulation. *Mechanisms of Development,* 120**,** 117-130.

Fink, R. I., Kolterman, O. G., Griffin, J. & Olefsky, J. M. 1983. Mechanisms Of insulin resistance in aging. *Journal of Clinical Investigation,* 71**,** 1523-35.

Fisher, P. J., Bulur, P. A., Vuk-Pavlovic, S., Prendergast, F. G. & Dietz, A. B. 2008. Dendritic cell microvilli: a novel membrane structure associated with the multifocal synapse and T-cell clustering. *Blood,* 112**,** 5037-5045.

Fisher, S. J. & Kahn, C. R. 2003. Insulin signaling is required for insulin's direct and indirect action on hepatic glucose production. *Journal of Clinical Investigation,* 111**,** 463-8.

Fleischmann, M. & Iynedjian, P. 2000. Regulation of sterol regulatory-element binding protein 1 gene expression in liver: role of insulin and protein kinase B/cAkt. *Biochemical Journal,* 349**,** 13-17.

Franceschini, A., Szklarczyk, D., Frankild, S., Kuhn, M., Simonovic, M., Roth, A., Lin, J., Minguez, P., Bork, P., Von Mering, C. & Jensen, L. J. 2013. STRING v9.1: protein-protein interaction networks, with increased coverage and integration. *Nucleic Acids Research,* 41**,** D808-15.

Franke, T. F., Kaplan, D. R., Cantley, L. C. & Toker, A. 1997. Direct regulation of the Akt proto-oncogene product by phosphatidylinositol-3, 4-bisphosphate. *Science,* 275**,** 665-668.

FRASER, R., BOSANQUET, A. & DAY, W. 1978. Filtration of chylomicrons by the liver may influence cholesterol metabolism and atherosclerosis. *Atherosclerosis,* 29**,** 113-123.

Fraser, R., Cogger, V. C., Dobbs, B., Jamieson, H. A., Warren, A., Hilmer, S. N. & Le Couteur, D. G. 2012. The liver sieve and atherosclerosis. *Pathology,* 44**,** 181-186.

Fraser, R., Day, W. & Fernando, N. 1986. Review: the liver sinusoidal cells. Their role in disorders of the liver, lipoprotein metabolism and atherogenesis. *Pathology,* 18**,** 5-11.

Fraser, R., Dobbs, B. R. & Rogers, G. W. 1995. Lipoproteins and the liver sieve: the role of the fenestrated sinusoidal endothelium in lipoprotein metabolism, atherosclerosis, and cirrhosis. *Hepatology,* 21**,** 863-874.

Friedman, J. E., Ishizuka, T., Liu, S., Farrell, C. J., Bedol, D., Koletsky, R. J., Kaung, H.-L. & Ernsberger, P. 1997. Reduced insulin receptor signaling in the obese spontaneously hypertensive Koletsky rat. *American Journal of Physiology- Endocrinology and Metabolism,* 273**,** E1014-E1023.

Friedman, S. L. 2008. Hepatic stellate cells: protean, multifunctional, and enigmatic cells of the liver. *Physiological Reviews,* 88**,** 125-172.

Fujimoto, T. 1993. Calcium pump of the plasma membrane is localized in caveolae. *The Journal of Cell Biology,* 120**,** 1147-1157.

Fukutomi, T., Zhou, Y., Kawai, S., Eguchi, H., Wands, J. R. & LI, J. 2005. Hepatitis C virus core protein stimulates hepatocyte growth: Correlation with upregulation of wnt-1 expression. *Hepatology,* 41**,** 1096-1105.

Funyu, J., Mochida, S., Inao, M., Matsui, A. & Fujiwara, K. 2001. VEGF can act as vascular permeability factor in the hepatic sinusoids through upregulation of porosity of endothelial cells. *Biochemical and Biophysical Research Communications,* 280**,** 481-485.

Furrer, K., Rickenbacher, A., Tian, Y., Jochum, W., Bittermann, A. G., Kach, A., Humar, B., Graf, R., Moritz, W. & Clavien, P. A. 2011. Serotonin reverts age-related capillarization and failure of regeneration in the liver through a VEGF-dependent pathway. *Proceedings of the National Academy of Sciences of the United States of America,* 108**,** 2945-50.

Gagliano, N., Arosio, B., Grizzi, F., Masson, S., Tagliabue, J., Dioguardi, N., Vergani, C. & Annoni, G. 2002. Reduced collagenolytic activity of matrix metalloproteinases and development of liver fibrosis in the aging rat. *Mechanisms of Ageing and Development,* 123**,** 413-425.

Ganesan, L. P., Mohanty, S., Kim, J., Clark, K. R., Robinson, J. M. & Anderson, C. L. 2011. Rapid and efficient clearance of blood-borne virus by liver sinusoidal endothelium. *PLoS Pathology,* 7**,** e1002281-e1002281.

Geloneze, B., Vasques, A. C. J., Stabe, C. F. C., Pareja, J. C., Rosado, L. E. F. P. D., Queiroz, E. C. D. & Tambascia, M. A. 2009. HOMA1-IR and HOMA2-IR indexes in identifying insulin resistance and metabolic syndrome: Brazilian Metabolic Syndrome Study (BRAMS). *Arquivos Brasileiros de Endocrinologia & Metabologia,* 53**,** 281-287.

Gerlach, J. C., Zeilinger, K., Spatkowski, G., Hentschel, F., Schnoy, N., Kolbeck, S., Schindler, R. K. & Neuhaus, P. 2001. Large-Scale Isolation of Sinusoidal Endothelial Cells from Pig and Human Liver. *Journal of Surgical Research,* 100**,** 39-45.

Ghany, M. & Hoofnagle, J. H. 2005. Approaches to the patient with liver disease. *Harrisons Principles of Internal Medicine,* 16**,** 1808.

Goresky, C. A. 1963. A linear method for determining liver sinusoidal and extravascular volumes. *American Journal of Physiology--Legacy Content,* 204**,** 626-640.

Goresky, C. A., Bach, G. G. & Nadeau, B. E. 1973. On the uptake of materials by the intact liver. The transport and net removal of galactose. *Journal of Clinical Investigation,* 52**,** 991.

Goresky, C. A. & Silverman, M. 1964. Effect of correction of catheter distortion on calculated liver sinusoidal volumes. *American Journal of Physiology--Legacy Content,* 207**,** 883-892.

Govindarajan, S. & Bonacini, M. 2003. Liver biopsy and histopathological diagnosis. *Textbook of Gastroenterology***,** 2449-2479.

Gregg, S. Q., Gutierrez, V., Robinson, A. R., Woodell, T., Nakao, A., Ross, M. A., Michalopoulos, G. K., Rigatti, L., Rothermel, C. E., Kamileri, I., Garinis, G., Stolz, D. B. & Niedernhofer, L. J. 2011. A mouse model of accelerated liver aging due to a defect in DNA repair. *Hepatology*.

Groop, L. C., Bonadonna, R. C., Delprato, S., Ratheiser, K., Zyck, K., Ferrannini, E. & Defronzo, R. A. 1989. Glucose and free fatty acid metabolism in non-insulin-dependent diabetes mellitus. Evidence for multiple sites of insulin resistance. *Journal of Clinical Investigation,* 84**,** 205.

Gu, H., Marth, J. D., Orban, P. C., Mossmann, H. & Rajewsky, K. 1994. Deletion of a DNA polymerase beta gene segment in T cells using cell type-specific gene targeting. *Science,* 265**,** 103-106.

Gustafson, T. A., He, W., Craparo, A., Schaub, C. D. & O'neill, T. J. 1995. Phosphotyrosine-dependent interaction of SHC and insulin receptor substrate 1 with the NPEY motif of the insulin receptor via a novel non-SH2 domain. *Molecular and Cellular Biology,* 15**,** 2500-2508.

Ha, C. W., Lam, Y. Y. & Holmes, A. J. 2014. Mechanistic links between gut microbial community dynamics, microbial functions and metabolic health. *World Journal of Gastroenterology,* 20**,** 16498-517.

Hall, R. K., Wang, X. L., George, L., Koch, S. R. & Granner, D. K. 2007. Insulin represses phosphoenolpyruvate carboxykinase gene transcription by causing the rapid disruption of an active transcription complex: a potential epigenetic effect. *Molecular Endocrinology,* 21**,** 550-563.

Hanson, R. W. & Reshef, L. 1997. Regulation of phosphoenolpyruvate carboxykinase (GTP) gene expression. *Annual Review of Biochemistry,* 66**,** 581-611.

Harris, M. I., Flegal, K. M., Cowie, C. C., Eberhardt, M. S., Goldstein, D. E., Little, R. R., Wiedmeyer, H.-M. & Byrd-Holt, D. D. 1998. Prevalence of diabetes, impaired fasting glucose, and impaired glucose tolerance in US adults: the Third National Health and Nutrition Examination Survey, 1988–1994. *Diabetes Care,* 21**,** 518-524.

Harrison, S. A., Brunt, E. M., Goodman, Z. D. & Di Bisceglie, A. M. 2006. Diabetic hepatosclerosis: diabetic microangiopathy of the liver. *Archives of Pathology & Laboratory Medicine,* 130**,** 27.

Hartz, A., Kent, S., James, P., Xu, Y., Kelly, M. & Daly, J. 2006. Factors that influence improvement for patients with poorly controlled type 2 diabetes. *Diabetes Research and Clinical Practice,* 74**,** 227-232.

Haslam, D. & James, W. 2005. Obesity lJ J. *Lancet,* 366**,** 1.

Heffelfinger, S. C., Hawkins, H. H., Barrish, J., Taylor, L. & Darlington, G. J. 1992. SK HEP-1: a human cell line of endothelial origin. *In Vitro Cellular & Developmental Biology-Animal,* 28**,** 136-142.

Henriksen, J. H., Horn, T. & Christoffersen, P. 1984. The blood-lymph barrier in the liver. A review based on morphological and functional concepts of normal and cirrhotic liver. *Liver,* 4**,** 221-232.

Herrlinger, C. & Klotz, U. Drug metabolism and drug interactions in the elderly. *Best practice & research. Clinical gastroenterology* **15**, 897-918 (2001).

Higuchi, H. & Gores, G. J. 2003. Mechanisms of liver injury: an overview. *Current Molecular Medicine,* 3**,** 483-490.

Hiles, I. D., Otsu, M., Volinia, S., Fry, M. J., Gout, I., Dhand, R., Panayotou, G., Ruiz-Larrea, F., Thompson, A. & Totty, N. F. 1992. Phosphatidylinositol 3-kinase: structure and expression of the 110 kd catalytic subunit. *Cell,* 70**,** 419-429.

Hilmer, S. N., Cogger, V. C., Fraser, R., Mclean, A. J., Sullivan, D. & Le Couteur, D. G. 2005. Age-related changes in the hepatic sinusoidal endothelium impede lipoprotein transfer in the rat. *Hepatology,* 42**,** 1349-54.

Hoehn, K. L., Hohnen-Behrens, C., Cederberg, A., Wu, L. E., Turner, N., Yuasa, T., Ebina, Y. & James, D. E. 2008. IRS1-independent defects define major nodes of insulin resistance. *Cell Metabolism,* 7**,** 421-33.

Holm, C., Østerlund, T., Laurell, H. & Contreras, J. A. 2000. Molecular mechanisms regulating hormone-sensitive lipase and lipolysis. *Annual Review of Nutrition,* 20**,** 365-393.

Holz, L. E., McCaughan, G. W., Benseler, V., Bertolino, P. & Bowen, D. G. 2008. Liver tolerance and the manipulation of immune outcomes. *Inflammation & Allergy-Drug Targets (Formerly Current Drug Targets-Inflammation & Allergy),* 7**,** 6-18.

Horn, T., Christoffersen, P. & Henriksen, J. H. 1987. Alcoholic liver injury: defenestration in noncirrhotic livers—a scanning electron microscopic study. *Hepatology,* 7**,** 77-82.

Horton, J. D., Goldstein, J. L. & Brown, M. S. 2002. SREBPs: activators of the complete program of cholesterol and fatty acid synthesis in the liver. *Journal of Clinical Investigation,* 109**,** 1125-1132.

Hovorka, R., Powrie, J., Smith, G., Sonksen, P., Carson, E. & Jones, R. 1993. Five-compartment model of insulin kinetics and its use to investigate action of chloroquine in NIDDM. *American Journal of Physiology-Endocrinology and Metabolism,* 265**,** E162-E175.

Inaba, R., Inaba, M. & Iwamura, K. 1984. Light microscopic and electron microscopic study on morphologic features resulting in the delay of ICG elimination in diabetic and non-diabetic fatty liver. *The Tokai Journal of Experimental and Clinical Medicine,* 9**,** 207-216.

Ito, K., Miyashita, Y. & Kasai, H. 1997. Micromolar and submicromolar Ca2+ spikes regulating distinct cellular functions in pancreatic acinar cells. *The EMBO Journal,* 16**,** 242-251.

Ito, Y., Sorensen, K. K., Bethea, N. W., Svistounov, D., McCuskey, M. K., Smedsrod, B. H. & McCuskey, R. S. 2007. Age-related changes in the hepatic microcirculation in mice. *Experimental Gerontology* 42**,** 789-97.

Iwakiri, Y. 2012. Endothelial dysfunction in the regulation of cirrhosis and portal hypertension. *Liver international,* 32**,** 199-213.

Iwakiri, Y. & Groszmann, R. J. 2007. Vascular endothelial dysfunction in cirrhosis. *Journal of Hepatology,* 46**,** 927-934.

Izzo, J. L. & Bartlett, J. W. 1969. Insulin-glucose dispersion and interaction system. Liver control mechanisms. *Archive of Internal Medicine,* 123**,** 272-83.

Jamieson, H., Day, W., Dobbs, B., Rogers, G. & Fraser, R. 1999. Is the fatty liver of diabetes, like that of alcoholism, related to an increased porosity of the liver sieve? *Cells Of The Hepatic Sinusoid,* 7**,** 96-98.

Jamieson, H., Dobbs, B., Day, W., Rogers, G. & Fraser, R. 2001. The liver sieve in diabetes: are the ultrastructural changes similar to those seen in alcoholism? *Cells Of The Hepatic Sinusoid,* 8**,** 123-124.

Jamieson, H. A., Cogger, V. C., Twigg, S. M., Mclennan, S. V., Warren, A., Cheluvappa, R., Hilmer, S. N., Fraser, R., De Cabo, R. & Le Couteur, D. G. 2007a. Alterations in liver sinusoidal endothelium in a baboon model of type 1 diabetes. *Diabetologia,* 50**,** 1969-76.

Jamieson, H. A., Hilmer, S. N., Cogger, V. C., Warren, A., Cheluvappa, R., Abernethy, D. R., Everitt, A. V., Fraser, R., De Cabo, R. & Le Couteur, D. G. 2007b. Caloric restriction reduces age-related pseudocapillarization of the hepatic sinusoid. *Experimental Gerontology,* 42**,** 374-8.

Jandhyala, S. M., Talukdar, R., Subramanyam, C., Vuyyuru, H., Sasikala, M. & Nageshwar Reddy, D. 2015. Role of the normal gut microbiota. *World Journal of Gastroenterology,* 21**,** 8787-803.

Jansen, P. L. 2002. Liver disease in the elderly. *Best Practice & Research Clinical Gastroenterology,* 16**,** 149-158.

Javitt, N. B. 1990. Hep G2 cells as a resource for metabolic studies: lipoprotein, cholesterol, and bile acids. *The FASEB Journal,* 4**,** 161-168.

Jensen, L. J., Kuhn, M., Stark, M., Chaffron, S., Creevey, C., Muller, J., Doerks, T., Julien, P., Roth, A., Simonovic, M., Bork, P. & Von Mering, C. 2009. STRING 8--a global view on proteins and their functional interactions in 630 organisms. *Nucleic Acids Research,* 37**,** D412-6.

Johnston, T. P. 2004. The P-407-induced murine model of dose-controlled hyperlipidemia and atherosclerosis: a review of findings to date. *Journal of Cardiovascular Pharmacology,* 43**,** 595-606.

Johnston, T. P. & Palmer, W. K. 1993. Mechanism of poloxamer 407-induced hypertriglyceridemia in the rat. *Biochemical Pharmacology,* 46**,** 1037-42.

Johnston, T. P. & Waxman, D. J. 2008. Circulating free fatty acids are increased independently of PPARgamma activity after administration of poloxamer 407 to mice. *Canadian Journal of Physiology and Pharmacology,* 86**,** 643-9.

Jones, C. N., Pei, D., Staris, P., Polonsky, K. S., Chen, Y.-I. & Reaven, G. M. 1997. Alterations in the glucose-stimulated insulin secretory dose-response curve and in insulin clearance in nondiabetic insulin-resistant individuals. *The Journal of Clinical Endocrinology & Metabolism,* 82**,** 1834-1838.

Jörneskog, G., Kalani, M., Kuhl, J., Båvenholm, P., Katz, A., Allerstrand, G., Alvarsson, M., Efendic, S., Östenson, C.-G., Pernow, J., Wahren, J. & Brismar, K. 2005. Early Microvascular Dysfunction in Healthy Normal-Weight Males With Heredity for Type 2 Diabetes. *Diabetes Care,* 28**,** 1495-1497.

Kabanov, A. V., Batrakova, E. V. & Alakhov, V. Y. 2002. Pluronic block copolymers as novel polymer therapeutics for drug and gene delivery. *Journal of Controlled Release,* 82**,** 189-212.

Kahn, C. R., Flier, J. S., Bar, R. S., Archer, J. A., Gorden, P., Martin, M. M. & Roth, J. 1976. The syndromes of insulin resistance and acanthosis nigricans: insulin-receptor disorders in man. *New England Journal of Medicine,* 294**,** 739-745.

Kahn, C. R. & White, M. 1988. The insulin receptor and the molecular mechanism of insulin action. *Journal of Clinical Investigation,* 82**,** 1151.

Kahn, E., Baarine, M., Dauphin, A., Ragot, K., Tissot, N., Seguin, A., Menetrier, F., Kattan, Z., Bachelet, C. M., Frouin, F. & Lizard, G. 2011. Impact of 7-ketocholesterol and very long chain fatty acids on oligodendrocyte lipid membrane organization: evaluation via LAURDAN and FAMIS spectral image analysis. *Cytometry A,* 79**,** 293-305.

Kalyan, K., Basu, D., Soundararaghavan, J., Kapoor, N., Jain, R., Surange, S., Bhardwaj, V., Srivastava, A., Buch, A. C. & Panicker, N. K. 2006. Nonalcoholic steatohepatitis-a histological perspective. *Indian Journal of Pathology and Microbiology,* 49**,** 163-172.

Kanehisa, M. & Goto, S. 2000. KEGG: kyoto encyclopedia of genes and genomes. *Nucleic Acids Research,* 28**,** 27-30.

Kanehisa, M., Goto, S., Sato, Y., Kawashima, M., Furumichi, M. & Tanabe, M. 2014. Data, information, knowledge and principle: back to metabolism in KEGG. *Nucleic Acids Research,* 42**,** D199-205.

Kaplowitz, N. Biochemical and cellular mechanisms of toxic liver injury. *Seminars In Liver Disease,* 2001. 137-144.

Karikoski, M., Irjala, H., Maksimow, M., Miiluniemi, M., Granfors, K., Hernesniemi, S., Elima, K., Moldenhauer, G., Schledzewski, K. & Kzhyshkowska, J. 2009. Clever-1/Stabilin-1 regulates lymphocyte migration within lymphatics and leukocyte entrance to sites of inflammation. *European Journal of Immunology,* 39**,** 3477-3487.

Kasai, H. & Augustine, G. J. 1990. Cytosolic Ca2+ gradients triggering unidirectional fluid secretion from exocrine pancreas. *Nature,* 348, 735-738

Kasuga, M., Karlsson, F. A. & Kahn, C. R. 1982. Insulin stimulates the phosphorylation of the 95,000-dalton subunit of its own receptor. *Science,* 215**,** 185-187.

Kawaguchi, T., Taniguchi, E., Itou, M., Sakata, M., Sumie, S. & Sata, M. 2011. Insulin resistance and chronic liver disease. *World Journal of Hepatology* 3**,** 99-107.

Kawai, H. F., Kaneko, S., Honda, M., Shirota, Y. & Kobayashi, K. 2001. α-fetoprotein-producing hepatoma cell lines share common expression profiles of genes in various categories demonstrated by cDNA microarray analysis. *Hepatology,* 33**,** 676-691.

Kiernan, F. 1833. The anatomy and physiology of the liver. *Philosophical Transactions of the Royal Society of London,* 123**,** 711-770.

Kleemann, R., Van Erk, M., Verschuren, L., Van Den Hoek, A. M., Koek, M., Wielinga, P. Y., Jie, A., Pellis, L., Bobeldijk-Pastorova, I. & Kelder, T. 2010. Time-resolved and tissue-specific systems analysis of the pathogenesis of insulin resistance. *PloS one,* 5**,** e8817.

Kline, M. A., Butler, E. O. C., Hinzey, A., Sliman, S., Kotha, S. R., Marsh, C. B., Uppu, R. M. & Parinandi, N. L. 2010. A simple method for effective and safe removal of membrane cholesterol from lipid rafts in vascular endothelial cells: implications in oxidant-mediated lipid signaling. *Free Radicals and Antioxidant Protocols.* Springer.

Klover, P. J., Mooney, R. A., Nowak, I. A. & Senn, J. J. 2002. Interleukin-6 induces cellular insulin resistance in hepatocytes. *Diabetes,* 51, 3391-3399.

Kmiec, Z. 2001. Cooperation of liver cells in health and disease. *Advances in Anatomy Embryology and cell biology,* 161, 1-151.

Knutson, V. P., Ronnett, G. V. & Lane, M. D. 1982. Control of insulin receptor level in 3T3 cells: effect of insulin-induced down-regulation and dexamethasone-induced up-regulation on rate of receptor inactivation. *Proceedings of the National Academy of Sciences of the United States of America,* 79**,** 2822-2826.

Kotronen, A., Vehkavaara, S., Seppala-Lindroos, A., Bergholm, R. & Yki-Jarvinen, H. 2007. Effect of liver fat on insulin clearance. *American Journal of Physiology- Endocrinology and Metabolism,* 293**,** E1709-15.

Krauss, R. M. 2004. Lipids and lipoproteins in patients with type 2 diabetes. *Diabetes Care,* 27**,** 1496-1504.

Kubota, N., Tobe, K., Terauchi, Y., Eto, K., Yamauchi, T., Suzuki, R., Tsubamoto, Y., Komeda, K., Nakano, R. & Miki, H. 2000. Disruption of insulin receptor substrate 2 causes type 2 diabetes because of liver insulin resistance and lack of compensatory beta-cell hyperplasia. *Diabetes,* 49**,** 1880-1889.

Kullak-Ublick, G. A., Stieger, B., Hagenbuch, B. & Meier, P. J. Hepatic transport of bile salts. *Seminars in Liver Disease,* 2000. 273-292.

Krasinski, S.D., Cohn, J.S., Schaefer, E.J. & Russell, R.M. Postprandial plasma retinyl ester response is greater in older subjects compared with younger subjects. Evidence for delayed plasma clearance of intestinal lipoproteins. *J Clin Invest* **85**, 883-892 (1990).

Kumar, S. & O'Rahilly, S. 2005. *Insulin resistance: Insulin action and its disturbances in disease,* John Wiley & Sons.

Kuntz, E. & Kuntz, H.-D. 2009. *Hepatology: Textbook and atlas,* Springer Science & Business Media.

Kusunoki, M., Tsutsumi, K., Hara, T., Ogawa, H., Nakamura, T., Miyata, T., Sakakibara, F., Fukuzawa, Y., Suga, T., Kakumu, S. & Nakaya, Y. 2002. Correlation between lipid and glycogen contents in liver and insulin resistance in high-fat-fed rats treated with the lipoprotein lipase activator NO-1886. *Metabolism,* 51**,** 792-5.

Kzhyshkowska, J., Gratchev, A., Schmuttermaier, C., Brundiers, H., Krusell, L., Mamidi, S., Zhang, J., Workman, G., Sage, E. H. & Anderle, C. 2008. Alternatively activated macrophages regulate extracellular levels of the hormone placental lactogen via receptor-mediated uptake and transcytosis. *The Journal of Immunology,* 180**,** 3028-3037.

Kzhyshkowska, J., Workman, G., Cardó-Vila, M., Arap, W., Pasqualini, R., Gratchev, A., Krusell, L., Goerdt, S. & Sage, E. H. 2006. Novel function of alternatively activated macrophages: stabilin-1-mediated clearance of SPARC. *The Journal of Immunology,* 176**,** 5825-5832.

Latry, P., Bioulac-Sage, P., Echinard, E., Gin, H., Boussarie, L., Grimaud, J. & Balabaud, C. 1987. Perisinusoidal fibrosis and basement membrane-like material in the livers of diabetic patients. *Human Pathology,* 18**,** 775-780.

Lavan, B. E., Lane, W. S. & Lienhard, G. E. 1997. The 60-kDa phosphotyrosine protein in insulin-treated adipocytes is a new member of the insulin receptor substrate family. *Journal of Biological Chemistry,* 272**,** 11439-11443.

Le Bail, B., Bioulac‐Sage, P., Senuita, R., Quinton, A., Saric, J. & Balabaud, C. 1990. Fine structure of hepatic sinusoids and sinusoidal cells in disease. *Journal of Electron Microscopy Technique,* 14**,** 257-282.

Le Couteur, D. G., Cogger, V. C., Markus, A. M., Harvey, P. J., Yin, Z. L., Ansselin, A. D. & Mclean, A. J. 2001. Pseudocapillarization and associated energy limitation in the aged rat liver. *Hepatology,* 33**,** 537-43.

Le Couteur, D. G., Fraser, R., Cogger, V. C. & Mclean, A. J. 2002. Hepatic pseudocapillarisation and atherosclerosis in ageing. *Lancet,* 359**,** 1612-5.

Le Couteur, D.G., Hilmer, S.N., Glasgow, N., Naganathan, V. & Cumming, R.G. Prescribing in older people. *Australian family physician* **33**, 777-781 (2004).

Le Couteur, D. G., Fraser, R., Hilmer, S., Rivory, L. P. & Mclean, A. J. 2005. The hepatic sinusoid in aging and cirrhosis - Effects on hepatic substrate disposition and drug clearance. *Clinical Pharmacokinetics.,* 44**,** 187-200.

Le Couteur, D. G. & Lakatta, E. G. 2010. A vascular theory of aging. *The Journals of Gerontology Series A: Biological Sciences and Medical Sciences,* 65**,** 1025-1027.

Le Couteur, D. G. & Mclean, A. J. 1998. The aging liver. Drug clearance and an oxygen diffusion barrier hypothesis. *Clinical Pharmacokinetics,* 34**,** 359-73.

Le Couteur, D. G., Tay, S. S., Solon-Biet, S., Bertolino, P., Mcmahon, A. C., Cogger, V. C., Colakoglu, F., Warren, A., Holmes, A. J., Pichaud, N., Horan, M., Correa, C., Melvin, R. G., Turner, N., Ballard, J. W., Ruohonen, K., Raubenheimer, D. & Simpson, S. J. 2014. The Influence of Macronutrients on Splanchnic and Hepatic Lymphocytes in Aging Mice. *The Journals of Gerontology Series A: Biological Sciences and Medical Sciences* 70,1499-507

Le Couteur, D. G., Warren, A., Cogger, V. C., Smedsrod, B., Sorensen, K. K., De Cabo, R., Fraser, R. & McCuskey, R. S. 2008. Old Age and the hepatic sinusoid. *Anatomical Record (Hoboken),* 291**,** 672-83.

Leavens, K. F. & Birnbaum, M. J. 2011. Insulin signaling to hepatic lipid metabolism in health and disease. *Critical Reviews in Biochemistry and Molecular Biology,* 46**,** 200-215.

Lebel, M. 2001. Human Genome and Diseases: A new series of reviews in CMLS¶ Werner Syndrome: genetic and molecular basis of a premature aging disorder. *Cellular and Molecular Life Sciences CMLS,* 58**,** 857-867.

Lee, J. H., Oh, J. H. & Lee, Y. J. 2012. Effects of experimental hyperlipidemia on the pharmacokinetics of tadalafil in rats. *Journal of Pharmacy & Pharmaceutical Sciences,* 15**,** 528-37.

Lee, K. P., Simpson, S. J., Clissold, F. J., Brooks, R., Ballard, J. W., Taylor, P. W., Soran, N. & Raubenheimer, D. 2008. Lifespan and reproduction in Drosophila: New insights from nutritional geometry. *Proceedings of the National Academy of Sciences of the United States of America,* 105**,** 2498-503.

Lehr, S., Kotzka, J., Herkner, A., Sikmann, A., Meyer, H. E., Krone, W. & Müller-Wieland, D. 2000. Identification of major tyrosine phosphorylation sites in the human insulin receptor substrate Gab-1 by insulin receptor kinase in vitro. *Biochemistry,* 39**,** 10898-10907.

Lesurtel, M. & Clavien, P. A. 2014. Platelet-derived serotonin: translational implications for liver regeneration. *Hepatology,* 60**,** 30-3.

Lewis, G. F., Carpentier, A., Adeli, K. & Giacca, A. 2002. Disordered fat storage and mobilization in the pathogenesis of insulin resistance and type 2 diabetes. *Endocrine Reviews,* 23**,** 201-229.

Lewis, G. F., Zinman, B., Groenewoud, Y., Vranic, M. & Giacca, A. 1996. Hepatic glucose production is regulated both by direct hepatic and extrahepatic effects of insulin in humans. *Diabetes,* 45**,** 454-462.

Li, C., Palmer, W. & Johnston, T. 1996. Disposition of poloxamer 407 in rats following a single intraperitoneal injection assessed using a simplified colorimetric assay. *Journal Of Pharmaceutical And Biomedical Analysis,* 14**,** 659-665.

Li, R., Oteiza, A., Sørensen, K. K., Mccourt, P., Olsen, R., Smedsrød, B. & Svistounov, D. 2011. Role of liver sinusoidal endothelial cells and stabilins in elimination of oxidized low-density lipoproteins. *American Journal of Physiology-Gastrointestinal and Liver Physiology,* 300**,** G71-G81.

Liu, B., Wang, M., Wang, X., Zhao, D., Liu, D., Liu, J., Chen, P.-J., Yang, D., He, F. & Tang, L. 2013. Liver sinusoidal endothelial cell lectin inhibits CTL-dependent virus clearance in mouse models of viral hepatitis. *The Journal of Immunology,* 190**,** 4185-4195.

Liu, Z., Jahn, L. A., Wei, L., Long, W. & Barrett, E. J. 2002. Amino acids stimulate translation initiation and protein synthesis through an Akt-independent pathway in human skeletal muscle. *The Journal of Clinical Endocrinology & Metabolism,* 87**,** 5553-5558.

Maassen, J., Burgering, B., Medema, R., Osterop, A., Van Der Zon, G., Möller, W. & Bos, J. 1992. The role of ras proteins in insulin signal transduction. *Hormone metabolic research,* 24**,** 214-218.

Macsween, R., Desmet, V., Roskams, T. & Scothorne, R. 2002. Developmental anatomy and normal structure. *Pathology of the Liver,* 4**,** 1-66.

Magnusson, I., Rothman, D., Katz, L., Shulman, R. & Shulman, G. 1992. Increased rate of gluconeogenesis in type II diabetes mellitus. A 13C nuclear magnetic resonance study. *Journal of Clinical Investigation,* 90**,** 1323.

Magnusson, S. & Berg, T. 1989. Extremely rapid endocytosis mediated by the mannose receptor of sinusoidal endothelial rat liver cells. *Biochemical Journal,* 257**,** 651-656.

Majumdar, S., Genders, A. J., Inyard, A. C., Frison, V. & Barrett, E. J. 2012. Insulin entry into muscle involves a saturable process in the vascular endothelium. *Diabetologia,* 55**,** 450-6.

Malarkey, D. E., Johnson, K., Ryan, L., Boorman, G. & Maronpot, R. R. 2005. New insights into functional aspects of liver morphology. *Toxicologic Pathology,* 33**,** 27-34.

Marchesini, G., Brizi, M., Bianchi, G., Tomassetti, S., Bugianesi, E., Lenzi, M., Mccullough, A. J., Natale, S., Forlani, G. & Melchionda, N. 2001. Nonalcoholic fatty liver disease a feature of the metabolic syndrome. *Diabetes,* 50**,** 1844-1850.

De Leeuw, M. A., Brouwer, A. & Knook, D. L. 1990. Sinusoidal endothelial cells of the liver: fine structure and function in relation to age. *Journal Of Electron Microscopy Technique,* 14**,** 218-236.

Mariat, D., Firmesse, O., Levenez, F., Guimaraes, V., Sokol, H., Dore, J., Corthier, G. & Furet, J. P. 2009. The Firmicutes/Bacteroidetes ratio of the human microbiota changes with age. *BMC Microbiology,* 9**,** 123.

Marquet-De Rouge, P., Clamagirand, C., Facchinetti, P., Rose, C., Sargueil, F., Guihenneuc-Jouyaux, C., Cynober, L., Moinard, C. & Allinquant, B. 2013. Citrulline diet supplementation improves specific age-related raft changes in wild-type rodent hippocampus. *Age (Dordr),* 35**,** 1589-606.

Martinez‐Hernandez, A. & Martinez, J. 1991. The role of capillarization in hepatic failure: Studies in carbon tetrachloride-induced cirrhosis. *Hepatology,* 14**,** 864-874.

Maskarinec, S. A., Hannig, J., Lee, R. C. & Lee, K. Y. C. 2002. Direct Observation of Poloxamer 188 Insertion into Lipid Monolayers. *Biophysical Journal,* 82**,** 1453-1459.

Massip, L., Garand, C., Paquet, E. R., Cogger, V. C., O'reilly, J. N., Tworek, L., Hatherell, A., Taylor, C. G., Thorin, E., Zahradka, P., Le Couteur, D. G. & Lebel, M. 2010. Vitamin C restores healthy aging in a mouse model for Werner syndrome. *FASEB Journal,* 24**,** 158-72.

Masyuk AI, Masyuk TV, LaRusso NF. Cholangiocyte primary cilia in liver health and disease. Developmental Dynamics. 2008;237(8):2007-12.

Matsuda, M., Liu, Y., Mahankali, S., Pu, Y., Mahankali, A., Wang, J., Defronzo, R. A., Fox, P. T. & Gao, J.-H. 1999. Altered hypothalamic function in response to glucose ingestion in obese humans. *Diabetes,* 48**,** 1801-1806.

Matsumoto, M., Ogawa, W., Teshigawara, K., Inoue, H., Miyake, K., Sakaue, H. & Kasuga, M. 2002. Role of the insulin receptor substrate 1 and phosphatidylinositol 3-kinase signaling pathway in insulin-induced expression of sterol regulatory element binding protein 1c and glucokinase genes in rat hepatocytes. *Diabetes,* 51**,** 1672-1680.

Matsumoto, T., Komori, R., Magara, T., Ui, T., Kawakami, M., Tokuda, T., Takasaki, S., Hayashi, H., Jo, K. & Hano, H. 1979. A study on the normal structure of the human liver, with special reference to its angioarchitecture. *Jikeikai Medical Journal,* 26**,** 1-40.

Matsunol, K. & Ezaki, T. 2000. Dendritic cell dynamics in the liver and hepatic lymph. *International Review of Cytology,* 197**,** 83-136.

Matthews, D., Hosker, J., Rudenski, A., Naylor, B., Treacher, D. & Turner, R. 1985. Homeostasis model assessment: insulin resistance and β-cell function from fasting plasma glucose and insulin concentrations in man. *Diabetologia,* 28**,** 412-419.

Mcauley, K. A., Williams, S. M., Mann, J. I., Walker, R. J., Lewis-Barned, N. J., Temple, L. A. & Duncan, A. W. 2001. Diagnosing insulin resistance in the general population. *Diabetes Care,* 24**,** 460-464.

McCuskey, R. S. 2000. Morphological mechanisms for regulating blood flow through hepatic sinusoids. *Liver,* 20**,** 3-7.

McCuskey, R. S. 2008. The hepatic microvascular system in health and its response to toxicants. *The Anatomical Record,* 291**,** 661-671.

McCuskey, R. S. & Reilly, F. D. Hepatic microvasculature: dynamic structure and its regulation. *Seminars in Liver Disease,* 1993. 1-12.

McCuskey, R. S., Reilly, F. D., McCuskey, P. A. & Dimlich, R. 1978. In vivo microscopy of the hepatic microvascular system. *Bibliotheca Anatomica***,** 73-76.

Mcgary, C. T., Raja, R. & Weigel, P. H. 1989. Endocytosis of hyaluronic acid by rat liver endothelial cells. Evidence for receptor recycling. *Biochemical Journal,* 257**,** 875-884.

Mcguire, R. F., Bissell, D. M., Boyles, J. & Roll, F. J. 1992. Role of extracellular matrix in regulating fenestrations of sinusoidal endothelial cells isolated from normal rat liver. *Hepatology,* 15**,** 989-997.

Mclean, A. J., Cogger, V. C., Chong, G. C., Warren, A., Markus, A. M., Dahlstrom, J. E. & Le Couteur, D. G. 2003. Age-related pseudocapillarization of the human liver. *Journal of Pathology,* 200**,** 112-7.

Mclean, A. J. & Le Couteur, D. G. 2004. Aging biology and geriatric clinical pharmacology. *Pharmacological Reviews,* 56**,** 163-84.

Mclean, A. J. & Morgan, D. J. 1991. Clinical pharmacokinetics in patients with liver disease. *Clinical Pharmacokinetics,* 21**,** 42-69.

Mcmahon, A. C., Parry, S. N., Benson, V. L., Witting, P. K. & Le Couteur, D. G. 2013. Beneficial effects of the synthetic antioxidant tert-butyl bisphenol on the hepatic microcirculation in a rat model of diabetes mellitus. *Acta Diabetologica,* 50**,** 645-9.

Medlock, E. S. & Haar, J. L. 1983. The liver hemopoietic environment: I. Developing hepatocytes and their role in fetal hemopoiesis. *The Anatomical Record,* 207**,** 31-41.

Meier, J. J., Veldhuis, J. D. & Butler, P. C. 2005. Pulsatile insulin secretion dictates systemic insulin delivery by regulating hepatic insulin extraction in humans. *Diabetes,* 54**,** 1649-1656.

Melmed, S., Polonsky, K. S., Larsen, P. R. & Kronenberg, H. M. 2011. *Williams Textbook Of Endocrinology,* Elsevier Health Sciences.

Michael, M. D., Kulkarni, R. N., Postic, C., Previs, S. F., Shulman, G. I., Magnuson, M. A. & Kahn, C. R. 2000. Loss of insulin signaling in hepatocytes leads to severe insulin resistance and progressive hepatic dysfunction. *Molecular Cell,* 6**,** 87-97.

Millar, J. S., Cromley, D. A., Mccoy, M. G., Rader, D. J. & Billheimer, J. T. 2005. Determining hepatic triglyceride production in mice: comparison of poloxamer 407 with Triton WR-1339. *Journal of Lipid Research,* 46**,** 2023-2028.

Mitchell, S. J., Huizer-Pajkos, A., Cogger, V. C., Mclachlan, A. J., Le Couteur, D. G. & Hilmer, S. N. 2010. Poloxamer 407 increases the recovery of paracetamol in the isolated perfused rat liver. *Journal of Pharmaceutical Sciences,* 100**,** 334-40.

Mitchell, S. J., Huizer-Pajkos, A., Cogger, V. C., Mclachlan, A. J., Le Couteur, D. G., Jones, B., De Cabo, R. & Hilmer, S. N. 2012. The influence of old age and poloxamer-407 on the hepatic disposition of diazepam in the isolated perfused rat liver. *Pharmacology,* 90**,** 233-41.

Moghimi, S. M. 1999. Re-establishing the long circulatory behaviour of poloxamine-coated particles after repeated intravenous administration: applications in cancer drug delivery and imaging. *Biochimica et Biophysica Acta,* 1472**,** 399-403.

Mönkemöller, V., Schüttpelz, M., Mccourt, P., Sørensen, K., Smedsrød, B. & Huser, T. 2014. Imaging fenestrations in liver sinusoidal endothelial cells by optical localization microscopy. *Physical Chemistry Chemical Physics,* 16**,** 12576-12581.

Mook-Kanamori, D. O., Romisch-Margl, W., Kastenmuller, G., Prehn, C., Petersen, A. K., Illig, T., Gieger, C., Wang-Sattler, R., Meisinger, C., Peters, A., Adamski, J. & Suhre, K. 2014. Increased amino acids levels and the risk of developing of hypertriglyceridemia in a 7-year follow-up. *Journal of Endocrinology Investigations,* 37**,** 369-74.

Mori, T., Okanoue, T., Sawa, Y., Hori, N., Ohta, M. & Kagawa, K. 1993. Defenestration of the sinusoidal endothelial cell in a rat model of cirrhosis. *Hepatology,* 17**,** 891-897.

Mousavi, S. A., Sporstøl, M., Fladeby, C., Kjeken, R., Barois, N. & Berg, T. 2007. Receptor-mediated endocytosis of immune complexes in rat liver sinusoidal endothelial cells is mediated by FcγRIIb2. *Hepatology,* 46**,** 871-884.

Muller, M. J., Willmann, O., Rieger, A., Fenk, A., Selberg, O., Lautz, H. U., Burger, M., Balks, H. J., Von Zur Muhlen, A. & Schmidt, F. W. 1992. Mechanism of insulin resistance associated with liver cirrhosis. *Gastroenterology,* 102**,** 2033-41.

Munday, M. R. & Hemingway, C. J. 1999. The regulation of acetyl-CoA carboxylase—a potential target for the action of hypolipidemic agents. *Advances in Enzyme Regulation,* 39**,** 205-234.

Murata, K. & Nakashima, H. 1985. Clinical and metabolic studies on Werner's syndrome: with special reference to disorders of lipid and liver function. *Werner's Syndrome and Human Aging.* Springer.

Myers, M. G., Backer, J. M., Sun, X. J., Shoelson, S., Hu, P., Schlessinger, J., Yoakim, M., Schaffhausen, B. & White, M. F. 1992. IRS-1 activates phosphatidylinositol 3'-kinase by associating with src homology 2 domains of p85. *Proceedings of the National Academy of Sciences of the United States of America,* 89**,** 10350-10354.

Nagai, T., Yokomori, H., Yoshimura, K., Fujimaki, K., Nomura, M., Hibi, T. & Oda, M. 2004. Actin filaments around endothelial fenestrae in rat hepatic sinusoidal endothelial cells. *Medical Electron Microscopy,* 37**,** 252-255.

Nagata, J., Guerra, M. T., Shugrue, C. A., Gomes, D. A., Nagata, N. & Nathanson, M. H. 2007. Lipid rafts establish calcium waves in hepatocytes. *Gastroenterology,* 133**,** 256-267.

Najjar, S. M. 2002. Regulation of insulin action by CEACAM1. *Trends in Endocrinology & Metabolism,* 13**,** 240-245.

Nakae, J., Kitamura, T., Silver, D. L. & Accili, D. 2001. The forkhead transcription factor Foxo1 (Fkhr) confers insulin sensitivity onto glucose-6-phosphatase expression. *Journal of Clinical Investigation,* 108**,** 1359.

Nakae, J., Park, B.-C. & Accili, D. 1999. Insulin stimulates phosphorylation of the forkhead transcription factor FKHR on serine 253 through a Wortmannin-sensitive pathway. *Journal of Biological Chemistry,* 274**,** 15982-15985.

Nakatani, K., Kaneda, K., Seki, S. & Nakajima, Y. 2004. Pit cells as liver-associated natural killer cells: morphology and function. *Medical Electron Microscopy,* 37**,** 29-36.

Nandi, A., Kitamura, Y., Kahn, C. R. & Accili, D. 2004. *Mouse Models of Insulin Resistance*.

O'reilly, J. N., Cogger, V. C., Fraser, R. & Le Couteur, D. G. 2010. The effect of feeding and fasting on fenestrations in the liver sinusoidal endothelial cell. *Pathology,* 42**,** 255-8.

Oda, M., Tsukada, N., Komatsu, H., Kaneko, K., Nakamura, M. & Tsuchiya, M. 1986. Electron microscopic localizations of actin, calmodulin and calcium in the hepatic sinusoidal endothelium in the rat. *Cells Of The Hepatic Sinusoid,* 1**,** 511-512.

Oda, M., Yokomori, H., Han, J., Kamegaya, Y., Ogi, M. & Nakamura, M. 2001. Hepatic sinusoidal endothelial fenestrae are a stationary type of fused and interconnected caveolae. *Cells of the Hepatic Sinusoid,* 8**,** 94-98.

Ogawa, W., Matozaki, T. & Kasuga, M. 1998. Role of binding proteins to IRS-1 in insulin signalling. *Molecular And Cellular Biochemistry,* 182**,** 13-22.

Ohtani, Y., Wang, B.-J., Poonkhum, R. & Ohtani, O. 2003. Pathways for movement of fluid and cells from hepatic sinusoids to the portal lymphatic vessels and subcapsular region in rat livers. *Archives Of Histology And Cytology,* 66**,** 239-252.

Onori, P., Morini, S., Franchitto, A., Sferra, R., Alvaro, D. & Gaudio, E. 2000. Hepatic microvascular features in experimental cirrhosis: a structural and morphometrical study in CCl 4-treated rats. *Journal Of Hepatology,* 33**,** 555-563.

Owen, D. M., Gaus, K., Magee, A. I. & Cebecauer, M. 2010. Dynamic organization of lymphocyte plasma membrane: lessons from advanced imaging methods. *Immunology,* 131**,** 1-8.

Owen, D. M., Lanigan, P. M., Dunsby, C., Munro, I., Grant, D., Neil, M. A., French, P. M. & Magee, A. I. 2006. Fluorescence lifetime imaging provides enhanced contrast when imaging the phase-sensitive dye di-4-ANEPPDHQ in model membranes and live cells. *Biophysical Journal,* 90**,** L80-L82.

Oya, J., Nakagami, T., Yamamoto, Y., Fukushima, S., Takeda, M., Endo, Y. & Uchigata, Y. 2014. Effects of age on insulin resistance and secretion in subjects without diabetes. *Internal Medicine,* 53**,** 941-7.

Burnham, K. P., & Anderson, D.R. 2002. *MODEL SELECTION AND MULTIMODEL INFERENCE: A practical information-theoretic approach.* , New York, USA, , Springer.

Palmer, W. K., Emeson, E. E. & Johnston, T. P. 1998. Poloxamer 407-induced atherogenesis in the C57BL/6 mouse. *Atherosclerosis,* 136**,** 115-23.

Paolella, G., Mandato, C., Pierri, L., Poeta, M., Di Stasi, M. & Vajro, P. 2014. Gut-liver axis and probiotics: their role in non-alcoholic fatty liver disease. *World Journal of Gastroenterology,* 20**,** 15518-31.

Pap, M. & Cooper, G. M. 2002. Role of translation initiation factor 2B in control of cell survival by the phosphatidylinositol 3-kinase/Akt/glycogen synthase kinase 3β signaling pathway. *Molecular And Cellular Biology,* 22**,** 578-586.

Park, S.-Y., Jung, M.-Y., Lee, S.-J., Kang, K.-B., Gratchev, A., Riabov, V., Kzhyshkowska, J. & Kim, I.-S. 2009. Stabilin-1 mediates phosphatidylserine-dependent clearance of cell corpses in alternatively activated macrophages. *Journal of Cell Science,* 122**,** 3365-3373.

Parton, R. G. 2003. Caveolae—from ultrastructure to molecular mechanisms. *Nature Reviews Molecular Cell Biology,* 4**,** 162-167.

Pasarín, M., La Mura, V., Gracia-Sancho, J., García-Calderó, H., Rodríguez-Vilarrupla, A., García-Pagán, J. C., Bosch, J. & Abraldes, J. G. 2012. Sinusoidal Endothelial Dysfunction Precedes Inflammation and Fibrosis in a Model of NAFLD. *PLoS ONE,* 7**,** e32785.

Perriello, G., Pampanelli, S., Del Sindaco, P., Lalli, C., Ciofetta, M., Volpi, E., Santeusanio, F., Brunetti, P. & Bolli, G. B. 1997. Evidence of increased systemic glucose production and gluconeogenesis in an early stage of NIDDM. *Diabetes,* 46**,** 1010-1016.

Pessin, J. E. & Saltiel, A. R. 2000. Signaling pathways in insulin action: molecular targets of insulin resistance. *Journal of Clinical Investigation,* 106**,** 165.

Petersen, K. F. & Shulman, G. I. 2002. Pathogenesis of skeletal muscle insulin resistance in type 2 diabetes mellitus. *The American Journal Of Cardiology,* 90**,** 11-18.

Pike, L. J. 2009. The challenge of lipid rafts. *Journal of Lipid Research,* 50**,** S323-S328.

Pilkis, S. J. & Granner, D. 1992. Molecular physiology of the regulation of hepatic gluconeogenesis and glycolysis. *Annual Review Of Physiology,* 54**,** 885-909.

Plum, L., Belgardt, B. F. & Brüning, J. C. 2006. Central insulin action in energy and glucose homeostasis. *Journal of Clinical Investigation,* 116**,** 1761.

Popper, H. 1985. Aging and the liver. *Progress in Liver Diseases,* 8**,** 659-683.

Popper, H., Elias, H. & Petty, D. E. 1952. Vascular pattern of the cirrhotic liver. *American Journal Of Clinical Pathology,* 22**,** 717.

Poy, M. N., Yang, Y., Rezaei, K., Fernström, M. A., Lee, A. D., Kido, Y., Erickson, S. K. & Najjar, S. M. 2002. CEACAM1 regulates insulin clearance in liver. *Nature Genetics,* 30**,** 270-276.

Prevo, R., Banerji, S., Ni, J. & Jackson, D. G. 2004. Rapid plasma membrane-endosomal trafficking of the lymph node sinus and high endothelial venule scavenger receptor/homing receptor stabilin-1 (FEEL-1/CLEVER-1). *Journal of Biological Chemistry,* 279**,** 52580-52592.

Puigserver, P., Rhee, J., Donovan, J., Walkey, C. J., Yoon, J. C., Oriente, F., Kitamura, Y., Altomonte, J., Dong, H. & Accili, D. 2003. Insulin-regulated hepatic gluconeogenesis through FOXO1–PGC-1α interaction. *Nature,* 423**,** 550-555.

R-DEVELOPMENT-CORE-TEAM. 2015 *R: A language and environment for statistical computing* [Online]. http://www.R-project.Org.

Raines, S. M., Richards, O. C., Schneider, L. R., Schueler, K. L., Rabaglia, M. E., Oler, A. T., Stapleton, D. S., Genove, G., Dawson, J. A., Betsholtz, C. & Attie, A. D. 2011. Loss of PDGF-B activity increases hepatic vascular permeability and enhances insulin sensitivity. *American Journal of Physiology Endocrinology and Metabolism,* 301**,** E517-26.

Rametta, R., Mozzi, E., Dongiovanni, P., Motta, B. M., Milano, M., Roviaro, G., Fargion, S. & Valenti, L. 2013. Increased insulin receptor substrate 2 expression is associated with

steatohepatitis and altered lipid metabolism in obese subjects. *International Journal of Obesity (London),* 37**,** 986-92.

Ramos, F. J., Langlais, P. R., Hu, D., Dong, L. Q. & Liu, F. 2006. Grb10 mediates insulin-stimulated degradation of the insulin receptor: a mechanism of negative regulation. *American Journal of Physiology-Endocrinology and Metabolism,* 290**,** E1262-E1266.

Reaven, G., Hollenbeck, C. & Chen, Y.-D. 1989. Relationship between glucose tolerance, insulin secretion, and insulin action in non-obese individuals with varying degrees of glucose tolerance. *Diabetologia,* 32**,** 52-55.

Reaven, G. M. 1995. Pathophysiology of insulin resistance in human disease. *Physiological Reviews,* 75**,** 473-486.

Rebrin, K., Steil, G. M., Getty, L. & Bergman, R. N. 1995. Free fatty acid as a link in the regulation of hepatic glucose output by peripheral insulin. *Diabetes,* 44**,** 1038-1045.

Reeves, H. L. & Friedman, S. L. 2002. Activation of hepatic stellate cells-a key issue in liver fibrosis. *Frontiers of Bioscience,* 7**,** 808-826.

Rogers, G., Dobbs, B. & Fraser, R. 1992. Decreased hepatic uptake of cholesterol and retinol in the dimethylnitrosamine rat model of cirrhosis. *Liver,* 12**,** 326-329.

Rojas, J. M. & Schwartz, M. W. 2014. Control of hepatic glucose metabolism by islet and brain. *Diabetes, Obesity and Metabolism,* 16 Suppl 1**,** 33-40.

Rose, D. W., Saltiel, A. R., Majumdar, M., Decker, S. J. & Olefsky, J. M. 1994. Insulin receptor substrate 1 is required for insulin-mediated mitogenic signal transduction. *Proceedings of the National Academy of Sciences of the United States of America,* 91**,** 797-801.

Ross, M. H., Kaye, G. I. & Pawlina, W. 2003. *Histology: a text and atlas: with cell and molecular biology*, Lippincott Williams & Wilkins.

Roth, R. A. & Cassell, D. J. 1983. Insulin receptor: evidence that it is a protein kinase. *Science,* 219**,** 299-301.

Rudovich, N. N., Rochlitz, H. J. & Pfeiffer, A. F. 2004. Reduced hepatic insulin extraction in response to gastric inhibitory polypeptide compensates for reduced insulin secretion in normal-weight and normal glucose tolerant first-degree relatives of type 2 diabetic patients. *Diabetes,* 53**,** 2359-2365.

Saito, M., Matsuura, T., Masaki, T., Maehashi, H. & Braet, F. 2004. Study of the reappearance of sieve plate-like pores in immortalized sinusoidal endothelial cells–Effect of actin inhibitor in mixed perfusion cultures. *Comparative Hepatology,* 3**,** S28.

Sakaue, M., Bowtell, D. & Kasuga, M. 1995. A dominant-negative mutant of mSOS1 inhibits insulin-induced Ras activation and reveals Ras-dependent and-independent insulin signaling pathways. *Molecular And Cellular Biology,* 15**,** 379-388.

Saltiel, A. R. & Kahn, C. R. 2001. Insulin signalling and the regulation of glucose and lipid metabolism. *Nature,* 414**,** 799-806.

Sánchez-Valle, V., C Chavez-Tapia, N., Uribe, M. & Méndez-Sánchez, N. 2012. Role of oxidative stress and molecular changes in liver fibrosis: a review. *Current Medicinal Chemistry,* 19**,** 4850-4860.

Sando, H., Lee, Y. S., Iwamoto, Y., Ikeuchi, M. & Kosaka, K. 1980. Isoproterenol-stimulated C-peptide and insulin secretion in diabetic and nonobese normal subjects: decreased hepatic extraction of endogenous insulin in diabetes. *The Journal of Clinical Endocrinology & Metabolism,* 51**,** 1143-1149.

Sandqvist, M., Strindberg, L., Schmelz, M., Lonnroth, P. & Jansson, P. A. 2011. Impaired delivery of insulin to adipose tissue and skeletal muscle in obese women with

postprandial hyperglycemia. *Journal of Clinical Endocrinology and Metabolism,* 96**,** E1320-4.
Saxena, R. & Theise, N. Canals of Hering: recent insights and current knowledge. *Seminars in Liver Disease*, 2004. GEORG THIEME VERLAG, 43-48.
Schaffner, F. & Popper, H. 1963. Capillarization of hepatic sinusoids in man. *Gastroenterology,* 44**,** 239-42.
Schiff, E. R., Sorrell, M. F. & Maddrey, W. C. 2007. *Schiff's Diseases of the Liver*, Lippincott Williams & Wilkins.
Schmucker, D. L. 1998. Aging and the liver: an update. *The Journals of Gerontology Series A: Biological Sciences and Medical Sciences,* 53**,** B315-B321.
Schmucker, D. L. 2005. Age-related changes in liver structure and function: implications for disease? *Experimental Gerontology,* 40**,** 650-659.
Schwartz, M. W., Woods, S. C., Porte, D., Seeley, R. J. & Baskin, D. G. 2000. Central nervous system control of food intake. *Nature,* 404**,** 661-671.
Selimoğlu, M. A., Aydoğdu, S. & Yağci, R. V. 2002. Lipid parameters in childhood cirrhosis and chronic liver disease. *Pediatrics International,* 44**,** 400-403.
Senoo, H. 2004. Structure and function of hepatic stellate cells. *Medical Electron Microscopy,* 37**,** 3-15.
Seow, T. K., Liang, R. C., Leow, C. K. & Chung, M. 2001. Hepatocellular carcinoma: from bedside to proteomics. *Proteomics,* 1**,** 1249-1263.
Sesti, G. 2006. Pathophysiology of insulin resistance. *Best Practice & Research Clinical Endocrinology & Metabolism,* 20**,** 665-679.
Shaw, L. M. 2011. The insulin receptor substrate (IRS) proteins: at the intersection of metabolism and cancer. *Cell Cycle,* 10**,** 1750-1756.
Shayeganpour, A., Korashy, H., Patel, J. P., El-Kadi, A. O. & Brocks, D. R. 2008. The impact of experimental hyperlipidemia on the distribution and metabolism of amiodarone in rat. *International Journal Of Pharmaceutics,* 361**,** 78-86.
Shepherd, P., Withers, D. & Siddle, K. 1998. Phosphoinositide 3-kinase: the key switch mechanism in insulin signalling. *Biochemistry Journal,* 333**,** 471-490.
Sibal, L., Law, H. N., Gebbie, J., Dashora, U. K., Agarwal, S. C. & Home, P. 2006. Predicting the Development of Macrovascular Disease in People with Type 1 Diabetes. *Annals of the New York Academy of Sciences,* 1084**,** 191-207.
Simpson, S. J., Le Couteur, D. G. & Raubenheimer, D. 2015. Putting the balance back in diet. *Cell,* 161**,** 18-23.
Simpson, S. J. & Raubenheimer, D. 2012. *The nature of nutrition. A unifying framework form animal adaption to human obesity*, Princeton, Princeton University Press.
Singleton, J. R., Smith, A. G., Russell, J. W. & Feldman, E. L. 2003. Microvascular Complications of Impaired Glucose Tolerance. *Diabetes,* 52**,** 2867-2873.
Slayter, E. M. 1992. *Light and Electron Microscopy*, Cambridge University Press.
Smedsrød, B. 2004. Clearance function of scavenger endothelial cells. *Comparative Hepatology,* 3**,** S22.
Smedsrød, B., Pertoft, H., Gustafson, S. & Laurent, T. 1990. Scavenger functions of the liver endothelial cell. *Biochemical Journal,* 266**,** 313.
Solon-Biet, S., Mcmahon, A., Ballard, J. W. O., Ruohonen, K., Wu, L., Cogger, V., Warren, A., Huang, X., Pichaud, N., Melvin, R. G., Gokarn, R., Khalil, M., Turner, N., Cooney, G., Sinclair, D., Raubenheimer, D., Le Couteur, D. & Simpson, S. 2014. The ratio of

macronutrients, not caloric intake, dictates cardiometabolic health, aging and longevity in ad libitum-fed mice. *Cell Metabolism,* 19**,** 418-430.

Solon-Biet, S. M., Walters, K. A., Simanainen, U. K., Mcmahon, A. C., Ruohonen, K., Ballard, J. W., Raubenheimer, D., Handelsman, D. J., Le Couteur, D. G. & Simpson, S. J. 2015. Macronutrient balance, reproductive function, and lifespan in aging mice. *Proceedings of the National Academy of Sciences of the United States of America,* 112**,** 3481-6.

Song, S. H., Mcintyre, S. S., Shah, H., Veldhuis, J. D., Hayes, P. C. & Butler, P. C. 2000. Direct Measurement of Pulsatile Insulin Secretion from the Portal Vein in Human Subjects 1. *The Journal of Clinical Endocrinology & Metabolism*, 85**,** 4491-4499.

Sorensen, A., Mayntz, D., Raubenheimer, D. & Simpson, S. J. 2008. Protein-leverage in mice: the geometry of macronutrient balancing and consequences for fat deposition. *Obesity,* 16**,** 566-71.

Sorensen, K. K., Mccourt, P., Berg, T., Crossley, C., Le Couteur, D. G., Wake, K. & Smedsrod, B. 2012. The scavenger endothelial cell - a new player in homeostasis and immunity. *American Journal of Physiology Regul Integrative and Comparative Physiology*

Spector, I., Braet, F., Shochet, N. R. & Bubb, M. R. 1999. New anti-actin drugs in the study of the organization and function of the actin cytoskeleton. *Microscopy Research and Technique,* 47**,** 18-37.

Steffan, A. M., Gendrault, J. L. & Kirn, A. 1987. Increase in the number of fenestrae in mouse endothelial liver cells by altering the cytoskeleton with cytochalasin B. *Hepatology,* 7**,** 1230-1238.

Steffan, A. M., Pereira, C. A., Bingen, A., Valle, M., Martin, J. P., Koehren, F., Royer, C., Gendrault, J. L. & Kirn, A. 1995. Mouse hepatitis virus type 3 infection provokes a decrease in the number of sinusoidal endothelial cell fenestrae both in vivo and in vitro. *Hepatology,* 22**,** 395-401.

Steinberg, P., Lafranconi, W. M., Wolf, C. R., Waxman, D. J., Oesch, F. & Friedberg, T. 1987. Xenobiotic metabolizing enzymes are not restricted to parenchymal cells in rat liver. *Molecular Pharmacology,* 32**,** 463-470.

Strazzabosco M. The cholangiopathies: Disorders of biliary epithelia.Gastroenterology. 2004;127(5):1565-77.

Sun, X. J., Crimmins, D., Myers, M., Miralpeix, M. & White, M. 1993. Pleiotropic insulin signals are engaged by multisite phosphorylation of IRS-1. *Molecular and Cellular Biology,* 13**,** 7418-7428.

Sun, X. J., Rothenberg, P., Kahn, C. R., Backer, J. M., Araki, E., Wilden, P. A., Cahill, D. A., Goldstein, B. J. & White, M. F. 1991. Structure of the insulin receptor substrate IRS-1 defines a unique signal transduction protein. *Nature,* 352**,** 73-77.

Sun, X. J., Wang, L.-M. & Zhang, Y. 1995. Role of IR5-2 in insulin and. *Nature,* 377**,** 173.

Svistounov, D., Warren, A., Mcnerney, G. P., Owen, D. M., Zencak, D., Zykova, S. N., Crane, H., Huser, T., Quinn, R. J., Smedsrod, B., Le Couteur, D. G. & Cogger, V. C. 2012. The Relationship between fenestrations, sieve plates and rafts in liver sinusoidal endothelial cells. *PLoS One,* 7**,** e46134.

Szklarczyk, D., Franceschini, A., Kuhn, M., Simonovic, M., Roth, A., Minguez, P., Doerks, T., Stark, M., Muller, J., Bork, P., Jensen, L. J. & Von Mering, C. 2011. The STRING database in 2011: functional interaction networks of proteins, globally integrated and scored. *Nucleic Acids Research,* 39**,** D561-8.

Taguchi, K., Yamanaka-Okumura, H., Mizuno, A., Nakamura, T., Shimada, M., Doi, T. & Takeda, E. 2014. Insulin resistance as early sign of hepatic dysfunction in liver cirrhosis. *Journal of Medical Investigations,* 61**,** 180-9.

Takamura, T., Misu, H., Ota, T. & Kaneko, S. 2012. Fatty liver as a consequence and cause of insulin resistance: lessons from type 2 diabetic liver. *Endocrinology Journal,* 59**,** 745-63.

Tamemoto, H., Kadowaki, T., Tobe, K., Yagi, T., Sakura, H., Hayakawa, T., Terauchi, Y., Ueki, K., Kaburagi, Y. & Satoh, S. 1994. Insulin resistance and growth retardation in mice lacking insulin receptor substrate-1. *Nature,* 372, 182-186

Tamura, Y., Adachi, H., Osuga, J.-I., Ohashi, K., Yahagi, N., Sekiya, M., Okazaki, H., Tomita, S., Iizuka, Y. & Shimano, H. 2003. FEEL-1 and FEEL-2 are endocytic receptors for advanced glycation end products. *Journal of Biological Chemistry,* 278**,** 12613-12617.

Tanabe, M. & Goto, M. 2001. Elevation of serum hyaluronan level in Werner's syndrome. *Gerontology,* 47**,** 77-81.

Taniguchi, C. M., Emanuelli, B. & KAHN, C. R. 2006. Critical nodes in signalling pathways: insights into insulin action. *Nature Reviews Molecular Cell Biology,* 7**,** 85-96.

Teutsch, H. F., Schuerfeld, D. & Groezinger, E. 1999. Three-dimensional reconstruction of parenchymal units in the liver of the rat. *Hepatology,* 29**,** 494-505.

Thirone, A. C., Huang, C. & Klip, A. 2006. Tissue-specific roles of IRS proteins in insulin signaling and glucose transport. *Trends in Endocrinology & Metabolism,* 17**,** 72-78.

Tsuchiya, K. & Accili, D. 2013. Liver sinusoidal endothelial cells link hyperinsulinemia to hepatic insulin resistance. *Diabetes,* 62**,** 1478-89.

Turner, N., Kowalski, G. M., Leslie, S. J., Risis, S., Yang, C., Lee-Young, R. S., Babb, J. R., Meikle, P. J., Lancaster, G. I., Henstridge, D. C., White, P. J., Kraegen, E. W., Marette, A., Cooney, G. J., Febbraio, M. A. & Bruce, C. R. 2013. Distinct patterns of tissue-specific lipid accumulation during the induction of insulin resistance in mice by high-fat feeding. *Diabetologia,* 56**,** 1638-48.

Ullrich, A. & Schlessinger, J. 1990. Signal transduction by receptors with tyrosine kinase activity. *Cell,* 61**,** 203-212.

Vaag, A., Alford, F., Henriksen, F., Christopher, M. & Beck-Nielsen, H. 1995. Multiple defects of both hepatic and peripheral intracellular glucose processing contribute to the hyperglycaemia of NIDDM. *Diabetologia,* 38**,** 326-336.

Van Der Smissen, P., Van Bossuyt, H., Charels, K. & Wisse, E. 1986. The structure and function of the cytoskeleton in sinusoidal endothelial cells in the rat liver. *Cells Of The Hepatic Sinusoid,* 1**,** 517-522.

Vermijlen, D., Luo, D., Froelich, C. J., Medema, J. P., Kummer, J. A., Willems, E., Braet, F. & Wisse, E. 2002. Hepatic natural killer cells exclusively kill splenic/blood natural killer-resistant tumor cells by the perforin/granzyme pathway. *Journal of Leukocyte Biology,* 72**,** 668-76.

Vidal-Vanaclocha, F. & Barbera, E. 1985. Fenestration patterns in endothelial cells of rat liver sinusoids. *Journal of Ultrastructure Research,* 90**,** 115-123.

Viola, A. & Gupta, N. 2007. Tether and trap: regulation of membrane-raft dynamics by actin-binding proteins. *Nature Reviews Immunology,* 7**,** 889-896.

Vollmar, B., Pradarutti, S., Richter, S. & Menger, M. D. 2002. In vivo quantification of ageing changes in the rat liver from early juvenile to senescent life. *Liver,* 22**,** 330-341.

Wake, K. 1980. Perisinusoidal stellate cells (fat-storing cells, interstitial cells, lipocytes), their related structure in and around the liver sinusoids, and vitamin A-storing cells in extrahepatic organs. *International Review Of Cytology*.

Wallace, T. & Matthews, D. 2002. The assessment of insulin resistance in man. *Diabetic Medicine,* 19**,** 527-534.

Wanless, I. R., Belgiorno, J. & Huet, P. 1996. Hepatic sinusoidal fibrosis induced by cholesterol and stilbestrol in the rabbit: 1. Morphology and inhibition of fibrogenesis by dipyridamole. *Hepatology,* 24**,** 855-864.

Warren, A., Benseler, V., Cogger, V. C., Bertolino, P. & Le Couteur, D. G. 2011. The impact of poloxamer 407 on the ultrastructure of the liver and evidence for clearance by extensive endothelial and kupffer cell endocytosis. *Toxicologic Pathology,* 39**,** 390-7.

Warren, A., Bertolino, P., Benseler, V., Fraser, R., McCaughan, G. W. & Le Couteur, D. G. 2007. Marked changes of the hepatic sinusoid in a transgenic mouse model of acute immune-mediated hepatitis. *Journal of Hepatology,* 46**,** 239-46.

Warren, A., Bertolino, P., Cogger, V. C., Mclean, A. J., Fraser, R. & Le Couteur, D. G. 2005. Hepatic pseudocapillarization in aged mice. *Experimental Gerontology,* 40**,** 807-12.

Warren, A., Cogger, V. C., Arias, I. M., McCuskey, R. S. & Le Couteur, D. G. 2010. Liver sinusoidal endothelial fenestrations in caveolin-1 knockout mice. *Microcirculation,* 17**,** 32-8.

Warren, A., Le Couteur, D. G., Fraser, R., Bowen, D. G., McCaughan, G. W. & Bertolino, P. 2006. T lymphocytes interact with hepatocytes through fenestrations in murine liver sinusoidal endothelial cells. *Hepatology,* 44**,** 1182-90.

Warton, D. I. & Hui, F. K. C. 2010. The arcsine is asinine: the analysis of proportions in ecology. *Ecology,* 92**,** 3-10.

Wasan, K. M., Subramanian, R., Kwong, M., Goldberg, I. J., Wright, T. & Johnston, T. P. 2003. Poloxamer 407-mediated alterations in the activities of enzymes regulating lipid metabolism in rats. *Journal of Pharmacy & Pharmaceutical Sciences,* 6**,** 189-97.

Watanabe, T., Tanaka, Y. & Kimula, Y. 1984. A cytophotometrical study on the centenarian hepatocyte. *Virchows Archiv B,* 46**,** 265-268.

Waters, S., Yamauchi, K. & Pessin, J. 1993. Functional expression of insulin receptor substrate-1 is required for insulin-stimulated mitogenic signaling. *Journal of Biological Chemistry,* 268**,** 22231-22234.

Weintraub, M.S., *et al.* Clearance of chylomicron remnants in normolipidaemic patients with coronary artery disease: case control study over three years. *Bmj* **312**, 935-939 (1996).

Weyer, C., Bogardus, C., Mott, D. M. & Pratley, R. E. 1999a. The natural history of insulin secretory dysfunction and insulin resistance in the pathogenesis of type 2 diabetes mellitus. *Journal of Clinical Investigation,* 104**,** 787.

Weyer, C., Bogardus, C. & Pratley, R. E. 1999b. Metabolic characteristics of individuals with impaired fasting glucose and/or impaired glucose tolerance. *Diabetes,* 48**,** 2197-2203.

White, M. F. 1998. The IRS-signalling system: a network of docking proteins that mediate insulin action. *Molecular And Cellular Biochemistry,* 182**,** 3-11.

Wick, M. J., Dong, L. Q., Hu, D., Langlais, P. & Liu, F. 2001. Insulin receptor-mediated p62dok tyrosine phosphorylation at residues 362 and 398 plays distinct roles for binding GTPase-activating protein and Nck and is essential for inhibiting insulin-stimulated activation of Ras and Akt. *Journal of Biological Chemistry,* 276**,** 42843-42850.

Wieland, A., Frank, D. N., Harnke, B. & Bambha, K. 2015. Systematic review: microbial dysbiosis and nonalcoholic fatty liver disease. *Alimentary Pharmacology & Therapeutics,* 42**,** 1051-63.

Wild, S., Roglic, G., Green, A., Sicree, R. & King, H. 2004. Global prevalence of diabetes estimates for the year 2000 and projections for 2030. *Diabetes Care,* 27**,** 1047-1053.

Winau, F., Hegasy, G., Weiskirchen, R., Weber, S., Cassan, C., Sieling, P. A., Modlin, R. L., Liblau, R. S., Gressner, A. M. & Kaufmann, S. H. 2007. Ito cells are liver-resident antigen-presenting cells for activating T cell responses. *Immunity,* 26**,** 117-129.

Wisse, E. 1970. An electron microscopic study of the fenestrated endothelial lining of rat liver sinusoids. *Journal of Ultrastructure Research,* 31**,** 125-150.

Wisse, E. 1972. An ultrastructural characterization of the endothelial cell in the rat liver sinusoid under normal and various experimental conditions, as a contribution to the distinction between endothelial and Kupffer cells. *Journal Of Ultrastructure Research,* 38**,** 528-562.

Wisse, E., Braet, F., Luo, D., De Zanger, R., Jans, D., Crabbe, E. & Vermoesen, A. 1996. Structure and function of sinusoidal lining cells in the liver. *Toxicologic Pathology,* 24**,** 100-111.

Wisse, E., De Zanger, R., Charels, K., Van Der Smissen, P. & McCuskey, R. 1985. The liver sieve: considerations concerning the structure and function of endothelial fenestrae, the sinusoidal wall and the space of Disse. *Hepatology,* 5**,** 683-692.

Wisse, E., Luo, D., Vermijlen, D., Kanellopoulou, C., De Zanger, R. & Braet, F. 1997. On the function of pit cells, the liver-specific natural killer cells. *Seminars in Liver Disease,* 17**,** 265-286.

Wisse, E., Noordende, J., Meulen, J. & Daems, W. T. 1976. The pit cell: description of a new type of cell occurring in rat liver sinusoids and peripheral blood. *Cell And Tissue Research,* 173**,** 423-435.

Withers, D. J., Burks, D. J., Towery, H. H., Altamuro, S. L., Flint, C. L. & White, M. F. 1999. Irs-2 coordinates Igf-1 receptor-mediated β-cell development and peripheral insulin signalling. *Nature Genetics,* 23**,** 32-40.

Withers, D. J., Gutierrez, J. S., Towery, H., Burks, D. J., Ren, J.-M., Previs, S., Zhang, Y., Bernal, D., Pons, S. & Shulman, G. I. 1998. Disruption of IRS-2 causes type 2 diabetes in mice. *Nature,* 391**,** 900-904.

Wout, Z. G., Pec, E. A., Maggiore, J. A., Williams, R. H., Palicharla, P. & Johnston, T. P. 1992. Poloxamer 407-mediated changes in plasma cholesterol and triglycerides following intraperitoneal injection to rats. *Journal of Parenteral Science & Technology,* 46**,** 192-200.

Wynne, H. A., Cope, L. H., Mutch, E., Rawlins, M. D., Woodhouse, K. W. & James, O. F. 1989. The effect of age upon liver volume and apparent liver blood flow in healthy man. *Hepatology,* 9**,** 297-301.

Xie, G., Wang, X., Wang, L., Wang, L., Atkinson, R. D., Kanel, G. C., Gaarde, W. A. & Deleve, L. D. 2012. Role of differentiation of liver sinusoidal endothelial cells in progression and regression of hepatic fibrosis in rats. *Gastroenterology,* 142**,** 918-927. e6.

Xu, B., Broome, U., Uzunel, M., Nava, S., Ge, X., Kumagai-Braesch, M., Hultenby, K., Christensson, B., Ericzon, B.-G. & Holgersson, J. 2003. Capillarization of hepatic sinusoid by liver endothelial cell-reactive autoantibodies in patients with cirrhosis and chronic hepatitis. *The American Journal Of Pathology,* 163**,** 1275-1289.

Yamada, K. & Noguchi, T. 1999. Nutrient and hormonal regulation of pyruvate kinase gene expression. *Biochemistry Journal,* 337**,** 1-11.

Yamamura, K. 1999. Transformation using (x + 0.5) to stabilize the variance of populations. *Researches on Population Ecology,* 41**,** 229-234.

Yokomori, H., Oda, M., Yoshimura, K., Nagai, T., Ogi, M., Nomura, M. & Ishii, H. 2003. Vascular endothelial growth factor increases fenestral permeability in hepatic sinusoidal endothelial cells. *Liver International,* 23**,** 467-475.

Yoon, J. C., Puigserver, P., Chen, G., Donovan, J., Wu, Z., Rhee, J., Adelmant, G., Stafford, J., Kahn, C. R. & Granner, D. K. 2001. Control of hepatic gluconeogenesis through the transcriptional coactivator PGC-1. *Nature,* 413**,** 131-138.

Youngren, J. 2007. Regulation of insulin receptor function. *Cellular and Molecular Life Sciences,* 64**,** 873-891.

Zhang, X., Li, Z., Liu, D., Xu, X., Shen, W. & Mei, Z. 2009. Effects of probucol on hepatic tumor necrosis factor-α, interleukin-6 and adiponectin receptor-2 expression in diabetic rats. *Journal of Gastroenterology and Hepatology,* 24**,** 1058-1063.

Zhu, M., De Cabo, R., Lane, M. A. & Ingram, D. K. 2004. Caloric restriction modulates early events in insulin signaling in liver and skeletal muscle of rat. *Annals of the New York Academy of Sciences,* 1019**,** 448-52.

APPENDICES

APPENDIX 1

Supplementary information for Chapter 3: Insulin tolerance test showing similar performance between young and old group.

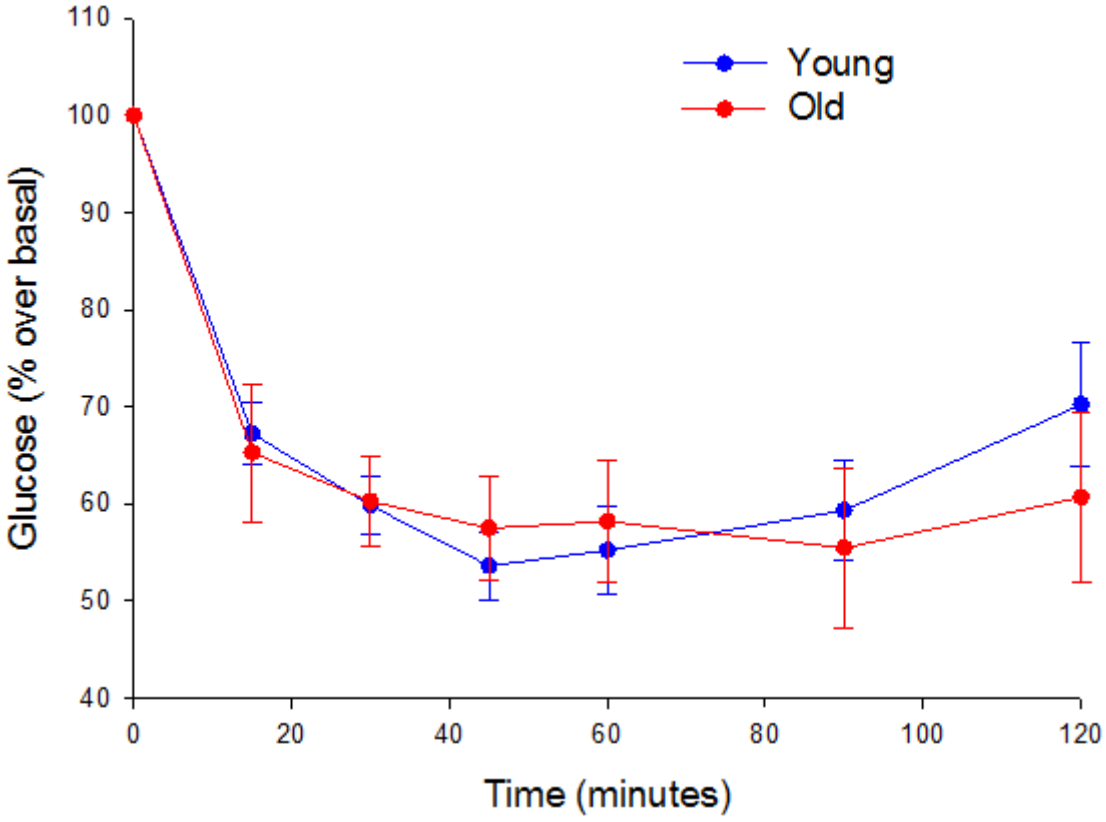

APPENDIX 2

Supplementary information for Chapter 3: RT-PCR data for insulin signaling pathway in young vs old livers

Symbol	Well	AVG ΔC_t (Ct (GOI) - Ave Ct (HKG))		2^-ΔC_t		Fold Change	T-TEST	Fold Up- or Down-Regulation
		OLD	YOUNG	OLD	YOUNG	OLD /YOUNG	p value	OLD /YOUNG
Acaca	A01	3.11	2.33	1.2E-01	2.0E-01	0.58	0.294059	-1.71
Acox1	A02	5.05	6.38	3.0E-02	1.2E-02	2.52	0.965517	2.52
Adra1d	A03	9.45	10.32	1.4E-03	7.8E-04	1.83	0.342633	1.83
Aebp1	A04	7.88	6.60	4.2E-03	1.0E-02	0.41	0.402924	-2.42
Akt1	A05	4.15	4.00	5.6E-02	6.3E-02	0.90	0.814608	-1.11
Akt2	A06	6.83	8.03	8.8E-03	3.8E-03	2.30	0.863440	2.30
Akt3	A07	7.14	7.38	7.1E-03	6.0E-03	1.18	0.600176	1.18
Araf	A08	2.64	2.74	1.6E-01	1.5E-01	1.08	0.685440	1.08
Bcl2l1	A09	6.30	5.66	1.3E-02	2.0E-02	0.64	0.511245	-1.55
Braf	A10	5.00	5.19	3.1E-02	2.7E-02	1.14	0.961619	1.14
Cap1	A11	2.44	3.16	1.8E-01	1.1E-01	1.65	0.322493	1.65
Cbl	A12	7.53	7.76	5.4E-03	4.6E-03	1.17	0.952396	1.17
Cebpa	B01	2.33	2.18	2.0E-01	2.2E-01	0.91	0.732909	-1.10
Cebpb	B02	6.27	7.75	1.3E-02	4.6E-03	2.80	0.996637	2.80
Cfd	B03	7.67	8.33	4.9E-03	3.1E-03	1.58	0.539415	1.58
Dok1	B04	9.19	10.19	1.7E-03	8.5E-04	2.01	0.341850	2.01
Dok2	B05	9.17	9.79	1.7E-03	1.1E-03	1.53	0.394094	1.53
Dok3	B06	9.31	9.86	1.6E-03	1.1E-03	1.46	0.421388	1.46
Dusp14	B07	8.27	7.45	3.2E-03	5.7E-03	0.57	0.780596	-1.76
Eif2b1	B08	4.71	4.08	3.8E-02	5.9E-02	0.64	0.272332	-1.55
Eif4ebp1	B09	1.85	1.24	2.8E-01	4.2E-01	0.66	0.306678	-1.53
Ercc1	B10	7.74	9.01	4.7E-03	1.9E-03	2.42	0.801794	2.42
Fasn	B11	3.80	-0.91	7.2E-02	1.9E+00	**0.04**	**0.022161**	**-26.22**
Fbp1	B12	8.02	8.14	3.9E-03	3.5E-03	1.09	0.859602	1.09
Fos	C01	7.14	8.67	7.1E-03	2.5E-03	2.90	0.789263	2.90
Frs2	C02	6.62	6.94	1.0E-02	8.1E-03	1.25	0.505022	1.25
Frs3	C03	5.82	7.04	1.8E-02	7.6E-03	2.33	0.711226	2.33
G6pc	C04	7.95	6.89	4.0E-03	8.4E-03	0.48	0.672318	-2.08
Gab1	C05	5.29	5.70	2.6E-02	1.9E-02	1.32	0.796305	1.32
Gcg	C06	6.57	7.70	1.1E-02	4.8E-03	2.18	0.659937	2.18

Symbol	Well	AVG ΔC_t (Ct (GOI) - Ave Ct (HKG))		$2^{-\Delta C_t}$		Fold Change	T-TEST	Fold Up- or Down-Regulation
		OLD	YOUNG	OLD	YOUNG	OLD /YOUNG	p value	OLD /YOUNG
Gck	C07	6.22	6.58	1.3E-02	1.0E-02	1.28	0.789675	1.28
Gpd1	C08	7.75	7.34	4.6E-03	6.2E-03	0.75	0.542770	-1.33
Grb10	C09	6.06	6.65	1.5E-02	1.0E-02	1.51	0.698559	1.51
Grb2	C10	6.82	8.10	8.8E-03	3.7E-03	2.42	0.753414	2.42
Gsk3b	C11	8.84	10.07	2.2E-03	9.3E-04	2.34	0.324282	2.34
Hk2	C12	6.37	7.40	1.2E-02	5.9E-03	2.04	0.594500	2.04
Hras	D01	5.97	6.82	1.6E-02	8.9E-03	1.80	0.448238	1.80
Igf1r	D02	9.29	8.83	1.6E-03	2.2E-03	0.73	0.928575	-1.37
Igf2	D03	4.72	6.40	3.8E-02	1.2E-02	**3.21**	0.822011	**3.21**
Igfbp1	D04	9.45	9.57	1.4E-03	1.3E-03	1.09	0.477142	1.09
Ins1	D05	9.45	10.32	1.4E-03	7.8E-04	1.83	0.342633	1.83
Ins2	D06	7.44	9.41	5.8E-03	1.5E-03	**3.93**	0.196303	**3.93**
Insl3	D07	6.61	8.45	1.0E-02	2.9E-03	**3.60**	0.598694	**3.60**
Insr	D08	2.46	2.86	1.8E-01	1.4E-01	1.32	0.813029	1.32
Irs1	D09	3.77	3.50	7.3E-02	8.9E-02	0.83	0.845756	-1.21
Irs2	D10	4.55	5.13	4.3E-02	2.8E-02	1.50	0.363243	1.50
Jun	D11	3.66	2.75	7.9E-02	1.5E-01	0.53	0.247933	-1.87
Klf10	D12	7.21	6.06	6.7E-03	1.5E-02	0.45	0.531329	-2.23
Kras	E01	4.77	4.76	3.7E-02	3.7E-02	0.99	0.756316	-1.01
Ldlr	E02	6.48	7.70	1.1E-02	4.8E-03	2.33	0.728540	2.33
Lep	E03	7.17	8.40	6.9E-03	3.0E-03	2.34	0.817543	2.34
Map2k1	E04	3.11	3.09	1.2E-01	1.2E-01	0.99	0.728693	-1.01
Mapk1	E05	4.74	4.46	3.7E-02	4.6E-02	0.82	0.748205	-1.22
Mtor	E06	9.45	10.32	1.4E-03	7.8E-04	1.83	0.342633	1.83
Nos2	E07	7.70	8.94	4.8E-03	2.0E-03	2.36	0.898031	2.36
Npy	E08	7.33	8.50	6.2E-03	2.8E-03	2.26	0.880665	2.26
Pck2	E09	6.22	5.92	1.3E-02	1.7E-02	0.81	0.712001	-1.23
Pdpk1	E10	4.94	4.86	3.3E-02	3.4E-02	0.94	0.950127	-1.06
Pik3ca	E11	6.87	8.17	8.5E-03	3.5E-03	2.47	0.846339	2.47
Pik3cb	E12	8.86	10.32	2.1E-03	7.8E-04	2.74	0.296042	2.74
Pik3r1	F01	3.18	3.15	1.1E-01	1.1E-01	0.98	0.692093	-1.02
Pik3r2	F02	5.97	5.30	1.6E-02	2.5E-02	0.63	0.464881	-1.59
Pklr	F03	6.24	4.80	1.3E-02	3.6E-02	0.37	0.464414	-2.71
Pparg	F04	9.45	9.94	1.4E-03	1.0E-03	1.41	0.404963	1.41
Ppp1ca	F05	2.65	2.72	1.6E-01	1.5E-01	1.05	0.961231	1.05
Prkcg	F06	7.51	8.98	5.5E-03	2.0E-03	2.78	0.660055	2.78
Prkcz	F07	7.05	6.57	7.5E-03	1.0E-02	0.72	0.980219	-1.39
Prl	F08	7.20	8.70	6.8E-03	2.4E-03	2.82	0.811913	2.82

Symbol	Well	AVG ΔC_t (Ct (GOI) - Ave Ct (HKG))		$2^{-\Delta C_t}$		Fold Change	T-TEST	Fold Up- or Down-Regulation
		OLD	YOUNG	OLD	YOUNG	OLD /YOUNG	p value	OLD /YOUNG
Ptpn1	F09	6.93	8.58	8.2E-03	2.6E-03	3.14	0.713847	3.14
Raf1	F10	1.89	2.55	2.7E-01	1.7E-01	1.58	0.363834	1.58
Retn	F11	9.45	10.32	1.4E-03	7.8E-04	1.83	0.342633	1.83
Rps6ka1	F12	7.87	9.15	4.3E-03	1.8E-03	2.43	0.661146	2.43
Rras	G01	4.90	4.07	3.4E-02	6.0E-02	0.56	0.477690	-1.78
Rras2	G02	3.97	4.70	6.4E-02	3.9E-02	1.66	0.329842	1.66
Serpine1	G03	5.59	5.51	2.1E-02	2.2E-02	0.94	0.806348	-1.06
Shc1	G04	5.09	5.11	2.9E-02	2.9E-02	1.01	0.729800	1.01
Slc27a4	G05	7.29	8.70	6.4E-03	2.4E-03	2.66	0.899783	2.66
Slc2a1	G06	7.26	8.72	6.5E-03	2.4E-03	2.76	0.835286	2.76
Slc2a4	G07	6.46	7.41	1.1E-02	5.9E-03	1.93	0.922519	1.93
Sos1	G08	6.28	5.85	1.3E-02	1.7E-02	0.74	0.568297	-1.34
Srebf1	G09	1.82	1.09	2.8E-01	4.7E-01	0.60	0.291791	-1.66
Tg	G10	9.45	10.21	1.4E-03	8.4E-04	1.70	0.355179	1.70
Ucp1	G11	9.26	10.32	1.6E-03	7.8E-04	2.08	0.333236	2.08
Vegfa	G12	6.48	7.75	1.1E-02	4.6E-03	2.42	0.782530	2.42
Actb	H01	-1.03	-1.43	2.0E+00	2.7E+00	0.76	0.658113	-1.31
B2m	H02	2.82	1.90	1.4E-01	2.7E-01	0.53	0.769787	-1.89
Hprt1	H03	-0.84	0.20	1.8E+00	8.7E-01	2.06	0.922424	2.06
Ldha	H04	0.42	0.03	7.5E-01	9.8E-01	0.77	0.809575	-1.30
Rplp1	H05	-1.36	-0.71	2.6E+00	1.6E+00	1.57	0.388136	1.57

Legend:

Fold-Change (2^(- Delta Delta Ct)) is the normalized gene expression (2^(- Delta Ct)) in the Test Sample divided the normalized gene expression (2^(- Delta Ct)) in the Control Sample.

Fold-Regulation represents fold-change results in a biologically meaningful way. Fold-change values greater than one indicate a positive- or an up-regulation, and the fold-regulation is equal to the fold-change

Fold-change values less than one indicate a negative or down-regulation, and the fold-regulation is the negative inverse of the fold-change.
Fold-change and fold-regulation values greater than 2 are indicated in red; fold-change values less than 0.5 and fold-regulation values less than -2 are indicated in blue.

p-values: The p values are calculated based on a Student's t-test of the replicate 2^(- Delta Ct) values for each gene in the control group and treatment groups, and p values less than 0.05 are indicated in red.

Comments:

A: This gene's average threshold cycle is relatively high (> 30) in either the control or the test sample, and is reasonably low in the other sample (< 30).

These data mean that the gene's expression is relatively low in one sample and reasonably detected in the other sample suggesting that the actual fold-change value is at least as large as the calculated and reported fold-change result.

This fold-change result may also have greater variations if p value > 0.05; therefore, it is important to have a sufficient number of biological replicates to validate the result for this gene.

B: This gene's average threshold cycle is relatively high (> 30), meaning that its relative expression level is low, in both control and test samples, and the p-value for the fold-change is either unavailable or relatively high (p > 0.05).

This fold-change result may also have greater variations; therefore, it is important to have a sufficient number of biological replicates to validate the result for this gene.

C: This gene's average threshold cycle is either not determined or greater than the defined cut-off (deault 35), in both samples meaning that its expression was undetected, making this fold-change result erroneous and un-interpretable.

APPENDIX 3:

Supplementary information for Chapters 3 & 4: Quantitative phosphoproteomics of 47 peptides containing insulin-regulated sites from the KEGG insulin signaling pathway for old vs young and control vs P407 group. Z-scores of >+/-1.0 were considered significant. Log2 values are provided to show statistical variation.

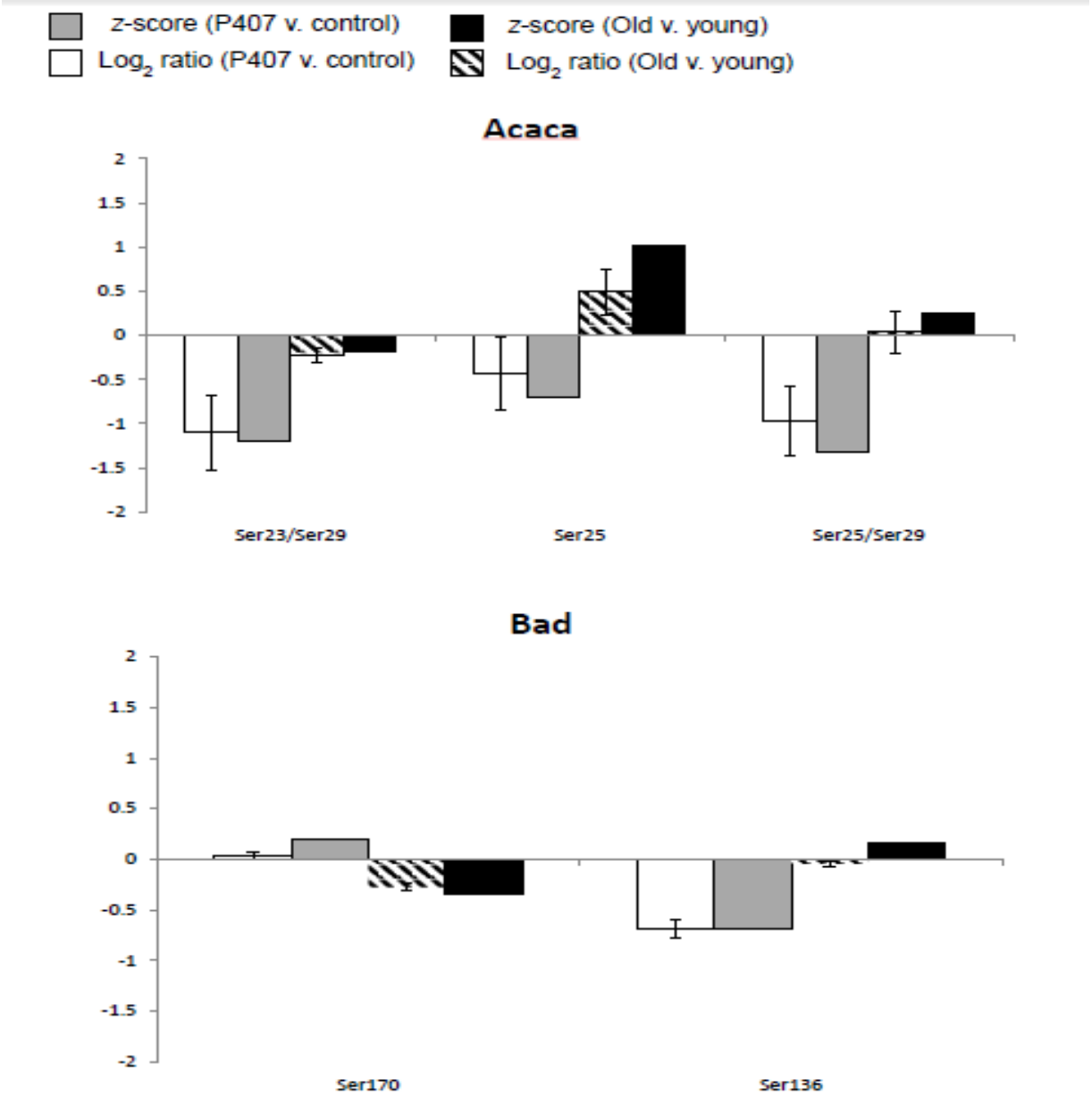

APPENDIX 4

Supplementary information for Chapter 4: Average MID outflow curves for pyruvate and the extracellular marker sucrose for (a) control and (b) P407 rats. There are no changes in the volume of distribution of pyruvate for both groups.

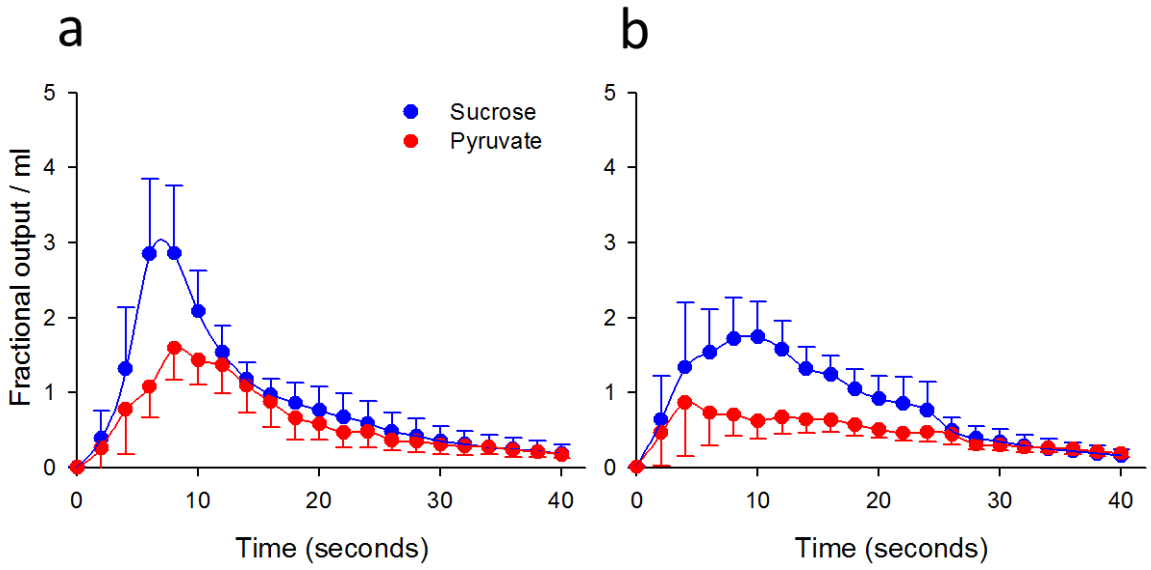

APPENDIX 5

Supplementary information for Chapter 4: RT-PCR data for insulin signaling pathway in Control vs P407 livers

Symbol	Well	AVG ΔC_t (Ct (GOI) - Ave Ct (HKG))		$2^{-\Delta C_t}$		Fold Change	T-TEST	Fold Up- or Down-Regulation
		P407	Saline	P407	Saline	P407 /Saline	p value	P407 /Saline
Acaca	A01	5.57	5.30	2.1E-02	2.5E-02	0.83	0.883138	-1.20
Acox1	A02	2.79	2.10	1.4E-01	2.3E-01	0.62	N/A	-1.62
Adra1d	A03	14.67	N/A	3.8E-05	N/A	**N/A**	N/A	**N/A**
Aebp1	A04	10.31	10.92	7.9E-04	5.2E-04	1.53	0.168876	1.53
Akt1	A05	5.86	6.12	1.7E-02	1.4E-02	1.20	0.555182	1.20
Akt2	A06	5.04	5.27	3.0E-02	2.6E-02	1.18	0.605222	1.18
Akt3	A07	9.65	9.65	1.2E-03	1.2E-03	1.00	0.917337	-1.00
Araf	A08	4.09	3.69	5.9E-02	7.7E-02	0.76	N/A	-1.31
Bcl2l1	A09	5.98	5.40	1.6E-02	2.4E-02	0.67	0.168497	-1.49
Braf	A10	7.66	7.80	4.9E-03	4.5E-03	1.10	0.511738	1.10
Cap1	A11	5.01	5.07	3.1E-02	3.0E-02	1.05	0.732696	1.05
Cbl	A12	9.68	10.05	1.2E-03	9.4E-04	1.30	0.407195	1.30
Cebpa	B01	3.67	6.27	7.9E-02	1.3E-02	**6.08**	0.950302	**6.08**
Cebpb	B02	12.79	12.65	1.4E-04	1.6E-04	0.90	N/A	-1.11
Cfd	B03	4.32	4.13	5.0E-02	5.7E-02	0.88	0.706524	-1.14
Dok1	B04	10.94	10.94	5.1E-04	5.1E-04	1.00	0.607590	1.00
Dok2	B05	12.17	12.12	2.2E-04	2.2E-04	0.97	0.722672	-1.03
Dok3	B06	10.00	11.15	9.7E-04	4.4E-04	2.21	0.083272	2.21
Dusp14	B07	9.72	9.60	1.2E-03	1.3E-03	0.92	0.577725	-1.08
Eif2b1	B08	7.00	7.31	7.8E-03	6.3E-03	1.24	N/A	1.24
Eif4ebp1	B09	4.97	4.98	3.2E-02	3.2E-02	1.00	0.966788	1.00
Ercc1	B10	11.91	11.99	2.6E-04	2.5E-04	1.06	0.874044	1.06
Fasn	B11	3.81	4.29	7.1E-02	5.1E-02	1.40	N/A	1.40

Symbol	Well	AVG ΔC_t (Ct (GOI) - Ave Ct (HKG))		$2^{-\Delta C_t}$		Fold Change	T-TEST	Fold Up- or Down-Regulation
		P407	Saline	P407	Saline	P407 /Saline	p value	P407 /Saline
Fbp1	B12	1.80	1.47	2.9E-01	3.6E-01	0.80	0.502627	-1.26
Fos	C01	10.57	10.77	6.6E-04	5.7E-04	1.15	0.745289	1.15
Frs2	C02	7.57	7.39	5.3E-03	5.9E-03	0.89	0.419211	-1.13
Frs3	C03	12.21	12.40	2.1E-04	1.8E-04	1.14	0.509824	1.14
G6pc	C04	4.98	3.17	3.2E-02	1.1E-01	**0.28**	0.841671	**-3.53**
Gab1	C05	8.92	8.99	2.1E-03	2.0E-03	1.05	0.909824	1.05
Gcg	C06	14.67	N/A	3.8E-05	N/A	**N/A**	N/A	**N/A**
Gck	C07	6.55	5.77	1.1E-02	1.8E-02	0.58	N/A	-1.72
Gpd1	C08	3.87	3.46	6.8E-02	9.1E-02	0.75	0.553015	-1.33
Grb10	C09	12.21	12.34	2.1E-04	1.9E-04	1.09	0.605081	1.09
Grb2	C10	3.71	3.83	7.6E-02	7.0E-02	1.09	N/A	1.09
Gsk3b	C11	6.79	6.93	9.1E-03	8.2E-03	1.11	0.726290	1.11
Hk2	C12	12.22	12.62	2.1E-04	1.6E-04	1.33	0.380887	1.33
Hras	D01	3.37	3.25	9.7E-02	1.1E-01	0.92	0.813262	-1.09
Igf1r	D02	11.65	11.63	3.1E-04	3.2E-04	0.98	0.863731	-1.02
Igf2	D03	12.16	12.28	2.2E-04	2.0E-04	1.09	0.576069	1.09
Igfbp1	D04	2.69	2.49	1.5E-01	1.8E-01	0.87	0.931905	-1.15
Ins1	D05	11.76	13.16	2.9E-04	1.1E-04	2.63	N/A	2.63
Ins2	D06	12.79	13.16	1.4E-04	1.1E-04	1.29	N/A	1.29
Insl3	D07	11.97	12.65	2.5E-04	1.6E-04	1.60	N/A	1.60
Insr	D08	5.44	5.88	2.3E-02	1.7E-02	1.35	0.227271	1.35
Irs1	D09	5.58	5.47	2.1E-02	2.3E-02	0.92	0.655403	-1.09
Irs2	D10	8.80	9.62	2.2E-03	1.3E-03	1.76	**0.026492**	1.76
Jun	D11	6.91	7.43	8.3E-03	5.8E-03	1.44	0.441436	1.44
Klf10	D12	7.66	7.78	4.9E-03	4.6E-03	1.08	0.663021	1.08
Kras	E01	7.66	7.48	4.9E-03	5.6E-03	0.88	0.310540	-1.13
Ldlr	E02	5.63	6.27	2.0E-02	1.3E-02	1.55	0.278261	1.55
Lep	E03	14.67	N/A	3.8E-05	N/A	**N/A**	N/A	**N/A**
Map2k1	E04	6.25	6.31	1.3E-02	1.3E-02	1.05	0.967957	1.05

Symbol	Well	AVG ΔC_t (Ct (GOI) - Ave Ct (HKG))		$2^{-\Delta C_t}$		Fold Change	T-TEST	Fold Up- or Down-Regulation
		P407	Saline	P407	Saline	P407 /Saline	p value	P407 /Saline
Mapk1	E05	3.93	3.98	6.6E-02	6.3E-02	1.03	0.755070	1.03
Mtor	E06	7.07	7.00	7.5E-03	7.8E-03	0.95	0.748041	-1.05
Nos2	E07	13.20	12.65	1.1E-04	1.6E-04	0.68	N/A	-1.46
Npy	E08	7.95	7.37	4.1E-03	6.0E-03	0.67	0.380978	-1.49
Pck2	E09	4.99	5.84	3.1E-02	1.8E-02	1.79	0.184082	1.79
Pdpk1	E10	6.53	6.55	1.1E-02	1.1E-02	1.01	N/A	1.01
Pik3ca	E11	6.84	6.98	8.7E-03	7.9E-03	1.10	0.689183	1.10
Pik3cb	E12	6.91	7.01	8.3E-03	7.8E-03	1.07	0.798322	1.07
Pik3r1	F01	6.65	5.81	1.0E-02	1.8E-02	0.56	0.188509	-1.79
Pik3r2	F02	8.40	8.53	3.0E-03	2.7E-03	1.09	0.804854	1.09
Pklr	F03	3.86	2.86	6.9E-02	1.4E-01	0.50	0.477493	-2.00
Pparg	F04	10.40	10.21	7.4E-04	8.5E-04	0.88	0.749064	-1.14
Ppp1ca	F05	3.57	3.67	8.4E-02	7.9E-02	1.07	0.633707	1.07
Prkcg	F06	12.43	12.62	1.8E-04	1.6E-04	1.14	0.587596	1.14
Prkcz	F07	8.73	8.95	2.4E-03	2.0E-03	1.16	0.775432	1.16
Prl	F08	12.79	12.62	1.4E-04	1.6E-04	0.89	0.757958	-1.13
Ptpn1	F09	7.38	7.69	6.0E-03	4.8E-03	1.24	0.562210	1.24
Raf1	F10	3.73	3.92	7.5E-02	6.6E-02	1.14	0.453272	1.14
Retn	F11	14.67	13.16	3.8E-05	1.1E-04	0.35	N/A	-2.85
Rps6ka1	F12	7.12	7.18	7.2E-03	6.9E-03	1.04	0.944111	1.04
Rras	G01	5.37	5.85	2.4E-02	1.7E-02	1.39	0.235829	1.39
Rras2	G02	5.35	6.16	2.4E-02	1.4E-02	1.75	N/A	1.75
Serpine1	G03	11.18	11.67	4.3E-04	3.1E-04	1.40	0.765379	1.40
Shc1	G04	5.22	5.56	2.7E-02	2.1E-02	1.27	0.643608	1.27
Slc27a4	G05	7.79	7.78	4.5E-03	4.6E-03	0.99	0.956394	-1.01
Slc2a1	G06	11.55	10.78	3.3E-04	5.7E-04	0.59	0.262772	-1.70
Slc2a4	G07	12.79	13.16	1.4E-04	1.1E-04	1.29	N/A	1.29
Sos1	G08	6.78	6.66	9.1E-03	9.9E-03	0.92	0.898960	-1.09
Srebf1	G09	9.09	9.58	1.8E-03	1.3E-03	1.41	N/A	1.41

Symbol	Well	AVG ΔC_t (Ct (GOI) - Ave Ct (HKG))		$2^{-\Delta C_t}$		Fold Change	T-TEST	Fold Up- or Down-Regulation
		P407	Saline	P407	Saline	P407 /Saline	p value	P407 /Saline
Tg	G10	11.90	10.99	2.6E-04	4.9E-04	0.53	**0.010198**	-1.88
Ucp1	G11	13.22	12.14	1.1E-04	2.2E-04	0.47	N/A	-2.11
Vegfa	G12	4.95	4.90	3.2E-02	3.4E-02	0.96	0.857308	-1.04
Actb	H01	0.68	0.92	6.3E-01	5.3E-01	1.19	0.551329	1.19
B2m	H02	-2.55	-2.89	5.8E+00	7.4E+00	0.79	0.059386	-1.27
Hprt1	H03	1.68	0.98	3.1E-01	5.1E-01	0.62	0.239562	-1.63
Ldha	H04	0.34	0.88	7.9E-01	5.4E-01	1.46	0.108750	1.46
Rplp1	H05	-0.15	0.10	1.1E+00	9.3E-01	1.19	0.175467	1.19

Legend:

Fold-Change (2^(- Delta Delta Ct)) is the normalized gene expression (2^(- Delta Ct)) in the Test Sample divided the normalized gene expression (2^(- Delta Ct)) in the Control Sample.

Fold-Regulation represents fold-change results in a biologically meaningful way. Fold-change values greater than one indicate a positive- or an up-regulation, and the fold-regulation is equal to the fold-change

Fold-change values less than one indicate a negative or down-regulation, and the fold-regulation is the negative inverse of the fold-change.
Fold-change and fold-regulation values greater than 2 are indicated in red; fold-change values less than 0.5 and fold-regulation values less than -2 are indicated in blue.

p-values: The p values are calculated based on a Student's t-test of the replicate 2^(- Delta Ct) values for each gene in the control group and treatment groups, and p values less than 0.05 are indicated in red.

Comments:

A: This gene's average threshold cycle is relatively high (> 30) in either the control or the test sample, and is reasonably low in the other sample (< 30).

These data mean that the gene's expression is relatively low in one sample and reasonably detected in the other sample suggesting that the actual fold-change value is at least as large as the calculated and reported fold-change result.

This fold-change result may also have greater variations if p value > 0.05; therefore, it is important to have a sufficient number of biological replicates to validate the result for this gene.

B: This gene's average threshold cycle is relatively high (> 30), meaning that its relative expression level is low, in both control and test samples, and the p-value for the fold-change is either unavailable or relatively high (p > 0.05).

This fold-change result may also have greater variations; therefore, it is important to have a sufficient number of biological replicates to validate the result for this gene.

C: This gene's average threshold cycle is either not determined or greater than the defined cut-off (deault 35), in both samples meaning that its expression was undetected, making this fold-change result erroneous and un-interpretable.

APPENDIX 6

Supplementary Information for Chapter 6

Supplementary Fig. 1 Circulating C19 levels and LSEC fenestration frequency

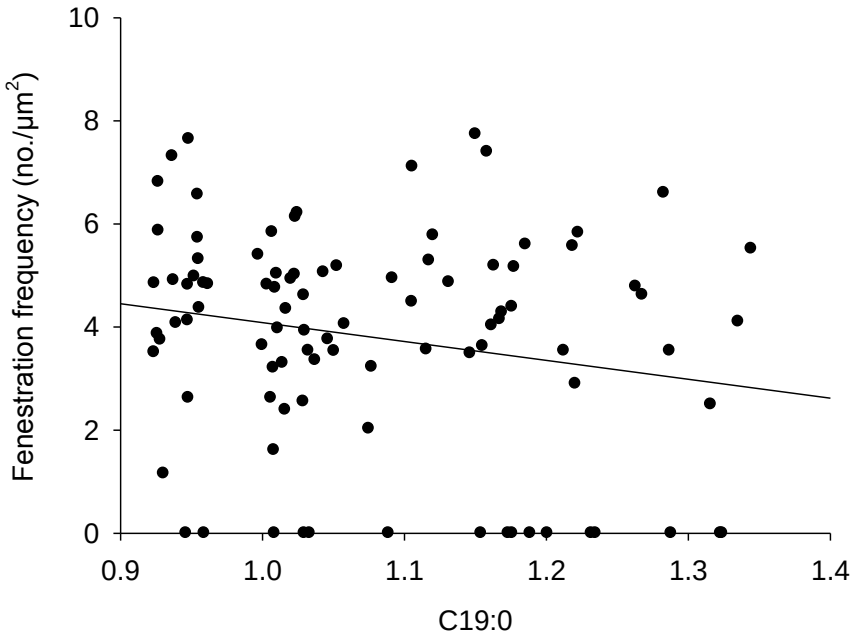

Supplementary Table 1.

Top model set based on Akaike Information Criterion corrected for small sample size (AICc) for the effects of bacterial abundance on fenestration diameter. Given for each model is the model form, degrees of freedom (df), models log likelihood (logLik), AICc, change in AICc from the top model (ΔAICc) and model weight (1 indicates the intercept).

Model Form	df	logLik	AICc	ΔAICc	weight
z.Bacteroidaceae + 1	3	-341.329	688.988	0	0.204
z.Rikenellaceae + 1	3	-341.541	689.412	0.424	0.165
z.Bacteroidaceae + z.Clostridiaceae + 1	4	-340.868	690.291	1.303	0.106
z.Clostridiaceae + z.Rikenellaceae + 1	4	-340.946	690.448	1.46	0.098
1	2	-343.203	690.568	1.581	0.093
z.Bacteroidaceae + z.Rikenellaceae + 1	4	-341.032	690.62	1.632	0.09
z.Lachnospiraceae + z.Rikenellaceae + 1	4	-341.12	690.795	1.808	0.083
z.Bacteroidaceae + z.Eubacteriaceae + 1	4	-341.148	690.853	1.865	0.08
z.Bacteroidaceae + z.Lachnospiraceae + 1	4	-341.151	690.857	1.869	0.08

Supplementary Table 2.

The Relative Importance (RI) of abundance of bacterial families in explaining fenestration diameter. Model averaged coefficient (Coef.) estimates (Est.), their Standard Error (SE), and Lower to Upper 95% Confidence Interval (LCI and UCI) are given. Also given are model averaged coefficients Est. with shrinkage.

Coef.	RI	Est.	SE	LCI	UCI	Est. (Shrinkage)
(Intercept)	NA	87.545	2.399	82.843	92.247	87.545
z.Bacteroidaceae	0.561	-9.174	5.442	-19.84	1.492	-5.149
z.Rikenellaceae	0.436	-8.849	5.935	-20.482	2.784	-3.862
z.Clostridiaceae	0.205	-5.451	5.517	-16.264	5.362	-1.116
z.Lachnospiraceae	0.163	3.777	5.188	-6.391	13.945	0.615
z.Eubacteriaceae	0.08	2.81	4.838	-6.672	12.292	0.226

Supplementary Table 3.

Top model set based on Akaike Information Criterion corrected for small sample size (AICc) for the effects of bacterial abundance on percentage porosity of fenestration (proportion logit-transformed). Given for each model is the model form, degrees of freedom (df), models log likelihood (logLik), AICc, change in AICc from the top model (ΔAICc) and model weight (1 indicates the intercept).

Model Form	df	logLik	AICc	ΔAICc	weight
1	2	-46.384	96.931	0	0.128
z.Ruminococcaceae + 1	3	-45.307	96.944	0.013	0.127
z.Eubacteriaceae + 1	3	-45.71	97.748	0.817	0.085
z.Lachnospiraceae + 1	3	-45.71	97.748	0.818	0.085
z.Lachnospiraceae + z.Rikenellaceae + 1	4	-44.624	97.803	0.873	0.083
z.Clostridiaceae + z.Rikenellaceae + 1	4	-44.656	97.867	0.937	0.08
z.Rikenellaceae + z.Ruminococcaceae + 1	4	-44.794	98.143	1.212	0.07
z.Clostridiaceae + 1	3	-45.954	98.237	1.306	0.066
z.Rikenellaceae + 1	3	-45.989	98.306	1.375	0.064
z.Lachnospiraceae + z.Ruminococcaceae + 1	4	-44.97	98.496	1.566	0.058
z.Bacteroidaceae + 1	3	-46.174	98.677	1.747	0.053
z.Lachnospiraceae + z.Rikenellaceae + z.Ruminococcaceae + 1	5	-43.918	98.682	1.751	0.053
z.Bacteroidaceae + z.Ruminococcaceae + 1	4	-45.156	98.868	1.937	0.048

Supplementary Table 4.

The Relative Importance (RI) of abundance of bacterial families in explaining percentage porosity of fenestration (proportion logit-transformed). Model averaged coefficient (Coef.) estimates (Est.), their Standard Error (SE), and Lower to Upper 95% Confidence Interval (LCI and UCI) are given. Also given are model averaged coefficients Est. with shrinkage.

Coef.	RI	Est.	SE	LCI	UCI	Est. (Shrinkage)
(Intercept)	NA	-3.281	0.051	-3.381	-3.181	-3.281
z.Ruminococcaceae	0.356	0.141	0.105	-0.065	0.347	0.05
z.Eubacteriaceae	0.085	0.117	0.104	-0.087	0.321	0.01
z.Lachnospiraceae	0.279	0.134	0.114	-0.089	0.357	0.037
z.Rikenellaceae	0.349	-0.141	0.117	-0.37	0.088	-0.049
z.Clostridiaceae	0.146	-0.147	0.123	-0.388	0.094	-0.021
z.Bacteroidaceae	0.102	-0.061	0.104	-0.265	0.143	-0.006

Supplementary Table 5.

Top model set based on Akaike Information Criterion corrected for small sample size (AICc) for the effects of bacterial abundance on fenestration frequency (log + 0.5). Given for each model is the model form, degrees of freedom (df), models log likelihood (logLik), AICc, change in AICc from the top model (ΔAICc) and model weight (1 indicates the intercept).

Model Form	df	logLik	AICc	ΔAICc	weight
z.Bacteroidaceae + z.Lachnospiraceae + 1	4	-84.532	177.619	0	0.476
z.Bacteroidaceae + z.Lachnospiraceae + z.Ruminococcaceae + 1	5	-83.865	178.575	0.957	0.295
z.Bacteroidaceae + z.Eubacteriaceae + z.Lachnospiraceae + 1	5	-84.12	179.084	1.466	0.229

Supplementary Table 6.

The Relative Importance (RI) of abundance of bacterial families in explaining fenestration frequency (log + 0.5). Model averaged coefficient (Coef.) estimates (Est.), their Standard Error (SE), and Lower to Upper 95% Confidence Interval (LCI and UCI) are given. Also given are model averaged coefficients Est. with shrinkage.

Coef.	RI	Est.	SE	LCI	UCI	Est. (Shrinkage)
(Intercept)	NA	1.33	0.086	1.161	1.499	1.33
z.Bacteroidaceae	1	-0.603	0.179	-0.954	-0.252	-0.603
z.Lachnospiraceae	1	0.422	0.183	0.063	0.781	0.422
z.Ruminococcaceae	0.295	-0.2	0.18	-0.553	0.153	-0.059
z.Eubacteriaceae	0.229	-0.157	0.18	-0.51	0.196	-0.036

Supplementary Table 7.

Top model set based on Akaike Information Criterion corrected for small sample size (AICc) for the effects of fatty acids on fenestration diameter. Given for each model is the model form, degrees of freedom (df), models log likelihood (logLik), AICc, change in AICc from the top model (ΔAICc) and model weight (1 indicates the intercept).

Model Form	df	logLik	AICc	ΔAICc	weight
z.Very.long + 1	3	-421.656	849.576	0	0.164
z.Saturated + 1	3	-422.219	850.702	1.126	0.093
1	2	-423.29	850.711	1.135	0.093
z.Medium.chain + z.Very.long + 1	4	-421.207	850.859	1.283	0.086
z.Long + z.Very.long + 1	4	-421.293	851.031	1.455	0.079
z.Medium.chain + z.Saturated + 1	4	-421.344	851.132	1.556	0.075
z.Medium.chain + z.Saturated + z.Very.long + 1	5	-420.241	851.156	1.58	0.074
z.Unsaturated + z.Very.long + 1	4	-421.41	851.265	1.69	0.07
z.Saturated + z.Very.long + 1	4	-421.418	851.28	1.704	0.07
z.Long + 1	3	-422.558	851.379	1.804	0.066
z.Essential.FA + z.Very.long + 1	4	-421.486	851.416	1.84	0.065
z.Long + z.Medium.chain + z.Very.long + 1	5	-420.399	851.472	1.896	0.063

Supplementary Table 8.

The Relative Importance (RI) of each fatty acid group in explaining fenestration diameter. Model averaged coefficient (Coef.) estimates (Est.), their Standard Error (SE), and Lower to Upper 95% Confidence Interval (LCI and UCI) are given. Also given are model averaged coefficients Est. with shrinkage.

Coef.	RI	Est.	SE	LCI	UCI	Est. (Shrinkage)
(Intercept)	NA	85.998	2.158	81.768	90.228	85.998
z.Very.long	0.672	-7.779	4.672	-16.936	1.378	-5.229
z.Saturated	0.313	-6.981	5.692	-18.137	4.175	-2.182
z.Medium.chain	0.299	6.422	5.355	-4.074	16.918	1.921
z.Long	0.209	-4.809	4.597	-13.819	4.201	-1.005
z.Unsaturated	0.07	-2.964	4.349	-11.488	5.56	-0.209
z.Essential.FA	0.065	-2.49	4.391	-11.096	6.116	-0.162

Supplementary Table 9.

Top model set based on Akaike Information Criterion corrected for small sample size (AICc) for the effects of fatty acids on fenestration frequency (log + 0.5). Given for each model is the model form, degrees of freedom (df), models log likelihood (logLik), AICc, change in AICc from the top model (ΔAICc) and model weight (1 indicates the intercept).

Model Form	df	logLik	AICc	ΔAICc	weight
z.Medium.chain + 1	3	-122.869	252.001	0	0.122
1	2	-124.052	252.234	0.233	0.109
z.Saturated + 1	3	-123.126	252.516	0.515	0.094
z.Long + 1	3	-123.295	252.853	0.852	0.08
z.Essential.FA + 1	3	-123.441	253.146	1.145	0.069
z.Medium.chain + z.Very.long + 1	4	-122.465	253.375	1.375	0.061
z.Essential.FA + z.Medium.chain + 1	4	-122.467	253.378	1.377	0.061
z.Unsaturated + 1	3	-123.691	253.645	1.644	0.054
z.Saturated + z.Very.long + 1	4	-122.623	253.691	1.69	0.052
z.Essential.FA + z.Long + z.Saturated + 1	5	-121.513	253.7	1.699	0.052
z.Long + z.Medium.chain + 1	4	-122.637	253.719	1.718	0.052
z.Medium.chain + z.Unsaturated + 1	4	-122.682	253.808	1.807	0.049
z.Essential.FA + z.Medium.chain + z.Unsaturated + 1	5	-121.567	253.808	1.807	0.049
z.Medium.chain + z.Saturated + 1	4	-122.72	253.884	1.883	0.048
z.Essential.FA + z.Unsaturated + 1	4	-122.748	253.94	1.939	0.046

Supplementary Table 10.
The Relative Importance (RI) of each fatty acid group in explaining fenestration frequency (log + 0.5). Model averaged coefficient (Coef.) estimates (Est.), their Standard Error (SE), and Lower to Upper 95% Confidence Interval (LCI and UCI) are given. Also given are model averaged coefficients Est. with shrinkage.

Coef.	RI	Est.	SE	LCI	UCI	Est. (Shrinkage)
(Intercept)	NA	1.199	0.093	1.017	1.381	1.199
z.Medium.chain	0.443	0.271	0.201	-0.123	0.665	0.12
z.Saturated	0.247	0.535	0.717	-0.87	1.94	0.132
z.Long	0.184	-0.553	1.423	-3.342	2.236	-0.102
z.Essential.FA	0.278	0.828	0.916	-0.967	2.623	0.23
z.Very.long	0.114	-0.191	0.208	-0.599	0.217	-0.022
z.Unsaturated	0.199	-0.486	0.93	-2.309	1.337	-0.097

Supplementary Table 11.

Top model set based on Akaike Information Criterion corrected for small sample size (AICc) for the effects of fatty acids on percentage porosity of fenestration (proportion logit-transformed). Given for each model is the model form, degrees of freedom (df), models log likelihood (logLik), AICc, change in AICc from the top model (ΔAICc) and model weight (1 indicates the intercept).

Model Form	df	logLik	AICc	ΔAICc	weight
z.Saturated + 1	3	-57.756	121.776	0	0.134
z.Long + 1	3	-57.832	121.927	0.151	0.124
z.Medium.chain + z.Saturated + 1	4	-56.743	121.93	0.155	0.124
1	2	-58.905	121.941	0.165	0.123
z.Saturated + I (z.Saturated^2) + 1	4	-57.23	122.905	1.129	0.076
z.Essential.FA + z.Long + 1	4	-57.278	123.001	1.225	0.072
z.Unsaturated + 1	3	-58.479	123.223	1.447	0.065
z.Essential.FA + z.Long + z.Medium.chain + 1	5	-56.334	123.342	1.566	0.061
z.Long + z.Medium.chain + 1	4	-57.457	123.359	1.583	0.061
z.Long + z.Unsaturated + 1	4	-57.565	123.575	1.799	0.054
z.Very.long + 1	3	-58.674	123.611	1.835	0.053
z.Essential.FA + 1	3	-58.683	123.63	1.855	0.053

Supplementary Table 12.
The Relative Importance (RI) of each fatty acid group in explaining percentage porosity of fenestration (proportion logit-transformed). Model averaged coefficient (Coef.) estimates (Est.), their Standard Error (SE), and Lower to Upper 95% Confidence Interval (LCI and UCI) are given. Also given are model averaged coefficients Est. with shrinkage.

Coef.	RI	Est.	SE	LCI	UCI	Est. (Shrinkage)
(Intercept)	NA	-3.386	0.047	-3.478	-3.294	-3.386
z.Saturated	0.333	-0.2	0.124	-0.443	0.043	-0.067
z.Long	0.372	-0.235	0.182	-0.592	0.122	-0.087
z.Medium.chain	0.245	0.14	0.116	-0.087	0.367	0.034
I (z.Saturated^2)	0.076	0.078	0.078	-0.075	0.231	0.006
z.Essential.FA	0.186	0.141	0.209	-0.269	0.551	0.026
z.Unsaturated	0.119	0.016	0.185	-0.347	0.379	0.002
z.Very.long	0.053	-0.063	0.095	-0.249	0.123	-0.003

Supplementary Table 13

Top model set based on Akaike Information Criterion corrected for small sample size (AICc) for the effects of amino acids on fenestration diameter. Given for each model is the model form, degrees of freedom (df), models log likelihood (logLik), AICc, change in AICc from the top model (ΔAICc) and model weight (1 indicates the intercept).

Model Form	df	logLik	AICc	ΔAICc	weight
z.Aliphatic + z.Hydroxyl.or.Sulfur.Selenium + 1	4	-413.077	834.604	0	0.324
z.Hydroxyl.or.Sulfur.Selenium + 1	3	-414.456	835.179	0.575	0.243
1	2	-415.897	835.926	1.322	0.168
z.Essential + z.Hydroxyl.or.Sulfur.Selenium + 1	4	-413.952	836.353	1.749	0.135
z.Acidic.and.their.Amide + z.Aliphatic + z.Hydroxyl.or.Sulfur.Selenium + 1	5	-412.88	836.442	1.838	0.129

Supplementary Table 14.

The Relative Importance (RI) of each amino acid group in explaining fenestration diameter. Model averaged coefficient (Coef.) estimates (Est.), their Standard Error (SE), and Lower to Upper 95% Confidence Interval (LCI and UCI) are given. Also given are model averaged coefficients Est. with shrinkage.

Coef.	RI	Est.	SE	LCI	UCI	Est. (Shrinkage)
(Intercept)	NA	86.115	2.097	82.005	90.225	86.115
z.Aliphatic	0.454	-10.536	6.402	-23.084	2.012	-4.781
z.Hydroxyl.or.Sulfur.Selenium	0.832	11.779	6.558	-1.075	24.633	9.805
z.Essential	0.135	-6.007	6.144	-18.049	6.035	-0.813
z.Acidic.and.their.Amide	0.129	3.137	5.167	-6.99	13.264	0.406

Supplementary Table 15.

Top model set based on Akaike Information Criterion corrected for small sample size (AICc) for the effects of amino acids on fenestration frequency (log + 0.5). Given for each model is the model form, degrees of freedom (df), models log likelihood (logLik), AICc, change in AICc from the top model (ΔAICc) and model weight (1 indicates the intercept).

Model Form	df	logLik	AICc	ΔAICc	weight
1	2	-126.953	258.039	0	0.219
z.Aliphatic + z.Basic + 1	4	-125.26	258.97	0.931	0.137
z.Basic + 1	3	-126.384	259.034	0.995	0.133
z.Aromatic + 1	3	-126.391	259.048	1.009	0.132
z.Aromatic + z.Basic + 1	4	-125.504	259.458	1.42	0.108
z.Aliphatic + z.Essential + 1	4	-125.595	259.639	1.6	0.098
z.Aliphatic + 1	3	-126.773	259.812	1.773	0.09
z.Hydroxyl.or.Sulfur.Selenium + 1	3	-126.863	259.992	1.953	0.082

Supplementary Table 16.

The Relative Importance (RI) of each amino acid group in explaining fenestration frequency (log + 0.5). Model averaged coefficient (Coef.) estimates (Est.), their Standard Error (SE), and Lower to Upper 95% Confidence Interval (LCI and UCI) are given. Also given are model averaged coefficients Est. with shrinkage.

Coef.	RI	Est.	SE	LCI	UCI	Est. (Shrinkage)
(Intercept)	NA	1.155	0.098	0.963	1.347	1.155
z.Aliphatic	0.326	-0.345	0.313	-0.958	0.268	-0.112
z.Basic	0.378	0.295	0.232	-0.16	0.75	0.112
z.Aromatic	0.24	-0.23	0.201	-0.624	0.164	-0.055
z.Essential	0.098	0.521	0.348	-0.161	1.203	0.051
z.Hydroxyl.or.Sulfur.Selenium	0.082	0.083	0.198	-0.305	0.471	0.007

Supplementary Table 17.

Top model set based on Akaike Information Criterion corrected for small sample size (AICc) for the effects of amino acids on percentage porosity of fenestration (proportion logit-transformed). Given for each model is the model form, degrees of freedom (df), models log likelihood (logLik), AICc, change in AICc from the top model (ΔAICc) and model weight (1 indicates the intercept).

Model Form	df	logLik	AICc	ΔAICc	weight
z.Aliphatic + z.Aromatic + z.Essential + 1	5	-52.651	115.983	0	0.177
z.Aliphatic + z.Essential + 1	4	-54.176	116.801	0.818	0.118
z.Aliphatic + z.Aromatic + z.Essential + z.Non.essential + 1	6	-51.964	116.894	0.911	0.112
z.Aliphatic + z.Basic + 1	4	-54.28	117.01	1.027	0.106
z.Acidic.and.their.Amide + z.Aliphatic + z.Aromatic + z.Essential + 1	6	-52.122	117.21	1.227	0.096
z.Aliphatic + z.Aromatic + z.Essential + z.Hydroxyl.or.Sulfur.Selenium + 1	6	-52.16	117.285	1.302	0.093
z.Aliphatic + z.Essential + z.Hydroxyl.or.Sulfur.Selenium + 1	5	-53.44	117.562	1.579	0.081
z.Aliphatic + z.Hydroxyl.or.Sulfur.Selenium + 1	4	-54.6	117.65	1.667	0.077
z.Aliphatic + z.Aromatic + z.Basic + 1	5	-53.526	117.734	1.751	0.074
z.Aliphatic + z.Aromatic + z.Basic + z.Essential + 1	6	-52.496	117.958	1.975	0.066

Supplementary Table 18.

The Relative Importance (RI) of each amino acid group in explaining percentage porosity of fenestration (proportion logit-transformed). Model averaged coefficient (Coef.) estimates (Est.), their Standard Error (SE), and Lower to Upper 95% Confidence Interval (LCI and UCI) are given. Also given are model averaged coefficients Est. with shrinkage.

Coef.	RI	Est.	SE	LCI	UCI	Est. (Shrinkage)
(Intercept)	NA	-3.407	0.046	-3.497	-3.317	-3.407
z.Aliphatic	1	-0.431	0.188	-0.799	-0.063	-0.431
z.Aromatic	0.618	-0.175	0.107	-0.385	0.035	-0.108
z.Essential	0.743	0.352	0.182	-0.005	0.709	0.261
z.Non.essential	0.112	0.174	0.154	-0.128	0.476	0.02
z.Basic	0.246	0.175	0.136	-0.092	0.442	0.043
z.Acidic.and.their.Amide	0.096	0.118	0.119	-0.115	0.351	0.011
z.Hydroxyl.or.Sulfur.Selenium	0.25	0.177	0.147	-0.111	0.465	0.044